

A Parametric Investigation on the Influence and Inhibition Performance on CO₂ Corrosion of Carbon Steel



Lesor IKEH (B.Eng., M.Eng, M.Sc)

School of Computing, Science and Engineering
College of Science and Technology
University of Salford, Salford, UK

Submitted in Partial Fulfilment of the Requirements of the
Degree of Doctor of Philosophy, August 2017.

DECLARATION

I hereby declare that except where specific reference is made to the work of others, the contents of this dissertation are original and have not been submitted in whole or in part for consideration for any other degree or qualification in this, or any other University. This dissertation is the result of my own work and includes nothing which is the outcome of work done in collaboration, except where specifically indicated in the text. This dissertation contains less than 65,000 words including appendices, bibliography, footnotes, Tables and equations and has less than 150 Figures.

Lesor Ikeh

.....

July, 2017

Supervisors:

Dr. C G Enyi

.....

Signature

.....

Date

Prof. G.G Nasr

.....

Signature

.....

Date

ABSTRACT

The deposition of hydrate and corrosion in the pipeline remain a major challenge in the petroleum industry. Internal corrosion slows and decreases the production of oil and gas when associated with free water and reacts with organic acid. Experiments had shown that the corrosion products (ferrous and anhydrous ions) combine together to form a precipitate on iron surface that are porous and non-protective. To prevent these occurrence, Mono-Ethylene glycol (MEG) is been utilized in the pipeline as an antifreeze and anti-corrosion agent. It has been observed that the MEG need to be separated from acetic acid (HAc) and acid gases which enhances corrosion of mild steel in the oil field environment. Mono-Ethylene glycol and acetic acid also has an adverse effect of lowering the solubility of mineral salts and causing a higher risk of corrosion problem

The goal of this investigation is to determine the combined effect of acetic acid and mono-ethylene glycol on corrosion of carbon steel in CO₂ saturated environment at three different temperatures of 25°C, 50°C and 80°C using a 3.5% wt. NaCl solution. (Weight loss) and (electrochemical) measurements using Linear polarization resistance (LPR), Electrochemical Impedance Spectroscopy (EIS) and Potentiodynamic polarization(PDP) were employed in measuring the corrosion rate as a function of time on HAc and MEG concentrations. In addition, the efficiencies of three corrosion inhibitor based chemicals (the phosphate ester and the Oleic imidazoline salt) at different concentrations were also evaluated. Furthermore, the link between the nature of the film formed on the electrode material and the corrosion characteristics were investigated using the Scanning Electron Microscope (SEM), X-ray diffraction (XRD) and X-ray photoelectron scan (XPS).

The weight loss results shows that the corrosion rate with HAc increases rapidly as the concentration of HAc was added to the solutions compared to the solution without HAc. The average corrosion rate with HAc at 25°C is about 0.72 mm/yr and increased to 1.05 mm/yr at 50°C. The highest corrosion rate was noted at 80°C with approximately 2.71 mm/yr. However, addition of 20% and 80% MEG reduced the corrosion rate at all temperatures studied.

The electrochemical measurement results obtained show the corrosion rate in the presence of HAc increases as different concentrations of HAc were added to the system, and decrease with increased in exposure time as a result of protective film formed on the electrode surface. At 25°C, the average corrosion rate increases from 2.6 mm/y to 3.07 mm/yr. The applications of inhibitors lower the corrosion rate at all temperatures with average corrosion rate of 0.21 mm/yr, 0.44 mm/yr and 0.56 mm/yr at 25°C, 50°C and 80°C respectively. Similarly, the Nyquist and Bode plots of the EIS results indicate that the diameter of the depressed semi-circle decreases as different concentration of HAc and MEG were added to the solution, and the capacitive semi-circle sizes also decreases on addition of 20% and 80% MEG to the system. This decreased in corrosion rate can be attributed to the formation of iron carbonate film on the surface of the steel sample.

The surface examination of the exposed samples reviews that a dense layer of iron carbonate and localized corrosion were observed in the absence of HAc at 80°C. On addition of HAc and MEG, the layers of the film became porous. High magnification of the scan results shows a small pits and localized corrosion on the electrode surface. The EDX and XPS analyses on the samples reviews that some of the elements are absence on addition of HAc to the solution.

ACKNOWLEDGEMENTS

Firstly, I would like to express my sincere gratitude to my advisors, Dr. C. G Enyi and Prof. G.G Nasr for their invaluable support, guidance, and encouragement during my Ph.D. study at the University of Salford, Manchester.

I would also like to thank Dr. Amir Nourian, Dr. Abubakar Abbas, Dr. Martin Burby, Dr. Musa Abuhesa and the technician Mr. Alan Wells for their immense contributions and insightful comments and encouragement.

My deepest gratitude also goes to Prof. Mike Onyekonwu, Prof. Joseph Ajienska and Prof. Dulu Appah of the University of Port Harcourt, Nigeria for their support and encouragement throughout my study.

My sincere thanks also goes to Dr. Steven Nicholas of the University of Manchester for provide me an opportunity to join their team as a visiting research student that gave me access to the laboratory and research facilities at the University of Manchester. Without their support it would not have been possible to complete this research

I would also like to thank the following: Mohammed Abubakar, Dr. Sunday Aribo, Emmanuel Udofia, Abdulati Rafefi and others are too numerous to mention.

I would like to express my deep gratitude to mother Mrs Christianah Kaizer Ikeh, My Uncle Chief Christopher Pianen, and Mr John Teenwini, My brothers Douglas Ikeh, Barika Ikeh, Barile Ikeh, and John Wadum.

Also, my deepest gratitude goes to my wife Mrs. Ziisorle Cynthia Lesor-Ikeh, My Daughter Miss Kiale MaryAnne Lesor-Ikeh, My Son Mr. Dormene Ivan Lesor-Ikeh for their for their prayers, patience and encouragement during my study.

Finally, to God Almighty for his grace, protection, guidance, Mercy and love and to My dearest mother Virgin Mary for her intercession, the gift and power of the Rosary.

DEDICATION

Dedicated to the memory of my departed Father, Brothers and Sisters May their souls and the soul of all the faithful departed rest in peace. Amen

Nomenclature

<i>ba, bc</i>	<i>anodic and cathodic Tafel slope, V/decade</i>
<i>cr and cp</i>	<i>concentrations of reactants and products, Kmol/m^3</i>
CR	<i>corrosion rate, mm/yr</i>
<i>E_{corr}</i>	<i>corrosion potential, mV</i>
F	<i>Faraday constant, (96,490 C/equiv.)</i>
HAc	<i>acetic acid concentration, ppm</i>
<i>i_{Corr}</i>	<i>corrosion current density, A/m^2</i>
<i>i_a</i>	<i>anodic current density, A/m^2</i>
<i>i_c</i>	<i>cathodic current density, A/m^2</i>
<i>i_{ct}</i>	<i>charge transfer component of the total current density, A/m^2</i>
<i>inh</i>	<i>inhibitor</i>
MEG	<i>monoEthylene glycol, %</i>
P_{CO_2}	<i>partial pressure of carbon dioxide, bar</i>
η	<i>inhibition efficiency, %</i>
ρ	<i>density, kg/m^3</i>
R	<i>universal gas constant, (8.3143 J/(mol K))</i>
FeCO_3	<i>iron carbonate</i>
T	<i>absolute temperature, K</i>
<i>v</i>	<i>velocity, m/s</i>
LPR	<i>Linear polarization resistance</i>
AC	<i>AC Impedance</i>
OCP	<i>Open circuit potential</i>
SEM	<i>Scanning electron microscope</i>

<i>XRD</i>	<i>X-Ray diffraction</i>
<i>XPS</i>	<i>X-Ray photoelectron spectroscopy</i>
<i>PDP</i>	<i>Potentiodynamic polarization</i>
<i>EDX</i>	<i>Energy dispersive X-Ray</i>
<i>EIS</i>	<i>Electrochemical impedance spectroscopy</i>
<i>BE</i>	<i>Binding energy</i>
<i>mm/yr</i>	<i>Millimeter per year</i>
<i>NACE</i>	<i>National Association of Corrosion Engineers</i>
<i>pH</i>	<i>Minus log of activity of pH</i>
<i>R_p</i>	<i>Polarization resistance</i>
<i>R_s</i>	<i>Solution resistance</i>
<i>MIC</i>	<i>Microbiologically induced corrosion</i>
<i>C_{dl}</i>	<i>Double layer capacitance</i>
<i>M</i>	<i>Atomic mass</i>
<i>n</i>	<i>Number of electrons bythe corrosion reaction</i>
<i>mpy</i>	<i>Milli-inch per year</i>

Conversion Table

Conversion criteria

Composed entity	Conversion factors		
	g/m^2h	Mm/yr	Mm/yr
mm/year	$0.116 \times s.g$	1.0	39.4
mm/month	$1.39 \times s.g$	12	479
mm/48h	$20.80 \times s.g$	180	7185

S.g= specific gravity

Corrosion rate units with appropriate value of K

Corrosion rate Units Desired	Constant (K) in CR
Mils per year (mpy)	3.45×10^6
Inches per year (ipy)	3.45×10^3
Inches per month (ipm)	2.87×10^2
Millimeters per year (mm/yr)	8.76×10^4
Micrometers per year ($\mu m/yr$)	8.76×10^7
Picometers per second (pm/s)	2.78×10^6
Grams per square per hours ($g/m^2.h$)	$1.00 \times 10^4 \times D^A$
Milligrams per square decimetre per day (mdd)	$2.40 \times 10^6 \times D^A$
Micrograms per square meter per second ($\mu g/m^2.s$)	$2.78 \times 10^6 \times D^A$

N/B: Density is not needed to calculate the corrosion rate in these units. The density in the constant K cancels out the density in the corrosion rate equation.

Simple chart to convert data between the most common corrosion units

	mA cm⁻²	mm year⁻¹	mpy	g m⁻² day⁻¹
mA cm⁻²	1	3.28 M/nd	29 M/nd	8.95 M/n
mm year⁻¹	0.306 nd/M	1	39.4	2.74 d
mpy	0.00777 nd/M	0.0254	1	0.0694 d
g m⁻² day⁻¹	0.112 n/M	0.365 /d	14.4 /d	1

PUBLICATIONS

- L. Ikeh, G.C Enyi and G.G Nasr; Petroleum Technology Research Group, School of Computing, Science and Engineering, University of Salford, Manchester, “Effects of acetic acid and mono-ethylene glycol on iron carbonate dissolution in de-aerated environment”. The European Corrosion Congress, 6 – 10 September, 2015, Graz, Austria.
- L. Ikeh, G.C Enyi and G.G Nasr; Petroleum Technology Research Group, School of Computing, Science and Engineering, University of Salford, Manchester, “Inhibition performance of mild steel corrosion in the presence of CO₂, HAc and MEG” SPE International Oilfield Corrosion Conference and Exhibition, 9 – 10 May, 2016 Aberdeen, Scotland, UK, Paper no. SPE-179942-MS
- L. Ikeh, G.C Enyi and G.G Nasr; Petroleum Technology Research Group, School of Computing, Science and Engineering, University of Salford, Manchester, Influence of Acetic Acid and Mono-Ethylene Glycol on Polarization behaviour of Mild Steel Corrosion in De-aerated Environment. Corrosion Conference and Expo, March 26 – 30, 2017, New Orleans, Louisiana, USA.

TABLE OF CONTENTS

DEDICATION.....	IV
NOMENCLATURE.....	V
LIST OF FIGURES	XV
CHAPTER 1 INTRODUCTION.....	1
1.1 Introduction	1
1.2 Assessment of corrosion failure in industry	1
1.3 Contribution to knowledge	6
1.4 Overall aim and objectives	6
1.5 Thesis Outlines	7
CHAPTER 2 LITERATURE REVIEW.....	9
2.1 Introduction	9
2.2 Thermodynamic aspects of aqueous corrosion	9
2.2.1 Potential-pH (Pourbaix) diagram	10
2.3 Driving force for corrosion	13
2.3.1 The standard hydrogen potential.....	13
2.3.2 The electrode potential at equilibrium	14
2.3.3 The electrode potential during corrosion	15
2.3.4 The electrical double layer (EDL).....	16
2.3.5 The relationship between EDL chemistry, voltage and current	17
2.4 Classification of corrosion	18
2.4.1 Uniform (general) corrosion.....	19

2.4.2	Crevice corrosion	21
2.4.3	Pitting corrosion	21
2.4.4	Mesa corrosion	22
2.4.5	Erosion-corrosion	23
2.4.6	Flow Induced Corrosion.....	24
2.4.7	Microbiologically-induced corrosion.....	25
2.5	Expressions and measurement of corrosion rate	27
2.5.1	Weight loss method.....	27
2.5.2	The potential-time measurement.....	27
2.6	Factors influencing CO ₂ corrosion	28
2.6.1	Effect of iron concentration.....	28
2.6.2	Effect of pH.....	29
2.6.3	Effect of CO ₂ partial pressure	31
2.6.4	Effect of operating temperature.....	31
2.6.5	Effect of velocity.....	32
2.7	Assessment of CO ₂ corrosion prediction models.....	32
2.7.1	Mechanistic model	32
2.7.2	Semi-empirical model	33
2.7.3	Empirical model	34
2.7.4	Norsok CO ₂ corrosion model	35
2.8	Acetic acid corrosion of carbon steel in CO ₂ environment.....	36
2.9	Hydrate formation in the oil and gas industry.....	44
2.9.1	The influence of MEG in oil and gas industry.....	46

2.9.2	Corrosion inhibition of carbon steel in CO ₂ environment	48
CHAPTER 3 APPARATUS, MATERIALS AND PROCEDURES		50
3.1	Overview	50
3.2	Phase 1: Weight loss test.....	54
3.2.1	Apparatus	54
3.2.2	Test material.....	54
3.2.3	Test procedure.....	60
3.2.4	Error and Accuracy	62
3.3	Phase - II: Electrochemical Test.....	62
3.3.1	Apparatus	63
3.3.2	Test material.....	64
3.3.3	Test procedure.....	66
3.3.4	Error and Accuracy	67
3.3.5	Measuring techniques.....	67
3.4	Phase - III: Surface Analysis Examination	77
3.4.1	Apparatus, test materials and procedures for SEM and XRD.....	77
3.4.2	Apparatus, test materials and procedures for XPS	80
(iii)	Procedures of the XPS.....	83
CHAPTER 4 RESULTS AND DISCUSSIONS		85
4.1	Introduction	85
4.2	Phase – I: Weight loss	85
4.2.1	Weight loss with HAc	86
4.2.2	Weight loss with HAc, MEG and corrosion inhibitors	99

4.3	Phase – II: Electrochemical test results	105
4.3.1	OCP with HAc	105
4.3.2	OCP with HAc and MEG.....	108
4.3.3	LPR results	113
4.3.4	EIS results	115
(i)	EIS with HAc	115
(ii)	EIS with HAc and MEG.....	120
(i)	EIS results with HAc, MEG and corrosion inhibitors.....	126
4.3.5	Potentiodynamic polarization results	133
4.4	Phase – III: Surface analysis results	143
4.4.1	SEM observations of samples in solutions with HAc.....	143
4.4.2	SEM observations of samples in solutions with HAc and	144
	MEG	144
4.4.3	SEM observations of samples in solutions with HAc, MEG and corrosion inhibitors	146
4.4.4	XPS spectrum analysis.....	149
i.	O 1s spectra	149
ii.	C 1s spectra	149
iii.	N 1s spectra	150
iv.	Fe 2p spectra.....	150
	CHAPTER 5.....	156
	CONCLUSIONS AND FURTHER WORK.....	156
5.1	Conclusions	156

5.2 Further work	159
REFERENCES.....	162
APPENDIX A	169
APPENDIX B	176
POTENTIODYNAMIC POLARIZATION (PDP) PARAMETERS OBTAINED	
FOR CARBON STEEL ELECTRODES SATURATED IN 3.5% WT.	
NACL SOLUTION CONTAINING HAC, 20% & 80% MEG, CORROSION	
INHIBITORS AT 25⁰C, 50⁰C AND 80⁰C	
	176
APPENDIX C	LIST OF PUBLISH PAPERS
	182
ABSTRACT.....	201

LIST OF FIGURES

Figure 1-1: Overall corrosion costs and main industrial fields contributing to these costs [4].....	2
Figure 1-2: Annual cost of corrosion in the production and manufacturing industry [4]... 3	
Figure 2-1: Schematic description of corrosion processes of an iron bar in hydrochloric acid [5].....	10
Figure 2-2: Pourbaix diagram for the Fe-H ₂ O system [14]	12
Figure 2-3: Standard hydrogen electrode, SHE.	14
Figure 2-4: Electrochemical cell for electrode potential measurements for a non-equilibrium half-cell	15
Figure 2-5: Electrical double layer at a metal-solution interface [17].....	17
Figure 2-6: General corrosion on carbon steel [21]	19
Figure 2-7: Crevice corrosion in titanium -6 aluminium -4 vanadium [21]	21
Figure 2-8: Schematic diagram of pitting corrosion mechanism for X-65 carbon steel immersed in 3.5% NaCl solution [24].....	22
Figure 2-9: Mesa corrosion attack on carbon steel [25]	23
Figure 2-10: Example of erosion corrosion in steel feed water pump spacer [30]	25
Figure 2-11: Flow induced localized corrosion in CO ₂ environment	26
Figure 2-12: Microbiologically induced corrosion in a carbon steel weld	26
Figure 2-13: Factors influencing CO ₂ corrosion of carbon steel	30
Figure 2-14: Nomogram for predicting CO ₂ corrosion rate of carbon steel	34

Figure 2-15: Concentration of organic acid found in formation water	38
Figure 2-16: An overview of MEG process and challenges with respect to precipitation of salts [62]	45
Figure 2-17: Typical example of gas hydrates in a Sunsea hydrocarbon pipeline [63]....	46
Figure 3-1: An overview of experimental Apparatus, Materials and procedures.....	52
Figure 3-2: Details of Experimental Structure and Apparatus.....	53
Figure 3-3: show the picture of the test set-up for the weight loss experiment of this study.....	56
Figure 3-4: Carbon steel specimens used for the weight loss corrosion test in this study.	56
Figure 3-5: Schematic drawing of 3-electrode glass cell used in the electrochemical test	63
Figure 3-6: Mechanical polishing machine in preparation for tests	64
Figure 3-7: Mechanical spot weld machine for test.....	64
Figure 3-8: Test samples after 6 hours exposure in the solution	65
Figure 3-9: Graphical representation of the polarization resistance.	70
Figure 3-10: Schematic diagram of the polarization curve demonstrating different anodic and cathodic regions, and showing the Tafel extrapolation method for estimation of corrosion current density (i_{corr}) and corrosion potential (E_{corr}).....	71
Figure 3-11: Schematic representation of a polarization curve showing pitting potential, metastable pitting region, repassivation region and, corrosion potential (E_{corr}).....	72
Figure 3-12: Nyquist plot with a single time constant and electrical circuit describing the plot.....	75
Figure 3-13: A Bode plot for single time constant for a corroding metal.....	76

Figure 3-14: A typical image of SEM for specimen's surface analysis.	79
Figure 3-15: A typical image of XRD for specimen's surface analysis	80
Figure 3-16: A typical image of Kratos Axis Ultra X-ray photoelectron Spectrometer used in this study.	82
Figure 3-17: Typical block diagram of an XPS spectrometer analysis	84
Figure 4-1: Corrosion rate as a function of time for 3.5% wt. NaCl solution containing HAc at 25°C.....	87
Figure 4-2: Corrosion rate as a function of time for 3.5% wt. NaCl solution containing HAc at 50°C.....	88
Figure 4-3: Corrosion rate as a function of time for 3.5% wt. NaCl solution containing HAc at 80°C.....	88
Figure 4-4: Corrosion rate as a function of time for solution with 500ppm HAc and MEG at 25°C.	91
Figure 4-5: Corrosion rate as a function of time for solution with 1000ppm HAc and MEG at 25°C.	91
Figure 4-6: Corrosion rate as a function of time for solution with 2500ppm HAc and MEG at 25°C.	92
Figure 4-7: Corrosion rate as a function of time for solution with 500ppm HAc and MEG at 50°C.	92
Figure 4-8: Corrosion rate as a function of time for solution with 1000ppm HAc and MEG at 50°C.	93
Figure 4-9: Corrosion rate as a function of time for solution with 2500ppm HAc and MEG at 50°C.	93

Figure 4-10: Corrosion rate as a function of time for solution with 500ppm HAc and MEG at 80°C.	94
Figure 4-11: Corrosion rate as a function of time for solution with 1000ppm HAc and MEG at 80°C.	94
Figure 4-12: Corrosion rate as a function of time for solution with 2500ppm HAc and MEG at 80°C.	95
Figure 4-13: Variation of corrosion rate as a function of immersion time recorded for carbon steel sample in 3.5% wt. NaCl solution containing 500ppm HAc MEG and inhibitors at 25°C.....	99
Figure 4-14: Variation of corrosion rate as a function of immersion time recorded for carbon steel sample in 3.5% wt. NaCl solution containing 1000ppm HAc, MEG and inhibitors at 25°C.....	100
Figure 4-15: Variation of corrosion rate as a function of immersion time recorded for carbon steel sample in 3.5% wt. NaCl solution containing 2500ppm HAc, MEG and inhibitors at 25°C.....	100
Figure 4-16: Variation of corrosion rate as a function of immersion time recorded for carbon steel sample in 3.5% wt. NaCl solution containing 500ppm HAc, MEG and inhibitors at 50°C.....	101
Figure 4-17: Variation of corrosion rate as a function of immersion time recorded for carbon steel sample in 3.5% wt. NaCl solution containing 1000ppm HAc, MEG and inhibitors at 50°C.....	102

Figure 4-18: Variation of corrosion rate as a function of immersion time recorded for carbon steel sample in 3.5% wt. NaCl solution containing 2500ppm HAc, MEG and inhibitors at 50°C.....	102
Figure 4-19: Variation of corrosion rate as a function of immersion time recorded for carbon steel sample in 3.5% wt. NaCl solution containing 500ppm HAc, MEG and inhibitors at 80°C.....	103
Figure 4-20: Variation of corrosion rate as a function of immersion time recorded for carbon steel sample in 3.5% wt. NaCl solution containing 1000ppm HAc, MEG and inhibitors at 80°C.....	104
Figure 4-21: Variation of corrosion rate as a function of immersion time recorded for carbon steel sample in 3.5% wt. NaCl solution containing 2500ppm HAc, MEG and inhibitors at 80°C.....	104
Figure 4-22: Corrosion potential of carbon steel electrodes immersed in 3.5% wt. NaCl solution containing different concentrations of HAc at 25°C.....	106
Figure 4-23: Corrosion potential of carbon steel electrodes immersed in 3.5% wt. NaCl solution containing different concentrations of HAc at 50°C.....	106
Figure 4-24: Corrosion potential of carbon steel electrodes immersed in 3.5% wt. NaCl solution containing different concentrations of HAc at 80°C.....	107
Figure 4-25: Free corrosion potential of carbon steel samples immersed in 3.5% wt. NaCl solutions containing HAc, 20% MEG and 80% MEG at 25°C	110
Figure 4-26: Free corrosion potential of carbon steel samples immersed in 3.5% wt. NaCl solutions containing HAc, 20% MEG and 80% MEG at 50°C	110

Figure 4-27: Free corrosion potential of carbon steel samples immersed in 3.5% wt. NaCl solutions containing HAc, 20% MEG and 80% MEG at 80°C	111
Figure 4-28: LPR measurements of carbon steel samples immersed in solution containing different concentrations of HAc at 25°C	114
Figure 4-29: LPR measurements of carbon steel samples immersed in solution containing different concentrations of HAc at 80°C	114
Figure 4-30: Nyquist plots for carbon steel samples in solutions containing HAc at 25°C after 6 hours	116
Figure 4-31: Bode plots for carbon steel samples in solutions containing HAc at 25°C after 6 hours	116
Figure 4-32: Nyquist plots for carbon steel samples in solutions containing HAc at 50°C after 6 hours	117
Figure 4-33: Bode plots for carbon steel samples in solutions containing HAc at 50°C after 6 hours	117
Figure 4-34: Nyquist plots for carbon steel samples in solutions containing HAc at 80°C after 6 hours	118
Figure 4-35: Bode plots for carbon steel samples in solutions containing HAc at 80°C after 6 hours.	118
Figure 4-36: Equivalent circuit diagram used to fit the EIS data	119
Figure 4-37: Nyquist plots for carbon steel coupons in 3.5% wt. NaCl solution containing HAc with 20% MEG and 80% MEG after 6 hours at 25°C	121
Figure 4-38: Bode plots for carbon steel coupons in 3.5% wt. NaCl solution containing HAc with 20% MEG and 80% MEG after 6 hours tests at 25°C	122

Figure 4-39: Nyquist plots for carbon steel coupons in 3.5% wt. NaCl solution containing HAC with 20% MEG and 80% MEG after 6 hours at 50°C	123
Figure 4-40: Bode plots for carbon steel coupons in 3.5% wt. NaCl solution containing HAC with 20% MEG and 80% MEG after 6 hours tests at 50°C	123
Figure 4-41: Nyquist plots for carbon steel coupons in 3.5% wt. NaCl solution containing HAC with 20% MEG and 80% MEG after 6 hours at 80°C	124
Figure 4-42: Bode plots for carbon steel coupons in 3.5% wt. NaCl solution containing HAC with 20% MEG and 80% MEG after 6 hours tests at 80°C	125
Figure 4-43: Nyquist plots for carbon steel coupons in 3.5% wt. NaCl solution containing HAC, 20% MEG, 80% MEG, and corrosion inhibitors for 6 hours at 25°C.....	130
Figure 4-44: Bode plots for carbon steel coupons in 3.5% wt. NaCl solution containing HAC, 20% MEG, 80% MEG, and corrosion inhibitors for 6 hours at 25°C.....	130
Figure 4-45: Nyquist plots for carbon steel coupons in 3.5% wt. NaCl solution containing HAC, 20% MEG, 80% MEG, and corrosion inhibitors for 6 hours at 50°C.....	131
Figure 4-46: Bode plots for carbon steel coupons in 3.5% wt. NaCl solution containing HAC, 20% MEG, 80% MEG, and corrosion inhibitors for 6 hours at 50°C.....	131
Figure 4-47: Nyquist plots for carbon steel coupons in 3.5% wt. NaCl solution containing HAC, 20% MEG, 80% MEG, and corrosion inhibitors for 6 hours at 80°C.....	132
Figure 4-48: Bode plots for carbon steel coupons in 3.5% wt. NaCl solution containing HAC, 20% MEG, 80% MEG, and corrosion inhibitors for 6 hours at 80°C.....	132
Figure 4-49: Potentiodynamic polarization curves for carbon steel electrodes in solutions containing HAC for 6 hours tests at 25°C.	134

Figure 4-50: Potentiodynamic polarization curves for carbon steel electrodes in solution containing HAc for 6 hours tests at 50°C	134
Figure 4-51: Potentiodynamic polarization curves for carbon steel electrodes in solution containing HAc for 6 hours tests at 80°C	135
Figure 4-52: Potentiodynamic curves for carbon steel electrodes saturated in solution containing HAc with 20% & 80% MEG at 25°C	136
Figure 4-53: Potentiodynamic curves for carbon steel electrodes saturated in solution containing HAc with 20% and 80% MEG at 50°C	138
Figure 4-54: Potentiodynamic curves for carbon steel electrodes saturated in solution containing HAc with 20% and 80% MEG at 80°C	138
Figure 4-55: Potentiodynamic curves for carbon steel samples saturated in 3.5% wt. NaCl solution containing different concentrations of HAc, MEG and inhibitors at 25°C.	141
Figure 4-56: Potentiodynamic curves for carbon steel samples saturated in 3.5% wt. NaCl solution containing different concentrations of HAc, MEG and inhibitors at 50°C	142
Figure 4-57: Potentiodynamic curves for carbon steel samples saturated in 3.5% wt. NaCl solution containing different concentrations of HAc, MEG and inhibitors at 80°C	142
Figure 4-58: SEM images (Left) and EDX spectrum (Right) of carbon steel samples exposed to 3.5% wt. NaCl solution and different concentrations of HAc for 6 hours. [A] 500ppm HAc [B] 1000ppm HAc [C] 2500 ppm HAc.	145
Figure 4-59: SEM images (Left) and EDX spectrum (Right) of carbon steel samples exposed to 3.5% wt. NaCl solution and 1000ppm HAc and different concentrations of MEG for 6 hours. [A] 20% MEG [B] 80% MEG	147

Figure 4-60: SEM images (Left) and EDX spectrum (Right) of carbon steel samples exposed to 3.5% wt. NaCl solution and 1000ppm HAc, 80% MEG and 10ppm of : [A] inhibitor XX [B] inhibitor YY [C] inhibitor ZZ.	148
Figure 4-61: The XPS deconvolution profiles for O 1s for carbon steel sample after 6 hours immersion period in 3.5% wt. NaCl solution in the presence of HAc, MEG and inhibitors.....	151
Figure 4-62: The XPS deconvolution profiles for C 1s for carbon steel sample after 6 hours immersion period in 3.5% wt. NaCl solution in the presence of HAc, MEG and inhibitors.....	151
Figure 4-63: The XPS deconvolution profiles for N 1s for carbon steel sample after 6 hours immersion period in 3.5% wt. NaCl solution in the presence of HAc, MEG and inhibitors.....	152
Figure 4-64: The XPS deconvolution profiles for Fe 2p for carbon steel sample after 6 hours immersion period in 3.5% wt. NaCl solution in the presence of HAc, MEG and inhibitors.....	152
Figure 4-65: The XPS deconvolution profiles for Cl 1s for carbon steel sample after 6 hours immersion period in 3.5% wt. NaCl solution in the presence of HAc, MEG and inhibitors.....	153
Figure 4-66: Variation of the XPS deconvolution profiles for different samples of carbon steel after 6 hours immersion period in 3.5% wt. NaCl solution in the presence of HAc, MEG and inhibitors.....	154

Figure 4-67: Variation of the XPS deconvolution profiles for different samples of carbon steel after 6 hours immersion period in 3.5% wt. NaCl solution in the presence of HAc, MEG and inhibitors including C % and O % respectively. 154

LIST OF TABLES

Table 1-1: Analysis of a selected number of failures in petroleum industries [3]	3
Table 1-2: Causes of corrosion-related failure in petroleum- related industries [3].....	4
Table 2-1: ASM classification of corrosion types [20].....	20
Table 2-2: Constant values of K_t at different temperatures.....	36
Table 2-3:Short chain organic acid found in formation water	37
Table 2-4: Proposed empirical thresholds for acetic acid in gas wells [44]	37
Table 2-5: Formation water analysis.....	39
Table 2-6: Characteristics of corrosion films [1].....	42
Table 3-1: Chemical composition of X-65 carbon steel that used in the experiments	55
Table 3-2: Chemical composition of sea water brine	57
Table 3-3: Properties of Acetic acid (HAc) used for the experiments.....	58
Table 3-4: Properties of Monoethylene glycol (MEG) used for the experiments	59
Table 3-5: Example of chemical and molecular structures of corrosion inhibitors constituent studied.	60
Table 3-6: Experimental matrix for the electrochemical test.....	65
Table 4-1: : Summary of average corrosion rate as a function of time for 3.5% wt. NaCl solution at 25°C, 50°C, 80°C.	89
Table 4-2: Summary of average corrosion rate as a function of time solution containing HAc and MEG at 25°C.	96
Table 4-3: Summary of average corrosion rate as a function of time solution containing HAc and MEG at 50°C.	97

Table 4-4: Summary of average corrosion rate as a function of time solution containing HAc and MEG at 80°C.....	98
Table 4-5: corrosion parameters obtained from polarization curves for carbon steel samples immersed in solution containing HAc at 25°C	107
Table 4-6: corrosion parameters obtained from polarization curves for carbon steel samples immersed in solution containing HAc at 50°C	108
Table 4-7: corrosion parameters obtained from polarization curves for carbon steel samples immersed in solution containing HAc at 80°C	108
Table 4-8: corrosion parameters obtained from polarization measurements of carbon steel samples in solutions containing HAc and MEG at 25°C.....	111
Table 4-9: corrosion parameters obtained from polarization measurements of carbon steel samples in solutions containing HAc and MEG at 50°C.....	112
Table 4-10: corrosion parameters obtained from polarization measurements of carbon steel samples in solutions containing HAc and MEG at 80°C	112
Table 4-11: Electrochemical parameters obtained for carbon steel electrode in solutions containing HAc at 25°C.....	119
Table 4-12: Electrochemical parameters obtained for carbon steel electrode in solutions containing HAc at 50°C.....	119
Table 4-13: Electrochemical parameters obtained for carbon steel electrode in solutions containing HAc at 80°C.....	120
Table 4-14: Electrochemical parameters obtained for carbon steel electrode in 3.5% wt. NaCl solutions containing different concentrations of HAc with 20% MEG and 80% MEG at 25°C	125

Table 4-15: Electrochemical parameters obtained for carbon steel electrode in 3.5% wt. NaCl solutions containing different concentrations of HAc with 20% MEG and 80% MEG at 50°C	126
Table 4-16: Electrochemical parameters obtained for carbon steel electrode in 3.5% wt. NaCl solutions containing different concentrations of HAc with 20% MEG and 80% MEG at 80°C	127
Table 4-17: Potentiodynamic polarization parameters obtained for carbon steel electrodes saturated in containing HAc at 25°C, 50°C and 80°C respectively.	135
Table 4-18: Potentiodynamic parameters for carbon steel samples saturated in solutions containing HAc with 20% and 80% MEG at 25°C	139
Table 4-19: Potentiodynamic parameters for carbon steel samples saturated in solutions containing HAc with 20% and 80% MEG at 50°C	139
Table 4-20: Potentiodynamic parameters for carbon steel samples saturated in solutions containing HAc with 20% and 80% MEG at 80°C	140
Table 4-21: Atomic percentage of XPS deconvolution profiles for carbon steel sample after 6 hours immersion period in 3.5% wt. NaCl solution in the presence of HAc, MEG and inhibitors	153

CHAPTER 1

Introduction

1.1 Introduction

In recent years, there have been several national costs of corrosion studies covering a range of countries including the United State of America and the United Kingdom [1]. The impact of corrosion on the oil and gas industry has been viewed in terms of its effect on capital expenditure (CAPEX) and operational expenditures (OPEX) as well as health, safety and environment (HSE) [2]. However, the direct costs related to corrosion degradation are estimated for industrial countries to be around 3-4% of the Gross Domestic Product (GDP). Kermani and Harrop [3] proposed that the corrosion of metallic structures poses a significant threat to a company's economy.

Koch [4] in their studies presents a summary of data from USA where a detailed analysis has been performed to be about 276 Billion dollars per year which correspond to about 3.1% of the gross domestic product (GDP) as presented in Figure 1-1 and Figure 1-2 respectively. These cost were determined by analyzing 26 industrial sectors in which corrosion is known to exist, and consists of the cost of design, manufacturing, construction and the cost of management [2].

1.2 Assessment of corrosion failure in industry

Corrosion can impose a significant cost penalty on the choice of material at the design stage, and its possible occurrence also has serious safety and environmental implications [1]. A corrosion failure can also have a very serious impact on the environment. In the offshore oil industry, leakage from subsea oil well tubulars and transmission pipelines or

the storage vessels and other equipment on offshore platforms poses the threat of pollution to the sea.

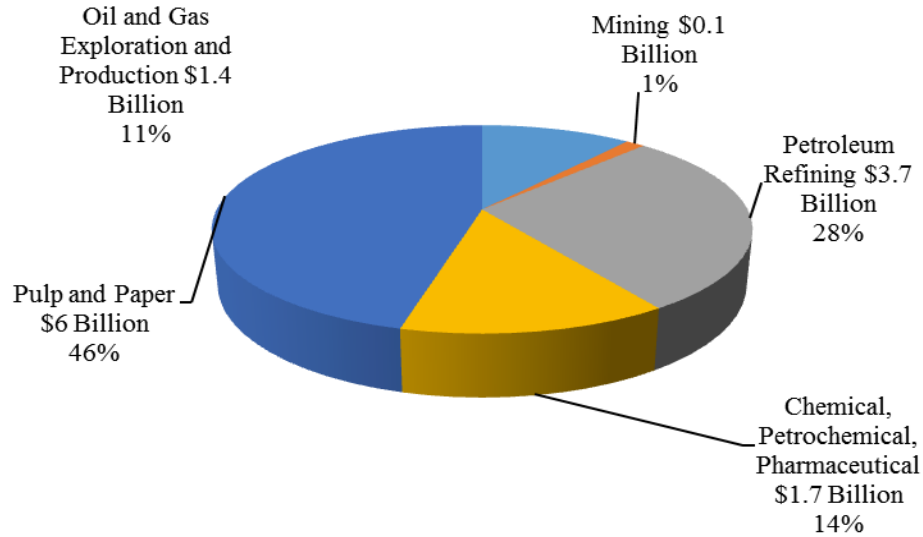


Figure 1-1: Overall corrosion costs and main industrial fields contributing to these costs [4]

Corrosion has been identified as the most common in-service cause of failure of pipelines and the cause of 6.4% of loss of containment failures of hazardous materials. Corrosion-related failures constitute over 25% of failures experienced in the oil and gas industry [3]. Kermani and Harrop [3] presented analyses of failures during in a limited industry-wide survey as summarized in Table 1-1 and Table 1-2.

Transportation of hydrocarbons and water in long distance flow lines from satellite fields to a platform or to shore results in new challenges to control hydrates, corrosion and scale. As the fluids cool down, water will condense and gas hydrates will form unless an inhibitor such as mono ethylene glycol (MEG) is present. The transportation of fluids in pipelines is a critical step in oil and gas production.

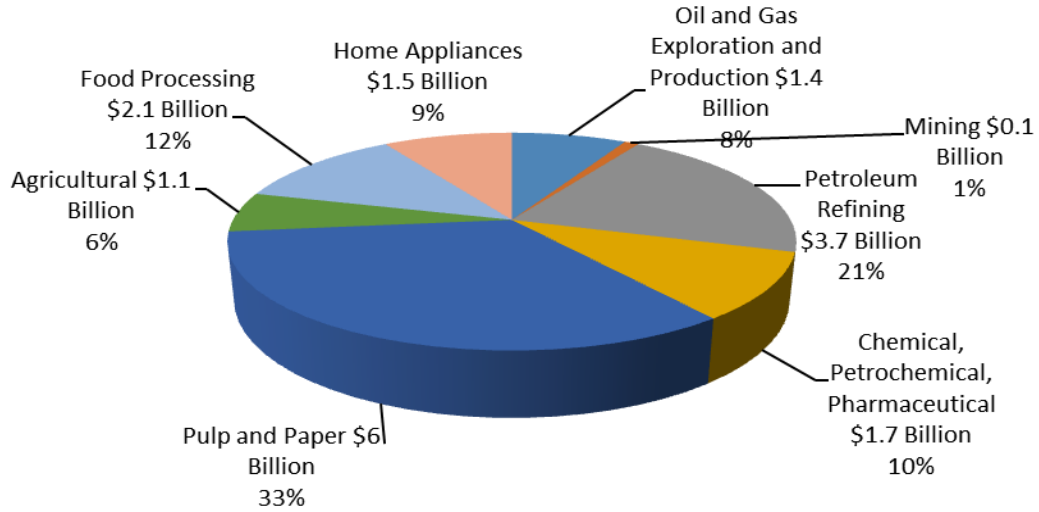


Figure 1-2: Annual cost of corrosion in the production and manufacturing industry [4]

Table 1-1: Analysis of a selected number of failures in petroleum industries [3]

Types of Failure	Frequency (%)
Corrosion (all types)	33
Fatigue	18
Mechanical damage/overload	14
Brittle fracture	9
Fabrication defects (excluding weld defects)	9
Welding defects	7
Others	10

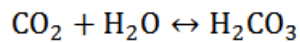
When it comes directly from the well, the fluid is usually unprocessed and multiphase and can be a mixture of oil, solids, gas and water. The presence of water leads to considerable corrosion problems on the internal walls of the pipelines. The liquid can contain corrosive species such as organic acids and dissolved corrosive gases such as

carbon dioxide (CO₂) or hydrogen sulphide (H₂S). Therefore the presence of these gases can lead to a very corrosion environment

Table 1-2: Causes of corrosion-related failure in petroleum- related industries [3]

Types of Failure	Total failure (%)
CO ₂ related	28
H ₂ S related	18
Preferential weld	18
Pitting	12
Erosion-Corrosion	9
Galvanic	6
Crevice	3
Impingement	3
Stress Corrosion	3

The carbon dioxide (CO₂) corrosion or sweet corrosion has been known for a long time and continues to be a problem in the oil and gas industry, costing billions of dollars every year [5]. The CO₂ is present in oil phase with water as a dissolved gas under high pressures commonly found in underground oil and gas reservoirs. In the dissolved state, it forms carbonic acid.



1-1

The pipeline costs are considerable part of the investment in subsea projects. For long-distance, large-diameter pipelines, they can become prohibitively high if the corrosivity of the fluid necessitates the use of corrosion-resistant alloys instead of carbon steel [6]. Therefore better understanding and control of the corrosion of carbon steel can increase its application range and have a large economic impact.

Carbon steel is used as the primary construction material for pipeline in oil and gas industry due to its low cost and availability. However, it is very susceptible to corrosion in CO₂ environments. Carbon dioxide corrosion has been of interest to many researchers [3, 7] in the oil and gas industry for many years and there exists many theories about the mechanism of CO₂ corrosion [8]. Similarly, there has been a great interest in understanding the effect of different factors on the mechanism of CO₂ corrosion and formation of iron carbonate film at the surface of the carbon steel because of the resulting corrosion rate.

Acetic acids (HAc) have been regarded as a source of hydrogen ions in its dissociation, increasing the acidification of the environment and the dissolution of the steel that leads to an increase in carbon steel corrosion rates, especially at low pH values. The acetic acid is the most common organic acid in multiphase systems containing brine [9]. The acetic acids content in oil wells plays a determining role in the severity of corrosion rate even when only small concentrations are present [10].

The precipitation of iron carbonate (FeCO₃) is an importance process for corrosion control in the oil industry. The precipitated corrosion film of FeCO₃ forms a layer of impermeable corrosion product which retards the corrosion process and lowers the corrosion rate by diffusion control. The formation of FeCO₃ plays an important role in the formation of protective layers [11]. When corrosion products are not deposited on the steel surface, very high corrosion rates of several millimeters per year can occur. The corrosion rate can be reduced substantially under conditions where FeCO₃ can precipitate on the steel surface and form a dense and protective corrosion product film. This occurs more easily at high temperature or high pH in the water phase. When hydrogen sulphide (H₂S) is present in addition to CO₂, iron sulphide (Fes) films are formed rather than FeCO₃ and protective films can be formed at lower temperature.

Corrosion inhibitor is one of the numerous methods used to protect against the corrosion process in the oil and gas industry. The inhibitors are commonly used to slow down corrosion process of mild steel in oilfield environment [12]. The inhibitors can reduce corrosion of metal by forming a protective film that can isolate the metal from the

aqueous corrosion environment. Water soluble and oil soluble inhibitors are the most commonly used in the oil and gas industry [13].

The mechanism of CO₂ corrosion and the kinetics of formation and removal of FeCO₃ film are not fully understood due to the complex reaction mechanisms, and the presence of many critical environmental factors such as pH, temperature, dissolved species concentrations and hydrodynamics that can change the corrosion rate. Similarly, there is little knowledge regarding the mechanism of CO₂ corrosion of acetic acid in CO₂ environment especially when MEG is involved. Hence, the main aim of this study is investigate comprehensively the carbon steel corrosion in CO₂ saturated environment.

1.3 Contribution to knowledge

The contribution to knowledge in this study is centered on where the combined effect of HAc and MEG have been employed to reduce the corrosion rate of carbon steel pipeline especially in the presence of HAc in CO₂ saturated environment. This study fills the corresponding gap which consequently abates the corrosion problems in their negative impact that facing the oil and gas industry.

1.4 Overall aim and objectives

The overall aim of this work is to understand the formation and dissolution of FeCO₃. In particular, this study will address the corrosion problem of carbon steel in CO₂ saturated environment especially when different concentration of HAc and MEG are involved.

The *objectives* of this study are:

- (i) To study the mechanism and corrosion rate of carbon steel in CO₂ environment especially when HAc is present using the weight loss and electrochemical methods
- (ii) To determine the synergistic behavior of HAc and MEG concentration on the corrosion rate of carbon steel in de-aerated environment using the weight loss and electrochemical measurements methods

- (iii) To quantify the combined effect of HAc, MEG and organic corrosion inhibitors on the corrosion rate of carbon steel in CO₂ environment using the weight loss, LPR, EIS and PDP measurement methods.
- (iv) To study and analyze the corrosion product film formed on the electrode surface using the XRD, SEM, EDX and XPS measurement techniques.

1.5 Thesis Outlines

The following paragraph gives a brief outline of the chapters in this thesis.

Chapter 1 presents the background and statement/contributions of knowledge of this research. It also highlights the aim and objectives of the studies

Chapter 2 presents the literature review on fundamental aspects of aqueous corrosion. This includes the thermodynamics of corrosion, the cell potential and the driving force for corrosion among others. It also presents the electrochemical aspect of corrosion, types of corrosion attack, and corrosion monitoring techniques. The knowledge of CO₂ corrosion mechanism and how the mechanism is affected by some environmental factors are also presented.

The second section of this chapter reviews the literature of short chain organic acid, the effect of MEG on CO₂ corrosion of carbon steel. CO₂ corrosion mitigation measures and the use of inhibitors are also presented.

Chapter 3 presents the experimental apparatus and procedures that are employed in this study. The use of surface analysis techniques such as the SEM, XRD and EDX are also discussed.

Chapter 4 reviewed the importance and use of X-ray photoelectron spectroscopy (XPS) in corrosion studies

Chapter 5 presents results obtained from this study based on the techniques in chapter 3. The first section presents results on the acetic acid corrosion, while the second section presents results on effect of acetic acid with MEG in CO₂ corrosion. The third section focuses on performance of inhibitors on CO₂ corrosion of carbon steel in the present of HAc and MEG.

Finally, **Chapter 6** presents the summary of conclusion from this work and offer potential means for future work to be carried out

CHAPTER 2

Literature Review

2.1 Introduction

This Chapter contains a survey of published work on fundamental principles of corrosion and short chain organic acid in CO₂ environment. It also includes review of literature on Mono-ethylene glycol and its importance in the oil and gas industry. Topics reviewed include acetic acid and its effect in CO₂ corrosion, electrochemical reactions of corrosion and the electrochemical techniques used in corrosion measurements are also discussed. CO₂ corrosion mitigation measures with the use of inhibitors are also included. The overview of these previous works will therefore highlights the gap that exist at present and hence the present investigation herewith.

2.2 Thermodynamic aspects of aqueous corrosion

In electrochemistry, thermodynamic considerations help us to understand under what conditions a corrosion reaction is possible. Even though the corrosion rates cannot be obtained yet, it is necessary to analyze thermodynamic stability of each specific metal-electrolyte interface [5]

Now considering a corrosion reaction processes of iron in acidic media as shown in Figure 2-1



Both anodic and the cathodic partial reactions take place at the same electrode, which means both partial reactions cannot be separated and therefore no external voltage difference can be measured.

In this present study, the thermodynamic stability of 3.5% wt. NaCl solution and HAc will be considered and used to determine the corrosion rate of carbon steel in CO₂ saturated environment.

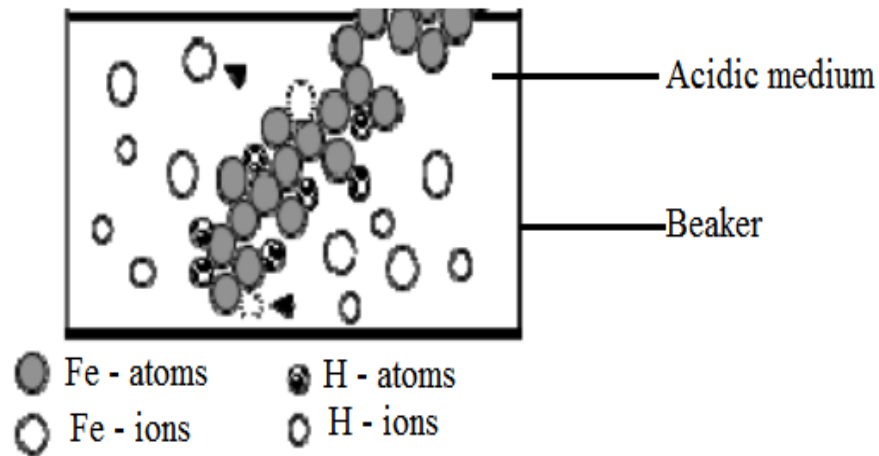


Figure 2-1: Schematic description of corrosion processes of an iron bar in hydrochloric acid [5].

2.2.1 Potential-pH (Pourbaix) diagram

The Pourbaix, E-pH diagram (Figure 2-2) due to the labeling of the two axes graphically represent the thermodynamic and electrochemical equilibrium between metal and water, indicating thermodynamically stable phases as a function of electrode potential and pH [14]. The vertical axis is labeled E for the voltage potential with respect to the standard hydrogen electrode (SHE) as calculated by the Nernst equation:

$$E = E^0 - \frac{0.0592}{n} \log \frac{[X]^x [Y]^y}{[C]^c [D]^d} \quad 2-4$$

The horizontal axis is labeled pH for the $-\log$ function of the H^+ ion activity:

$$pH = -\log_{10}(a_{H^+}) \quad 2-5$$

$$= \log_{10}\left(\frac{1}{a_{H^+}}\right) \quad 2-6$$

The Pourbaix diagrams provide much information on the behavior of a system as the pH and potential vary. It is suitable for studies of corrosion, electroplating, electrolysis, electrical cells, and water treatment since they are electrochemical maps indicating the domain of stability of ions, oxides and hydroxides [14]. The Pourbaix diagram is commonly used by corrosion Engineers to determine the pH and potential where a metal will be stable, corrode or form a passivating layer. The bottom of the diagram refers to reduced species Fe(s), or to the type of conditions that lead to reduction. The top of the diagram refers to oxidized or oxidizing conditions. The vertical lines indicate changes in acid base chemistry independent of E (e.g. $Fe^{3+}/Fe(OH)_3$). The horizontal lines indicate redox changes unaffected by pH (e.g. Fe/Fe^{2+} below pH 6) [15]. In this work and based on the Pourbaix diagram, the pH of 3.5% wt NaCl solution and potential of the electrode will be analyzed to determine the corrosion rate of carbon steel in CO_2 environment especially when different concentrations of HAc are added to the system.

Uses of the Pourbaix Diagrams:

- The Pourbaix diagram is very useful for estimation of the corrosion product and compositions that will form at any given potential and pH combinations
- To predict the spontaneous directions of the various reactions at given pH and E

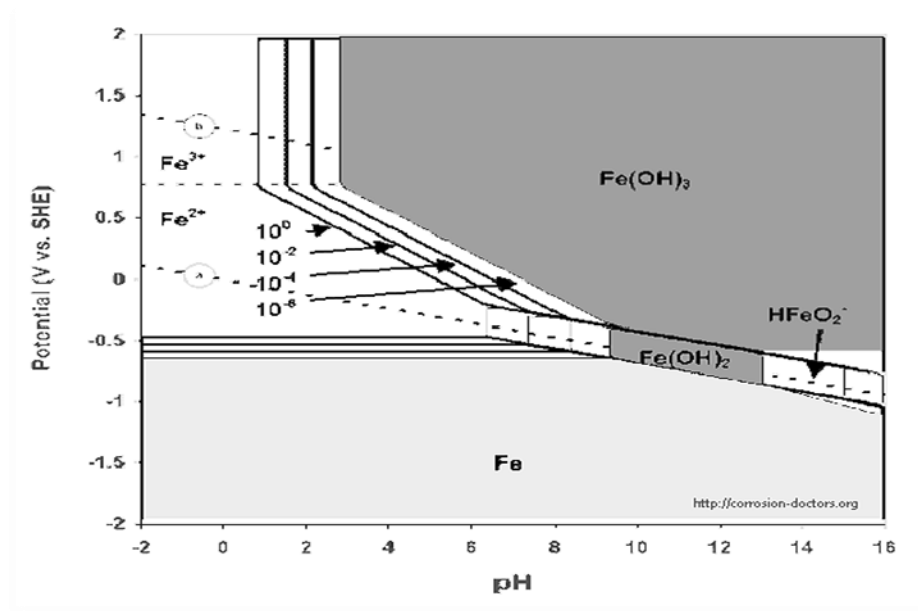


Figure 2-2: Pourbaix diagram for the Fe-H₂O system [14]

- The Pourbaix diagram can also be used to forecast which environmental pH and potential changes in solution composition will reduce or prevent corrosion attack
- To determine the boundaries of potential and pH that shows the immunity area (where only the reduced form of the metal is stable), corrosion area (where soluble corrosion products are the most stable), and passive area (where insoluble compounds are formed and may protect the metal against corrosion)
- It also gives an idea of the cathodic reaction product (i.e. hydrogen evolution or oxygen reaction) that is taking place during the process

The **limitations** of the Pourbaix diagram are:

- The Pourbaix diagrams are purely based on thermodynamic data and do not provide any information on the reactions
- Also, considerations of the Pourbaix diagram is given only to equilibrium conditions in specified environment and factors such as temperature, and velocity are not considered which may seriously affect the corrosion rate
- The activities of the species is arbitrarily selected as 10⁻⁶ gmol that is not realistic

- The Pourbaix diagrams deal with pure metals which are not much of interest to the engineers
- All soluble products are assumed to be protective which is not true as porosity, thickness, and adherence to substrate are important factors.

However, this present study will address some of the limitations of the pourbaix diagram.

2.3 Driving force for corrosion

The corrosion process in Figure 2-1 is an example of a spontaneous electrochemical cell reaction. The driving force of the reaction is a reversible cell voltage, expressed as the difference between the potentials of anode and cathode [16]. Reversible cell voltage and corresponding reversible cell potentials of the electrodes are determined by thermodynamic properties.

2.3.1 The standard hydrogen potential

In a corrosion cell, the potential difference between the anode and cathode can be measured using a voltage measuring device, but the absolute potential of the anode and cathode cannot be measured directly. In order to measure the potential of an electrode, it is necessary to compare this to a reference electrode (the standard hydrogen electrode, SHE). The hydrogen potential has been taken as a standard potential for convenient reference points for measuring and comparing the relative affinities of chemical substances for electrons under specified conditions. Therefore, the potential of hydrogen is taken to be zero at all temperatures. However, this study will consider the Ag/AgCl electrode as the reference electrode and platinum as the auxiliary electrode to measure and compare the potential of the working electrode (carbon steel) in a solution of 3.5% wt NaCl and HAc.

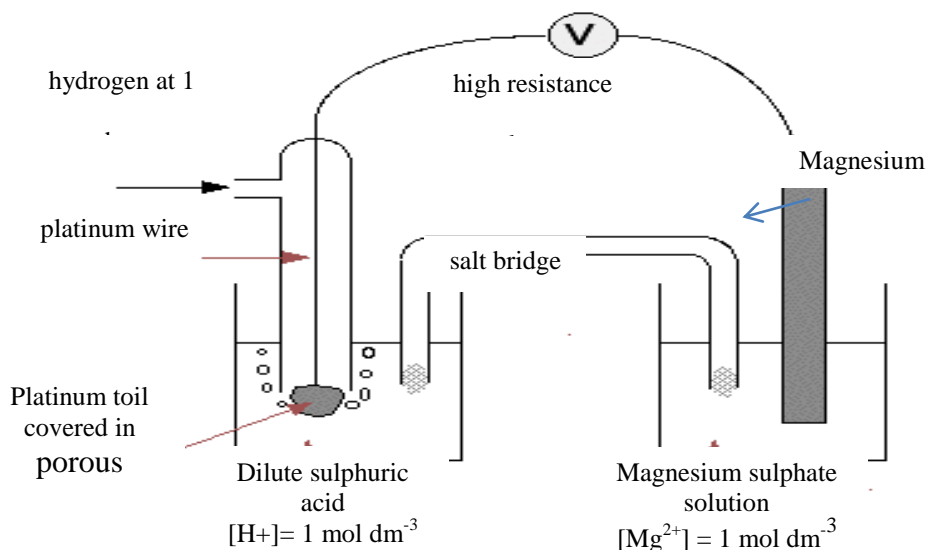


Figure 2-3: Standard hydrogen electrode, SHE.

The standard hydrogen electrode consists of a platinum electrode in a solution containing H^+ ions as shown in Figure 2-3. The solution (H_2SO_4) has a concentration of $1 \text{ mol} \cdot \text{dm}^{-3}$. As the hydrogen gas bubbles over the platinum electrode, the reaction becomes:



2.3.2 The electrode potential at equilibrium

The electrochemical cell provides information on the equilibrium electrode potential, ϵ_{eq} . At each metal-electrolyte interface, there is a tendency of metal ions from the solution to deposit on the metal electrode to make it positively charged. Alternatively, metal atoms of the electrode have a tendency to migrate into the solution as ions and leave behind the electrons at the electrode trying to make it negatively charged. Eventually, a point is reached when equilibrium is established where the rate of positively charge builds up is

equal to the negative charge. At this point, a potential difference develops between the electrode and the solution.

2.3.3 The electrode potential during corrosion

In measuring corrosion kinetics, $\varepsilon - \varepsilon_{eq}$ is the difference between the electrode potential for the metal and a solution where the rates of forward and backward reactions are not the same and the potential at equilibrium. In order to measure the electrode potential ε , an alternative experimental set up in Figure 2-4 is required which includes the voltmeter. In Figure 2-4, the voltmeter measures the electrode potential, ε while corrosion is taking place in the test metal M. A current I is applied that measured by the ammeter represents the corrosion rate which is a function of current and the concentration M^{2+} .

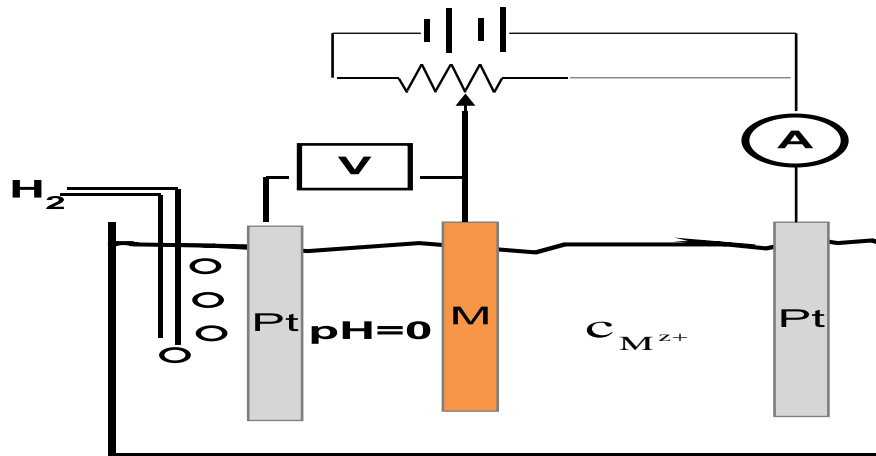


Figure 2-4: Electrochemical cell for electrode potential measurements for a non- equilibrium half-cell

2.3.4 The electrical double layer (EDL)

When a solid emerges in a polar solvent or an electrolyte solution, a redistribution of charges at the metal-electrolyte interface will develop as shown in Figure 2-5. It is well noticed that this interface will alter the solutions as the interactions between the electrode and the solution is quite different to those in the solution. In addition, there is an influence of the charge transfer for the electrode under potentiostatic measurements. These however lead to strong interactions occurring between the ions/molecules in electrolyte and the electrode surface. This region is known as the electrical double layer. The EDL is referred to as a special region of an electrode-electrolyte surface that contains a negative charge of electron and positive charge ions separated the electrolyte in a metal electrochemical reaction [17]. Different models have been developed to explain the process observed when electrochemical measurements are performed in electrolyte solutions.

The Barlow and Erdey-Gruz [18, 19] models are used to explain the interfacial structure of the electrical double layer known as the Helmholtz layer behaving like a charged capacitor as shown in Figure 2-5. The Figure 2-5 shows that some negatively charge ions are absorbed on the metal-electrode surface and polar water covers the rest of the surface, forming a protective layer. The following can also be deduced from Figure 2-5.

- The Inner Helmholtz Plane (IHP) is an ionic layer that consists of adsorbed dipole H_2O molecules. The majority of the anions do not penetrate this layer but some does. The inner potential on the boundary of this ionic plane is ϕ_1 .
- The Outer Helmholtz Plane (OHP) consists of a plane of adsorbed ions due to electrostatic forces in contact with a diffuse ionic layer at an inner potential ϕ_2
- The diffuse layer (DL) is a thick layer located in a region of diffusely ions in contact with the OHP and the bulk of solution at a potential range of $\phi_1 < \phi_{\text{diffuse}} < \phi_3$. Hence, the diffuse layer/bulk boundary is at $\phi_3 = \phi_b$

In view of this, the present study will relate the principle of electrical double layer to explain the behaviour that will be encountered when linear polarization resistance, LPR, electrochemical impedance spectroscopy, EIS and potentiodynamic scan, PDP measurements are performed on carbon steel electrode in 3.5% wt. NaCl solution containing different concentrations of acetic acid and mono-ethylene glycol.

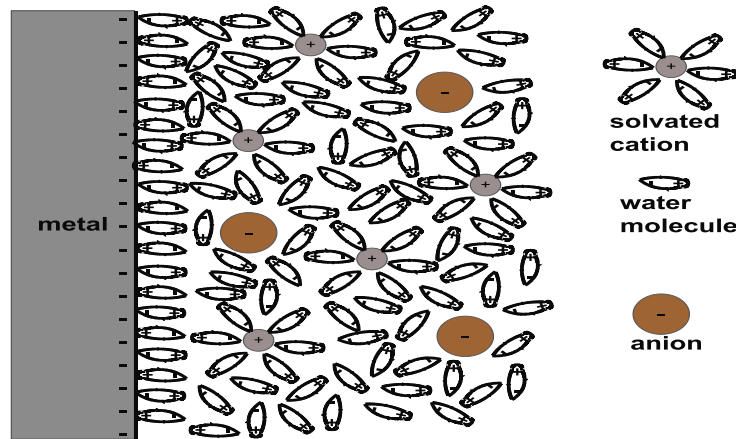


Figure 2-5: Electrical double layer at a metal-solution interface [17].

2.3.5 The relationship between EDL chemistry, voltage and current

However, unlike a chemical reaction which depends on the temperature (Arrhenius equation), an electrochemical reaction depends directly on the applied potential at the electrodes. The Butler-volmer equation is used to express the relationship between applied potential to the current as follows:

At the electrode surface, the redox reaction occurs as:



The reaction rate of the forward direction K_f and backward direction K_b depends on the applied potential E at the electrode:

$$K_f = K_0 \exp \left[-\frac{\alpha n F}{RT} (E - E_0) \right] \quad 2-9$$

$$K_b = K_0 \exp \left[\frac{(1 - \alpha) n F}{RT} (E - E_0) \right] \quad 2-10$$

In equation 2-9 and equation 2-10, K_f is the forward reaction (metal deposition, cathodic), K_b is the backward reaction (metal dissolution, anodic), E_0 is the standard potential of the redox reaction, E is the applied potential, R is the gas constant, F is the Faraday constant, T is the temperature, n is the number of electrons transferred (valency), K_0 is the standard rate constant and α is the transfer coefficient.

Combining equation 2-9 and equation 2-10 together gives:

$$i = nFA(K_f[O_x] - K_b[Red]) \quad 2-11$$

Where, A is the surface area of the electrode, $[O_x]$ and $[Red]$ are the concentrations of the oxidation and reduction.

2.4 Classification of corrosion

Corrosion occurs in different forms depending upon the metal involved, its size, shape as well as the nature and precise environmental conditions prevailing [20]. Each type of corrosion has a specific arrangement of anodes and cathodes and specific patterns and locations depending on the type can exist [20]. The most common corrosion types in CO_2 environment are classified in Table 2-1. In this study, different types of corrosion that will be encounter as a result of carbon steel samples immersed in a solutions containing 3.5% wt NaCl salt in the presence of HAc and MEG at different temperatures in order to

determine which types of corrosion and mechanism have taken place in the studied environment.

2.4.1 Uniform (general) corrosion

General or Uniform corrosion is regarded as a type of corrosion attack or the dissolution of the corroding surface that is more or less evenly distributed over the entire surface area of a metal. The attack occurs on materials that normally form un-protective film on the surface when corrosion occurs, and it allowed for corrosion to continue on the surface of the material uniformly. General corrosion is the most widely researched form of corrosion in the literature. General corrosion is much less severe in stainless steel than in other metals. In stainless steel, it only occurs when the stainless steel is at a pH value which is either very low (acid environments) or very high (alkaline environments) at high temperature [21].

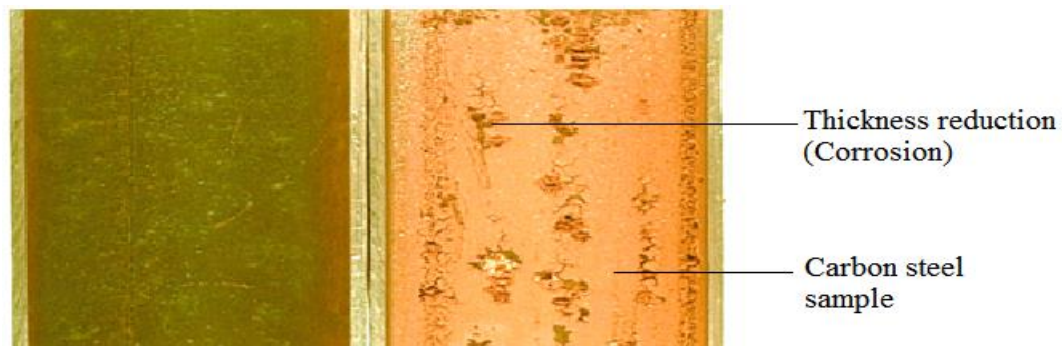


Figure 2-6: General corrosion on carbon steel [21]

Table 2-1: ASM classification of corrosion types [20].

General Corrosion	Localized Corrosion	Metallurgically Influenced Corrosion	Mechanically Assisted Degradation	Environmentally Induced Cracking
Corrosion attack dominated by uniform thinning <ul style="list-style-type: none"> • Atmospheric corrosion • Galvanic corrosion • Stray-current corrosion • General biological corrosion • Molten salt corrosion • Corrosion in liquid metals • High-temperature corrosion 	High rates of metal penetration at specific sites <ul style="list-style-type: none"> • Crevice corrosion • Filiform corrosion • Pitting corrosion • Localized biological corrosion 	Affected by alloy chemistry and heat treatment <ul style="list-style-type: none"> • Intergranular corrosion • Dealloying corrosion 	Corrosion with a mechanical component <ul style="list-style-type: none"> • Erosion corrosion • Fretting corrosion • Cavitation and water drop impingement • Corrosion fatigue 	Cracking produced by corrosion, in the presence of stress. <ul style="list-style-type: none"> • Stress-Corrosion Cracking (SCC) • Hydrogen Damage • Liquid metal embrittlement • Solid metal induced embrittlement.

2.4.2 Crevice corrosion

Crevice corrosion refers to a localized form of attack on a metal surface which is initiated by the extremely low availability of oxygen in a crevice. Crevice corrosion is likely to be a problem in stagnant solutions where a build-up of chlorides can occur. However, the severity of crevice corrosion is very dependent on the geometry of the crevice, the narrower and deeper the crevice, the more severe the corrosion. Crevice corrosion is initiated by differences in concentration of ions or dissolved gases in an electrolytic solution. Figure 2-7 shows typical example of crevice corrosion attack. As can be seen in Figure 2-7, a solution became trapped between a pipe and the flange on the left. However, the stagnant liquid in the crevice eventually had a lower dissolved oxygen concentration and crevice corrosion took over and destroyed the flange. In the absence of oxygen, the metal or its passive layer begin to oxidize.

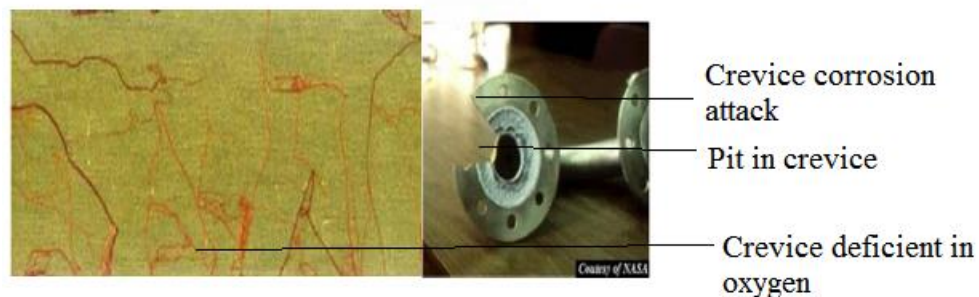


Figure 2-7: Crevice corrosion in titanium -6 aluminium -4 vanadium [21]

2.4.3 Pitting corrosion

Pitting corrosion is a localized phenomenon confined to small areas [22]. It occurs normally at very low velocities and in dew-point temperatures in gas-producing wells. The driving power in pitting corrosion is the lack of oxygen around a small area. This area becomes anodic while the area with excess of oxygen becomes cathodic. Schmitt et al [23] suggested that for a passive metal to be susceptible to pitting corrosion, two conditions have to be fulfilled: Presence of aggressive anions (element: Cl, F, Br, and I) inducing a local attack (dissolution) of the passive film, and the equilibrium potential of

the material must be higher than the pitting potential. Formation of micro-pits can be very damaging. Pitting factor (ratio of deepest pit to average penetration) can be used to evaluate the severity of pitting corrosion that is usually observed in metals and alloys [20]. Pitting tendency can be predicted through measurement of pitting potentials. The pitting susceptibility increases with temperature and CO_2 partial pressure.

Schmitt et al [23] studied the effects of temperature, Cl^- concentration, nature of anions and cations, as well as corrosion inhibitors on the pit initiation during the first stages of CO_2 corrosion of pure iron low-alloy steels at 5 bar CO_2 . They confirmed that almost all alloys might undergo pitting corrosion in CO_2 environments. They also showed that addition of leads inhibited localized corrosion through deposition at local anodes.

Pits are often initiated because of inhomogeneity of the metal surface, deposits or scale on the surface, or breaks in a protective film [24].

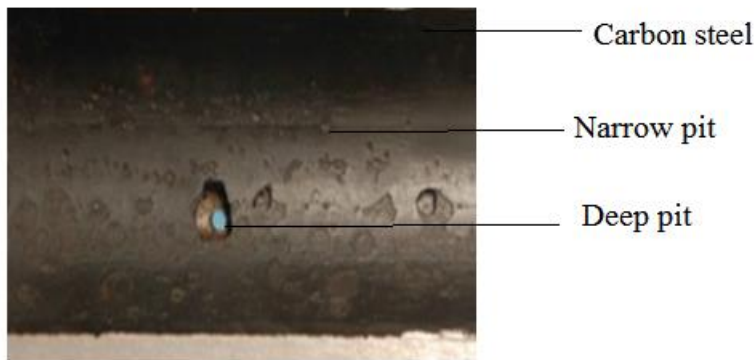


Figure 2-8: Schematic diagram of pitting corrosion mechanism for X-65 carbon steel immersed in 3.5% NaCl solution [24]

2.4.4 Mesa corrosion

Mesa corrosion is a stochastic pitting process. It is similar to normal pitting but the mechanism is observed at high flow rate where the steel surface is partly covered with a protective iron carbonate film. The attack is characterized by the formation of severely corroded regions separated with sharp steps from neighboring areas with much less

attack. Videm et al [25] showed that localized attack can be initiated and propagated under semi-stagnant conditions. The mechanism is based on film in a fine balance between film growth and film dissolution or mechanical film removal. Figure 2-9 shows an example of mesa corrosion attack and the mechanism of mesa attack under high flow rate. It is caused by the dissolution of iron under the corrosion film. In Figure 2-9 at a certain point, the film breaks and is removed by the high flow rate. However, the dissolution and removing of more film is a continuous process where more iron dissolves and film breaks off. Crolet [26] stated that mesa corrosion attack appeared to be only slightly sensitive to the velocity of water in pipe, but extremely dependent on fluid composition. Videm and co-workers [25] also showed that flow-induced mesa attack could occur in water saturated with FeCO_3 under turbulent flow conditions where film formation is prevented locally.



Figure 2-9: Mesa corrosion attack on carbon steel [25]

2.4.5 Erosion-corrosion

Erosion-corrosion is the deterioration of metals and alloys as a result of relative movement between surfaces and corrosion fluids. In erosion-corrosion, abrasion normally takes place depending on the rate of moving fluids. Erosion-corrosion due to

high velocity impingement occurs in steam condenser tubes, slide valves in petroleum refinery at high temperature, inlet pipes, cyclones and steam turbine blades.

Erosion-corrosion normally occurs under turbulent flow conditions. The flowing fluid may be single phase flow or multiphase flows with various combinations of gas, water, oil and sand that can cause severe erosion-corrosion of oil production systems [27]. The most severe erosion-corrosion problems occur under conditions of disturbed turbulent at sudden changes in the flow system geometry, such as bends, valves, fittings, and in pumps, compressors [28]. Surface defects in the form of small protrusions or depressions such as corrosion pits, deposits, and weld bends can give rise to disturbed flow on a smaller scale, but sufficient to initiate erosion-corrosion [27]. Erosion-corrosion occurs in many oil and gas industries, and can be a costly problem. Postlethwaite et al.[28] reported that the presence of solid particles in coal slurry transportation can increase the corrosion rate of steel pipelines greatly. Furthermore, Vankatesh [29] have shown that severe erosion and erosion-corrosion damage has damaged production from potentially high-capacity wells in the oil and gas industry

Cavitation damage in ship's propeller, pump impellers and hydraulic turbines are all special form of erosion corrosion. Cavitation is caused by formation and collapse of vapour bubbles in liquids closer to a metal surface. In this study, the bubble (3-electrode) cell technique will be utilized to examine erosion-corrosion of carbon steel in CO₂ saturated solutions containing different concentrations of HAc, MEG and inhibitors with little or no sand entrained in the solution. This will enable us characterize the corrosion rate and corrosion products formed on the carbon steel surfaces.

2.4.6 Flow Induced Corrosion

Flow-induced localized corrosion is a form of mesa attack at high flow rates by eating away the corrosion scales due to liquid vortices. In this type of damage, the corrosion started from the pits, or sites of mesa attack above critical intensities, and then propagates

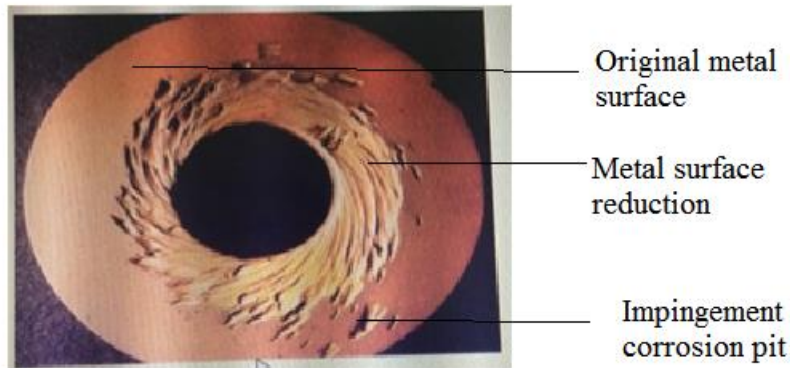


Figure 2-10: Example of erosion corrosion in steel feed water pump spacer [30]

by local turbulences created by the pits. The local turbulence combined with the stresses produced during scale growth may destroy existing scales [30]. Once the scale is damaged or destroyed, the flow conditions may stop the reformation of protective scale on the exposed metal. Figure 2-11 shows a typical example of flow induced localized corrosion in CO₂ environment. The influence of fluid flow on the corrosion of carbon steel in an environment containing CO₂, HAc and corrosion inhibitors will be considered in this work. This will enable us understand the mechanisms and processes that leads to localized corrosion in the presence of HAc.

2.4.7 Microbiologically-induced corrosion

Microbiologically-Induced corrosion refers to the deterioration of metals as a result of the metabolic activity of microorganisms. Different bacteria are known to cause microbiologically influenced corrosion of carbon steels, stainless steels, aluminium alloys and copper alloys in water and soils with pH 4-9 and temperature range of 10°C ~ 50°C. Microbiologically induced corrosion is caused by specific bacteria which feed on nutrients and other elements found in waters and soils. However, the primary source of sulphate reducing bacteria is sea water

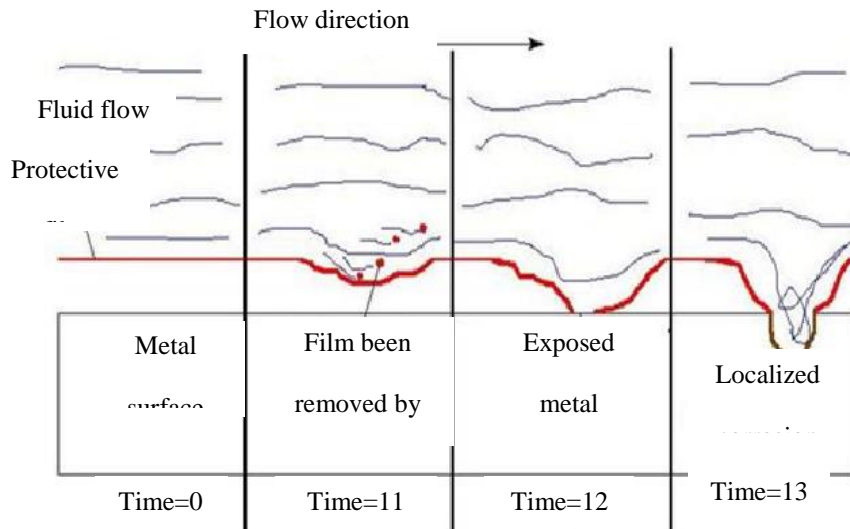


Figure 2-11: Flow induced localized corrosion in CO₂ environment

The bacteria (sulphate reducing bacteria) requires oxygen to become active (aerobic) and is responsible for most instances of accelerated corrosion damages to offshore steel structures. In this study, the effect of micro-organisms such as the biofilms on the corrosion of carbon steel will be study at different temperatures in CO₂ environment



Figure 2-12: Microbiologically induced corrosion in a carbon steel weld

2.5 Expressions and measurement of corrosion rate

Basically, there are three methods that are employed to express the corrosion rate of carbon steel in CO₂ environment as follows:

- Thickness reduction of the material per unit time
- Weight loss per unit area and unit time
- Corrosion current density, i_{Corr} .

2.5.1 Weight loss method

The assessment of corrosion rate is usually carried out using different corrosion techniques such as the gravimetric-based mass loss, quartz crystal microbalance-based mass loss can also be used to determine the corrosion rate of a metal. However, this study will look at some of the techniques that are common and relevant to this work and the corrosion industry such as the direct (weight loss/gain) measurement and the electrochemical (potential–time, polarization resistance, and the AC impedance) measurements.

2.5.2 The potential-time measurement

The potential– time measurement is one of the simplest methods used in assessing corrosion and corrosion rate. If a coupon is immersed in an electrolyte, a potential difference is established on the metal–electrolyte surface. This potential occurs without the application of any current on the metal. However with time, the potential will vary and comes to a constant value known as the open circuit potential (OCP).

The potential-time measurement is very easy and quick to determine. It gives an idea of the thermodynamic stability of a metal in its environment, and also determines the domain the metal lies in the pourbaix diagram [31]

The effect of electrolyte condition and changes can be easily understood with the potential-time measurement technique. For instance, the presence of acetic acid (HAc) can cause the potential to move to a more positive value with time indicating that the HAc protects the anode by reducing the anodic reaction. If the potential does not move to a positive direction or increases, it means that the corrosion reaction is cathodically control. If the potential value moves slightly to the positive direction, then it means that the reaction is controlled both by the cathodic and anodic reactions [32]

2.6 Factors influencing CO₂ corrosion

Carbon steel is regarded as one of the best pipeline materials for the oil and gas production from different reservoirs. Besides, the pipeline materials are usually corroded as results of environmental factors affecting the pipeline systems. Figure 2-13 illustrates the factors that influence CO₂ corrosion of carbon steel. In this investigation, the impact of some environmental parameters such as temperature, HAc concentration, pH and CO₂ partial pressure on the corrosion rate of carbon steel in saturated CO₂ environment, and under the influence of HAc, MEG and corrosion inhibitors will be analyze. This will lead us understand the particular types of corrosion taking place under such conditions.

2.6.1 Effect of iron concentration

The concentration of Fe²⁺ ions has a direct effect on the rate of corrosion, as it is part of the anode reaction. When Fe²⁺ concentration is reduced, the reaction equilibrium is shifted to the product side and the rate of corrosion increases.



The formation of FeCO₃ occurs in conditions where the concentration of Fe²⁺ ions in the aqueous phase exceeds the solubility range of FeCO₃. The increase of c_{Fe²⁺} results in

higher supersaturations, which accelerates the precipitation rate. At higher concentrations, more protective films formed. They are released continually so that different concentrations of ferrous ions also correspond to different concentrations of bicarbonate, which will lead to local changes in pH [26]. A ferrous ion concentration well below the solubility limit of FeCO_3 will not only prevent the formation of FeCO_3 containing films, but also dissolve the existing films [33]. This is represented in [box -2] in Figure 2-13

2.6.2 Effect of pH

The pH is the most important factor in FeCO_3 scale formation and it influences the solubility of FeCO_3 [34]. The pH influences the electrochemical reactions that lead to iron dissolution, and the precipitation of protective films on the pipe wall [35]. At favorable conditions, increasing pH decreases the FeCO_3 solubility and promotes its precipitation in the environment, resulting in lower corrosion rates.

Videm and Dugstad [33] reported that a good protection could be obtained at pH of 6.0 by FeCO_3 films even at room temperature. They also demonstrated that an increase in pH also made film formation more likely as a result of a reduction in the solubility of Fe^{2+} as represented in [box 3] in Figure 2-13.

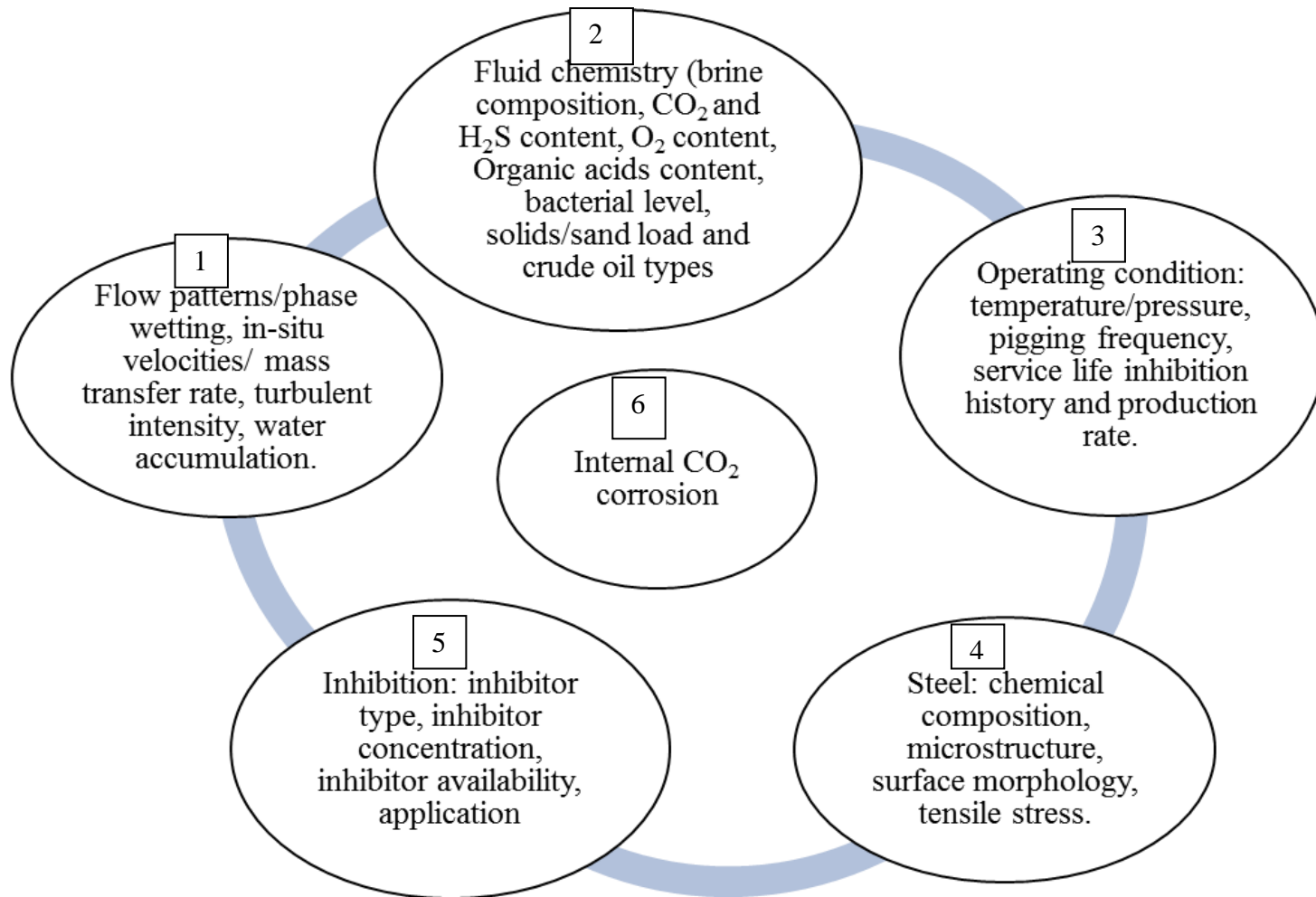


Figure 2-13: Factors influencing CO₂ corrosion of carbon steel

2.6.3 Effect of CO₂ partial pressure

In a CO₂ corrosion environment, an increase in CO₂ partial pressure typically leads to an increase in the corrosion rates. With increase in partial pressure, the concentration of H₂CO₃ increases and accelerates the cathodic reaction, and ultimately the corrosion rate. At higher pH, high CO₂ partial pressure leads to an increase in bicarbonate and carbonate ion concentration and higher supersaturation. This accelerates precipitation and scale formation. This is represented in [box -3] in Figure 2-13

2.6.4 Effect of operating temperature

Temperature affects the rate of corrosion indirectly through the formation of a protective film. It is known that increased temperature aids the formation of iron carbonate film by accelerating the kinetics of precipitation. The effect of temperature on corrosion rate is thought to be primarily due to its effect on CO₂ solubility. The solubility of FeCO₃ decreases as the temperature increases, creating a supersaturated environment. Using the Arrhenius principle, the relationship between the temperature and corrosion rate can be expressed as:

$$\frac{CR_1}{CR_2} = \exp \left[\frac{1}{T_1} - \frac{1}{T_2} \right] \quad 2-13$$

Where,

CR₁ and CR₂ are corrosion rates at temperature T₁ and T₂ respectively

T₁ and T₂ are absolute temperature in °K.

When the temperature is less than 60°C, the solubility of FeCO₃ is high and no protective film is formed unless the pH is raised, corrosion rate increases. Between 60°C and 80°C, the solubility of FeCO₃ decreases with temperature and the protective film starts to form hence corrosion rate decreases. At 80°C, a very protective film formed which reduces the corrosion rates [11]. This is shown in [box -3] in Figure 2-13

2.6.5 Effect of velocity

The hydrodynamics of flow affects corrosion in two different ways – the destruction of protective films, and the reduction of ion concentration near the pipe wall. Higher velocity is associated with higher turbulence and more effective mixing in the solution. It is suggested that the corrosion rate is diffusion controlled at low flow velocities and charge transfer controlled at high velocities. The diffusion rate increases with flow rate while charge transfer reaction is independent of flow [36].

In prior to film formation, high velocity leads to increased corrosion rate as the transport of cathodic species towards the steel surface is enhanced by turbulent transport. Also, the transport of Fe^{2+} ions away from the steel surface is also increased leading to a lower concentration of Fe^{2+} ions at the steel surface. The flow regime of the fluid is very important as it affects the formation of protective films. For laminar flow, films formation can occur. When the flow regime is turbulent, the protective film is removed and any further formation of a protective layer is prevented as shown in [box -1] in Figure 2-13

2.7 Assessment of CO₂ corrosion prediction models

Corrosion of pipelines in multiphase flow is one of the complex problems facing the oil and gas industries. Several researchers have significantly contributed to development of CO₂ corrosion models. The models to be considered are:

2.7.1 Mechanistic model

Mechanistic models provide mathematical formulations of the chemical and electrochemical phenomena of the corrosion using mass, energy and charge balances. In an aqueous CO₂ system, the processes commonly modelled by mechanistic approach include the electrochemical reactions at the surface along with the transport processes of species in the system.



This involves iron (Fe^{2+}) dissolution, hydrogen ion (H^+) reduction, carbon dioxide (CO_2) dissolution, and carbonic acid (H_2CO_3) formation and reduction. The three main cathodic reactions that take place are:

2.7.2 Semi-empirical model

The semi-empirical models are presented to resemble some of the physical principle of real system. The unknown parameters in the model are fitted in order to reproduce measured experimental corrosion data. The model is simple and can be evaluated easily. De Waard and Milliams [37] developed a semi – empirical model from their corrosion experiments using the weight loss coupons and linear polarization experiments. The model is based on the assumption of direct reduction of H_2CO_3 , and compared with correlation for the corrosion rate as a function of the partial pressure of CO_2 and temperature in glass cell laboratory data shown below:

$$\log V_{\text{corr}} = 7.96 - \frac{2320}{T + 273} - 5.55 \times 10^{-3}T + 0.67 \log p\text{CO}_2 \quad 2-17$$

Where V_{Corr} is the corrosion rate (mm/yr), T is the temperature ($^{\circ}\text{C}$) and $p\text{CO}_2$ is the CO_2 partial pressure (bar).

The constant 0.67 was obtained by assuming that the pH is a function of $p\text{CO}_2$ only. The temperature functions in Error! Reference source not found. was obtained by assuming arrhenius-type dependence for a charge transfer controlled process. They also assumed that the anodic process of iron dissolution proceeds via a pH-dependent mechanism. The

scope of de Waard and Milliams [37] model was revised on several occasions to extend its validity into areas where protective scales form and to account for high pH in brines, velocity, water. Despite all the theoretical shortcomings, the model of de Waard and Milliams stood as one of the important reference points for CO₂ corrosion research over the past two decades, and in its most recently revised form [38], is still used as an informal industrial standard. Figure 2-14 shows the Nomogram of CO₂ corrosion predicting model by de waard [37]

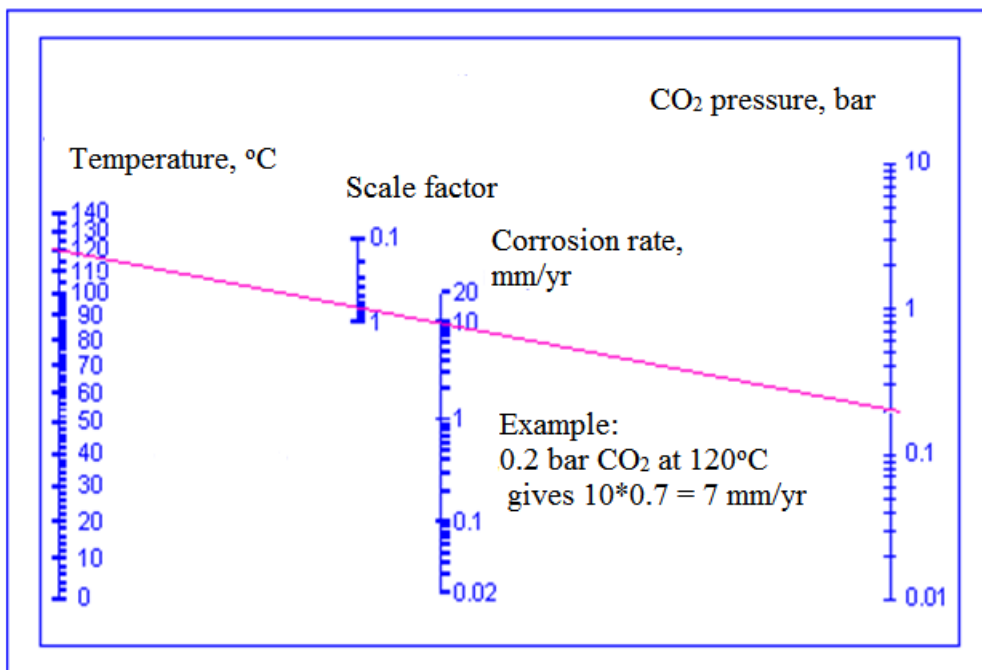


Figure 2-14: Nomogram for predicting CO₂ corrosion rate of carbon steel

2.7.3 Empirical model

Empirical models are correlation of measured corrosion rate in mm/yr to a number of input variables. Example of the empirical models was presented by Halvorsen [39]:

$$CR = K_T f_{CO_2}^{0.6} \left(\frac{S}{19} \right)^{0.15+0.03 \log \rho_{CO_2}} \quad 2-18$$

Where

CR = Corrosion rate, mm/yr;

K_T = Constant;

ρ_{CO_2} = Partial pressure of CO_2 , bar

S = Wall shear stress, pS

f = factor depending on CO_2

2.7.4 Norsok CO_2 corrosion model

The NORSOK M- 506 model is a pure empirical model based on laboratory data from single phase flow loops. It is an empirical corrosion rate model for carbon steel in water containing CO_2 at different temperatures, pH, CO_2 partial pressure, and wall shear stresses. According to Norsok [40] CO_2 corrosion within temperature range of 20°C to 120°C can be calculated using the empirical equation as:

$$CR = K_t \times f_{CO_2}^{0.62} \times \left(\frac{S}{19} \right)^{0.146+0.0324 \log f_{CO_2}} \times f(pH) \quad 2-19$$

Where

K_t is a temperature-related constant, given in Table 2-2 for a temperature range of 5°C to 150°C.

f (pH) is a factor depending on the pH of the solution.

This model primarily is meant as a guidance tool for material selection and for determination of the required corrosion allowance. The model is mainly made for pipelines systems where pure CO₂ corrosion is the dominating corrosion reaction.

Table 2-2: Constant values of K_t at different temperatures

Temperature (°C)	K_t
5	0.42
15	1.59
20	4.76
40	8.92
60	10.69
80	9.94
90	6.25
120	7.77
150	5.20

2.8 Acetic acid corrosion of carbon steel in CO₂ environment

Internal corrosion of pipelines constitutes a significant problem to the petroleum industry [1]. CO₂ corrosion in the presence of HAc is known as a major reason for premature failures in oil and gas pipelines which are usually made of carbon steel [3, 41]. Crolet et al [42] reported that the presence of acetic acid in a saturated aqueous solution with CO₂ increases the corrosion rate from 1.3 to 5.7 mm/yr in the North Sea.

Water and acidic gases such as carbon dioxide (CO₂), hydrogen sulphide (H₂S) and organic acids co-produced with the hydrocarbon constitute the corrosive environment. Carbon steel is presently the only economically feasible material for such pipelines, and the corrosion rates may reach about 10 mm/yr or more in the absence of mitigation measure like injection of corrosion inhibitors [43]

Table 2-3:Short chain organic acid found in formation water

Acid	Concentrations (mmol/l)	Concentrations (Mg/l)
Acetic acid	10.1	609
Propanoic acid	1.5	113
Formic acid	0.3	14
1-butanoic acid	0.3	27
Maloic acid	0.2	21
Oxalic acid	0.1	9

Table 2-4: Proposed empirical thresholds for acetic acid in gas wells [44]

Free HAc (meq/L)	Dominating acid	Corrosion process governed by
<0.1	CO ₂ becomes the dominant acid	CO ₂ corrosion
0.1 - 1	Mixed dominance of both acids	Mixed corrosion
>1	Essentially HAc	HAc corrosion. Independent of CO ₂

The presence of acetic acids (HAc) in oil and gas wells has been known since 1944 and its presence is frequent in oilfields when CO₂ is observed [3, 45]. Acetic acid is the most common organic acid in multiphase systems containing brine as shown in Table 2-3. The effect of acetic acid (HAc) on the corrosion rate of carbon steel in most of the oil and gas fields containing brine and CO₂ has been studied. It has been shown that acetic acids served as a corrosive agent in CO₂ corrosion. Nafday et al. [11] and Garsany et al.[41] have demonstrated that the presence of acetic acids decreases the protectiveness of iron carbonate films and this occur as a result of reduction in pH and a scale undermining effect.

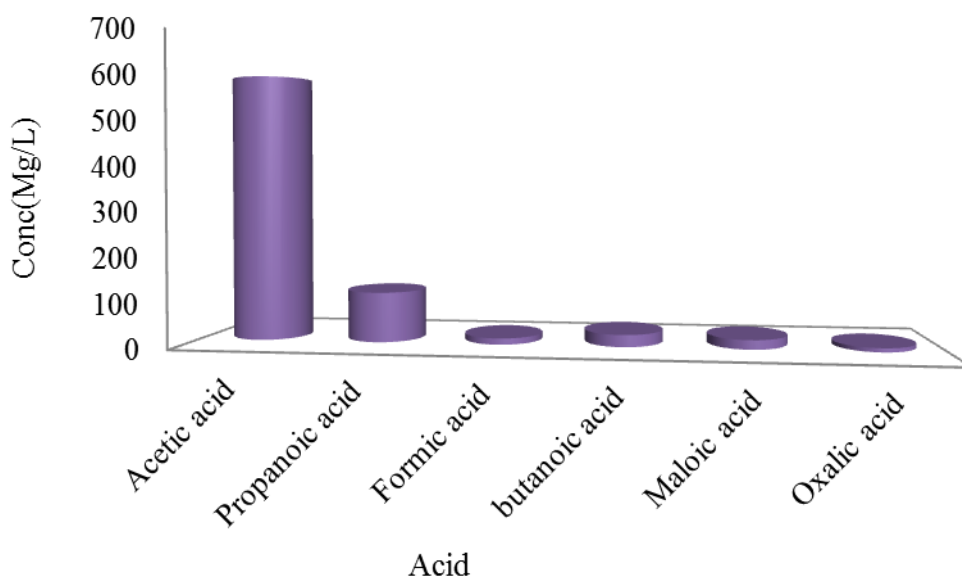


Figure 2-15: Concentration of organic acid found in formation water

The carbon steel corrosion in the presence of HAc is known as a major cause for premature failures in oil and gas pipelines that usually made of carbon steel [46].

In oilfield pipelines with low $p\text{CO}_2$, the corrosion issues are easily managed, but when small amounts of acetic acids are present, the corrosivity of the brine can change dramatically [26]. It has been shown that [9] the total quantity of organic acids in produced water in oil and gas system varies between 500-3000 ppm of which HAc contributes about 50-90% of organic acids. Similarly, a systematic investigation of field data showed that undissociated HAc concentration higher than 0.1-1 mM was a critical factor for CO_2 corrosion [26]

Many studies [1, 11, 46] have found that acetic acid main role is that of a corrosion promoter and also as a corrosion inhibitor. They concludes that the acetic acids may behave as corrosion inhibitors when the acids are absorbed on the metallic surface acting as a barrier between the metal and the environment

Table 2-5: Formation water analysis

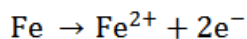
Component	Symbol	Concentration (mg/l)
Sodium	Na ⁺	2337
Potassium	K ⁺	90
Calcium	Ca ²⁺	75
Magnesium	Mg ²⁺	13
Barium	Ba ²⁺	12
Strontium	St ²⁺	2
Iron	Fe ²⁺	0
Chloride	Cl ⁻	3075
Sulphate	SO ₄ ²⁻	7
Alkalinity	HCO ₃ ⁻	1348
Bromide	Br ⁻	0
Organic acids (acetic acid)	C ₁ – C ₄	773

Similarly, it behaves as corrosion promoters by a reduction in pH and a scale undermining effect leading to localized corrosion. Garsany et al. [41] proposed that the role of acetic acid is to act as a reactant in the cathodic process which could have a significantly higher rate than the reduction of protons or carbonic acid in oilfield conditions. The three main cathodic reactions are [41]:



The reaction mechanism and kinetics of iron dissolution reaction with the overall reaction of equation 2-22 are affected by acetic acid, CO₂ partial pressure and pH [26].

Also, it is well established that HAc may retard the anodic reaction. This was particularly observed at room temperature where it led to a slight reduction in general corrosion rate, but increased the tendency of localized attack.



2-23

Crolet et al. [26] suggested that acetic acid species actually act as a weak inhibitor for anodic dissolution reaction of steel, and this is not due to any influence of acetic acid either on cathodic reduction of H^{+} or on anodic dissolution of iron, but rather to its effect on the protectiveness of the corrosion product layer. Dugstad [47] and Gunaltun et al. [9] reported results from field observations and laboratory investigations that the presence of HAc may induce a detrimental effect on the overall corrosion rate and the pitting morphology in sweet systems. Field experience has also shown that HAc is a key factor in the localized top-of-line corrosion attacks in gas-condensate pipelines. Similarly, the presence of HAc also tends to solubilize the dissolving iron ions and suppress FeCO_3 or oxide film formation, which can passivate the steel surface [33]. Pots and Hendriksen [48] stated that HAc along with other organic acids could hinder the protective corrosion product scales formed on top-of-the-line corrosion

Furthermore, Crolet et al. [26] determine the effect of acetic acid on the cathodic and anodic charge transfer mechanisms in the presence of CO_2 . They first studied the effect of acetic acid on potential sweeps at different pH levels and CO_2 partial pressures. It was found that the presence of acetic acid does not affect the cathodic limiting current density, but shows an inhibiting effect on the anodic charge transfer mechanism. Though, the acetate ions have a limited effect on the pH because of the buffering action, they can play a significant role in the hydrogen evolution reaction which is a rate-controlling step in the corrosion reaction.

Hedges and McVeigh [49] tested the effect of HAc on CO₂ corrosion at 60°C, 0.8 bar CO₂ partial pressure, 3% NaCl and synthetic formation water. It was found that the corrosion rates increased with increasing HAc concentration, and further increased again when more HAc was added to the cell. Nafday and Nesic [11] studied the effect of HAc on FeCO₃ corrosion product film protectiveness at 80°C in 3% wt NaCl and CO₂ partial pressure of 0.5 bars. The tests were carried out at relative FeCO₃ supersaturations of 32 and 162. It was found that no significant effect of HAc on FeCO₃ layer protectiveness or morphology was found in any of the tests. Ueda and Takabe [50] later investigated the effect of 0.5% (5000ppm) HAc on carbon and chromium bearing steels at 60-300°C using autoclave tests at 30 bar CO₂ partial pressure, and 5% NaCl. They found that the corrosion rate was considerably higher with HAc than with only CO₂. It was also observed that the corrosion rate is lower at 60°C where HAc related to the anodic inhibition. Liu et al [51] studied the effect of HAc using electrochemical impedance spectroscopy (EIS). They found that the surface chemical reactions of cathodic reduction were enhanced in the presence of HAc. Furthermore, they found that HAc can remove FeCO₃ layer. Zhang and Cheng [52] reported similar results and observed an increase in the current density of anodic reactions and localized corrosion on the surface of steel.

Dugstad et al [53] tested the effect of 12 ppm undissociated HAc under film forming conditions at 80°C using flow loop at CO₂ partial pressure of 2 bar, pH of 5.8, 0.1 % NaCl and supersaturation of 6-30ppm of Fe²⁺. It was found that though, the corrosion attack varied considerably between the different steels tested, the HAc caused more mesa attack on the steel surfaces. The corrosion films were more fragmented, with more pores and flaws, and the localized corrosion was more severe at high rates.

Consequently, from the literature review so far, a lot of works have been carried out on corrosion of carbon steel and the effect of acetic acid in diluted environment but lack knowledge and understanding regarding the corrosion of carbon steel when both HAc and MEG exist together in a typical wet gas system. Hence, in this work, the driving

mechanism of CO₂ corrosion and the effect of HAc and MEG on formation of protective films in CO₂ environment and at different temperatures will be discussed.

Table 2-6: Characteristics of corrosion films [1]

Corrosion film class	Temperature formation (°C)	Characteristics/nature	Growth habit and composition
Transparent	Forms at room temperature and below	<1 μm thick, once formed, it is very protective	Forming fast as temperature reduces to < room temperature mainly consisting of Fe and oxygen
Iron carbide	No range	<100 μm thick, metallic, conductive, and nonadherent	Spongy and brittle, consisting of Fe, and C.
Iron carbonate	Minimum required in laboratory conditions is 50°C to 70°C	Adherent, protective, and nonconductive	Cubic morphology, consisting of Fe, C, and O.
Iron carbonate + Iron carbide	Maximum temperature is 150°C	All depends on how FeCO ₃ is blended with Fe ₃ C	Consisting of ferrous carbide and ferrous carbonate

Singer et al. [54] studied top-of-line (TOL) corrosion in presence of HAc and CO₂ at 70°C, 0-1000ppm HAc. It was observed that the corrosion rate in TOL increased gradually with increasing HAc concentration and with increasing condensation rates, and the rates were gradually lower than in the bottom of the line. Furthermore, Mendez et al [55] extended the work of Singer et al. [54] to include the effect of glycol and pH control. It was found that little effect of HAc was seen on the TOL corrosion rate after 2 to 3 days exposure. Oblonsky et al. [56] found out that solid Fe₃O₄ and dissolved Fe²⁺ as the corrosion products in the corrosion of Fe in the solution saturated with argon, and in the presence of acetate ion. They found that acetate concentration had no effect on the chemical analysis of the corrosion product layer. Sun et al. [57] used a rotating cylinder electrode with glass cell bubble tests to investigate the effect of HAc on the part reactions

under N_2 and CO_2 atmospheric pressure and room temperature, HAc concentrations of 0-1000 ppm and 3 wt.-% NaCl. From the results obtained, it was showed that the HAc increased the cathodic current, and that the H_2 evolution from HAc was activation controlled at room temperature.

George et al. [46] basically used Sun [57] to further study the effect of HAc on the corrosion rate in the temperature range of 22-60°C, 0-1000ppm HAc concentration and 3 wt.-% NaCl, and developed an electrochemical/hydrodynamic model for the cathodic reaction taking into account the reduction of H^+ , H_2CO_3 and HAc from the bulk of the solution. It was observed that the cathodic current in presence of HAc was reduced in synthetic brine with high salt contents compared to 3 wt.-% NaCl. The mass loss data showed no significant difference between them.

Okafor and Nestic [58] reported that acetic acid can caused localized corrosion by removing iron carbonate layer. Similarly, George and Nestic [46] reported that the presence of HAc strongly affects the cathodic limiting current. The anodic reaction (iron dissolution) was unaffected or rapidly retarded with increasing HAc concentration at room temperature. Guo et al [51] studied the effect of HAc and Ac^- at 50°C, 1 bar CO_2 , and 100°C, 10 bar CO_2 . The polarization curves result shows an increased cathodic currents, and indication of inhibition of the anodic reaction with increasing HAc concentration of 0-360 ppm. Garber et al. [59] developed computer models to calculate downhole pH in presence of CO_2 and organic acids, and suggested to correlate corrosion and scaling tendency to deviation in pH from $FeCO_3$ saturation pH. Hurlen et al.[60] investigated the effect of acetate buffers on the cathodic reaction on iron (N_2 atmospheres, 25°C). They observed a limiting cathodic current that was dependent on stirring on HAc concentration, and the HAc had no effect in the potential region of activation controlled reaction.

Garsany et al. [41] used voltammetry to study the effect of HAc on the cathodic part reaction on platinum and steel in CO₂ environment at 25°C and 60°C. They observed a limiting cathodic current in HAc solutions, and the magnitude of the limiting current was proportional to the HAc concentrations and square root of the rotating disc rotation rate. This shows that the limitation is caused by the diffusion of HAc.

A lot of research work has been carried out on CO₂ corrosion and the effect of acetic acid in CO₂ corrosion environment. The literature review is a summary of work done so far. From the information gathered, there still lack of knowledge regarding corrosion of carbon steel presence of acetic acid and mono-ethylene glycol (MEG). The effect of some environmental parameters on scale dissolution that leads to pitting and localized corrosion in CO₂ saturated environment is not fully understood.

2.9 Hydrate formation in the oil and gas industry

One of the challenges facing producers today is assuring oil and gas flow through complex and costly long distance pipelines. Potential impediments include formation and deposition of hydrates, paraffin, scale and asphatenes in production facilities and corrosion constituents in the flow stream which may damage equipment and tabular.

Natural gas hydrates are crystalline compounds of water and gas which under pressure exist at temperatures considerably above the freezing point of water. They are formed as a result of physical combination of water and gas molecules. Hydrates formation needs to be avoided because it can cause serious operational and safety problems in pipelines and also can leads to production shut down. In order to prevent hydrate formation and corrosion in pipelines, Monoethylene glycol (MEG) needs to be injected at the inlet of the pipeline as an antifreeze and anticorrosion agent to reduce the water vapour pressure [61, 62].

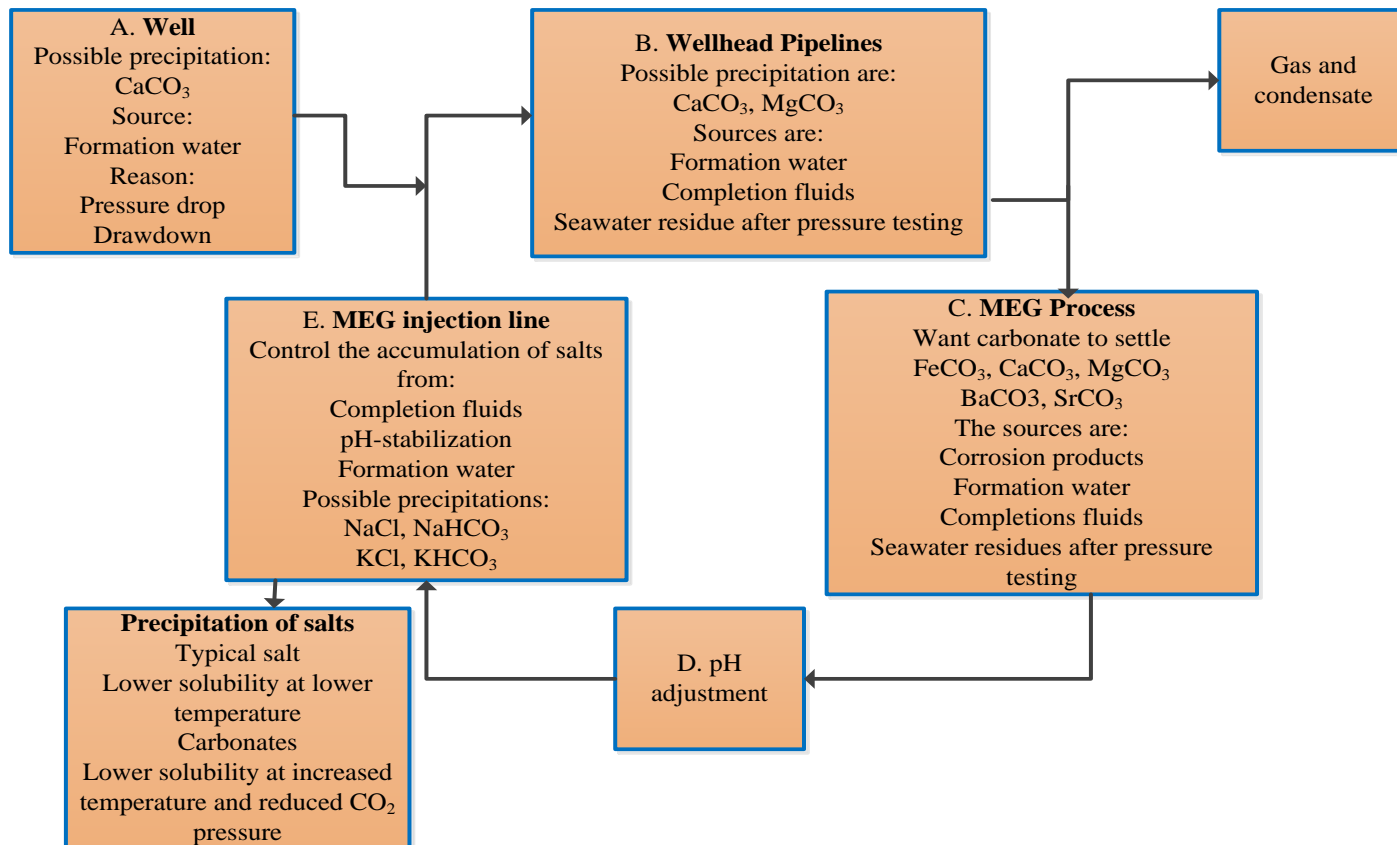


Figure 2-16: An overview of MEG process and challenges with respect to precipitation of salts [62]

However, for this process to be successful, the MEG needs to be avoided continuously from unwanted substances such as acetic acid. The presence of MEG changes the thermodynamics of the aqueous phase and lowers the solubility of most salts. MEG also changes the pH, the gas solubility and the acidity of CO₂. Controlling scale and corrosion in such systems requires good control of pH, salt solubility, gas solubility and the effect of MEG on these parameters [63].

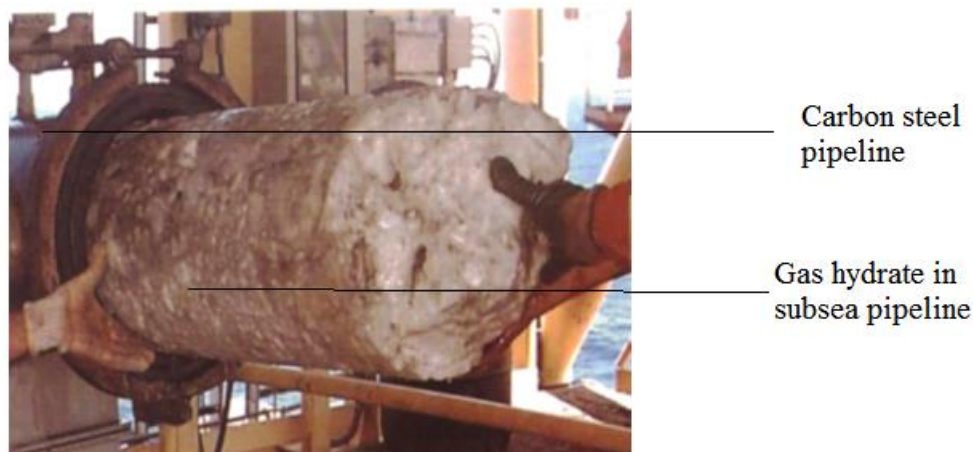


Figure 2-17: Typical example of gas hydrates in a Sunsea hydrocarbon pipeline [63]

2.9.1 The influence of MEG in oil and gas industry

The corrosion of carbon steel pipelines has been studied for many years and effect of various parameters such as pH, temperature and water chemistry are thoroughly researched [1]. The study of carbon steels in CO₂ saturated conditions can be complicated in the presence of different chemicals added into the system. In wet gas transportation pipelines, the hydrate formation is the common concern and mono ethylene glycol (MEG) is the preferred thermodynamic hydrate inhibitor [64].

MEG effect on CO₂ corrosion of carbon steel is not well understood [57]. It was reported that presence of MEG changed the physio-chemical properties of the aqueous phase [65].

The density of solution increased almost linearly, while the viscosity increased exponentially. Similarly, Lu et al [65] Show that CO₂ solubility decreased when MEG concentration increased to about 60 wt %. Another study [66] demonstrated that the CO₂ solubility in MEG/water mixture was a function of salt concentration. At high salt concentration (> 6 mole NaCl/kg solvent) CO₂ solubility increases with MEG concentration. The diffusivity of CO₂ in the solution mixture decreases with increasing MEG concentration [66]

De Waard and Milliams [37] demonstrated that addition of glycol to wet gas pipeline influenced CO₂ corrosion by lowers the dew point of water and consequently could reduce the severity of TOL corrosion. They also noticed that the corrosion rate at the BOL decreases when glycol mixes with the water phase. Gulbrandsen and Morard [13, 67] observed that MEG altered the anodic half reaction of the corrosion process and relates it to adsorption of MEG on the steel surface. The influence of other parameters in combination with MEG such as the presence of O₂, H₂S and the corrosion inhibitors [13] has been studied.

Consequently, despite the fact that many researches has been done related to CO₂ corrosion of carbon steel, there is little information available that are directly applicable to corrosion of carbon steel in the presence of HAc and MEG, more specifically to conditions seen in the oil and gas industry. In addition, several research [38, 43] has been carried out relating to internal corrosion protection of carbon steel pipelines, but the effect of acetic acid is not well known especially when pH stabilization with MEG are used for corrosion protection. This study will look at how HAc/MEG affect the dissolution of carbon steel in de-aerated environment, and develop corrosion protection strategies that will reduces the corrosion rate to an acceptable level in the oil field.

The next Chapter provides description of the apparatus, materials and testing in present investigation.

2.9.2 Corrosion inhibition of carbon steel in CO₂ environment

Corrosion processes are responsible for several losses in the oil and gas industry, and as such, prevention is one of the best ways to combat it. Many methods have been employed to prevent corrosion of carbon steel in CO₂ environment, and corrosion inhibition is one of the best methods. Corrosion inhibition is regarded as changes in composition of corrosive environments to reduce or prevent corrosion of carbon steel and alloys.

Several papers have been published on corrosion inhibition in CO₂ environment. Scully [68] presents a paper on the polarization resistance for determination of instantaneous corrosion rates and found out that the possible source of error in the polarization resistance is the high solution resistance and non-uniform current and potential distributions of the metal in the solution. Magana-Zavala et al [69] also studied EIS modelling of different behaviours of Ni and Ni oxide thin films for corrosion prevention in sour media. The results show that the nickel and nickel oxide films adopt different behaviours. Wang, H et al [70] studied the characterization of inhibitor and corrosion product film using electrochemical impedance spectroscopy and found out that the corrosion product layer without inhibitor is non-protective at lower temperature and low pressure environment. Chechirlian et al [71] also in his work proposed specific aspect of impedance measurements in low conductivity media. Itagaki et al [72] discussed anodic dissolution of Fe-Mo in sulfuric acid solution as investigated by EIS combined with channel flow double electrode. The results indicate that the Fe- 2.5% wt. Mo shows capacitive and inductive semi-circles and almost the same as that of the pure Fe. Pajkossy [73] in his work on impedance of rough capacitive electrodes and observed that a significant portion of capacitance dispersion are noted when studying polycrystalline solid.

Mansfeld et al [74] studied corrosion inhibition in neutral, aerated media using rotating cylinder electrode and found out that a second time constant occurs at high frequencies in NaCl medium.

Based on these, no published papers have been reported on the corrosion inhibition in the presence of HAc and MEG. This work will study the effect of three corrosion inhibitors on the corrosion rate of carbon steel in CO₂ environment especially when some concentrations of HAc and MEG are encounter in the system.

CHAPTER 3

Apparatus, Materials and Procedures

3.1 Overview

The aim of this experimental work was to study the synergistic effect of acetic acid (HAc) and mono-ethylene glycol (MEG) on carbon steel corrosion in CO₂ saturated environment under different conditions. This Chapter is divided into three phases as shown in Figure 3-1 and Figure 3-2 respectively.

The First Phase of the experimental work was carried out in test cell beakers using average weight loss measurement procedures at stagnant (no flow) conditions (**Section – I**)

The Second Phase of the study was carried out in a bubble cell glass beaker set up connected with corrosion monitoring systems such as linear polarization resistance (LPR), potentiodynamic polarization (PDP) and electrochemical impedance spectrum (EIS) (**Section - II**)

The Third Phase of the experimental work the surface analyses were studied using the scanning electron microscope (SEM), X-ray diffraction (XRD), Energy dispersion X-ray (EDX) and X-ray photoelectron spectroscopy (XPS) to monitor and characterized the surface of the samples prior to and after every experiments. This help to ascertain the extent of damage done and characterize the types of corrosion that has taken place on the surface of the metal (**Section - III**)

All the experiments were conducted in a simulated artificial sea water (3.5% wt NaCl) solution saturated with CO₂, temperatures of 25°C, 50°C and 80°C, 0.5 bar partial pressure

and pH of 6.0. Figure 3-1 and Figure 3-2 shows an overview of research experimental framework.

As can be seen, Figure 3-1 shows an overview of experimental apparatus, material preparation and testing as well as the corresponding procedures. Similarly, Figure 3-2 also illustrates the details structure of the experiments and the associated apparatus at a glance.

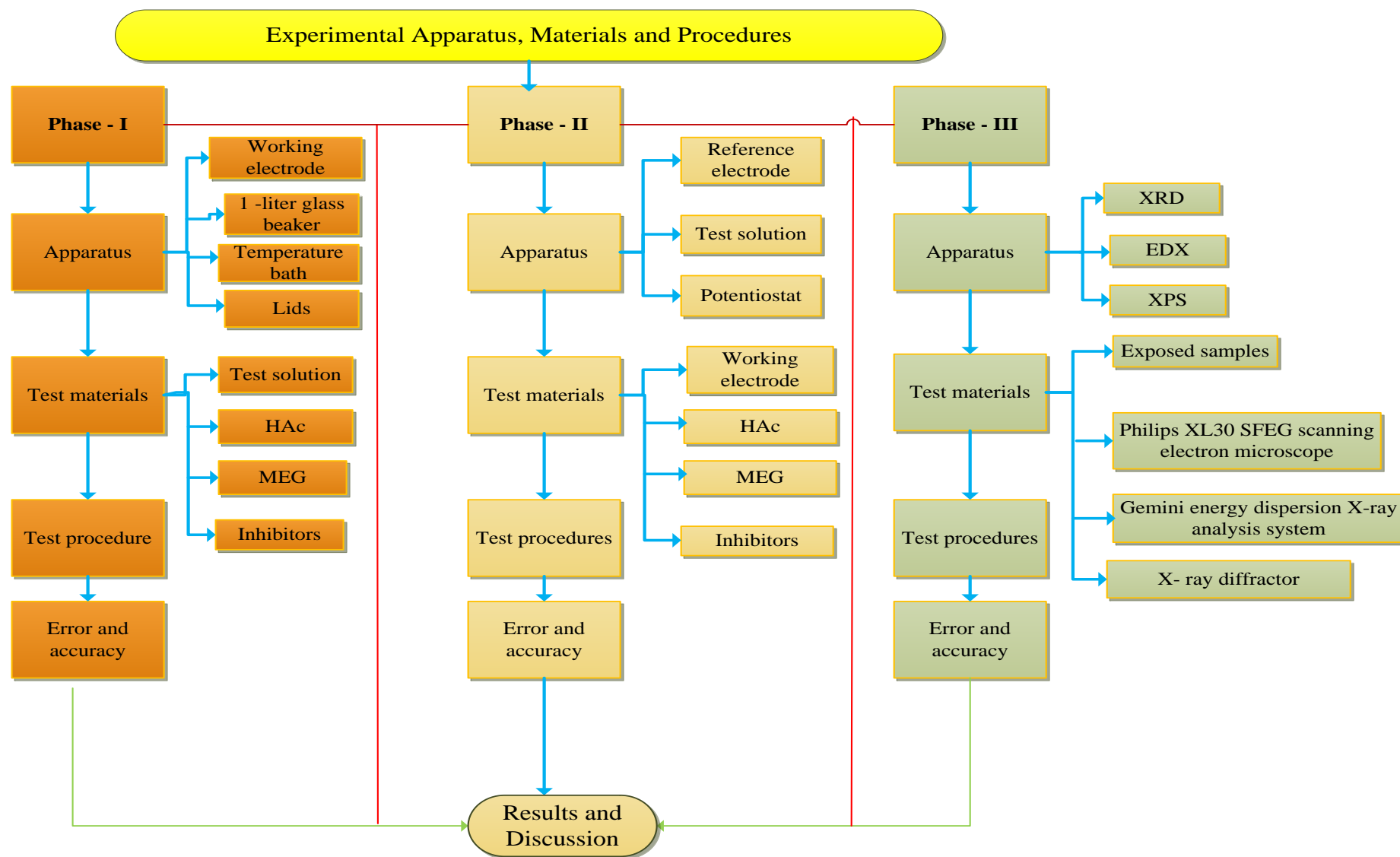


Figure 3-1: An overview of experimental Apparatus, Materials and procedures

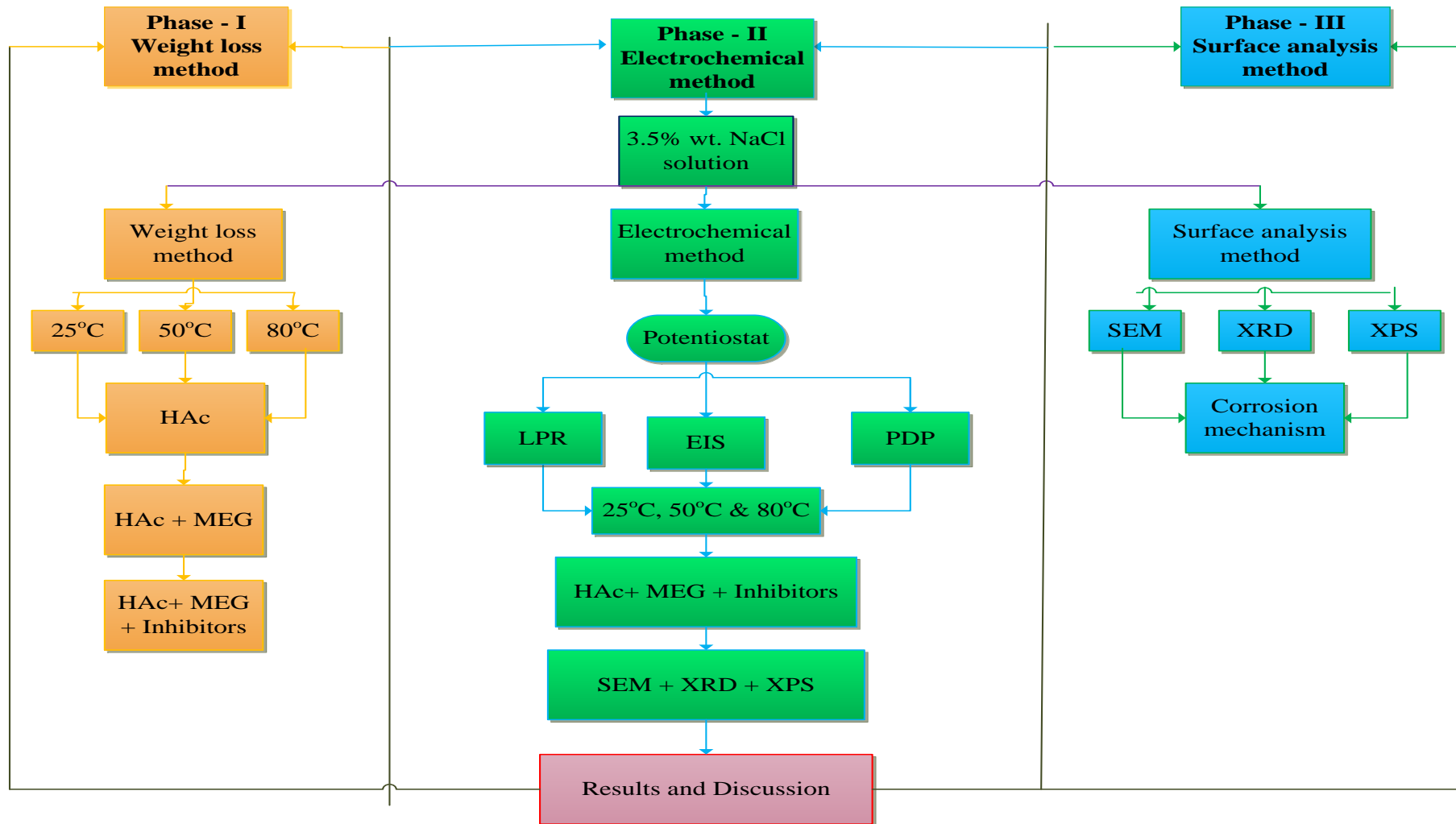


Figure 3-2: Details of Experimental Structure and Apparatus.

3.2 Phase 1: Weight loss test

Weight loss test monitoring is one of the fundamental methods of evaluating the usefulness of corrosion rate and corrosion control measurement in any environment. The process involves exposing a specimen (carbon steel material) to an environment for a period of time and then measuring the resultant weight loss after removing the corrosion product.

3.2.1 Apparatus

The apparatus used for the weight loss test include 1 liter glass beaker, carbon steel samples (electrode), water bath for temperature control, and copper wire for sample holder and plastic lids as shown in Figure 3-3

3.2.2 Test material

The principal samples investigated in this work were machined from commercial rods of X65 carbon steel with composition of 0.08%C, 0.25%Si and 1.54%Mn. The average chemical composition of the material is given in Table 3-1. The shape and typical dimensions of the samples for average weight loss are shown in Figure 3-4.

In every experiment, the specimen surfaces were polished successively with 80, 120, 240, 320, 600, 800 and 1200 grit SiC paper, degreased using acetone rinsed with distilled water/ethanol and then dried.

Table 3-1: Chemical composition of X-65 carbon steel that used in the experiments

Chemical Composition	Values (%)
C	0.08
Si	0.25
Mn	1.54
S	0.001
P	0.019
Sn	0.008
Cr	0.04
Ni	0.03
MO	0.01
Cu	0.12
Al	0.038

The following provides an overview of:

- (i) Test solution
- (ii) Acetic acid
- (iii) Mono-ethylene glycol
- (iv) Corrosion inhibitors

These intend to give an insight into the material preparations

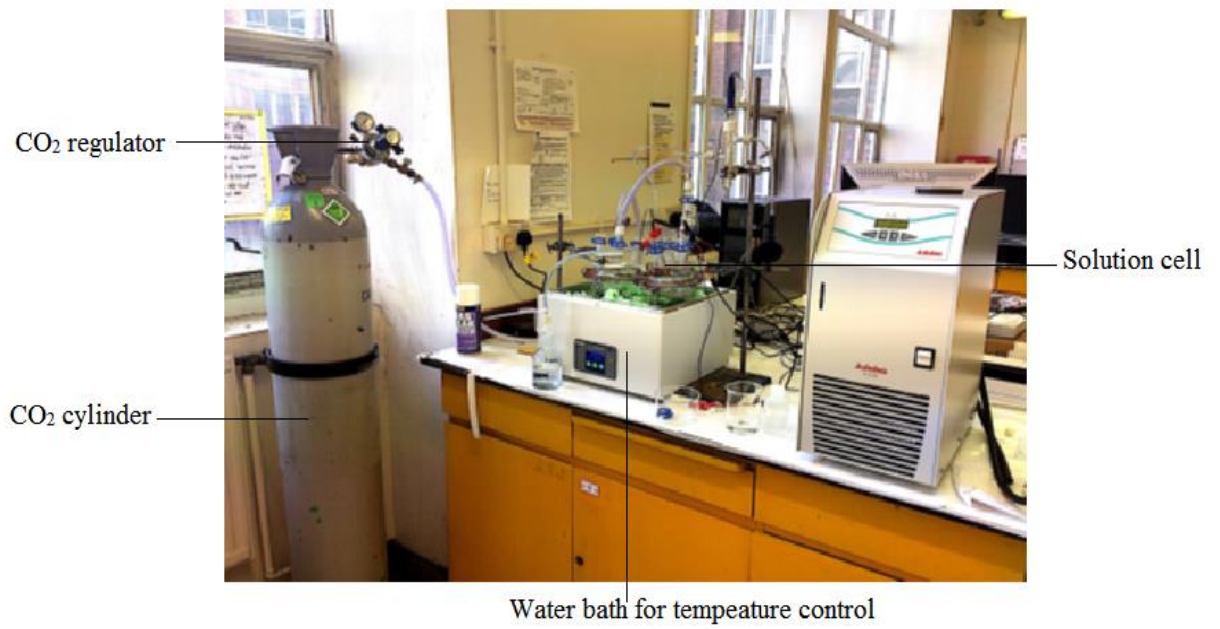


Figure 3-3: show the picture of the test set-up for the weight loss experiment of this study.

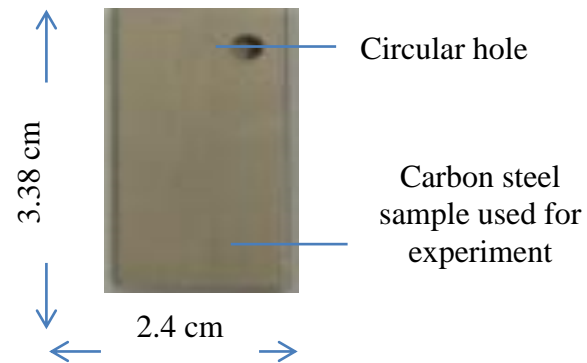


Figure 3-4: Carbon steel specimens used for the weight loss corrosion test in this study.

(i) Test solution

All experiments performed in this study were carried out using artificial simulated seawater (3.5% wt. NaCl) solutions saturated with CO₂. The solutions replicate typical seawater found in the oilfield environment with composition shown in Table 3-2. The fresh solutions were prepared with sodium chloride salt from LLK laboratories Ltd and distilled water.

Table 3-2: Chemical composition of sea water brine

Component	Composition(g/L)
CaCl ₂ .2H ₂ O	10.53
MgCl ₂	4.47
KCl	0.87
BaCl ₂ .2H ₂ O	0.449
SrCl ₂ .6H ₂ O	1.44
NaCl	74.78
NaHCO ₃	0.335

Each experiment was performed in 1 liter glass cell and at 0.54 bar partial pressure. In addition and prior to each test, the test cell solution was continuously purge with CO₂ for at least 2 hours before the experiment and bubbled throughout the duration of the test in order to completely dissolved oxygen from the system.

(ii) Acetic acid concentration

The molecular and structural formulas of the acetic acid used in this study are given in Table 3-3. In all tests, four different concentrations of 0ppm, 500ppm, 1000ppm and

2500ppm of HAc were added to the system of weight loss and the electrochemical test to examine their effect on the solution containing carbon steel.

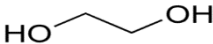
Table 3-3: Properties of Acetic acid (HAc) used for the experiments

Name	Properties
Chemical name	Ethanoic acid (Acetic acid)
Molecular formula	(C ₂ H ₄ O ₂ or CH ₃ COOH)
Molecular structure	$ \begin{array}{c} \text{H} \\ \\ \text{H}-\text{C}-\text{C} \\ \quad // \\ \text{H} \quad \text{O} \\ \quad \quad \backslash \\ \quad \quad \text{O}-\text{H} \end{array} $
Molecular weight	60.05 g/mol
Boiling point	117.9oC
Density	1.044 g/cm ³
Melting point	16.6oC

(iii) Mono-ethylene glycol concentration

The mono-ethylene glycol (MEG) studied in this work contains about 99.5% wt. purity and was supplied by Fishers chemical laboratory (analytical grade quantity). Any impurity in the MEG was certified by the supplier to be less than 0.001 mol %. Two different concentrations 20% MEG (referred as a rich MEG) and 80% MEG (referred as lean MEG) were examined in the tests.


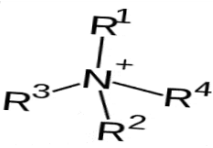
Table 3-4: Properties of Monoethylene glycol (MEG) used for the experiments

Name	Properties
Chemical name	Mono-ethylene glycol
Molecular formula	C ₂ H ₆ O ₂
Molecular structure	
Molecular weight	62.07 g/mol
Boiling point	197.3°C
Density	1.11 g/cm ³
Melting point	-12.9°C

(iv) Inhibitors concentration

Three different types of organic chemical corrosion inhibitors (the phosphate ester, the oleic imidazoline salt and the quaternary salt) were examined in this study. The formulation names given to the inhibitors studied are XX, YY and ZZ. The chemical packages of the inhibitors are based on their combinations of complex blends of esters, phosphoric acid, propionic acid and other organic constituents. Table 3-5 shows an example of the generic forms of the inhibitors studied.

Table 3-5: Example of chemical and molecular structures of corrosion inhibitors constituent studied.

Inhibitor	Active component	Chemical formula	Molecular structure
A	The phosphate ester	H_3PO_4	$ \begin{array}{c} O \\ \\ HO-P-OCH_3 \\ \\ OH \end{array} $
B	The Oleic imidazoline salt(OI)	$C_{18}H_{33}NaO_2$	
C	Quaternary salt		

3.2.3 Test procedure

The weight loss experiments in this study were carried out under laboratory conditions and 3.5% wt. NaCl solution. Carbon steel specimens with an exposed area of 8.11 cm² and rectangular in shape with a circular hole toward the top end as shown in Figure 3-4 were prepared by successfully ground with 80, 240, 320 and 400 with silicon grit paper and then polished with 600, 800 and 1200 silicon paper. The samples were then exposed to the prepared solution and CO₂ gas with partial pressure of 0.54 bar continuously bubble into the solution for the entire experiment duration. The samples were exposed to different conditions with average exposed time ranges from 24 – 72 hours. The test samples were suspended in the test solution by passing a plastic wire through the coupon and the wire was hung to a plastic rod held in place of the glass cell top holes. It was then

weighed using an electronic balance (Mettler Model AE163) and suspend into the solution.

In order to measure the weight loss and determine the corrosion rate, it is extremely important to remove the corrosion products formed on coupons. The corrosion products were carefully cleaned using Clarke's solution. The Clarke's solution used was prepared according to ASTM G1 specification [75] with the ratio of 1000ML of hydrochloric acid (specific gravity of 1.19), 20 grams of antimony trioxide (Sb_2O_3) and 50 grams of stannous chloride (SnCl_2). The samples were then rinsed thoroughly after cleaning with deionized water followed by ethanol and then dried with blower.

The corrosion rate was then determined by taking into account the initial total surface area of the sample and the mass lost before and after the test period using equation 3-1, corrosion rate equation [76] as:

$$CR = \frac{m_1 - m_3}{MW_{Fe} \times t \times S} \quad 3-1$$

Where,

CR = Corrosion rate, $\text{g}/\text{m}^2\text{h}$

m_1 = The weight of coupon prior to running experiments, g

m_3 = The weight of coupon after removing the scale, g

MW_{Fe} = The molecular weight of iron atom, g/mol

t = The exposed time, hr

S = The exposed coupon surface area, m^2

Converting equation 3-1 in mm/yr gives:

$$CR = \frac{m_1 - m_3}{MW_{Fe} \times t \times S} \left(\frac{\text{mol}}{\text{m}^2\text{h}} \right) \quad 3-2$$

$$CR = \frac{m_1 - m_3}{MW_{Fe} \times t \times S} \times \frac{365 \times 24 \times MW_{Fe}}{\rho} \text{ (mm/yr)} \quad 3-3$$

Where, ρ is the density of the coupon in kg/m^3 .

3.2.4 Error and Accuracy

The samples were weighed using electronic balance for within 0.1 mg and each sample was weighed three times. The accuracy of this device and other instruments used in the weight loss experiment could be affected air flow rates, CO₂ partial pressure and temperature readings. The electronic balance has an accuracy of $\pm 2\%$ and repeatability of $\pm 0.1\%$. The accuracy of the temperature probe was 0.05°C.

Phase – II description of this study is given in the following:

3.3 Phase - II: Electrochemical Test

Every corrosion is an electrochemical process of reduction and oxidation reactions. As corrosion occurred, electrons are given up by the electrode (oxidation) and accept by the elements (reduction) in the corroding electrolyte. However, because there is a flow of electron (current) in the electrode-electrolyte reaction, it can be measured and controlled electrochemically.

In this section of study, an electrochemical test will be employed to characterize the corrosion properties of carbon steel and its components in a solution of 3.5% wt. NaCl solution containing different concentrations of HAc, MEG and corrosion inhibitors.

3.3.1 Apparatus

The apparatus used in this study (Figure 3-5 to Figure 3-7) consisted of glass cell, ACM-Gill potentiostat, and thermometer, working electrode, counter electrode, reference electrode, grinding /polishing machine, spot welding machine and a PC.

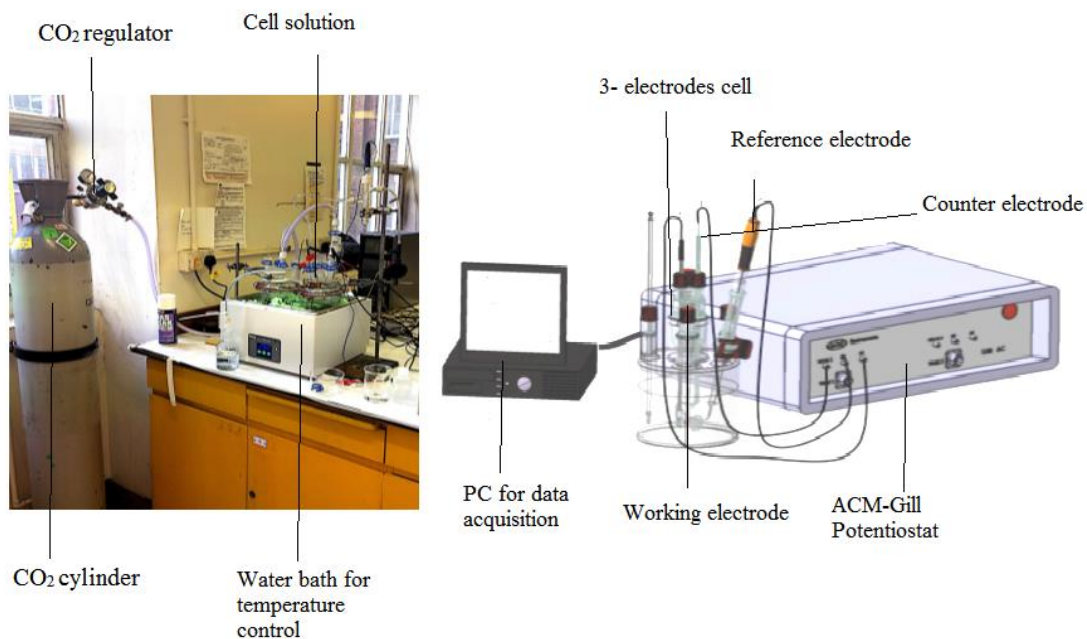


Figure 3-5: Schematic drawing of 3-electrode glass cell used in the electrochemical test



Figure 3-6: Mechanical polishing machine in preparation for tests

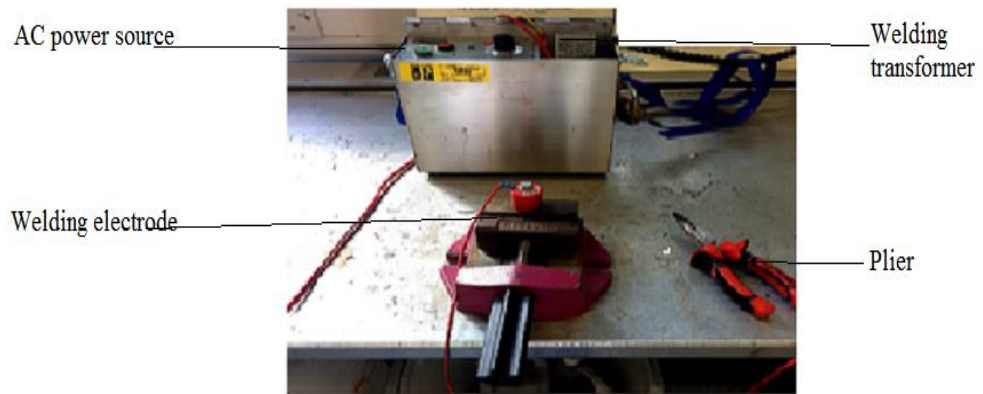


Figure 3-7: Mechanical spot weld machine for test

3.3.2 Test material

The principal samples investigated in this work were machined from commercial rods of X65 carbon steel with composition of material given in Table 3-1 and same preparation procedure shown in section 3.2.2.

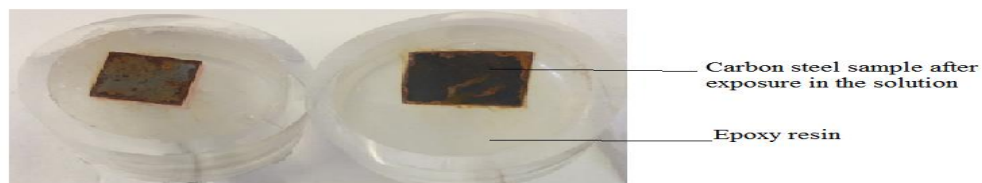


Figure 3-8: Test samples after 6 hours exposure in the solution

(i) Test solution

All experiments performed in this section of study were carried out using the same test solution as in Phase-1.

Table 3-6: Experimental matrix for the electrochemical test

Parameters	Values
Test material	Carbon steel X 65 grade.
Test solution	3.5% wt. NaCl
Temperature, °C	[25, 50 and 80]
PCO ₂ , bar	0.54
HAc Conc, ppm	[0, 500, 1000, 2500]
MEG Conc, %	[20, 80]
Inhibitors Conc, ppm	[3, 5 and 10]
Test duration, hrs	6
Measurement techniques	WL, OCP, LPR, EIS and PDP
LPR:	
Potential ramp :	-5 to +5 mV vs. E _{corr}
sweep rate :	0.1 mV/s
PDP	-600 mV to 150 mV Vs. E _{corr}
EIS	5KHz – 0.01 Hz

3.3.3 Test procedure

The electrochemical experiments using the bubble cell were carried out to examine the corrosion behaviour of carbon steel at different conditions in a 3.5% wt. NaCl solution. These tests were conducted at the Corrosion and Material Research Laboratory at the University of Manchester. The test assembly consisted of one-litre glass cell that was continuously bubbled with CO₂ for at least 2 hours prior to the experiment and throughout the duration of the test at a partial pressure of 0.54 bar, stable temperature water bath for temperature control.

The spot-weld sample is put in a 30mm acrylic mould, filled with araldite resin mixed with araldite hardener in a ratio of 10 parts resin to 1 part hardener, carefully stirring for about 5 minutes to avoid bubble formation. The mixture takes approximately 12 hours to set at room temperature or about 6 hours at 140 °C. Once the mixtures are set, the samples were mechanically polished using metallographic abrasive papers of different grades of 80, 120, 240, 320, 400, 600, 800 and 1200. The polishing using different paper grades was carried out in order to remove coatings from the surface of the sample and achieve a smooth surface with no dent, then degreased with acetone, rinsed with distilled water/ethanol and then air dried.

The electrochemical measurements were based on a three electrode system, using a commercially potentiostat- ACM Gill AC 930 Potentiostat/galvanostat with a computer control system. The reference electrode was the Ag/AgCl and the auxiliary electrode is a platinum electrode. The Open circuit potential (OCP), Linear Polarization Resistance (LPR), Electrochemical Impedance Spectroscopy (EIS) and Potentiodynamic scan (PDP) measurement were employed to measure the corrosion rate.

3.3.4 Error and Accuracy

The electrochemical measurements were performed with ACM-Gill Potentiostat and frequency response analyser in a three electrode cell arrangement. The EIS measurements were carried out at OCP with frequency range of 5 KHz to 0.01 Hz. The PDP was performed from -600mV to 150mV vs E_{corr} with respect to OCP at scan rate 0.1 mV/s.

The accuracy of the devices and instruments in the electrochemical tests could be affected by also air flow to the system, CO₂ partial pressure, temperature measurements, and stirring of the solutions.

The reference electrode has an accuracy of $\pm 5\text{mV}$ and repeatability of $\pm 1\%$.

3.3.5 Measuring techniques

The various measurement methods used in the electrochemical test described below includes the following:

- (i) Open circuit potential, OCP
- (ii) Linear polarization resistance, LPR
- (iii) Potentiodynamic polarization, PDP
- (iv) Electrochemical impedance spectroscopy, EIS

(i) Open circuit potential (OCP)

The measurement of an electrochemical potential is one of the basic measurements in electrochemistry. In this process, the potential of the working electrode that is not subjected to any external current as a function of time is measured. The potential of a metal in an aqueous solution is a function of the reactivity of the metal and oxidizing power of the solution. During the potential measurements, both the anodic and cathodic

reactions take place simultaneously on the electrode surface and are equilibrium and there is no net current.

The essence of potential measurement is to measure the potential of the specimen without affecting in any way electrochemistry reactions on the specimen surface. It is necessary to make the potential measurements with respect to a stable reference electrode so that any changes in the measured potential can be attributed to changes at the specimen/solution interface. When a suitable reference electrode is used, the potential of the working electrode can be controlled consistently and any changes in the measured potential during the test can be related to changes in the working electrode. Generally, a more positive OCP indicates that a metal surface is less prone towards electrochemical dissolution. Hence, the OCP can be used to indicate the likely resistance to corrosion of the metal or alloy in any conductive environment. In this study, a Ag/AgCl Saturated Calomel Electrode (SCE) with a potential V-SHE of +0.243V at 25°C was used.

(ii) Linear polarization resistance (LPR)

The linear polarization method is a direct current measurement technique.

It is one of the quickest, high sensitive and non-destructive techniques for determination of the corrosion rate of a metal [69, 71]. The basis of the LPR technique was developed by Stern and Geary [72]. It assumes that the exponential anodic and cathodic polarization curves are approximately to a straight line close to the free OCP, which is the potential difference between two electrodes (submerged in an electrolyte) when no electrical current flows between them [72].

In this study for the LPR measurements, the carbon steel electrodes are polarized using a DC with a maximum potential range of -20 to 20 millivolts (mV) from the OCP value and a scan rate of 0.1667 mV/s. The current flows when this voltage is applied are measured and then the polarization resistance can be calculated. Figure 3-9 shows a

typical graph of the potential plotted against current and the slope of the linear straight line is taken which gives a value of the polarization resistance, R_p .

$$R_p = \frac{\Delta E}{\Delta i} \quad 3-4$$

Where,

R_p = Polarization resistance, ohm.cm²

ΔE = Potential increment, V

Δi = Corresponding current densities increment in A/cm²

The corrosion current density (i_{corr}) is then calculated using the Stern and Geary equation [72] as:

$$i_{\text{corr}} = \frac{\beta_a \beta_c}{2.303 R_p (\beta_a + \beta_c)} \quad 3-5$$

Where,

i_{corr} = Corrosion current density, A/cm²

β_a = anodic Tafel constant, v

β_c = cathodic Tafel constant, v

R_p = Polarisation resistance, Ω .cm²

The corrosion current density i_{corr} is then converted to a corrosion rate using the Faraday's law given as:

$$m = \frac{i_{\text{corr}} M A t}{n F} \quad 3-6$$

Where,

m = Mass loss, g, i_{corr} = the corrosion current density, A/cm^2

M = The molar weight, g/mol

A = Area of the specimen, cm^2

t = Time of exposure, sec n = number of electrons involved in the reaction,

F = Faraday's constant,

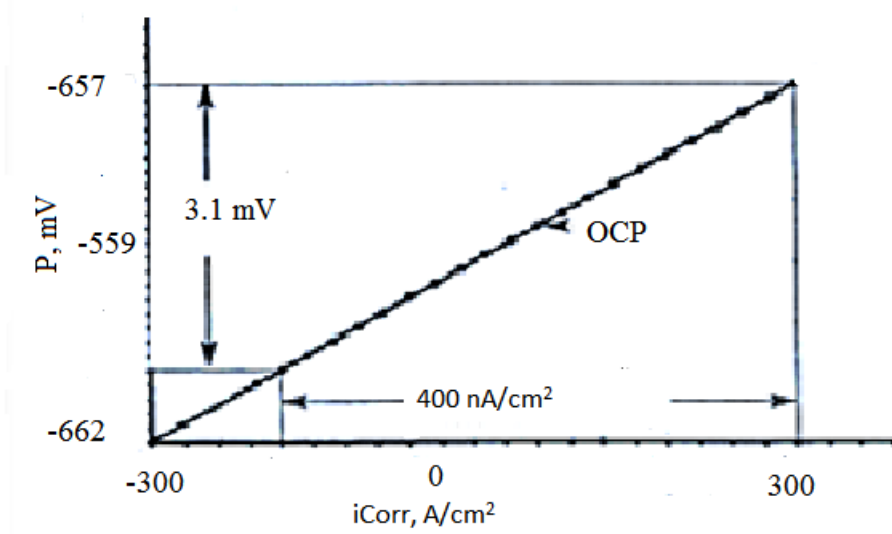


Figure 3-9: Graphical representation of the polarization resistance.

(iii) Potentiodynamic polarization (PDP)

The potentiodynamic polarization curve is an electrochemical technique used in corrosion testing to evaluate reaction kinetics. Electrochemical reaction kinetics is essential in evaluating the corrosion rate of a given metal exposed to the environment of interest. The potentiodynamic shows the correlations between the current flowing and the potential of the working electrode over a wide range. Thermodynamics may predict the possibility of corrosion occurring, but does not provide information on how slow or fast corrosion processes occur [73]. In evaluating the potentiodynamic measurements, the

electrochemical reactions occurred on the surface of the working electrode can be controlled. Consequently, the corrosion reaction of the specimen can be further understood by examining the cathodic and the anodic reaction processes.

The characterization of electrochemical kinetics can be achieved by evaluating at least three polarization parameters i.e corrosion current density i_{corr} , corrosion potential E_{corr} , and Tafel plot slopes b_a and b_c .

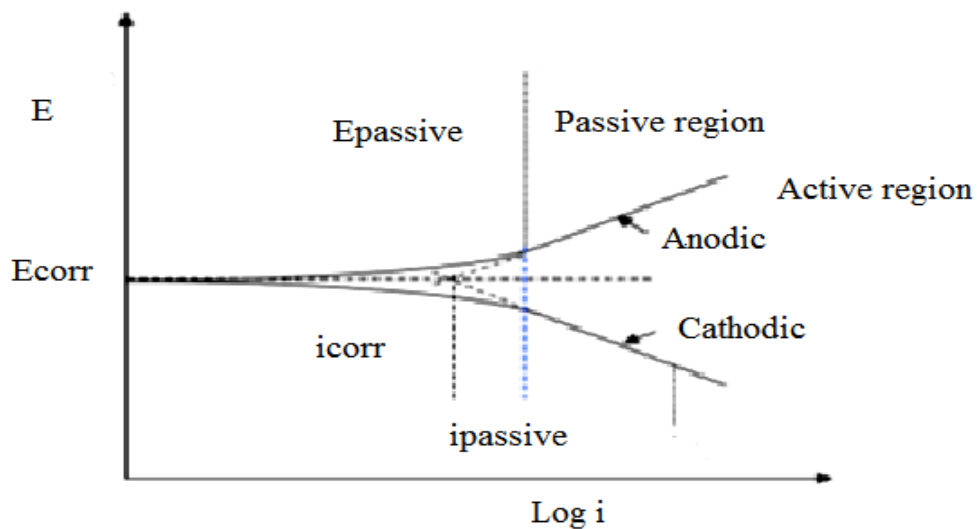


Figure 3-10: Schematic diagram of the polarization curve demonstrating different anodic and cathodic regions, and showing the Tafel extrapolation method for estimation of corrosion current density (i_{corr}) and corrosion potential (E_{corr}).

The polarization curve is measured by scanning the potential and recording the current [77]. Hence the corrosion rate can be estimated by observing the response to a controlled change from the steady state reaction that is created by applying the potential or current [78].

A potentiodynamic measurement is done by scanning the sample potential slowly through hundred millivolts from the open circuit potential through the anodic or cathodic direction and then the potentials are plotted against the logarithm of the measured current to obtain a polarization resistance graph as shown in Figure 3-10

Corrosion current density (i_{corr}) and corrosion potential (E_{corr}) can then be estimated from the polarization curve using the Tafel extrapolation of the anodic and cathodic slopes as shown in Figure 3-11

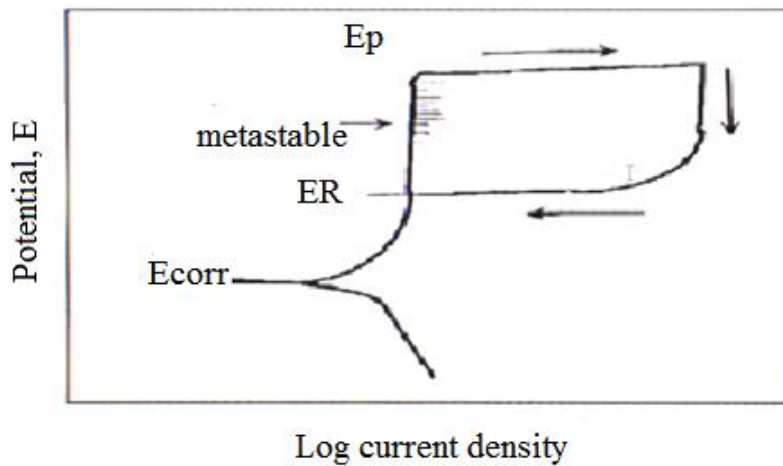


Figure 3-11: Schematic representation of a polarization curve showing pitting potential, metastable pitting region, repassivation region and, corrosion potential (E_{corr}).

(iv) Electrochemical impedance spectroscopy (EIS)

The electrochemical impedance spectroscopy, EIS is an electrochemical corrosion measurement technique that uses alternating current to determine the fundamental parameters of electrochemical reactions (corrosion rate) as well as corrosion mechanism. The EIS can give an insight into the process of corrosion and corrosion control method

that cannot be obtained easily by other DC methods such as the use of inhibitors and coatings in protecting the surface of the metal [71].

Using an electrolyte solution, a potential is applied to the sample and the resulting impedance of the electrode is measured. The impedance is defined as the ability of a circuit to resist the flow of alternating electrical current and is quantified by the equation:

$$Z = \frac{V_{ac}}{I_{ac}} \quad 3-7$$

Where Z is the impedance

A lot of research work has been carried out in corrosion engineering using the EIS measurement technique. Qiu et al [79] studied the properties of anodized aluminum using the EIS.

(v) Evaluation of corrosion rate using EIS

AC impedance technique has been extensively used in corrosion studies. Impedance analysis consists of applying a broad range of frequencies of AC signals to a solid state or aqueous system. An AC voltage is applied and the response current is measured. The data obtained is in the form of real and imaginary current or voltage. Based on the data obtained, the value of impedance (Z) is calculated.

Many researchers have used AC impedance in investigating the corrosion processes occurring at the metal as well as many other corroding interfaces. Yong et al [80] studied the effect of high temperatures on the corrosion behavior of super Austenitic stainless steel S32654 in polluted phosphoric acid. They found that the corrosion rates measured

using AC-impedance was in good agreement with the values obtained from weight loss measurements. Park and Pyum [75] analyzed the impedance spectra of pitted alloy 600 electrode in aqueous NaCl solution at high temperatures from 60°C to 150°C with different slopes. They concluded that the section with the smaller slope in lower frequency range was due to combination of resistive and capacitive elements in the pit wall. The section with the higher slope at higher frequencies was due to double layer charging at the pit bottom.

The experimental work in this study will include the use of EIS to measure the frequency response on carbon steel subjected to CO₂ corrosion environment with and without HAC. The results will also give an insight of the changes in corrosion rate on the surfaces of the material.

(i) Nyquist plot

Nyquist plot is a plot between real and imaginary values of impedance [76]. It is a semi-circle form from high frequency domain to low frequency domain. The Nyquist plot can have a single time constant which has one semi-circle or more time constant with more semi-circles. This plot could be used to compute the values of the uncompensated resistance (R_U) between the working electrode and the reference electrode, the polarization resistance (R_p) at the electrode-solution interface and double layer capacitance (C_{dl}) also at the electrode-solution interface.

Figure 3.12 shows an example of a Nyquist plot in a solution with single time constant

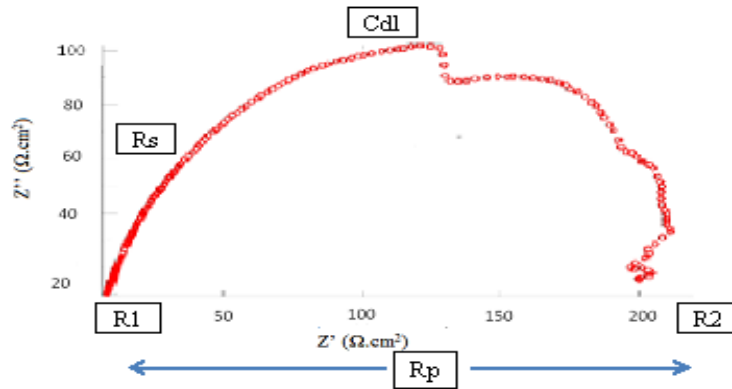


Figure 3-12: Nyquist plot with a single time constant and electrical circuit describing the plot.

In Figure 3.12, the point of the higher frequency is the solution resistance (R_1). The polarization resistance (R_p) is the diameter of the semi-circle, R_2 . The double layer capacitance, C_{dl} is derived from the maximum frequency of the imaginary impedance, Z'' and the polarization resistance, R_2

$$C_{dl} = \frac{1}{2\pi f_{max}} R_2 \quad 3-8$$

(ii) Bode plot

The Bode plot is a useful alternative to the Nyquist plot to avoid longer measurement time associated with low frequency. It is a plot of $\log |Z|$ for each frequency on the Y-axis against $\log \omega$ value on the X-axis. This form of plot permits examination of the

absolute impedance $|Z|$ and the phase shift ϕ of the resultant wave front, each as a function of frequency as calculated in the equation below.

$$|Z| = \sqrt{(Z')^2 + (Z'')^2} \tag{3-9}$$

$$\tan \phi = \frac{Z''}{Z'} \tag{3-10}$$

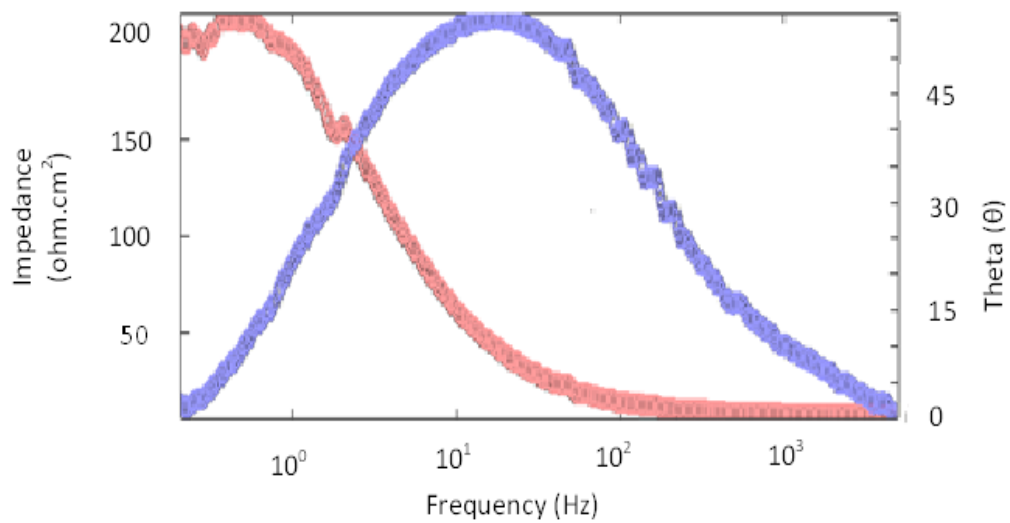


Figure 3-13: A Bode plot for single time constant for a corroding metal.

The following provides description of Phase-III (Surface analysis) of this investigation

3.4 Phase - III: Surface Analysis Examination

After corrosion tests, another important aspect of the study was to determine the damage mechanisms of the specimens tested. In this section, the surface analysis methods used in examining the corrosion products and to ascertain the types of corrosion that have occurred on the surface of the steel will be presented. The apparatus used for this section (Phase-III) include the Scanning Electron Microscope (SEM), X-Ray Diffraction (XRD) and Energy Dispersion X-ray (EDX) and X-ray Photoelectron Spectroscopy (XPS).

3.4.1 Apparatus, test materials and procedures for SEM and XRD

(i) SEM examination

Figure 3-14 shows the SEM apparatus used in this study. The Scanning Electron Microscopy (SEM) is a technique used for the observation and characterization of materials on a nanometer to micrometer scale. The SEM provides high-resolution and long-depth of field images of the sample surface and near surface. It was used to investigate and analyze the corroded surface of the materials. The basic principle involved in SEM consists of bombarding the surface sample to be examined under vacuum with a finely focused beam of electrons. A very fine focuses beam of electrons is scanned over the surface of the specimen. As the electron beam scans the specimen, it provides both the topographical information about the specimen as well penetrates the surface, interacts with the samples to cause effects such as electron backscattering, x-ray emission, secondary electron emission and cathode luminescence.

In this work, the test samples were examined using the Philips XL30 SFEG Scanning Electron Microscope, interfaced to the EDAX Energy Dispersive X-ray Analysis system. SEM micrographs were obtained using an accelerating voltage of 15KV with a spot size of 3 using secondary electron detection. The micrographs generated were acquired using system magnifications of 250x, 1000x, 2000x, 5000x and 10,000x. Figure 3-14 show a typical image of SEM for the analysis of surface test material.

(ii) EDX examination

The energy dispersive X-ray spectroscopy equally known as energy dispersive X-ray analysis is an analytical technique used to determine the chemical and elemental character of a sample. The EDX depends on the interaction of the X-ray and the sample. Each sample was examined by clamping in the sample holder of an FEI Quanta 250 field emission scanning electron microscope (SEM). The accelerating voltage was 15kV and images of the surface acquired at magnifications of 500x, 1000x and 5000x using the secondary electron detector (ETD). The spectra were acquired using an EDAX Gemini energy dispersive x-ray analyzer (EDX) attached to the SEM.

(i) X-ray diffraction (XRD)

Figure 3-15 show a typical XRD apparatus used in this investigation. The X-ray diffraction (XRD) is a non-destructive technique for characterizing corrosion materials. It provides information about structures, phases, orientations and other structural parameters as grain size, and crystal defects of materials. Analysis of the x-rays provides elemental analysis of the surface composition without any changes to the nature of the object under examination. In this study, the samples were run on the Bruker D8 advance X-ray Diffractometer. The conditions of analysis involved running test material from 10°

2-theta up to 90° 2-theta with a step size of 0.02 and step time of 2 seconds. Each crystalline phase was compared against standards from the International Centre for Diffraction Data (ICDD/JCPDS database). Figure 3-15 also show typical image of the XRD used in this study.



Figure 3-14: A typical image of SEM for specimen's surface analysis.



Figure 3-15: A typical image of XRD for specimen's surface analysis

(ii) Test Equipment

The test equipment include the Philips XL30 SFEG Scanning Electron Microscope, EDAX Gemini Energy Dispersive X-ray Analysis system, Bruker D8 advance X-ray Diffractometer, FEI Quanta 250 field emission scanning electron microscope (SEM) and secondary electron detector (ETD)

3.4.2 Apparatus, test materials and procedures for XPS

(i) Apparatus

Figure 3-16 shows the XPS apparatus that was in this investigation. The X-ray photoelectron spectroscopy is a technique used to determine composition based on the photoelectric effect. Basically, it's an instrument used for investigating the surface

chemistry of electrically conducting and non-conducting coupons. The XPS beam emits photoelectrons from the surface of the sample using either AlK α (1486.6 eV) or MgK α (1253.6 eV). The XPS provides information about the samples from the top 10nm of the sample with a spatial resolution between 3 μ m 100 μ m. The XPS works on a surface which is irradiated with X-rays (200-2000 eV) in vacuum to examine core-levels. The X-ray hits and transfers the energy to a core-level electron which is emitted from its initial state with a kinetic energy dependent on the incident X-ray as well as the binding energy of the atomic orbital where it originated. Finally, the energy and intensity of the emitted photoelectrons are analyzed to identify and determine the concentrations of the elements present in the sample tested.

The XPS is viewed as a quantitative spectroscopic approach that provides information regarding the elemental composition in parts per thousand levels, based on the elemental electronic and chemical state of the electrode surface. The XPS can measure the elemental composition, empirical formula, chemical state and electronic state of the elements within a material. Different reports have been presented on the use of XPS especially in the study of corrosion. Qiu et al [79] uses the XPS for surface composition characterization and corrosion product analysis on carbon steel exposed to sea water. Qualitative analysis of surface films and formation of iron carbonate on carbon steel surfaces had also been studied using the XPS [80]. Similarly Galicia et al[81] uses the XPS to studied 1018 carbon steel surface composition exposed to alkaline medium as a function of immersion time and confirmed film formation on the steel surface. Ochoa et al [82] uses the XPS to studied the formation and quantitative analysis of iron carbonate at carbon steel in respect to the structure of the carbon steel

The physical principle of the XPS is based upon a single photon in/electron out process. The energy of a photon of electromagnetic radiation is based on the Einstein equation given as:

$$E = h\nu$$

3-11

Where,

H is the Planck constant (6.6210^{-34} Js)

V is the frequency of the radiation (Hz)

(ii) Test materials of the XPS

The Axis Ultra DLD spectrometer Karros, Manchester (Figure 3-16) uses a monochromatic Al K_{α} X-ray source (1486.6 eV, 10 mA emission), and uses a delay line detector that enables fast acquisition of a narrow binding energy region which is used for sample position optimization (using a pertinent core level photoelectron peak).

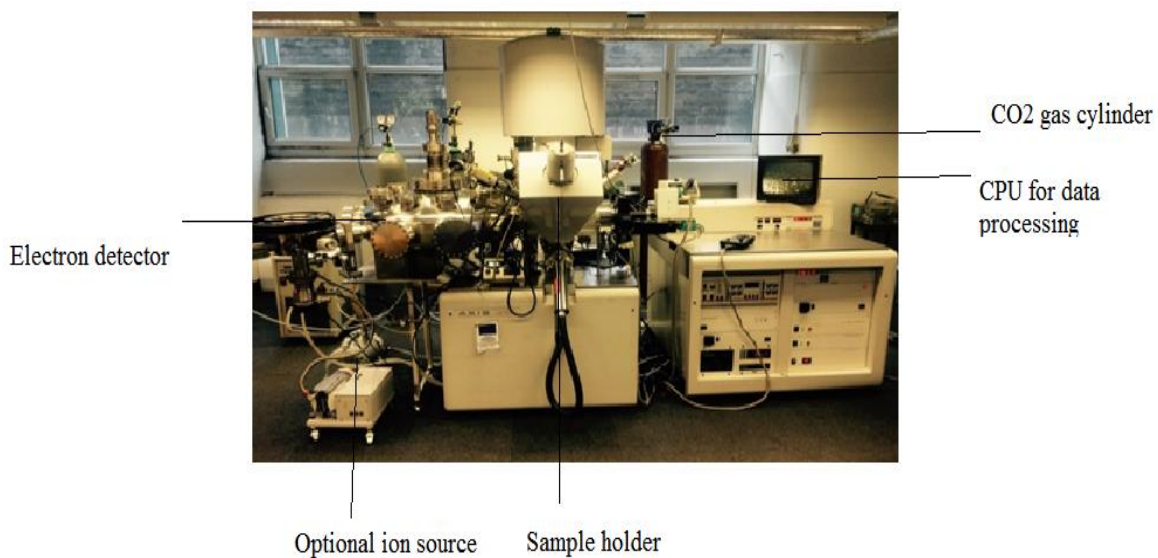


Figure 3-16: A typical image of Kratos Axis Ultra X-ray photoelectron Spectrometer used in this study.

An electromagnetic in the analysis chamber below the sample position is used to increase the yield of photoelectrons reaching the analyzer slits. A charge neutralizer was used to compensate for any differential charging or, *e.g.*, any poor connections between the sample and sample plate (and thus ground). Survey spectra of a wide binding energy region were acquired with pass energy of 80 eV while high-resolution narrow scans of the important atomic core levels were acquired using a pass energy of 20 eV. The experiments were performed under high vacuum at pressures $< 3 \times 10^{-8}$ mbar. Data were analyzed using CASAXPS (www.casaxps.com), where photoelectron peaks are typically fit with product-approximation Voigt functions (Gaussian-Lorentzian peaks with a mixing ratio of 0.3).

(iii) Procedures of the XPS

In order to carry out spectroscopic examination on carbon steel samples using the XPS, the sample is positioned in a suitable evacuated housing, an electron energy analyzer and a detector /data system analysis. This is however done in order to record the binding energy positions to the order of ± 0.1 eV, and also to resolve photoelectron energies to better than 1 eV. Figure 3-17 shows a block diagram of the XPS analysis. In summary, the basic procedure includes:

- Basics of ultra-high vacuum technology
- Generation of X-ray radiation
- Analysis in energy and detection of electrons
- Characterization of solid samples
- Computer control of the measurements
- Data analysis via computer software

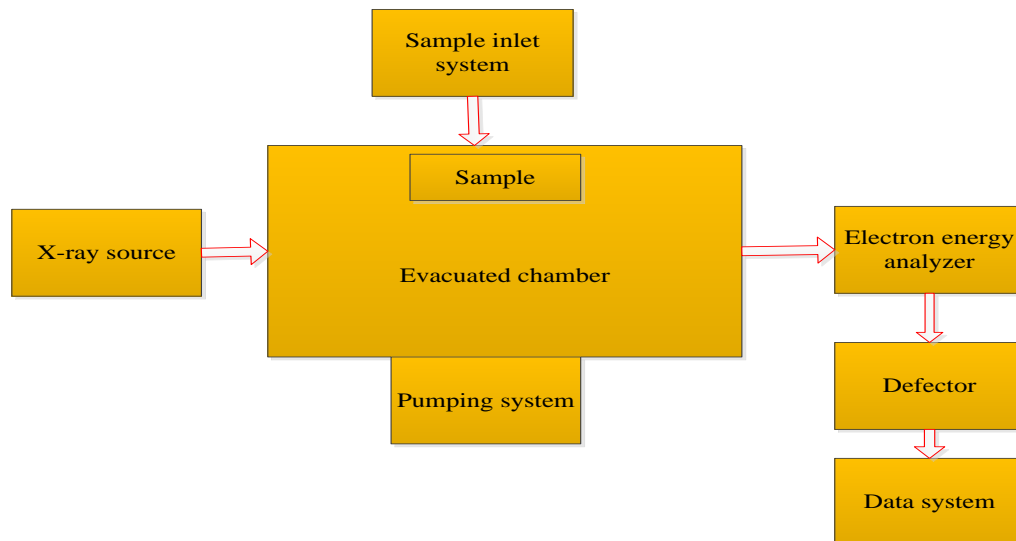


Figure 3-17: Typical block diagram of an XPS spectrometer analysis

The next Chapter of this work will provide comprehensive results and discussion using the apparatus, testing materials and procedures that were described above.

CHAPTER 4

Results and Discussions

4.1 Introduction

The experimental determination of the effect of acetic acid, mono-ethylene glycol and organic corrosion inhibitors on CO₂ corrosion of carbon steel under certain conditions at 25°C, 50°C and 80°C have been studied using the weight loss, electrochemical and surface analysis methods. This Chapter presents results and discussion of the results obtained from Phase – I, Phase – II and Phase - III of this study. The results of the weight loss (Phase - I) are presented first, followed by the results obtained from the electrochemical (Phase - II) tests and thereafter, the results obtained from the surface analysis (Phase - III) and the XPS tests are presented.

4.2 Phase – I: Weight loss

The Variations of average weight loss of carbon steel samples as a function of time in the presence of different concentrations of acetic acid, HAc are presented. The weight loss of the first test solution (3.5% wt. NaCl solution only), the second test solution (3.5% wt. NaCl solution with 500ppm), the third test solution (3.5% wt. NaCl solution with 1000ppm), and the four test solution (3.5% wt. NaCl solution with 2500ppm) at 25°C, 50°C and 80°C are presented in Figure 4-1 to Figure 4-3 and summarized in Table 4-1. The weight loss results had been converted to corrosion rate (mm/yr) for easy presentation and analyses using equation 3-1 to equation 3-3 respectively.

4.2.1 Weight loss with HAc

Figure 4-1 to Figure 4-3 shows the corrosion of carbon steel coupons immersed in 3.5% wt. NaCl solution in the presence of different concentrations of HAc at different temperatures studied. It is observed that an increase in the concentration of HAc leads to a general increase in corrosion rate irrespective of the concentrations added to the solutions. The corrosion rate for the blank solutions at all temperatures tested are lower compared to the corrosion rates with addition of HAc.

At 25°C (Figure 4-1), the corrosion rate at blank solution after 24hrs experiment is 0.72 mm/yr. On addition of 500ppm HAc, the corrosion rate increase to 0.86 mm/yr. Further addition of 2500ppm of HAc increases the corrosion rate drastically to 1.05 mm/yr. Similarly, after 168 hours test, the corrosion rate with 500ppm HAc raises to 1.31 mm/yr and 2.34 mm/yr on addition of 2500ppm HAc. These are detrimental increase in corrosion rate which are far above acceptable limits.

At 50°C (Figure 4-2), the corrosion rate for the blank solution is 0.70 mm/yr at the end of 24 hours test. Addition of 500ppm, 1000ppm and 2500ppm HAc also increased the corrosion rates to 0.85 mm/yr, 1.05 mm/yr and 1.67 mm/yr respectively. It is seen that a very low corrosion rate was observed after the durations of 168 hours experiments. After 168 hours test, the corrosion rate for 500ppm, 1000 ppm and 2500 ppm gradually increases to a maximum at 1.6 mm/yr, 2.54 mm/yr and 2.65 mm/yr at the end of the experiment.

Figure 4-3 shows a very high corrosion rate at 80°C even in the absence of HAc. It is noticed that the corrosion rate at blank solution is 1.5 mm/yr after 168 hours test. Addition of 500ppm and 2500ppm HAc accelerate the corrosion rate to approximately 2.04 mm/yr and 2.71 mm/yr respectively. Generally, it is noted that the increase in

corrosion rate observed on addition of different concentration of acetic acid is due to the presence of water and hydrogen ions contained in the acetic acid which influences the corrosion rate. The high corrosion rate observed at 80°C is however due to the fast reaction rate that occurs at higher temperatures. This confirmed that the rate of a chemical reaction increases with increased concentration of temperature and HAC.

Table 4-1 presents the summary of average corrosion rate as a function time for the conditions studied at 25°C, 50°C and 80°C. The error values in Table 4-1 show the percentage of error obtained after repeating the test for three times.

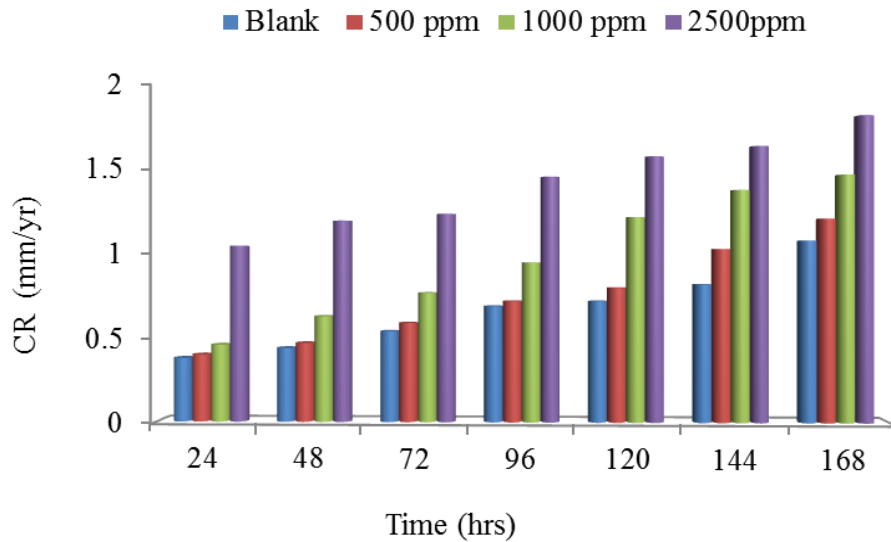


Figure 4-1: Corrosion rate as a function of time for 3.5% wt. NaCl solution containing HAc at 25°C.

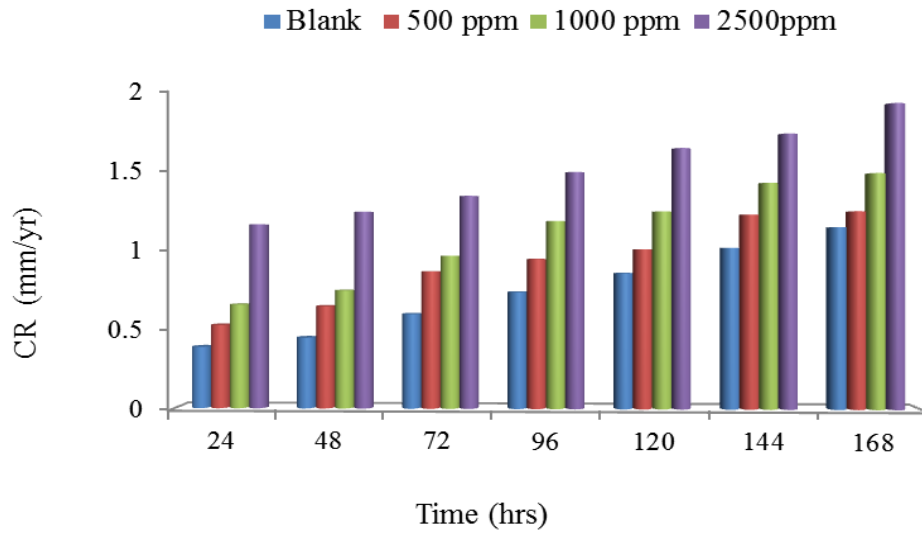


Figure 4-2: Corrosion rate as a function of time for 3.5% wt. NaCl solution containing HAC at 50°C

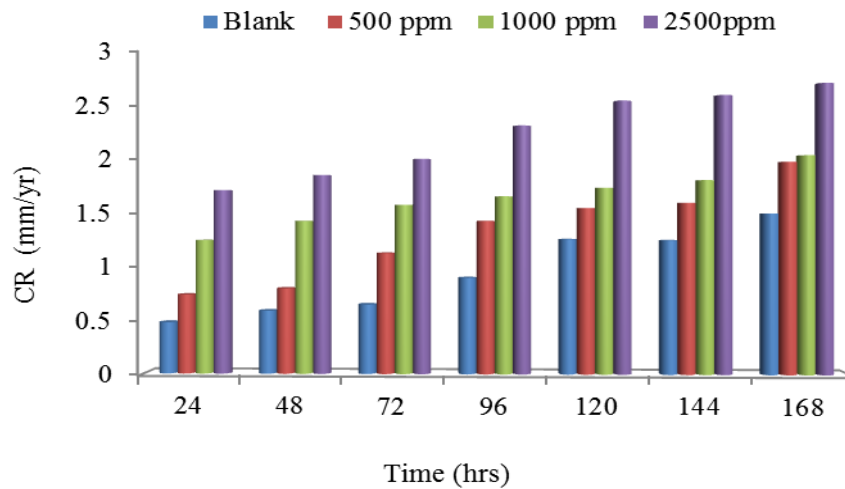


Figure 4-3: Corrosion rate as a function of time for 3.5% wt. NaCl solution containing HAC at 80°C

Table 4-1: Summary of average corrosion rate as a function of time for 3.5% wt. NaCl solution at 25°C, 50°C, 80°C.

T=25°C				
T(hrs)	0 ppm	500 ppm	1000 ppm	2500 ppm
24	0.38	0.4	0.46	1.05
48	0.44	0.47	0.63	1.2
72	0.54	0.59	0.77	1.24
96	0.69	0.72	0.95	1.46
120	0.72	0.8	1.22	1.58
144	0.82	1.03	1.38	1.64
168	1.08	1.21	1.47	1.82
ε (%)	0.04	0.01	0.02	0.05
T= 50°C				
T(hrs)	0 ppm	500 ppm	1000 ppm	2500 ppm
24	0.39	0.53	0.66	1.17
48	0.45	0.65	0.75	1.25
72	0.6	0.87	0.97	1.35
96	0.74	0.95	1.19	1.50
120	0.86	1.01	1.25	1.65
144	1.02	1.23	1.43	1.74
168	1.15	1.25	1.49	1.93
ε (%)	0.03	0.02	0.06	0.01
T=80°C				
T(hrs)	0 ppm	500 ppm	1000 ppm	2500 ppm
24	0.48	0.74	1.25	1.72
48	0.59	0.80	1.43	1.86
72	0.65	1.13	1.58	2.01
96	0.90	1.43	1.66	2.32
120	1.26	1.55	1.74	2.55
144	1.25	1.60	1.81	2.6
168	1.5	1.98	2.04	2.71
ε (%)	0.07	0.05	0.01	0.03

Weight loss with HAc and MEG

Figure 4-4 to Figure 4-12 present the weight loss of the carbon steel after 168 hours immersion in 3.5% wt. NaCl solution in the presence of HAc and MEG (rich MEG & lean MEG) at different temperatures. In general, it is observed that presence of MEG reduces the corrosion rate of carbon steel in all the condition tested.

At 25°C (Figure 4-4 to Figure 4-6), It is seen that a decreased in corrosion rate was observed in the solutions containing 20% and 80% MEG compared to the solutions without MEG. The corrosion rate for the solution with 500ppm HAc is approximately 1.6 mm/yr (Figure 4-4). On addition of 20% MEG and 80% MEG, the corrosion rate drops drastically to 1.31 mm/yr and 0.94 mm/yr after 168 hours of tests.

At 50°C (Figure 4-7 to Figure 4-9), the average corrosion rate after 168 hours immersion of carbon steel was 1.60 mm/yr. Addition of the lean MEG and rich MEG reduces the corrosion rate to 0.64 mm/yr and 0.81 mm/yr respectively. The decreased in corrosion rate in the presence of 20% MEG and 80% MEG concentrations are attributed to the reduction in pH of the solution.

At 80°C (Figure 4-10 to Figure 4-12), a lower corrosion rate is noticed in the presence of MEG. The corrosion rate decreased from 1.98 mm/yr in the presence of 500ppm HAc to 0.75 mm/yr and 0.78 mm/yr on addition of 20% and 80% MEG to the solutions. It is generally observed that the decreased in corrosion rate in the presence of MEG is due to the absorption of MEG on the carbon steel samples thereby hinder the cathodic and anodic reactions or interfere in the mechanism of cathodic and anodic reactions. This results corresponds with the result obtained using the electrochemical test in Phase – II results of this study. The summaries of results obtained from the weight loss test at different concentration of HAc, 20% MEG, 80% MEG and temperatures are presented in

Table 4-2 to Table 4-4. The percentage error was calculated from the average experiments after repeating each test for three times.

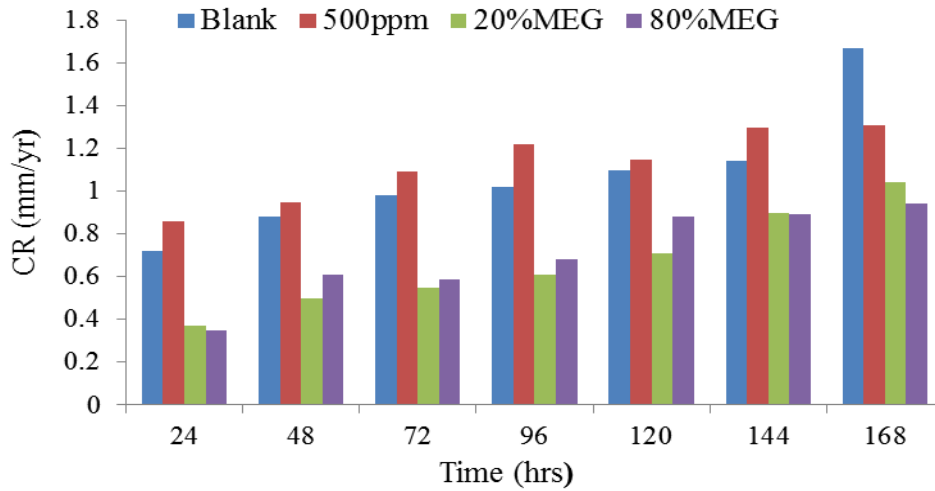


Figure 4-4: Corrosion rate as a function of time for solution with 500ppm HAc and MEG at 25°C.

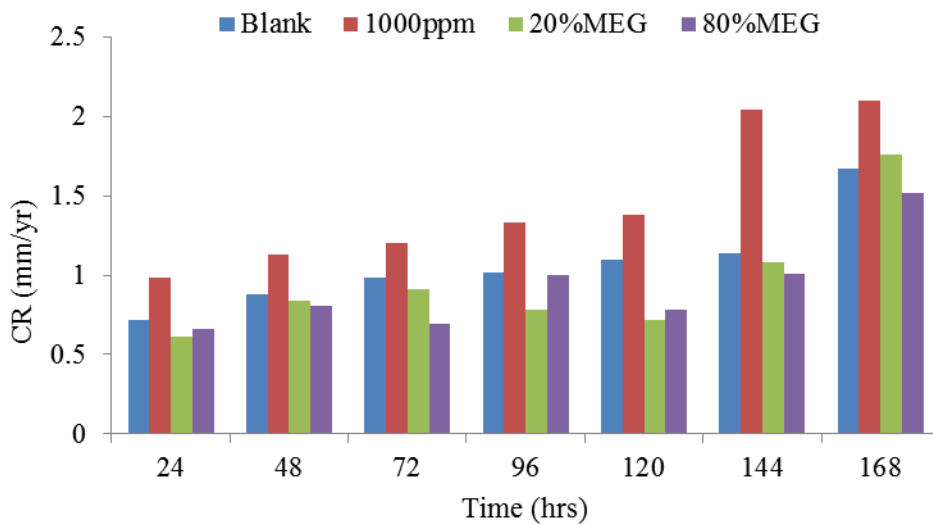


Figure 4-5: Corrosion rate as a function of time for solution with 1000ppm HAc and MEG at 25°C.

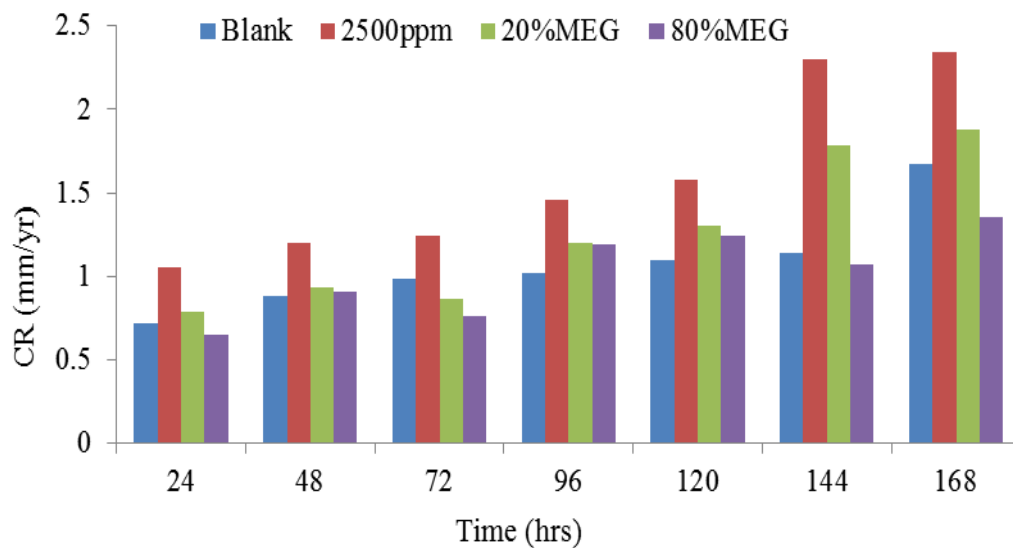


Figure 4-6: Corrosion rate as a function of time for solution with 2500ppm HAc and MEG at 25°C.

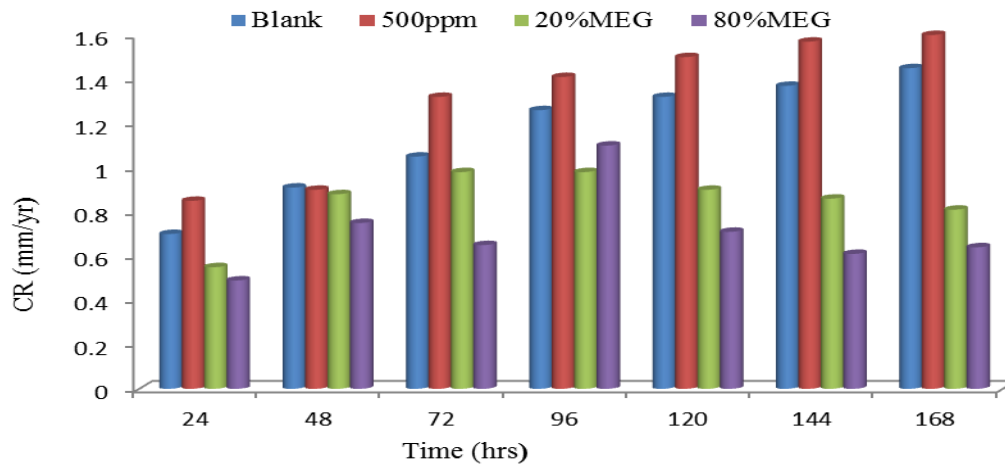


Figure 4-7: Corrosion rate as a function of time for solution with 500ppm HAc and MEG at 50°C.

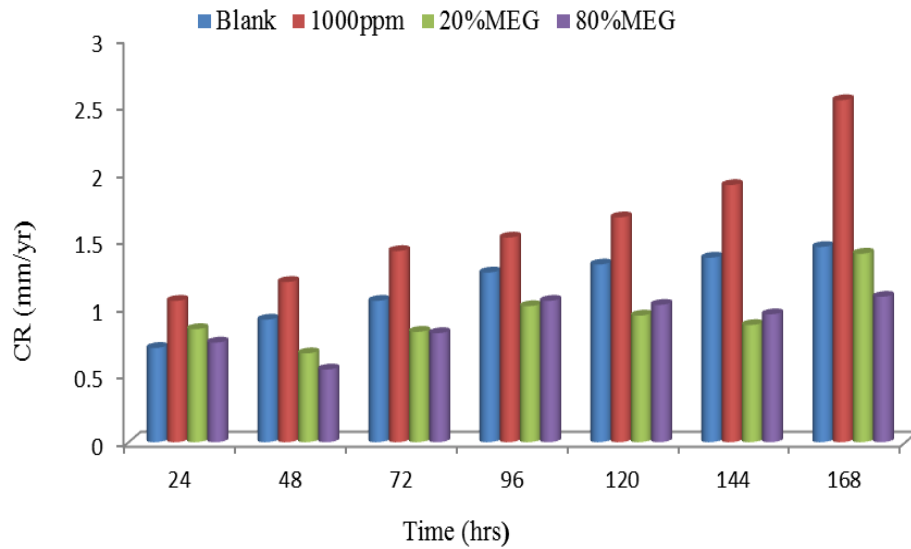


Figure 4-8: Corrosion rate as a function of time for solution with 1000ppm HAC and MEG at 50°C.

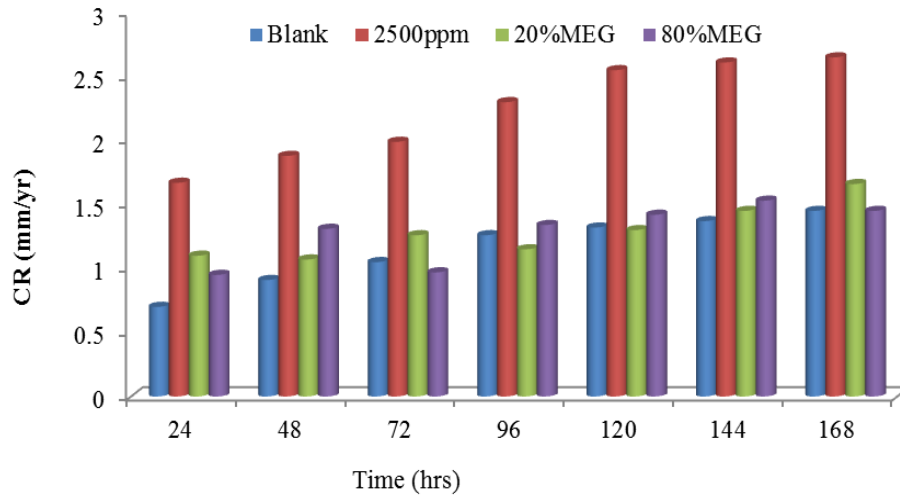


Figure 4-9: Corrosion rate as a function of time for solution with 2500ppm HAC and MEG at 50°C.

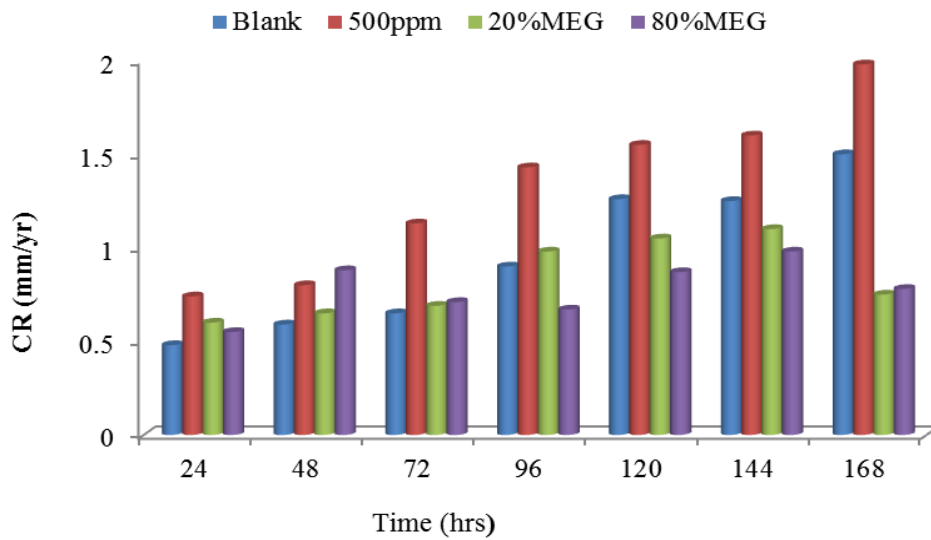


Figure 4-10: Corrosion rate as a function of time for solution with 500ppm HAC and MEG at 80°C.

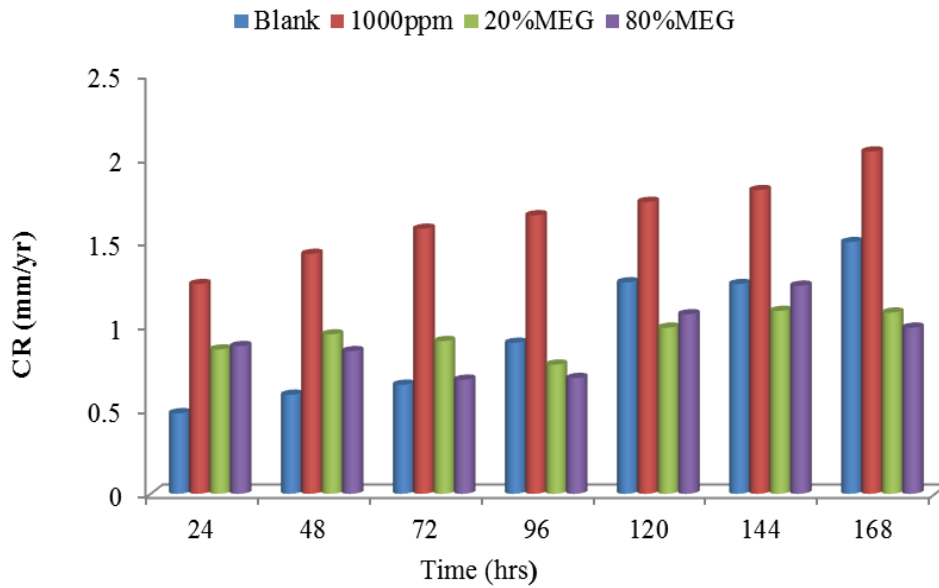


Figure 4-11: Corrosion rate as a function of time for solution with 1000ppm HAC and MEG at 80°C.

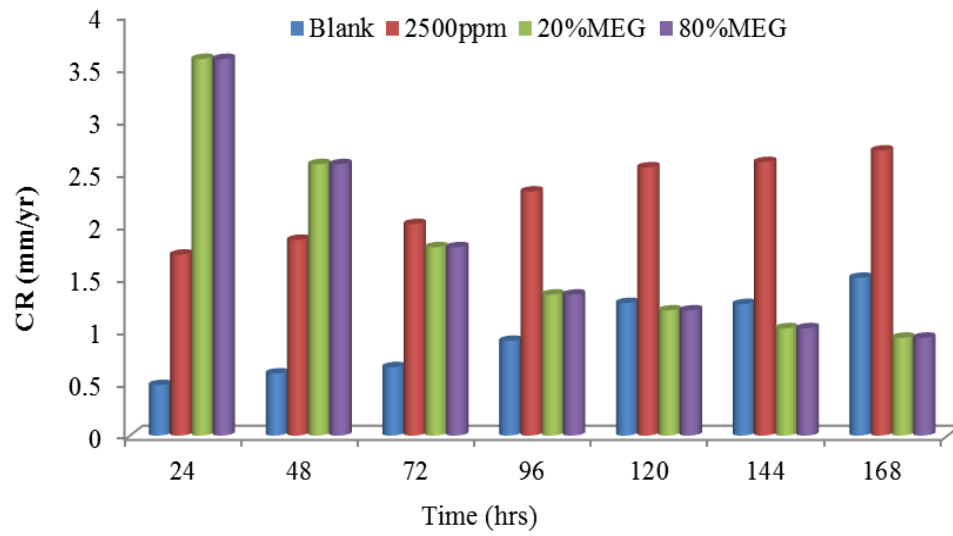


Figure 4-12: Corrosion rate as a function of time for solution with 2500ppm HAc and MEG at 80°C.

Table 4-2: Summary of average corrosion rate as a function of time solution containing HAc and MEG at 25°C.

Composition	Time (hours)							ϵ (%)
	24	48	72	96	120	144	168	
solution Only (Blank)	0.72	0.88	0.98	1.02	1.1	1.14	1.67	± 0.02
solution + 500ppm HAc	0.86	0.95	1.09	1.22	1.15	1.30	1.31	± 0.05
solution + 500ppm HAc + 20% MEG	0.37	0.50	0.55	0.61	0.71	0.90	1.04	± 0.01
solution + 500ppm HAc + 80% MEG	0.35	0.61	0.59	0.68	0.88	0.89	0.94	± 0.03
solution + 1000ppm HAc	0.98	1.13	1.20	1.33	1.38	2.04	2.1	± 0.08
solution + 1000ppm HAc + 20% MEG	0.61	0.84	0.91	0.78	0.72	1.08	1.76	± 0.01
solution + 1000ppm HAc + 80% MEG	0.66	0.81	0.69	1.0	0.78	1.01	1.52	± 0.04
solution + 2500ppm HAc	1.05	1.20	1.24	1.46	1.58	2.30	2.34	± 0.05
solution + 2500ppm HAc + 20% MEG	0.79	0.93	0.86	1.20	1.30	1.78	1.88	± 0.03
solution + 2500ppm HAc + 80% MEG	0.65	0.91	0.76	1.19	1.24	1.07	1.35	± 0.03

Table 4-3: Summary of average corrosion rate as a function of time solution containing HAc and MEG at 50°C.

Composition	Time (hrs)							ϵ(%)
	24	48	72	96	120	144	168	
solution Only (Blank)	0.70	0.91	1.05	1.26	1.32	1.37	1.45	± 0.01
solution + 500ppm HAc	0.85	0.90	1.32	1.41	1.50	1.57	1.60	± 0.05
solution + 500ppm HAc + 20% MEG	0.55	0.88	0.97	0.98	0.90	0.86	0.81	± 0.04
solution + 500ppm HAc + 80% MEG	0.49	0.75	0.65	1.1	0.71	0.61	0.64	± 0.02
solution + 1000ppm HAc	1.05	1.19	1.42	1.52	1.67	1.91	2.54	± 0.04
solution + 1000ppm HAc + 20% MEG	0.84	0.66	0.82	1.01	0.94	0.87	1.40	± 0.01
solution + 1000ppm HAc + 80% MEG	0.74	0.54	0.81	1.05	1.02	0.95	1.08	± 0.03
solution + 2500ppm HAc	1.67	1.88	1.92	2.30	2.55	2.61	2.65	± 0.06
solution + 2500ppm HAc + 20% MEG	1.10	1.07	1.26	1.15	1.30	1.45	1.66	± 0.05
solution + 2500ppm HAc + 80% MEG	0.95	1.31	0.97	1.34	1.42	1.53	1.45	± 0.05

Table 4-4: Summary of average corrosion rate as a function of time solution containing **HAc** and MEG at 80°C.

Composition	Time (hrs)							ε (%)
	24	48	72	96	120	144	168	
solution Only (Blank)	0.48	0.59	0.65	0.90	1.26	1.25	1.50	±0.03
solution + 500ppm HAc	0.74	0.80	1.13	1.43	1.55	1.60	1.98	±0.02
solution + 500ppm HAc + 20% MEG	0.60	0.65	0.69	0.98	1.05	1.10	0.75	±0.01
solution + 500ppm HAc + 80% MEG	0.55	0.88	0.71	0.67	0.87	0.98	0.78	±0.03
solution + 1000ppm HAc	1.25	1.43	1.58	1.66	1.74	1.81	2.04	±0.06
solution + 1000ppm HAc + 20% MEG	0.86	0.95	0.91	0.77	0.99	1.09	1.08	±0.05
solution + 1000ppm HAc + 80% MEG	0.88	0.85	0.68	0.69	1.07	1.24	0.99	±0.02
solution + 2500ppm HAc	1.72	1.86	2.01	2.32	2.55	2.60	2.71	±0.03
solution + 2500ppm HAc + 20% MEG	0.58	0.74	1.21	1.34	1.19	1.02	0.93	±0.05
solution + 2500ppm HAc + 80% MEG	0.77	0.69	0.92	1.28	1.54	1.09	1.91	±0.05

4.2.2 Weight loss with HAc, MEG and corrosion inhibitors

Figure 4-13 to Figure 4-21 present the weight loss results of carbon steel after 168 hours test in 3.5% wt NaCl solutions with 20% MEG, 80% MEG and three corrosion inhibitors. A decrease in the corrosion rate is achieved as a result of inhibitors added to the system. The increase in concentrations of the inhibitors also leads to the increase in surface coverage of the electrode and efficiency of the inhibition.

Figure 4-13 to Figure 4-15 show that the corrosion rate with HAc and MEG are 1.6 mm/yr and 1.2 mm/yr at 25°C. Injection of inhibitors reduces the corrosion rate drastically to a lower rate. The average corrosion rate with the presence of inhibitors is below 0.4 mm/yr after 168 hours test. This decrease in metal loss with inhibitors implies the inhibitors are absorbed on the surface of the carbon steel thereby preventing the reaction process of the cathodic and anodic reactions.

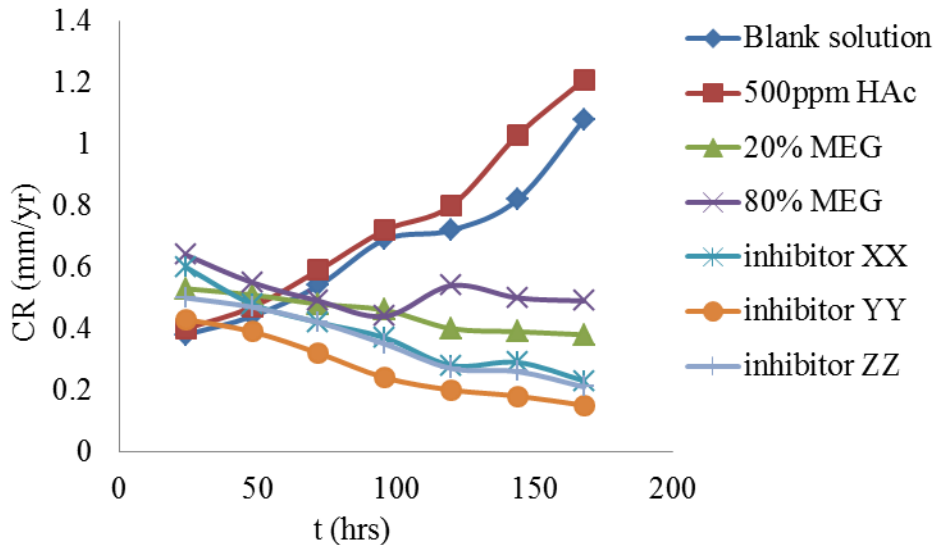


Figure 4-13: Variation of corrosion rate as a function of immersion time recorded for carbon steel sample in 3.5% wt. NaCl solution containing 500ppm HAc MEG and inhibitors at 25°C

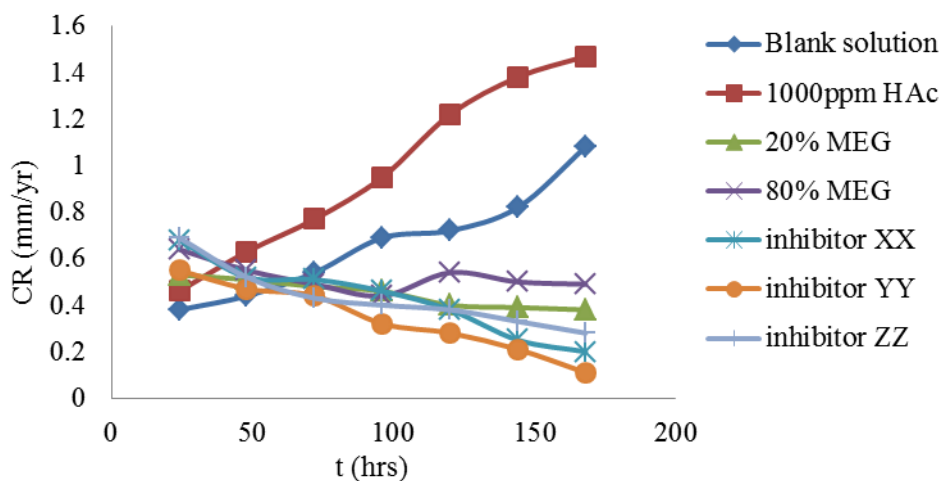


Figure 4-14: Variation of corrosion rate as a function of immersion time recorded for carbon steel sample in 3.5% wt. NaCl solution containing 1000ppm HAC, MEG and inhibitors at 25°C

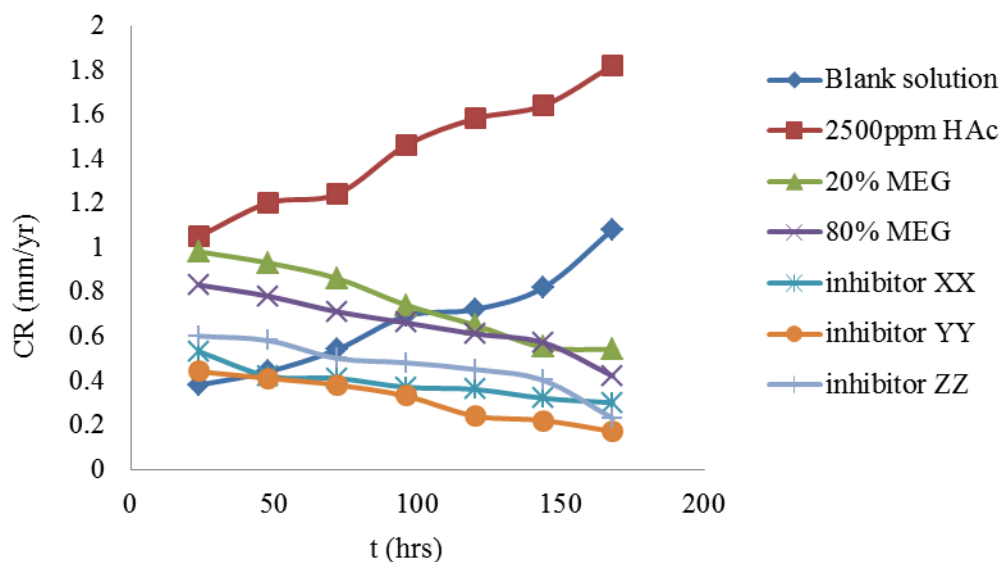


Figure 4-15: Variation of corrosion rate as a function of immersion time recorded for carbon steel sample in 3.5% wt. NaCl solution containing 2500ppm HAC, MEG and inhibitors at 25°C

At 50°C (Figure 4-16 to Figure 4-18), it is easily observed that the corrosion rate with and without inhibitors shows similar trends to the corrosion rate at 25°C., It is observed that inhibitor YY has lower corrosion rate compared to inhibitor XX and inhibitor ZZ. The final corrosion rate after 168 hours test is approximately 0.2 mm/yr. The results signified that the inhibitors are been absorbed to the surface of the electrode. This result is not in agreement with the results obtained by Hassan et al [83] which reveals that 5 ppm of the inhibitors is the most efficient due to its high inhibition performance. Figure 4-16 to Figure 4-18 also indicates that the inhibition efficiency increases with increase in concentration of the inhibitors applied.

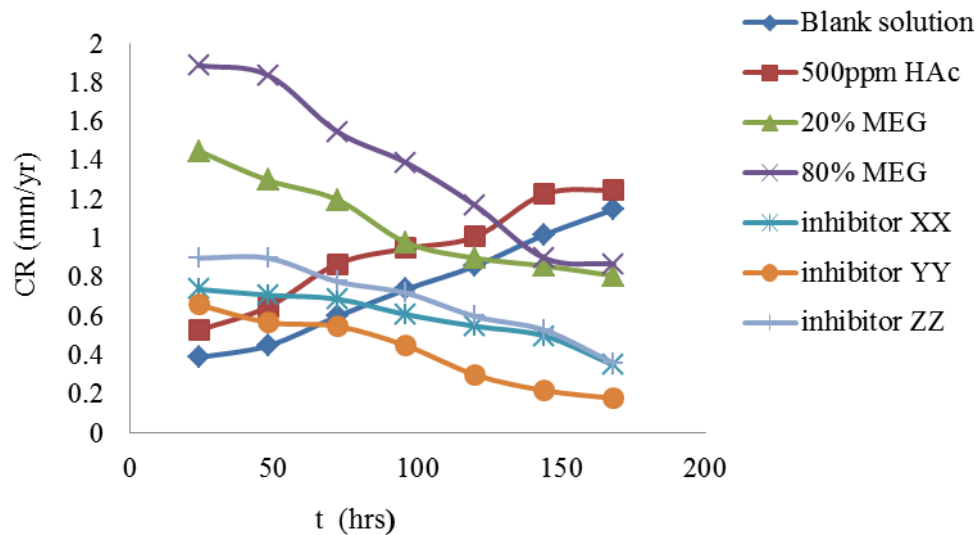


Figure 4-16: Variation of corrosion rate as a function of immersion time recorded for carbon steel sample in 3.5% wt. NaCl solution containing 500ppm HAc, MEG and inhibitors at 50°C

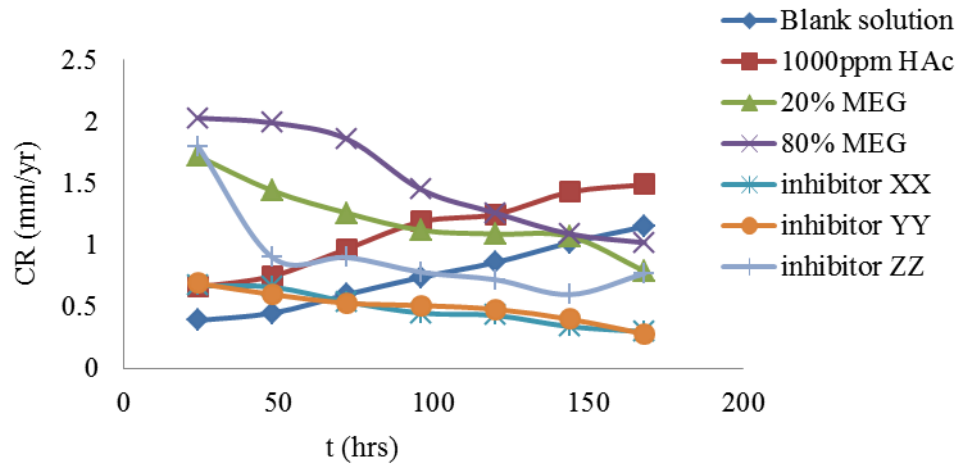


Figure 4-17: Variation of corrosion rate as a function of immersion time recorded for carbon steel sample in 3.5% wt. NaCl solution containing 1000ppm HAc, MEG and inhibitors at 50°C

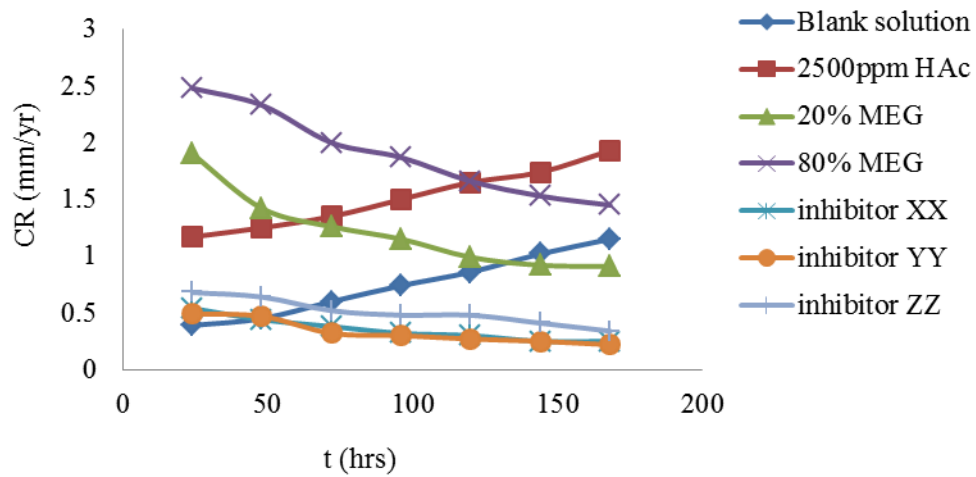


Figure 4-18: Variation of corrosion rate as a function of immersion time recorded for carbon steel sample in 3.5% wt. NaCl solution containing 2500ppm HAc, MEG and inhibitors at 50°C

The variation of inhibition efficiencies as a function of time calculated from the weight loss measurements for three types of inhibitors at 80°C are presented in Figure 4-19 to Figure 4-21. It is observed that the corrosion rate decreases with increase in inhibitor concentrations resulted in increased in inhibition efficiencies. The decreased in corrosion rate observed in Figure 4-19 to Figure 4-21 with the inhibitors are as a results of absorption and possible coverage of the inhibitor on the electrode surface. This indicates that higher absorption of the inhibitors on the carbon steel results in higher efficiencies of inhibition. Similar results was also reported by Xinglong et al [84] in his work on inhibition of the corrosion of cold rolled steel in hydrochloric acid solution by Tween-40. Comparing the results obtained to the results at 25°C and 50°C, it is obvious that increase in temperature decreases the inhibition efficiency showing that at higher temperature, corrosion of carbon steel prevails on absorption of the inhibitors at the electrode surface. This shows the effect of temperature on inhibited electrode-electrolyte reaction is complex.

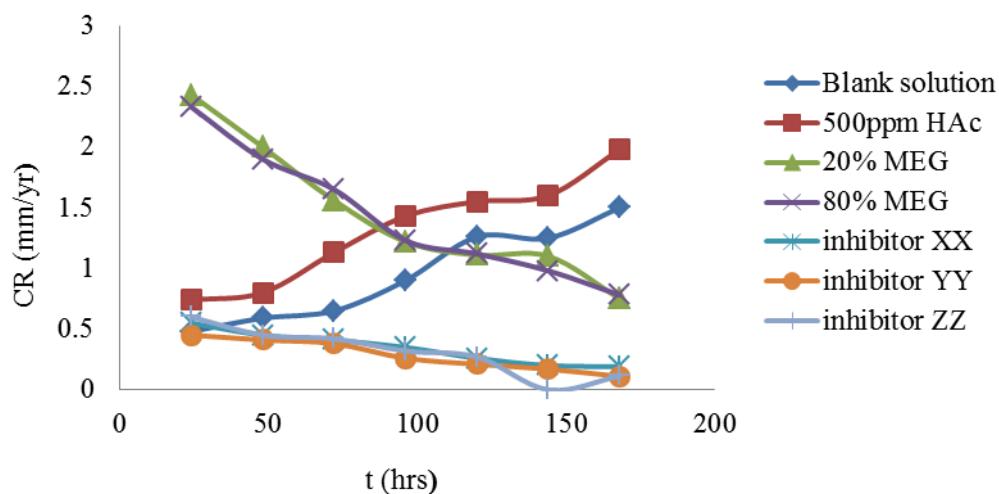


Figure 4-19: Variation of corrosion rate as a function of immersion time recorded for carbon steel sample in 3.5% wt. NaCl solution containing 500ppm HAC, MEG and inhibitors at 80°C

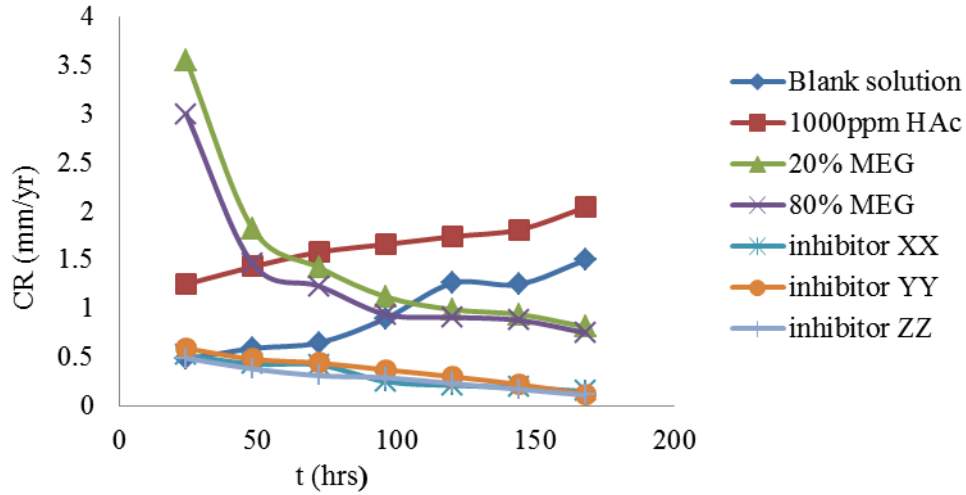


Figure 4-20: Variation of corrosion rate as a function of immersion time recorded for carbon steel sample in 3.5% wt. NaCl solution containing 1000ppm HAC, MEG and inhibitors at 80°C

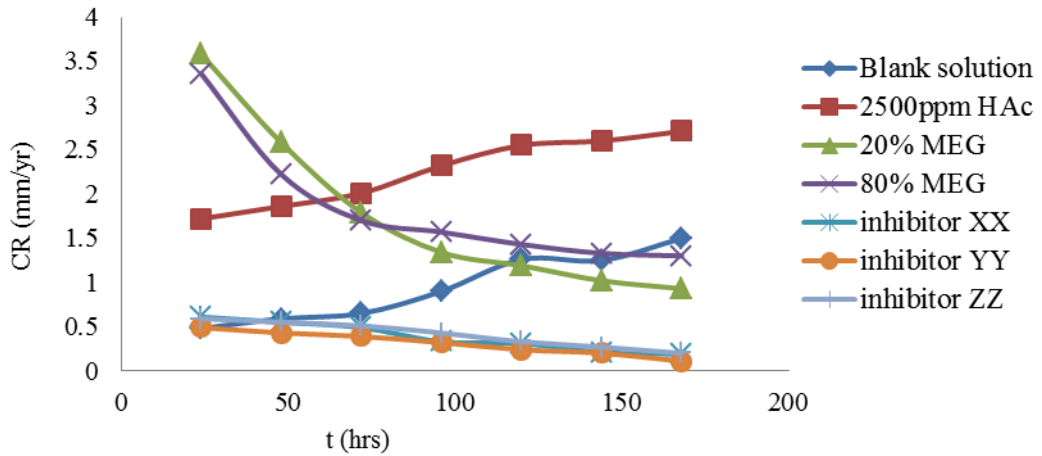


Figure 4-21: Variation of corrosion rate as a function of immersion time recorded for carbon steel sample in 3.5% wt. NaCl solution containing 2500ppm HAC, MEG and inhibitors at 80°C

4.3 Phase – II: Electrochemical test results

The open circuit potential (OCP) measures the corrosion potential E_{corr} of a corroding metal in a given solution when no current is passed over it. The OCP provide the basis for assessing the corrosion condition of a given electrode with respect to time. However, it is imperative to measure the OCP of a working electrode to ascertain regions of corrosion attack. A positive E_{corr} can be attributed to formation of physical barriers on the electrode that makes it less susceptible to corrosion, while a negative E_{corr} is an indication that the electrode is in active state and metal dissolution is possible.

In this section of the study, the variations of OCP of the carbon steel was measured as a function of time in 3.5% wt. NaCl solution containing different concentrations of HAC at different temperatures. These were carefully carried out to evaluate the effect of HAC on the Potential of carbon steel.

4.3.1 OCP with HAC

The variations of OCP of carbon steel electrode as a function of time in different concentrations of HAC for a period of 2 hours is shown in Figure 4-22 to Figure 4-24. From the plots (Figure 4-22 to Figure 4-24), it is seen that the potential of the electrode move upwards to the direction of positive potentials stipulating an initial corroding process of pre-immersion, air formed oxide film and an attack on the electrode. However, a stable potential were attained which coincide to the free corrosion potential of the working electrode. The different values of OCP and other parameters obtained from the polarization measurements of carbon steel samples immersed in 3.5% wt. NaCl solution containing 0ppm, 500ppm, 1000ppm, and 2500ppm of HAC at 25°C, 50°C and 80°C respectively are given in Table 4-5 to Table 4-7.

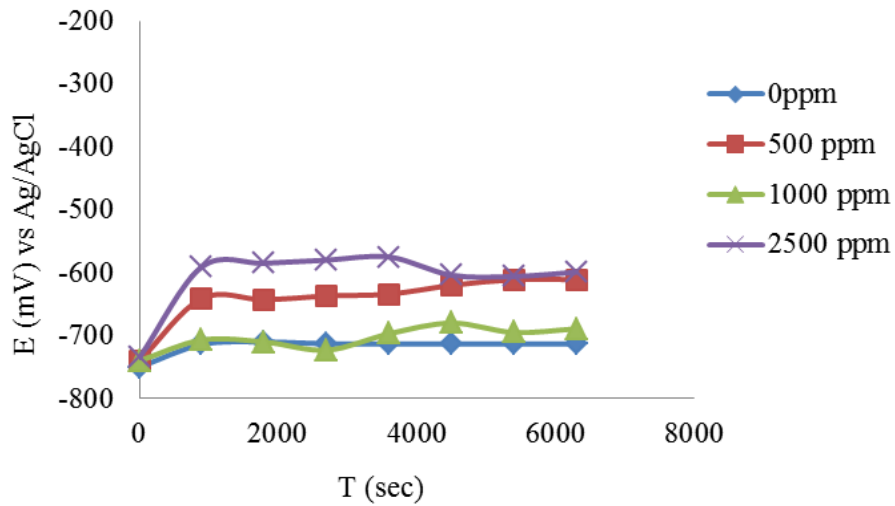


Figure 4-22: Corrosion potential of carbon steel electrodes immersed in 3.5% wt. NaCl solution containing different concentrations of HAc at 25°C

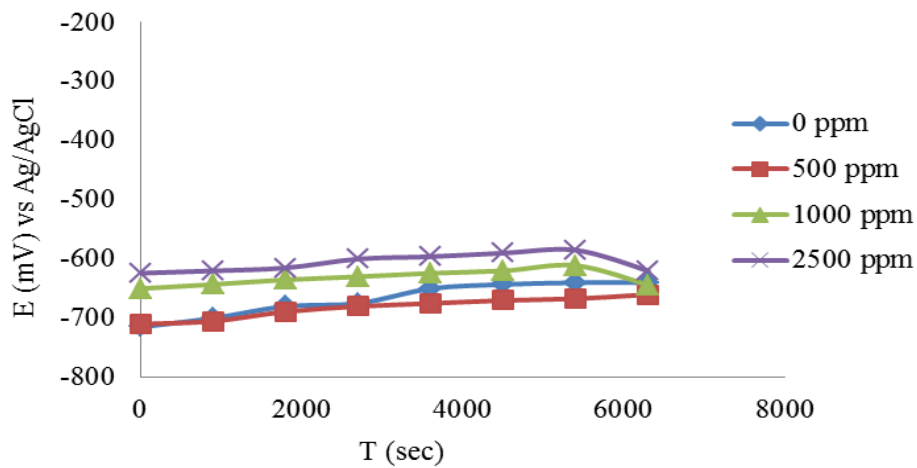


Figure 4-23: Corrosion potential of carbon steel electrodes immersed in 3.5% wt. NaCl solution containing different concentrations of HAc at 50°C

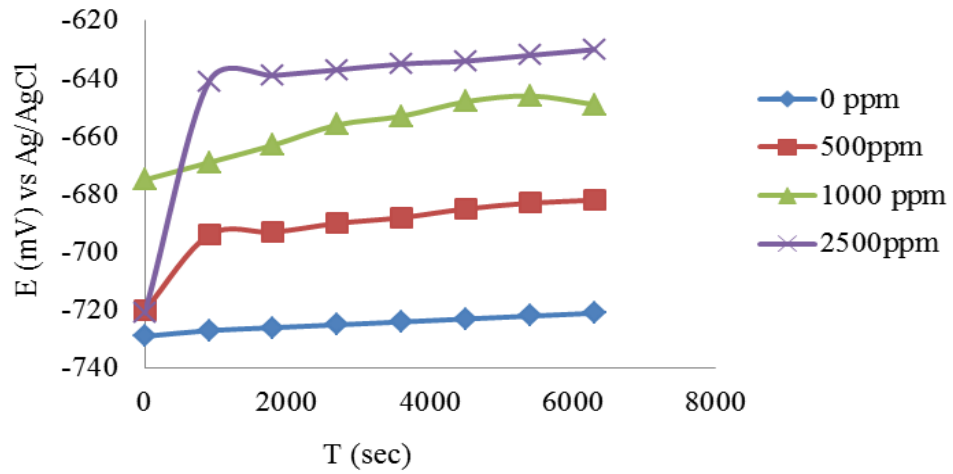


Figure 4-24: Corrosion potential of carbon steel electrodes immersed in 3.5% wt. NaCl solution containing different concentrations of HAC at 80°C

Table 4-5: corrosion parameters obtained from polarization curves for carbon steel samples immersed in solution containing HAC at 25°C

Conc(ppm)	OCP(mV)	E _{corr} (mV)	B	I _{corr} (mA/cm ²)	CR(mm/yr)
0	-750	-739	26	35.18	2.59
500	-740	-738	26	35.23	2.60
1000	-740	-735	26	35.37	2.61
2500	-735	-730	26	35.61	2.63
E (%)	±0.01	±0.02	±0.05	±0.05	±0.03

Table 4-6: corrosion parameters obtained from polarization curves for carbon steel samples immersed in solution containing HAc at 50°C

Conc(ppm)	OCP(mV)	E _{corr} (mV)	B	I _{corr} (μ A/cm ²)	CR(mm/yr)
0	-715	-712	26	36.52	2.70
500	-710	-695	26	37.41	2.76
1000	-650	-644	26	40.37	2.97
2500	-624	-618	26	42.07	3.10
(%) ϵ	± 0.05	± 0.02	± 0.01	0.03	± 0.05

Table 4-7: corrosion parameters obtained from polarization curves for carbon steel samples immersed in solution containing HAc at 80°C

Conc(ppm)	OCP(mV)	E _{corr} (mV)	(B)	I _{corr} (mA/cm ²)	CR(mm/yr)
0	-729	-690	26	37.68	2.78
500	-720	-650	26	40	2.95
1000	-675	-630	26	41.26	3.04
2500	-721	-615	26	42.27	3.12
(%) ϵ	± 0.02	± 0.04	± 0.03	± 0.02	± 0.05

4.3.2 OCP with HAc and MEG

Figure 4-25 to Figure 4-27 shows the plots of OCP as a function of time for carbon steel samples immersed in solution with the lean and rich MEG at different concentrations of

HAc after 6 hours tests. At equilibrium, no current was applied to the electrode and the net cathodic and anodic current was equal to zero. The OCP shows the rate of corroding on the electrode in the solutions as current was applied.

At 25°C (Figure 4-25), the OCP for the blank solution was approximately -521 mV after 6 hours of tests. Addition of 20% MEG and 80% MEG to different concentrations of HAc in the solutions raises the OCP -519 mV and -517 mV.

At 50°C (Figure 4-26), the OCP for the 3.5% wt. NaCl (blank) solution is approximately -604 mV. The addition of the lean and rich MEG increases the OCP to maximum values of -599 mV and -590 mV respectively. This implies that increase in the concentration of MEG increases the anodic reaction of the metal and reduces the corrosion rate. The addition of MEG at 80°C (Figure 4-27) also show a similar trends to those at 25°C and 50°C. At 80°C (Figure 4-27), the values of the OCP are reduced on addition of 20% MEG and 80% MEG as noticed. The OCP for the 3.5% wt. NaCl solution without MEG and HAc is approximately -625 mV after 6 hours of test. Injection of the lean MEG and the rich MEG elevates OCP to -624 mV and -623 mV respectively. These values show a little reduction in the values of the OCP at high temperature. Table 4-8 to Table 4-10 shows the OCP, E_{corr} , i_{corr} and corrosion rate values obtained from the polarization measurements.

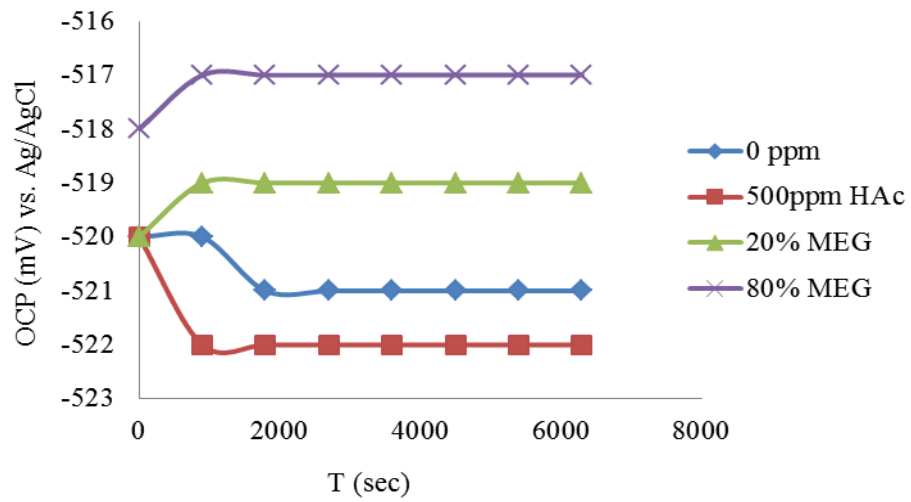


Figure 4-25: Free corrosion potential of carbon steel samples immersed in 3.5% wt. NaCl solutions containing HAc, 20% MEG and 80% MEG at 25°C

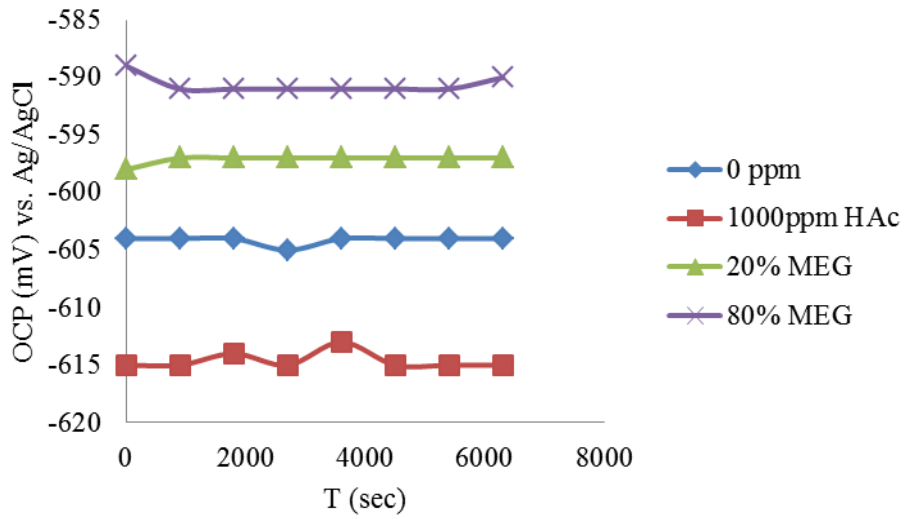


Figure 4-26: Free corrosion potential of carbon steel samples immersed in 3.5% wt. NaCl solutions containing HAc, 20% MEG and 80% MEG at 50°C

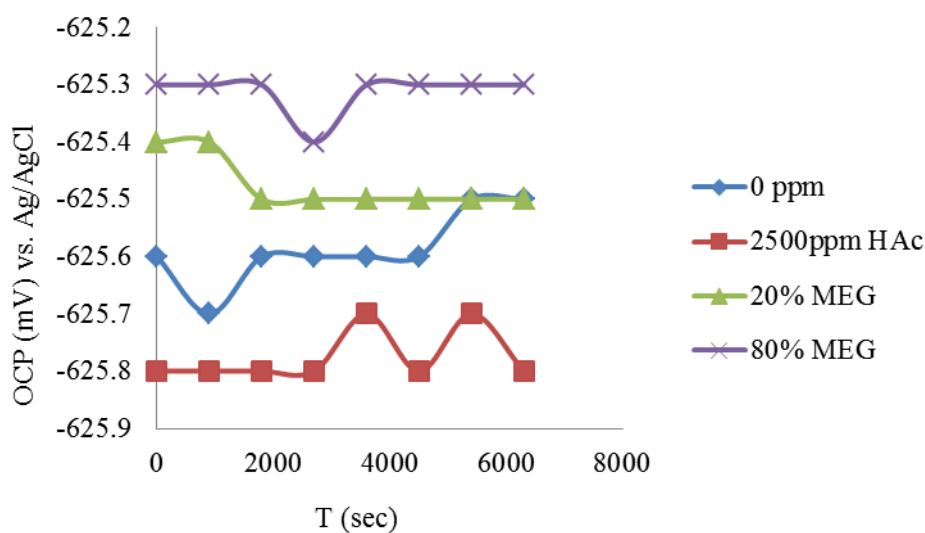


Figure 4-27: Free corrosion potential of carbon steel samples immersed in 3.5% wt. NaCl solutions containing HAc, 20% MEG and 80% MEG at 80°C

Table 4-8: corrosion parameters obtained from polarization measurements of carbon steel samples in solutions containing HAc and MEG at 25°C

Conc(ppm)	OCP(mV)	E _{corr} (mV)	B	I _{corr} (mA/cm ²)	CR(mm/yr)
0	-548	534	26	33.50	2.47
500	-537	534	26	48.68	3.58
1000	-521	517	26	50.29	3.70
2500	-546	540	26	48.14	3.54
(%) ε	±0.02	±0.01	±0.05	±0.02	±0.03

Table 4-9: corrosion parameters obtained from polarization measurements of carbon steel samples in solutions containing HAc and MEG at 50°C

Conc(ppm)	OCP(mV)	Ecorr(mV)	B	icorr(mA/cm²)	CR(mm/yr)
0	-591	604	26	43.04	3.17
500	-594	615	26	42.27	3.11
1000	-593	629	26	41.33	3.04
2500	-604	631	26	41.20	3.03
(%) ε	± 0.05	± 0.01	± 0.03	± 0.05	± 0.03

Table 4-10: corrosion parameters obtained from polarization measurements of carbon steel samples in solutions containing HAc and MEG at 80°C

Conc(ppm)	OCP(mV)	Ecorr(mV)	B	icorr(mA/cm²)	CR(mm/yr)
0	620	615	26	35.61	2.62
500	627	631	26	35.71	2.63
1000	642	656	26	35.96	2.65
2500	627	738	26	35.23	2.60
(%) ε	± 0.03	± 0.02	± 0.05	± 0.01	± 0.02

4.3.3 LPR results

The effect of different concentrations of HAc on the corrosion rate of carbon steel in 3.5% wt. NaCl solution were evaluated using the linear polarization resistance (LPR) technique. In this study and for the LPR measurements, the potential of the working electrode was scanned from -5 mV to +5 mV versus corrosion potential at a scan rate of 0.1 mV/s resulted in a straight line graph.

Figure 4-28 and Figure 4-29 shows a linear relationship of potential E_{corr} as a function of corrosion current density, i_{corr} for carbon steel samples after 6 hours immersion in solution containing different concentrations of HAc at 25°C and 80°C respectively. The slope obtained from the linear graph gives the polarization resistance, R_p . However, the corrosion rate is calculated from the measured polarization resistance R_p , using equation 4-1 to equation 4-4. From Figure 4-28 and Figure 4-29, it is noticed that both graphs exhibit a linear relationship between the potential and corrosion current density. Table 4-5 to Table 4-10 summarizes the results obtained from the LPR measurements at all temperatures studied.

$$R_p = \left(\frac{\Delta E}{\Delta i} \right) \quad 4-1$$

$$i_{\text{Corr}} = \frac{\beta}{R_p} \quad 4-2$$

$$\beta = \frac{\beta_a \beta_c}{2.303(b_a b_c)} \quad 4-3$$

$$CR = \frac{i_{\text{Corr}} \times M_w}{n \times F \times \rho} \text{ (mm/yr)} \quad 4-4$$

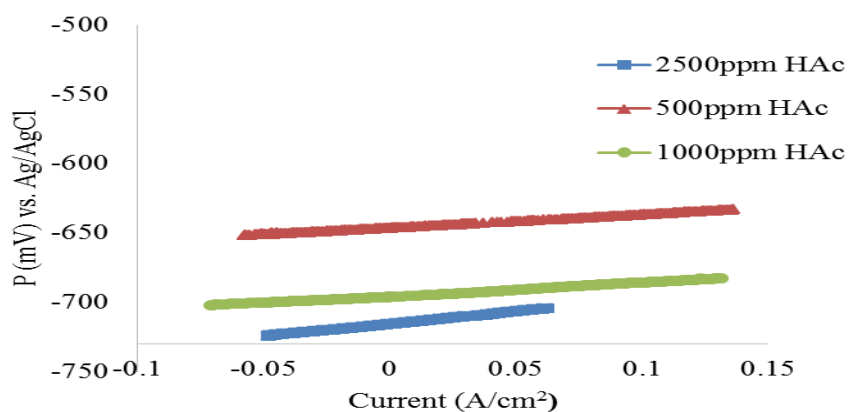


Figure 4-28: LPR measurements of carbon steel samples immersed in solution containing different concentrations of HAc at 25°C

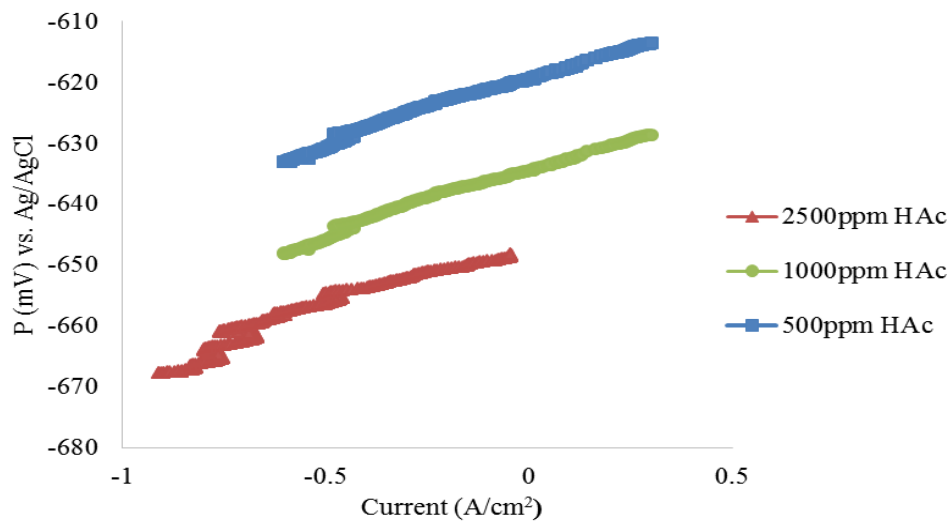


Figure 4-29: LPR measurements of carbon steel samples immersed in solution containing different concentrations of HAc at 80°C

4.3.4 EIS results

In electrochemistry, the linear polarization resistance (LPR) demonstrates only the changes in dissolution of the steel surface under certain conditions. On the other hand, the electrochemical impedance spectroscopies (EIS) are used as an alternative measurement to explain the mechanisms of electrochemical reactions that may occur at the metal-electrolyte interface.

In this study, the EIS was used to demonstrate the effect of acetic acid on CO₂ corrosion of carbon steel samples in 3.5% wt. NaCl solution. The impedance spectra was reported at the OCP and in the frequency range of 5KHz to 0.01Hz and alternative current amplitude of ± 5 mV.

(i) EIS with HAc

Figure 4-30 to Figure 4-35 presents the Nyquist and Bode experimental curves measured on the carbon steel coupons in CO₂ saturated environment at 25°C, 50°C, 80°C and at different concentrations of HAc.

It is seen (Figure 4-30 to Figure 4-35) that a large capacitive semi-circle at high frequencies are observed in the absence of HAc which is considered as the capacitance of double electrode layer between the electrode and the solution. On addition of more concentrations of HAc to the solution, the high frequency semi-circle decreases in size signifies an increase in corrosion rate and decrease in protectiveness of FeCO₃ layer that could have been formed. From the Bode plots (Figure 4-31, Figure 4-33 and Figure 4-35); the regions with high frequencies are regarded as the more porous medium with little or no protective layer. On the other hand, the low frequencies regions are the less porous region where a protective layer formation can be possible. If the protective layers are completely impact, the corrosion is controlled by a diffusion transfer process, while it is a charge transfer process when the protective layer is more porous at the electrode-electrolyte interface.

To confirm and verify the results obtained by the Nyquist and Bode plots, an equivalent circuit model diagram in Figure 4-36 was used to interpret results obtained from the plot. From Figure 4-36, R_s is the solution resistance, C_{dl} is the double layer capacitance, and R_t is the capacitive double layer. Table 4-11 to Table 4-13 summarizes the data obtained from the equivalent circuit diagram for different conditions studied.

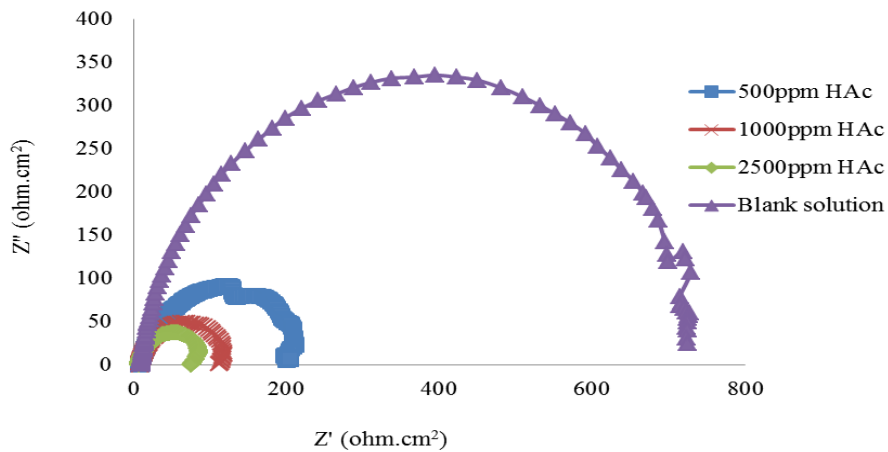


Figure 4-30: Nyquist plots for carbon steel samples in solutions containing HAc at 25°C after 6 hours

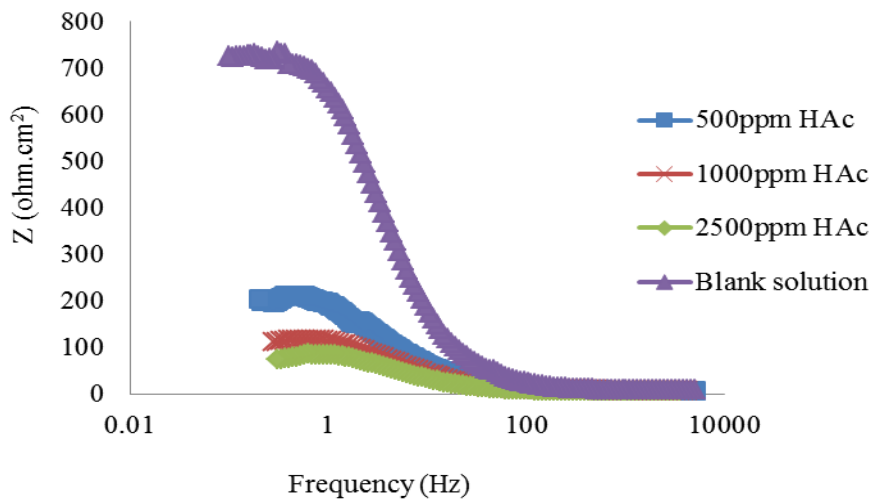


Figure 4-31: Bode plots for carbon steel samples in solutions containing HAc at 25°C after 6 hours

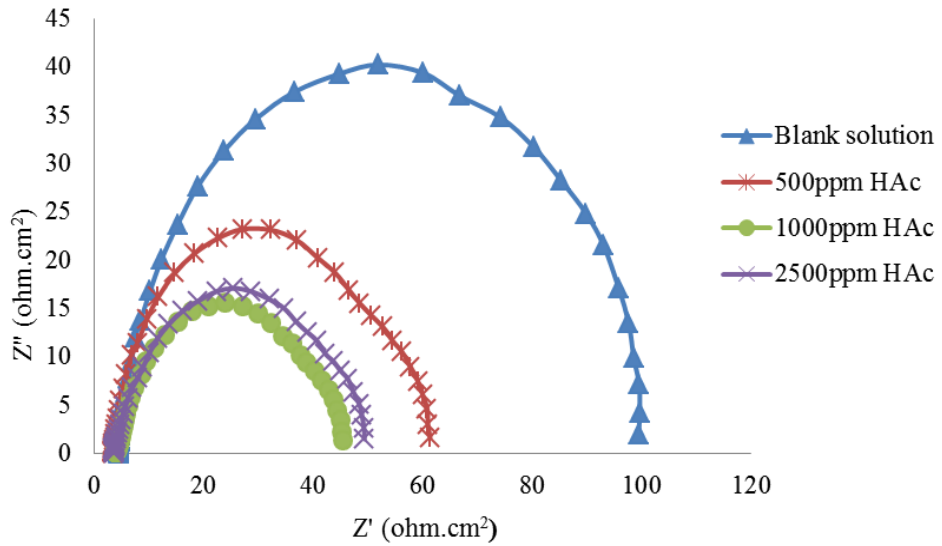


Figure 4-32: Nyquist plots for carbon steel samples in solutions containing HAc at 50°C after 6 hours

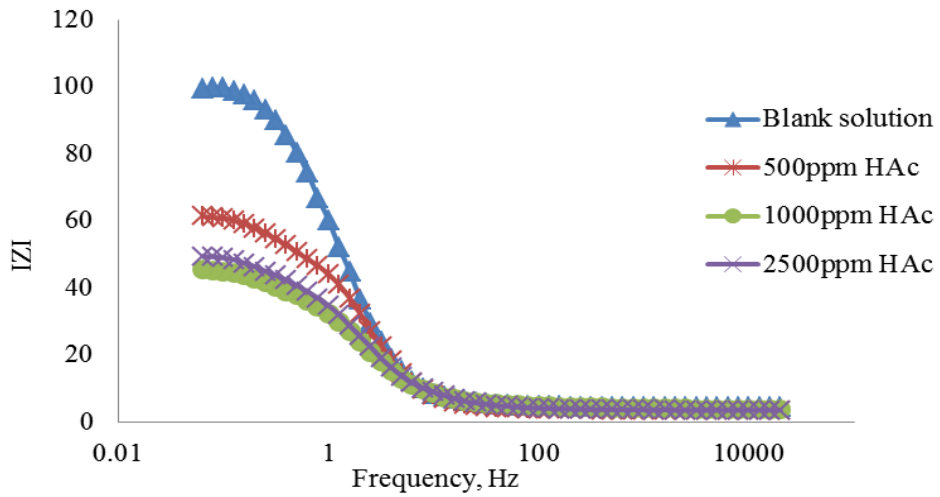


Figure 4-33: Bode plots for carbon steel samples in solutions containing HAc at 50°C after 6 hours

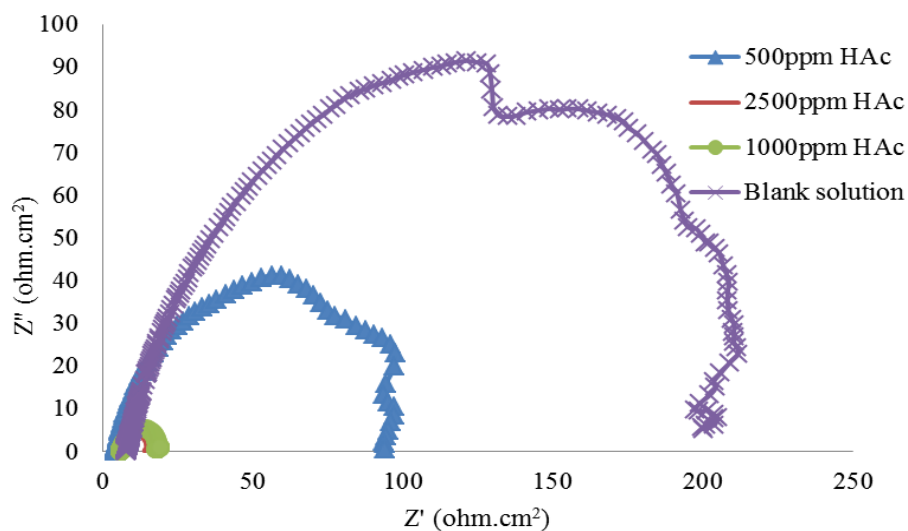


Figure 4-34: Nyquist plots for carbon steel samples in solutions containing HAC at 80°C after 6 hours

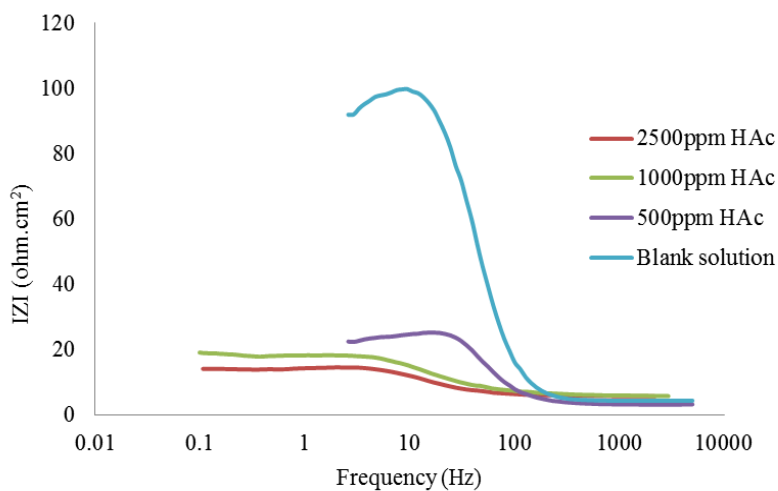


Figure 4-35: Bode plots for carbon steel samples in solutions containing HAC at 80°C after 6 hours.

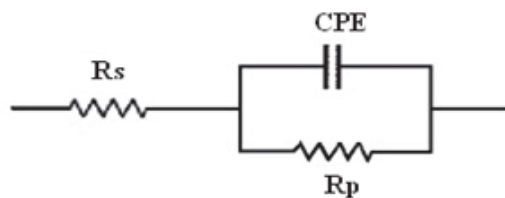


Figure 4-36: Equivalent circuit diagram used to fit the EIS data

Table 4-11: Electrochemical parameters obtained for carbon steel electrode in solutions containing HAc at 25°C

Conc(ppm)	R_{ct} ($\Omega \cdot \text{cm}^2$)	R_{sol} ($\Omega \cdot \text{cm}^2$)	C_{dl} (μF)	Θ ($^\circ$)
0	1.90	7.87	1.58	5.18
500	9.53	8.04	3.80	10.4
1000	6.97	6.62	1.12	8.4
2500	7.14	9.14	7.53	3.25
ε (%)	0.03	0.05	0.01	0.04

Table 4-12: Electrochemical parameters obtained for carbon steel electrode in solutions containing HAc at 50°C

Conc (ppm)	R_{ct} ($\Omega \cdot \text{cm}^2$)	R_{sol} ($\Omega \cdot \text{cm}^2$)	C_{dl} (μF)	Θ ($^\circ$)
0	2.87	3.22	4.15	6.75
500	3.07	4.11	5.99	3.30
1000	3.14	5.05	6.23	5.81
2500	3.38	6.64	7.58	7.33
ε (%)	0.02	0.01	0.01	0.05

Table 4-13: Electrochemical parameters obtained for carbon steel electrode in solutions containing HAc at 80°C

Conc (ppm)	R _{ct} (Ω.cm ²)	R _{sol} (Ω.cm ²)	C _{dl} (μF)	θ (°)
0	8.36	4.24	3.58	7.61
500	9.53	4.92	2.14	7.6
1000	9.01	5.76	1.01	10
2500	1.32	5.83	1.15	9.52
ε (%)	0.02	0.01	0.03	0.04

(ii) EIS with HAc and MEG

As mentioned previously, apart from the fact that the electrochemical impedance spectroscopy (EIS) can be used as an alternative measurements to predict the mechanisms of electrochemical reactions that occur at the metal-electrolyte interface, the EIS also can be used to evaluate the characteristics of corrosion reaction that occurs on the electrode surface such as the formation of scales. In addition, it can also be used to calculate the solution resistance (resistance due to a non-conductive metal-electrolyte).

The EIS measurements were employed to evaluate the behaviour of MEG and HAc on carbon steel electrodes immersed in a 3.5% wt. NaCl solution at 25°C, 50°C and 80°C respectively. The percentage of MEG injected to the solution were 20% MEG (referred to as rich MEG) and 80% MEG (referred to as lean MEG).

Figure 4-37 to Figure 4-42 depicts the Nyquist and Bode plots of the EIS measurements under different conditions. At lower temperature (Figure 4-37 and Figure 4-38), the Nyquist plots shows a large capacitive semicircle at very high frequencies that signifies high solution resistance for the blank solution (solution without MEG). The impedance value of the blank solution is so small compared to the impedance values with 20% and 80% MEG solution. However, on addition of 20%MEG and 80% MEG, the capacitance semi circles are depressed showing a charge transfer process taking place. The depressed semicircle is a characteristic of dispersion in frequencies and has been reported for

different physical phenomenon as roughness and other in homogeneities of solid surface taking place during corrosion. From the equivalent circuit diagram for modelling and calculations (Figure 4-36), the solution resistance value for the blank solution is approximately 8.1 ohms.cm². Addition of 20% MEG and 80% MEG increases the solution resistance to 9.20 ohms.cm² and 11.30 ohms.cm² respectively.

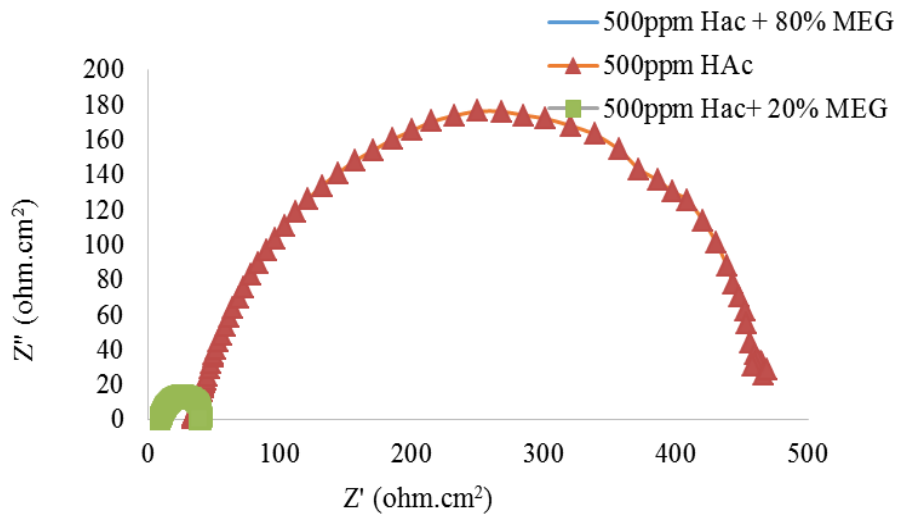


Figure 4-37: Nyquist plots for carbon steel coupons in 3.5% wt. NaCl solution containing HAc with 20% MEG and 80% MEG after 6 hours at 25°C

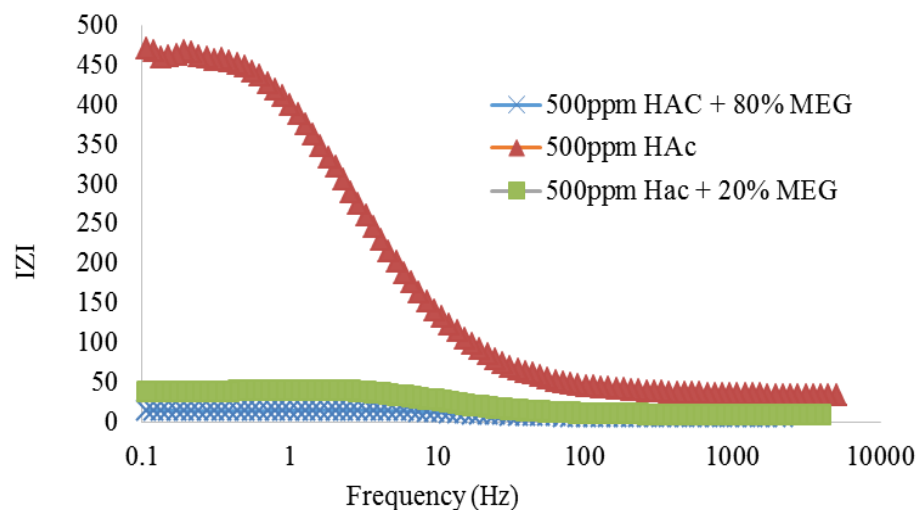


Figure 4-38: Bode plots for carbon steel coupons in 3.5% wt. NaCl solution containing HAC with 20% MEG and 80% MEG after 6 hours tests at 25°C

The Nyquist and Bode plots for carbon steel submerged in 3.5% wt. NaCl solution for different concentrations of HAC and MEG at 50°C is presented in Figure 4-39 and Figure 4-40. It was noticed that at addition of 20% MEG and 80% MEG to the solution shows high solution resistance compared to the solution resistance at lower temperature. The solution resistance for the blank solution at 50°C is 9.44 ohms.cm² compared to 8.1 ohms.cm² at 25°C. With 20% MEG and 80% MEG, the solution resistance increases to 10.2 ohms.cm² and 16.0 ohms.cm². Besides, it was noticed that the impedance values for the solution with HAC and the blank solutions are insignificant. The 20% MEG and 80% MEG both has higher impedance values indicating that the corrosion resistance of carbon steel materials with 20% MEG and 80% MEG are higher than the 3.5% wt NaCl solutions and the solution in the presence of HAC.

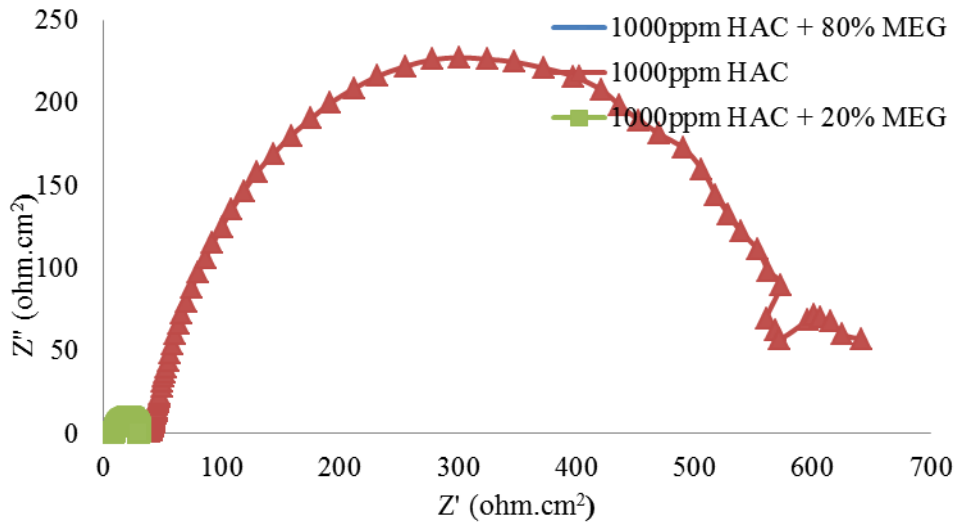


Figure 4-39: Nyquist plots for carbon steel coupons in 3.5% wt. NaCl solution containing HAC with 20% MEG and 80% MEG after 6 hours at 50°C

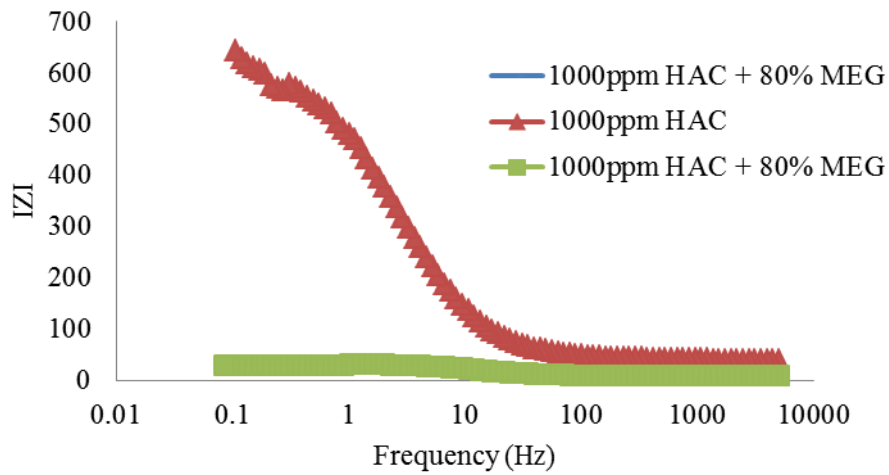


Figure 4-40: Bode plots for carbon steel coupons in 3.5% wt. NaCl solution containing HAC with 20% MEG and 80% MEG after 6 hours tests at 50°C

The Nyquist and Bode plots obtained from the EIS for carbon steel coupons in 3.5% wt. NaCl solution in the presence of HAc, 20% MEG, and 80% MEG at higher temperature are presented in Figure 4-41 and Figure 4-42 respectively. The trend of the plots indicate that the size of the Nyquist and Bode plots reduced drastically on addition of 20% MEG and 80% MEG compared to the Nyquist plots in the presence of HAc and the blank solution. The results in reality signify changes in the corrosion mechanisms as results of the MEG added to the system that reduces the corrosion rates. The higher impedance indicate high corrosion rate at high temperature. The addition of 20% MEG and 80% MEG reduces the capacitance semi-circles which is a function of the MEG concentrations. It proves that the double layer capacitance and charge transfer resistance is an indication of inhibition of the corrosion process.

Table 4-14 to Table 4-16 summarizes the parameters obtained from fitting the electrochemical impedance measurements using the equivalent circuit diagram in Figure 4-36. From Figure 4-36, C_{dl} is the capacitance due to electric double layer, R_{sol} is the solution resistance and R_{ct} is the resistance due to charge transfer by the corroding electrode.

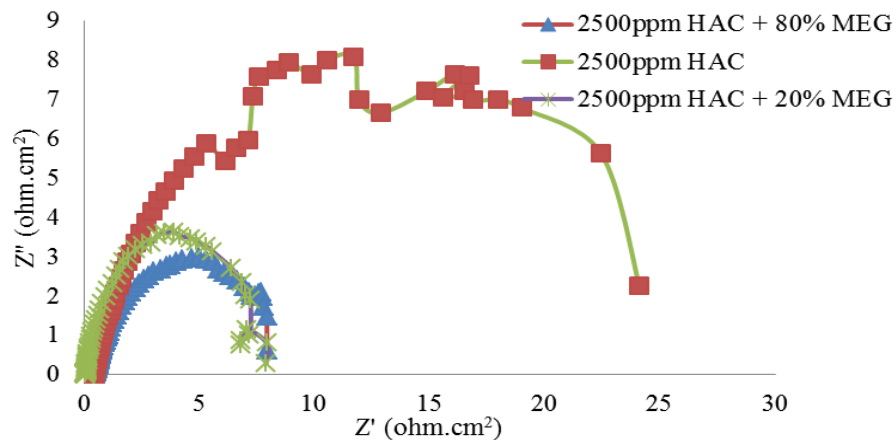


Figure 4-41: Nyquist plots for carbon steel coupons in 3.5% wt. NaCl solution containing HAc with 20% MEG and 80% MEG after 6 hours at 80°C

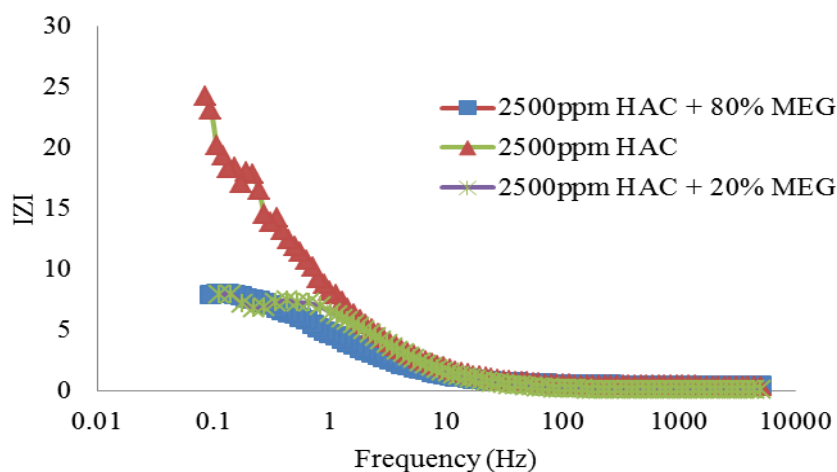


Figure 4-42: Bode plots for carbon steel coupons in 3.5% wt. NaCl solution containing HAC with 20% MEG and 80% MEG after 6 hours tests at 80°C

Table 4-14: Electrochemical parameters obtained for carbon steel electrode in 3.5% wt. NaCl solutions containing different concentrations of HAC with 20% MEG and 80% MEG at 25°C

Composition	R_{ct} ($\Omega.cm^2$)	R_{sol} ($\Omega.cm^2$)	C_{dl} (F)	Θ ($^\circ$)
Solution + 20% MEG + 0ppm HAC	35	8.1	197	0
Solution + 20% MEG + 500ppm HAC	64	9.20	69	65
Solution + 20% MEG + 1000ppm HAC	109	11,3	77	61
Solution + 20% MEG + 2500ppm HAC	210	10.21	34	83
Solution + 80% MEG + 0ppm HAC	48	13.6	22	89
Solution + 80% MEG + 500ppm HAC	76	12.9	56	72
Solution + 80% MEG + 1000ppm HAC	112	10.15	40	80
Solution + 80% MEG + 2500ppm HAC	230	11.8	76	61
(%) ϵ	± 0.02	± 0.05	± 0.01	± 0.02

Table 4-15: Electrochemical parameters obtained for carbon steel electrode in 3.5% wt. NaCl solutions containing different concentrations of HAc with 20% MEG and 80% MEG at 50°C

Composition	R_{ct} (Ω.cm²)	R_{sol} (Ω.cm²)	C_{dl} (F)	Θ (°)
Solution + 20% MEG + 0ppm HAc	57	9.44	146	26
Solution + 20% MEG + 500ppm HAc	75	16.0	80	59
Solution + 20% MEG + 1000ppm HAc	130	10.2	34	83
Solution + 20% MEG + 2500ppm HAc	240	11.8	54	73
Solution + 80% MEG + 0ppm HAc	65	9.05	60	70
Solution + 80% MEG + 500ppm HAc	77	9.95	39	80
Solution + 80% MEG + 1000ppm HAc	120	11	50	75
Solution + 80% MEG + 2500ppm HAc	248	10.2	57	71
(%)ε	±0.03	±0.04	±0.02	0±.02

(i) EIS results with HAc, MEG and corrosion inhibitors

The LPR measurements basically do not provide knowledge about the process of corrosion inhibition for the inhibitors evaluated. However, the EIS was employed to estimate the inhibitor mechanisms of the chemical reaction that might occur at the electrode-electrolyte surface when different concentrations of inhibitors are added to the system. Different studies by [68-70] had reported that when scale forming inhibitors are applied, the scale resistance due to the inhibitor can be obtained with EIS method. However results obtained in this investigation had shown that corrosion inhibition can also be obtained using the LPR and weight loss methods as presented in Figure 4-13 to Figure 4-21. As can be seen from Figure 4-13 to Figure 4-21, weight results shows decrease in resistance and reveal that corrosion inhibitors effect is an indication of thin

film that form on carbon steel surface and the inhibition efficiencies increase as a result of increased concentrations.

Table 4-16: Electrochemical parameters obtained for carbon steel electrode in 3.5% wt. NaCl solutions containing different concentrations of HAc with 20% MEG and 80% MEG at 80°C

Composition	R_{ct} (Ω.cm²)	R_{sol} (Ω.cm²)	C_{dl} (F)	θ (°)
Solution + 20% MEG + 0ppm HAc	45	7.5	130	34
Solution + 20% MEG + 500ppm HAc	66	9.08	55	72
Solution + 20% MEG + 1000ppm HAc	125	11.2	44	78
Solution + 20% MEG + 2500ppm HAc	208	10.65	56	72
Solution + 80% MEG + 0ppm HAc	58	11.5	64	68
Solution + 80% MEG + 500ppm HAc	65	9.8	40	80
Solution + 80% MEG + 1000ppm HAc	109	12	65	67
Solution + 80% MEG + 2500ppm HAc	221	10.5	70	64
ε (%)	0.02	0.05	0.03	0.01

Figure 4-43 to Figure 4-48 presents a typical EIS Nyquist and Bode plots of carbon steel in 3.5% wt. NaCl solution acquired in this work. The curves consist of one depressed semi-circle at high frequencies, and also one depressed semi-circle at lower frequencies. The depressed semi-circle at high frequencies is an indication of low conductivity of the solution that leads to solution resistance between the reference electrode and the working electrode in the presence of the inhibitors. At lower frequencies, the depressed semi-circle exhibited is due to carbon steel corrosion process in the solution.

In Figure 4-43 to Figure 4-48, it is discovered that a depressed capacitive semi-circle is noticed at high frequency range for the solution with inhibitors compared to the blank solution at low frequency range and inductive semi-circle are noticed. The depressed

capacitive semi-circle occurred as a result of time constant of the electric double layer and charge transfer resistance of the solution. The depressed inductive semi-circle noticed at the low frequency is as a result of adsorption relaxation of intermediates. The occurrence of single depressed semi-circle predicts that the corrosion inhibitors retard the acceleration of corrosion process during the dissolution of carbon steel. Paskossy [73] in his recent publications proposed that the depressed semi-circle is as a result of the carbon steel and differences in frequencies are due to the surface roughness and other inhomogeneities of the electrode.

At 25°C (Figure 4-43 and Figure 4-44,) the size of the depressed semi-circle of Nyquist plots on application of inhibitors XX and YY are almost the same compared to the size of inhibitor ZZ though with one single depressed semi-circle. These trends imply that almost the same inhibition mechanisms occur during the dissolution of carbon steel samples in the solution. It was also noticed that the impedance plots consist of a single capacitance loop at very high frequency.

The addition of the different concentration of the inhibitors to the solutions with 20% MEG and 80% MEG and HAc raised the capacitance of depressed semi-circles and was attributed to the double layer capacitance and charge transfer resistance undermining the corrosion process. The reduction of the depressed semi-circle was also noticed for the Nyquist plots with the application of inhibitor YY. This depicts that the corrosion process taking place with the application of inhibitor YY is charge transfer rather than activation controlled process.

In order to obtain useful information from the corrosion process such as the corrosion rate, the EIS data was analyzed using an equivalent circuit diagram of elements shown in Figure 4-36. In Figure 4-36, R_{ct} is the charge transfer resistance, R_s is the solution resistance, and C_{dl} is the electrical double layer of the capacitance.

Mansfeld et al [74] proposed an exponent, n in the impedance function as a deviation factor from the ideal behaviour for the depressed semi-circle at high frequency. According to Mansfeld et al, it is the capacitor in the equivalent circuit in Figure 4-36

which can be replaced by the constant phase element (CPE). The constant phase element (CPE) is regarded as an element whose depend on frequency and reflects the surface roughness such as those found in adsorption processes. The impedance function of the CPE can be written as:

$$Y_{CPE} = Y_0(j\omega)^n \quad 4-5$$

$$Z_{CPE} = \frac{1}{(Y_0j\omega)^n} \quad 4-6$$

Where

Y_0 is the magnitude of the CPE, j is the imaginary number ($j^2=-1$), ω is the phase angle of the CPE, and $n = \omega/(\frac{\pi}{2})$, n is an adjustable factor(surface roughness) that lies between

the values of 0.50 and 1.0. Y_0 and n can be derived from 4-7. The capacitor is an ideal factor when $n=1$. In order to compare the capacitive behaviour of different solutions, the initially obtained values of Y_0 and n are however converted into ideal capacitance values, C_{idl} . This is done by separating the purely imaginary contribution to the impedance

$$C_{idl} = \frac{Y_0\omega^{n-1}}{\sin(n\pi/2)} \quad 4-7$$

Appendixes A-1 to A-6 presents the summaries of parameters (R_{ct} , R_{sol} , C_{dl} and θ) obtained from the electrochemical impedance spectroscopy measurements of carbon steel saturated in 3.5% wt NaCl at various conditions studied using Figure 4-36, the equivalent circuit diagram.

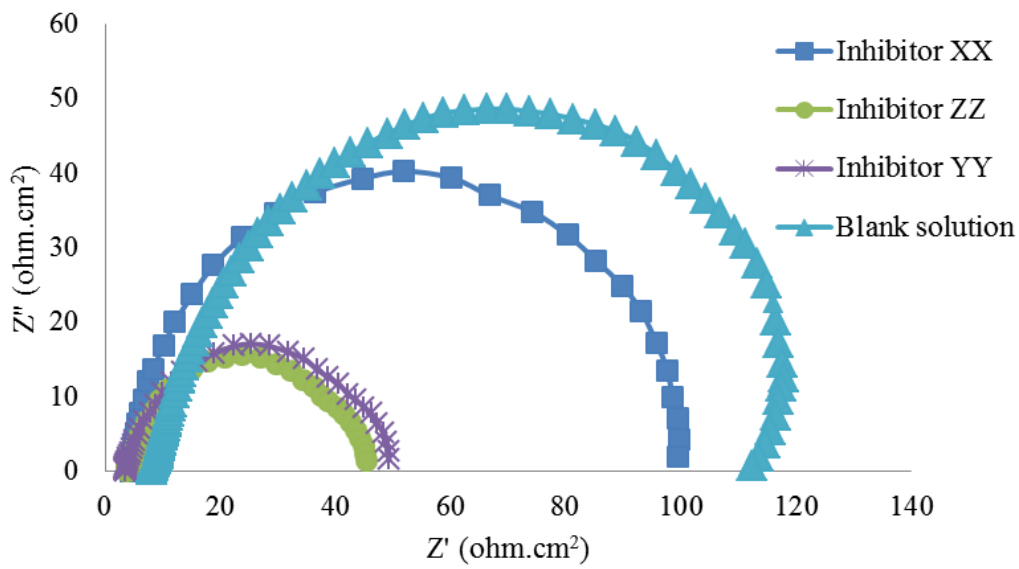


Figure 4-43: Nyquist plots for carbon steel coupons in 3.5% wt. NaCl solution containing HAc, 20% MEG, 80% MEG, and corrosion inhibitors for 6 hours at 25°C

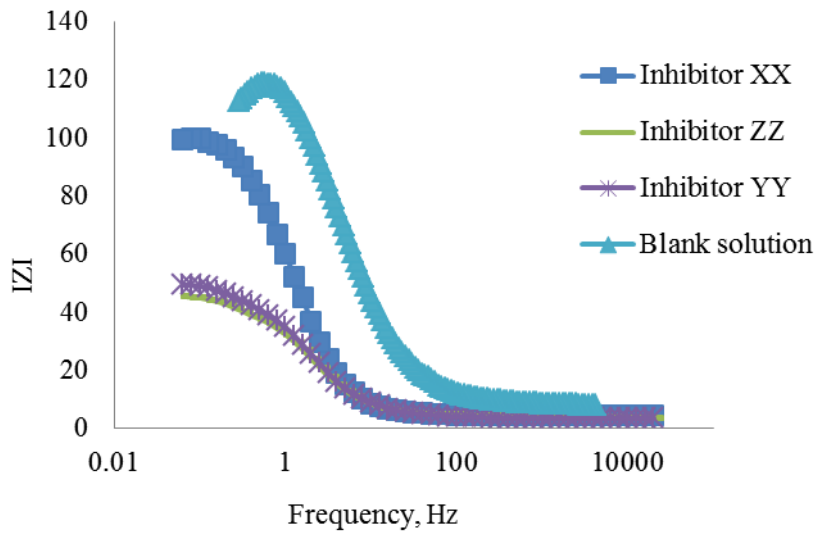


Figure 4-44: Bode plots for carbon steel coupons in 3.5% wt. NaCl solution containing HAc, 20% MEG, 80% MEG, and corrosion inhibitors for 6 hours at 25°C

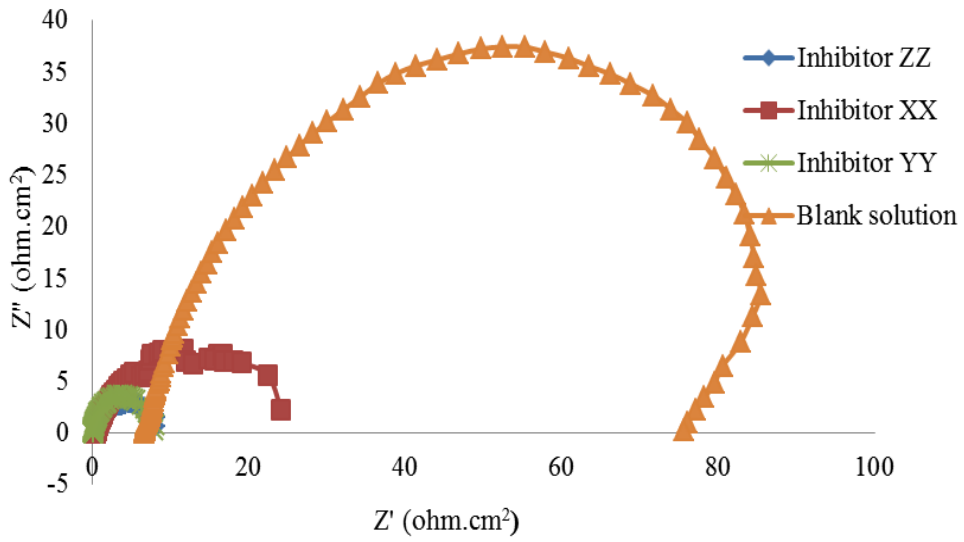


Figure 4-45: Nyquist plots for carbon steel coupons in 3.5% wt. NaCl solution containing HAc, 20% MEG, 80% MEG, and corrosion inhibitors for 6 hours at 50°C

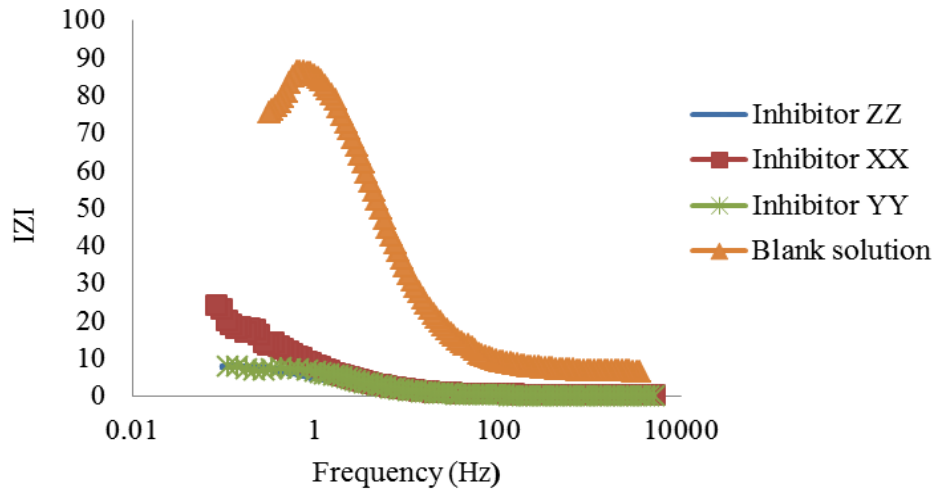


Figure 4-46: Bode plots for carbon steel coupons in 3.5% wt. NaCl solution containing HAc, 20% MEG, 80% MEG, and corrosion inhibitors for 6 hours at 50°C

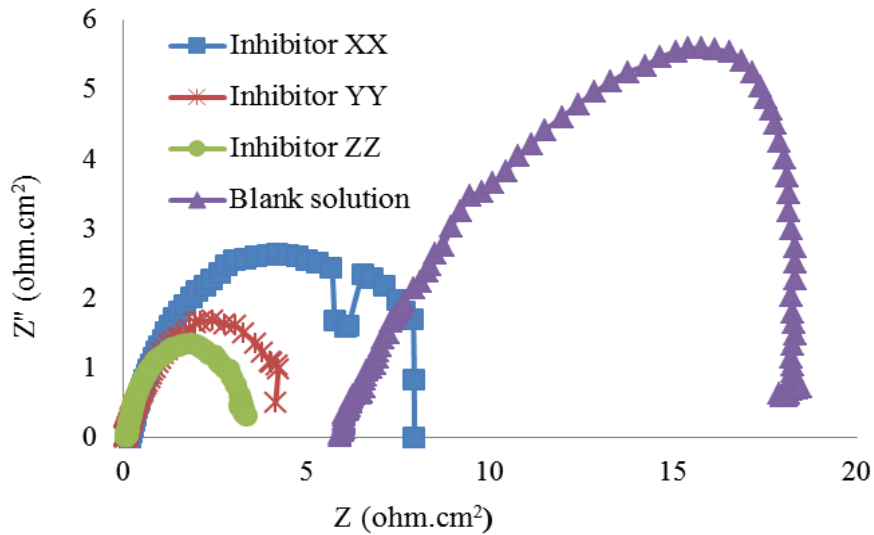


Figure 4-47: Nyquist plots for carbon steel coupons in 3.5% wt. NaCl solution containing HAc, 20% MEG, 80% MEG, and corrosion inhibitors for 6 hours at 80°C

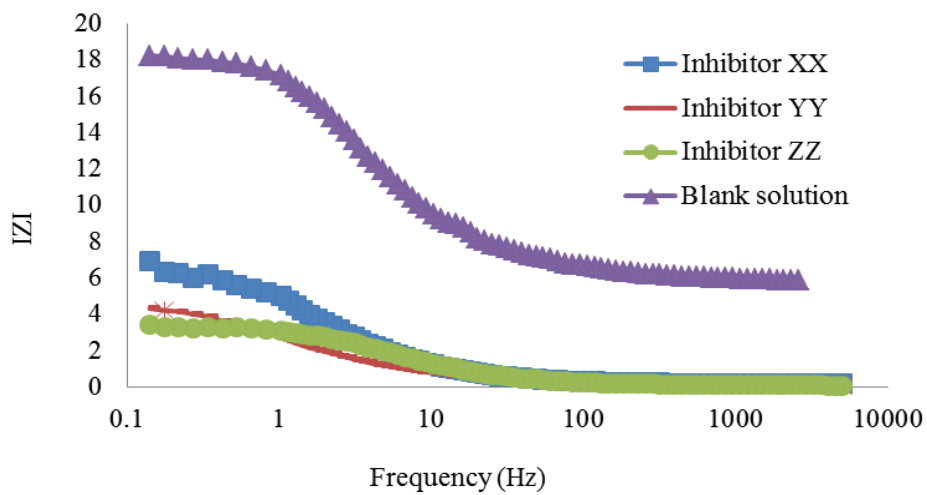


Figure 4-48: Bode plots for carbon steel coupons in 3.5% wt. NaCl solution containing HAc, 20% MEG, 80% MEG, and corrosion inhibitors for 6 hours at 80°C

4.3.5 Potentiodynamic polarization results

The potentiodynamic polarization (PDP) scan was employed to assess the effect of HAc concentrations on the corrosion rate of carbon steel immersed in 3.5% wt NaCl solution in de-aerated environment at three different temperatures. The measuring polarization was conducted in the potential range of -600 mV to 150 mV vs. E_{corr}

This section presents results and discussions of the following:

- (i) PDP with HAc
- (ii) PDP with HAc and MEG
- (iii) PDP with HAc, MEG and inhibitors

(i) PDP with HAc

Figure 4-49 to Figure 4-51 presents the potentiodynamic polarization curves for the experiments with and without HAc. It is noticed that there is an increase in corrosion current density, i_{corr} with a corresponding increase in corrosion potential, E_{corr} . These variations of corrosion current density and corrosion potential signify that an active dissolution of the electrode is taking place at the electrode–electrolyte interface. The increase in the concentration of HAc from 500ppm to 2500ppm increases the reaction process of the cathodic reaction than the anodic reaction in all cases studied. The samples in solution containing 2500ppm HAc have more negative potential than the ones in solutions containing 500ppm and 1000ppm HAc respectively. Table 4-17 summarizes the values obtained from the electrochemical parameters of potentiodynamic polarization tests at different conditions.

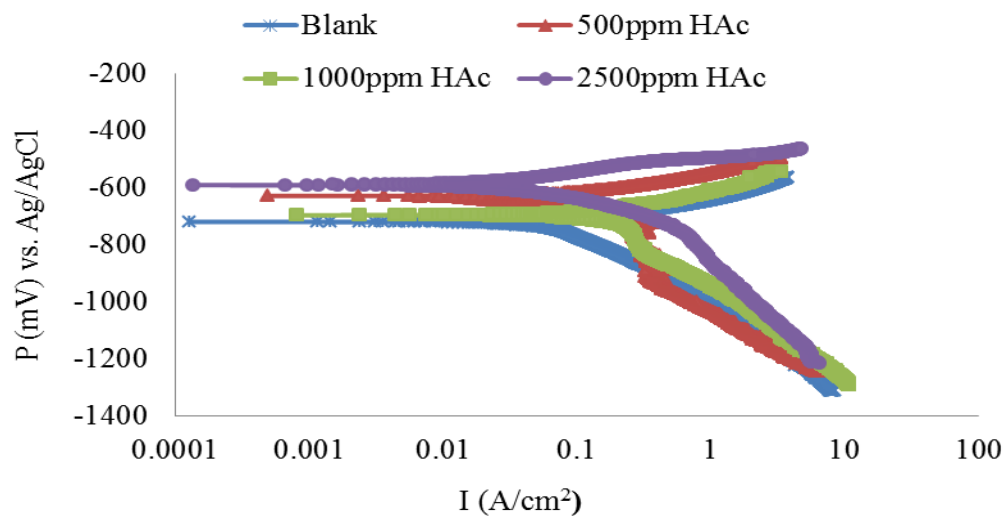


Figure 4-49: Potentiodynamic polarization curves for carbon steel electrodes in solutions containing HAc for 6 hours tests at 25°C.

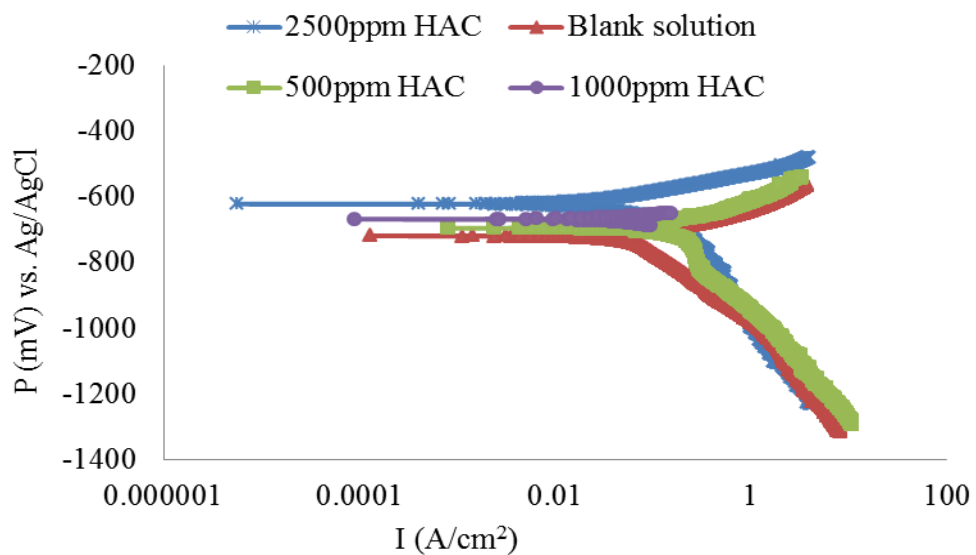


Figure 4-50: Potentiodynamic polarization curves for carbon steel electrodes in solution containing HAc for 6 hours tests at 50°C

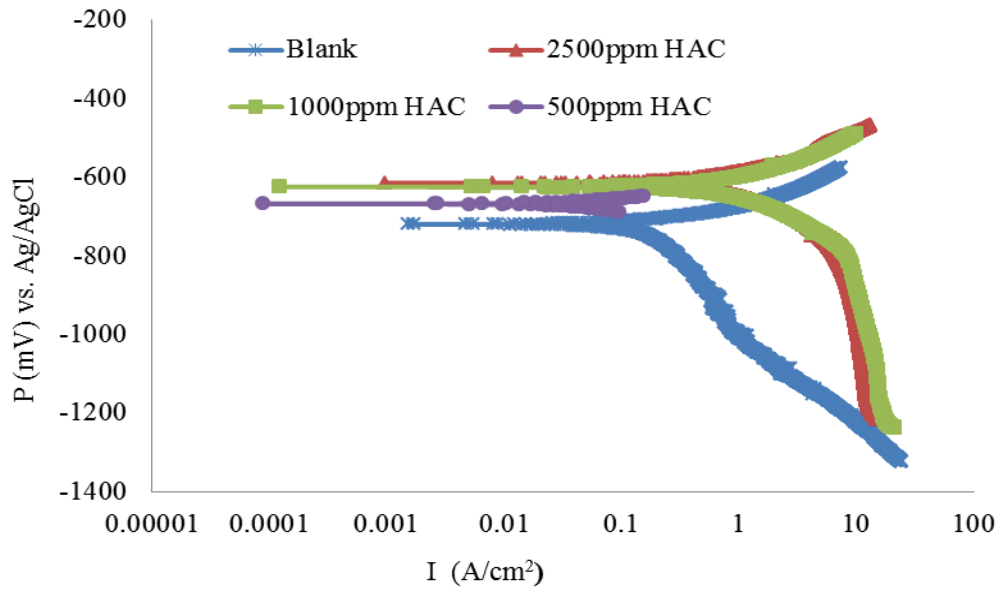


Figure 4-51: Potentiodynamic polarization curves for carbon steel electrodes in solution containing HAC for 6 hours tests at 80°C

Table 4-17: Potentiodynamic polarization parameters obtained for carbon steel electrodes saturated in containing HAC at 25°C, 50°C and 80°C respectively.

Conc. (ppm)	25°C			50°C			80°C		
	E _{corr} , mV	I _{corr} , μA/cm ²	CR, mm/yr	E _{corr} , mV	I _{corr} , μA/cm ²	CR, mm/yr	E _{corr} , mV	I _{corr} , μA/cm ²	CR, mm/yr
0	-712	0.2411	1.45	-670	0.2311	1.26	-722	0.5586	6.47
500	-643	0.1259	2.79	-632	0.1364	1.29	-719	0.6146	6.05
1000	-690	0.3070	2.27	-620	0.1827	1,32	-617	0.6885	7.98
2500	-612	0.1961	3.55	-628	0.1217	1.411	-632	0.8498	9.80
(%) ε	±0.02	±0.04	±0.01	±0.03	±0.03	±0.02	±0.05	±0.01	±0.02

(ii) PDP with HAC and MEG

Figure 4-52 to Figure 4-54 depicts the polarization curves of the carbon steel in the solution resulting from the addition of different concentrations of HAC with 20% and 80% MEG at low and high temperatures.

The polarization curves at 25°C (Figure 4-52) indicates that the corrosion potential (E_{corr}) moves upwards while the corrosion current density (i_{corr}) increases with the solution of acetic acid. This increase in corrosion potential (E_{corr}) is evidence that presence of HAC increases the corrosion rate of carbon steel in CO_2 solution. This result corresponds with that obtained from the linear polarization measurements. As can be seen, it is clear that the anodic reaction was not affected as a result of adding different concentrations of HAC. This also implies that at low temperatures, the reaction rate at the anode remain the same. The addition of 20% MEG and 80% MEG to the solutions decreases the corrosion potential (E_{corr}) and lower the corrosion current density (i_{corr}). The decreased in the corrosion potential and corrosion current density is as a result of adding 20% and 80% MEG to the solutions which retards the corrosion rate of the materials.

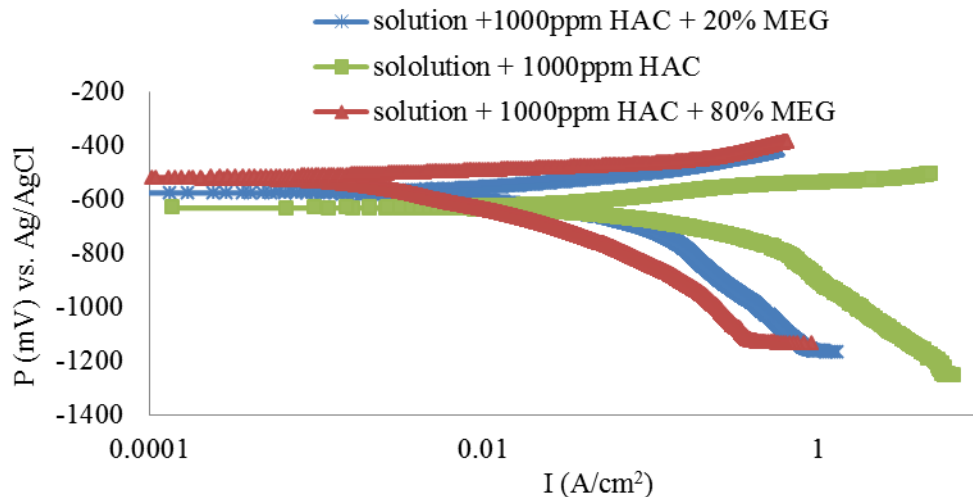


Figure 4-52: Potentiodynamic curves for carbon steel electrodes saturated in solution containing HAC with 20% & 80% MEG at 25°C

At 50°C, the polarization curves also shows that the addition of MEG affect the corrosion potential (E_{corr}) of the carbon steel. Figure 4-53, it is seen that the cathodic Tafel slope is more affected than the anodic Tafel slope.

At 80°C (Figure 4-54), it is noted that there is a decrease in corrosion current density (i_{corr}) as well as corrosion potential (E_{corr}) with addition of HAc to the solutions, indicating an active dissolution of the electrode materials taking place. The introduction of 20% MEG and 80% MEG to the solution drastically reduced the anodic reaction and move the cathodic reaction slightly towards lower corrosion current densities. As a result of increase in corrosion potential to the positive direction and decrease of the corrosion current density, it can be confirmed that MEG reduces the corrosion rate of carbon steel materials in a solution containing 3.5% wt. NaCl. This decrease in corrosion rate can be attributed to the fact that addition of 20% and 80% MEG reduces the anodic dissolution of the carbon steel and decelerate the growth of hydrogen reactions. Table 4-18 to Table 4-20 summarizes the resulted data obtained, including the corrosion potential, corrosion current density, corrosion rate as well as the inhibition efficiency for the carbon steel samples immersed in solutions with HAc, 20% and 80% MEG at three different temperatures. In Table 4-18 to Table 4-20, the inhibition performance efficiency was determined using equation 4-8 below:

$$\% = \left(\frac{i_{corr}^o - i_{corr}}{i_{corr}^o} \right) \times 100 \quad 4-8$$

Where

$i_{corr}^o - i_{corr}$ are the values for corrosion current density without and with MEG respectively

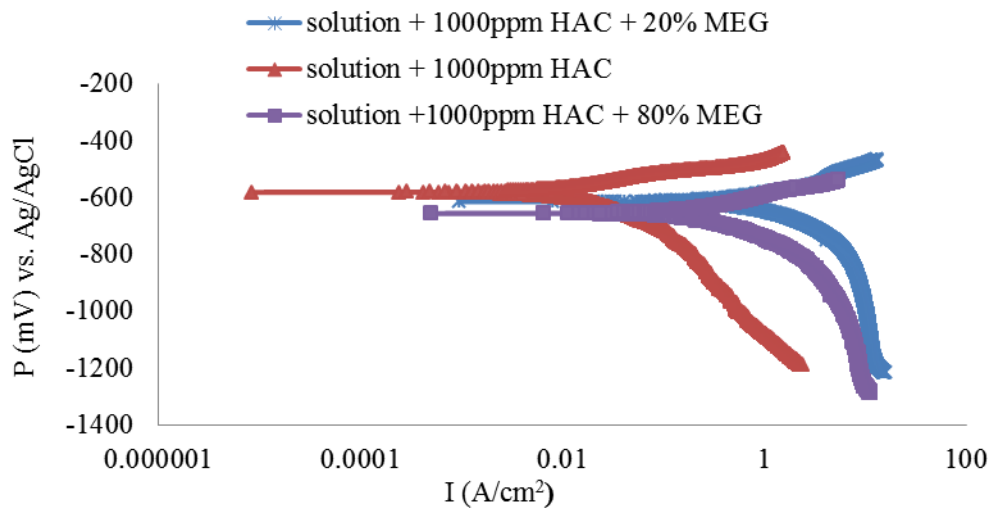


Figure 4-53: Potentiodynamic curves for carbon steel electrodes saturated in solution containing HAC with 20% and 80% MEG at 50°C

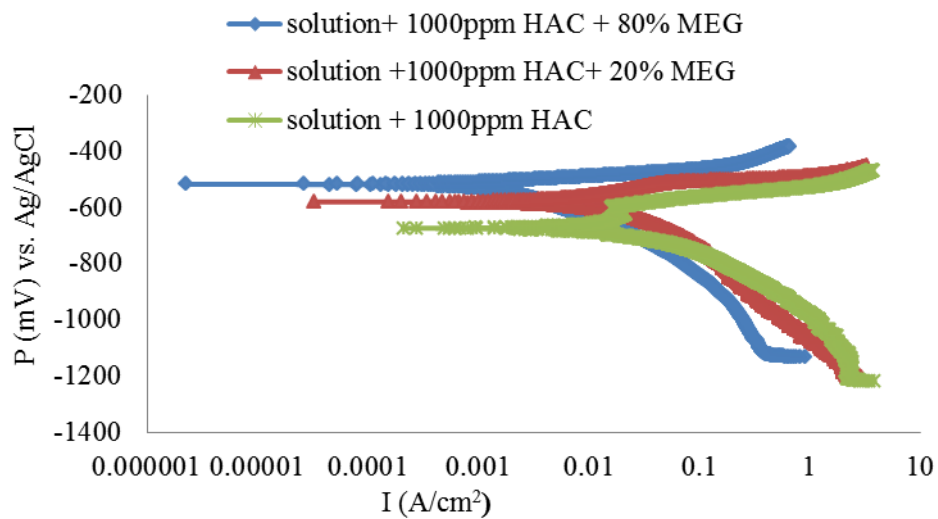


Figure 4-54: Potentiodynamic curves for carbon steel electrodes saturated in solution containing HAC with 20% and 80% MEG at 80°C

Table 4-18: Potentiodynamic parameters for carbon steel samples saturated in solutions containing HAc with 20% and 80% MEG at 25°C

Composition	E_{corr} (v)	I_{corr} (mA/cm²)	CR (mm/yr)	η_i (%)
Solution + 20% MEG + 0ppm HAc	-625	45	3.31	-
Solution + 20% MEG + 500ppm HAc	-620	21	1.54	53
Solution + 20% MEG + 1000ppm HAc	-618	18	1.32	60
Solution + 20% MEG + 2500ppm HAc	-615	29	2.13	35.5
Solution + 80% MEG + 0ppm HAc	-624	25	1.84	44
Solution + 80% MEG + 500ppm HAc	-622	22	1.62	51
Solution + 80% MEG + 1000ppm HAc	-618	27	1.99	40
Solution + 80% MEG + 2500ppm HAc	-611	34	2.50	24.4
ε (%)	±0.03	±0.01	±0.03	±0.04

Table 4-19: Potentiodynamic parameters for carbon steel samples saturated in solutions containing HAc with 20% and 80% MEG at 50°C

Composition	E_{corr} (v)	I_{corr} (mA/cm²)	CR (mm/yr)	η_i (%)
Solution + 20% MEG + 500ppm HAc	-638	30	2.21	33
Solution + 20% MEG + 1000ppm HAc	-635	11	0.81	75
Solution + 20% MEG + 2500ppm HAc	-627	28	2.06	37
Solution + 80% MEG + 0ppm HAc	-623	19	1.40	57
Solution + 80% MEG + 500ppm HAc	-618	21	1.54	53
Solution + 80% MEG + 1000ppm HAc	-615	33	2.43	27
Solution + 80% MEG + 2500ppm HAc	-612	24	1.76	47
ε(%)	±0.04	±0.01	±0.01	±0.03

Table 4-20: Potentiodynamic parameters for carbon steel samples saturated in solutions containing HAc with 20% and 80% MEG at 80°C

Composition	E_{corr} (v)	I_{corr} (mA/cm²)	CR (mm/yr)	η_p (%)
Solution + 20% MEG + 500ppm HAc	-574	15	1.10	67
Solution + 20% MEG + 1000ppm HAc	-570	24.3	1.79	46
Solution + 20% MEG + 2500ppm HAc	-565	27.6	2.03	38
Solution + 80% MEG + 0ppm HAc	-565	24	1.76	47
Solution + 80% MEG + 500ppm HAc	-578	38.2	2.81	15
Solution + 80% MEG + 1000ppm HAc	-577	28.	2.06	38
Solution + 80% MEG + 2500ppm HAc	-578	25	1.84	44
ε (%)	±0.02	±0.04	±0.02	±0.02

(iii) PDP with HAc, MEG and corrosion inhibitors

Figure 4-55 to Figure 4-57 shows the polarization curves with HAc, MEG and inhibitors at three temperatures studied. It is noted that the mechanism of carbon steel corrosion is controlled by mass transfer and activation control. The corrosion current density decreases as the potential of the electrode were scanned from the OCP in the anodic direction on adding different concentrations of inhibitors to the solutions. This indicates that the protective nature of the filmed form decreases due to the increase in concentration of inhibitors.

Figure 4-55 to Figure 4-57 also depicts that there is a decrease in the dissolution of carbon still on addition of different concentrations of inhibitors XX, YY and ZZ to the solution. The addition of the inhibitors moves the corrosion potential to a more positive potentials while reduces the values of the corrosion current density. This implies that the inhibitors reduces the corrosion of carbon steel to a minimum acceptable level and as a result depends on the concentration of the inhibitors applied to the system. The addition

of the corrosion inhibitors also affects the carbon steel corrosion by reduces the corrosion current densities. The reduction in corrosion current density indicates that the inhibitors with the solution interferes in the oxidation and reduction reaction preventing anodic dissolution by absorption of the inhibitor molecules on the steel surface. The efficiencies of the inhibition from the studies were calculated using equation 4-8. Appendixes A7 – A12 present the summaries of the kinetic parameters obtained from the potentiodynamic test of the solution containing HAC, MEG and three different types of corrosion inhibitors.

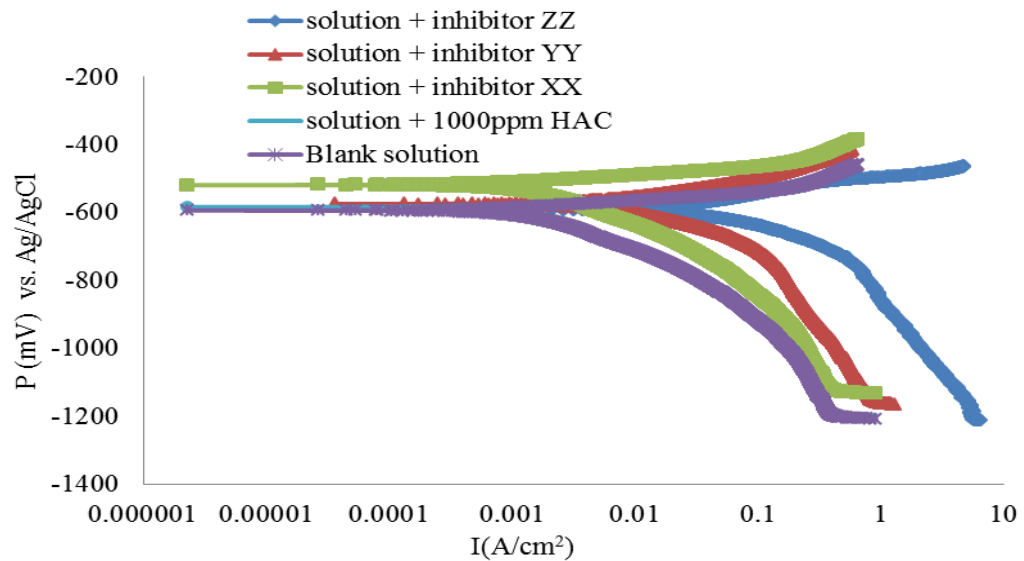


Figure 4-55: Potentiodynamic curves for carbon steel samples saturated in 3.5% wt. NaCl solution containing different concentrations of HAC, MEG and inhibitors at 25°C.

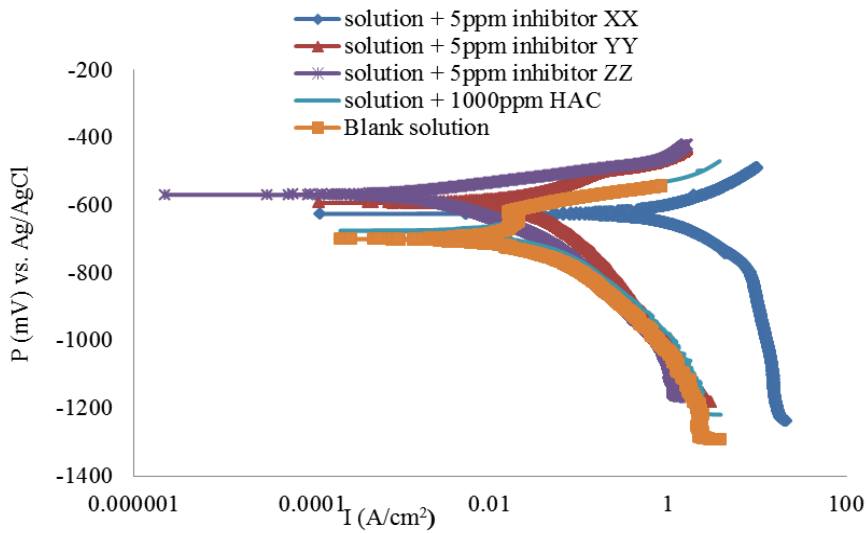


Figure 4-56: Potentiodynamic curves for carbon steel samples saturated in 3.5% wt. NaCl solution containing different concentrations of HAc, MEG and inhibitors at 50°C

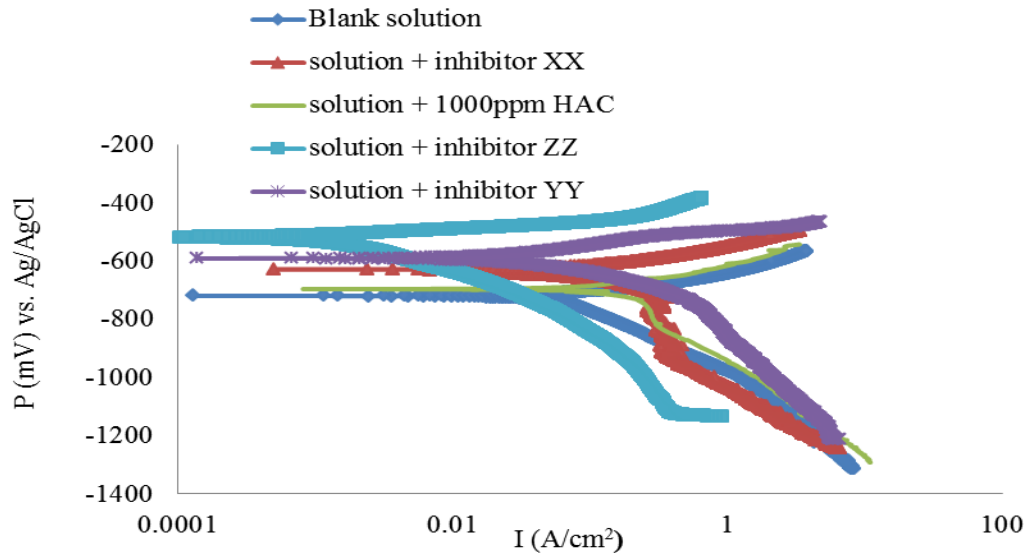


Figure 4-57: Potentiodynamic curves for carbon steel samples saturated in 3.5% wt. NaCl solution containing different concentrations of HAc, MEG and inhibitors at 80°C

4.4 Phase – III: Surface analysis results

The understanding of surface morphology, texture, and surface defects is of significant importance in electrochemistry. To determine the effect that these parameters have on the corrosion of carbon steel in CO₂ environment, the use of surface characterization analytical tools were employed.

In this section of work, the scanning electron microscopy (SEM) and energy dispersion X-ray (EDX) were utilized to study the metallic surface and determine the morphology of the corrosion product as well as to characterize the products formed on the carbon steel samples prior to and after 6 hours exposure.

The following discusses the results obtained for the surface analysis using SEM, XRD and XPS

4.4.1 SEM observations of samples in solutions with HAc

Figure 4-58 show the morphologies of carbon steel sample obtained in 3.5% wt. NaCl solution after 6 hours exposure in the presence of HAc. It is confirmed (Figure 4-58) that an amorphous corrosion product layers were formed on the surface of the blank solution compared to the surfaces where HAc was presence. In all cases in the absence of HAc, corrosion products are formed due to the presence of water, hydrogen sulphide and carbon dioxide. A compact layer composed of corrosion products such as iron carbonate (FeCO₃), oxides and sulphides are formed on carbon steel without HAc.

Addition of different concentration of HAc to the solution result in a less dense layer (corrosion film) formed on the surface as shown in (Figure 4-58 C & E). This less dense layer is an indication that the presence of HAc accelerates the dissolution of carbon steel materials and the solubility of iron carbonate increases in the presence of HAc irrespective of the pH of the solution.

Figure 4-58 (B, D F) shows the EDX analysis on the carbon steel in the presence of HAc. The results show an irregular discontinuous layer formed without any orientation. The peak is composed of iron Fe, Oxygen, O. This formation of peak is an indication of the presence of iron oxide and carbonate as a result of the corrosion product on the carbon steel. It is also observed that small amount of sulphur is observed as a result of iron sulphide presence.

4.4.2 SEM observations of samples in solutions with HAc and MEG

Figure 4-59 shows the SEM examination of carbon steel after 6 hours exposure to the solution of 3.5% wt. NaCl containing different concentration of HAc and MEG. It is confirmed that that in the absence of MEG irrespective of the percentage, a very rough surface is formed as a result of dissolution of carbon steel material. The presence of MEG increases the formation of protective film on the carbon steel surface. This implies that the addition of MEG to the solution favours the formation of protective film on the electrode, and the increased in the concentration of MEG generally decreases FeCO_3 solubility and favour protective film formation. It was reported by Dugstad [53] that transport of reactants and corrosion products through protective scale formation governs the rate of corrosion when a dense film are form.

Figure 4-59 (A, D &F) shows the EDX spectra obtained for carbon steel samples after 6 hours of exposure in solution containing HAc and MEG. In the presence of HAc, the EDX spectra shows some characteristics peaks of the elements contained in the carbon steel samples. Addition MEG to the solutions confirmed that some of the elements in the carbon steel generally increased

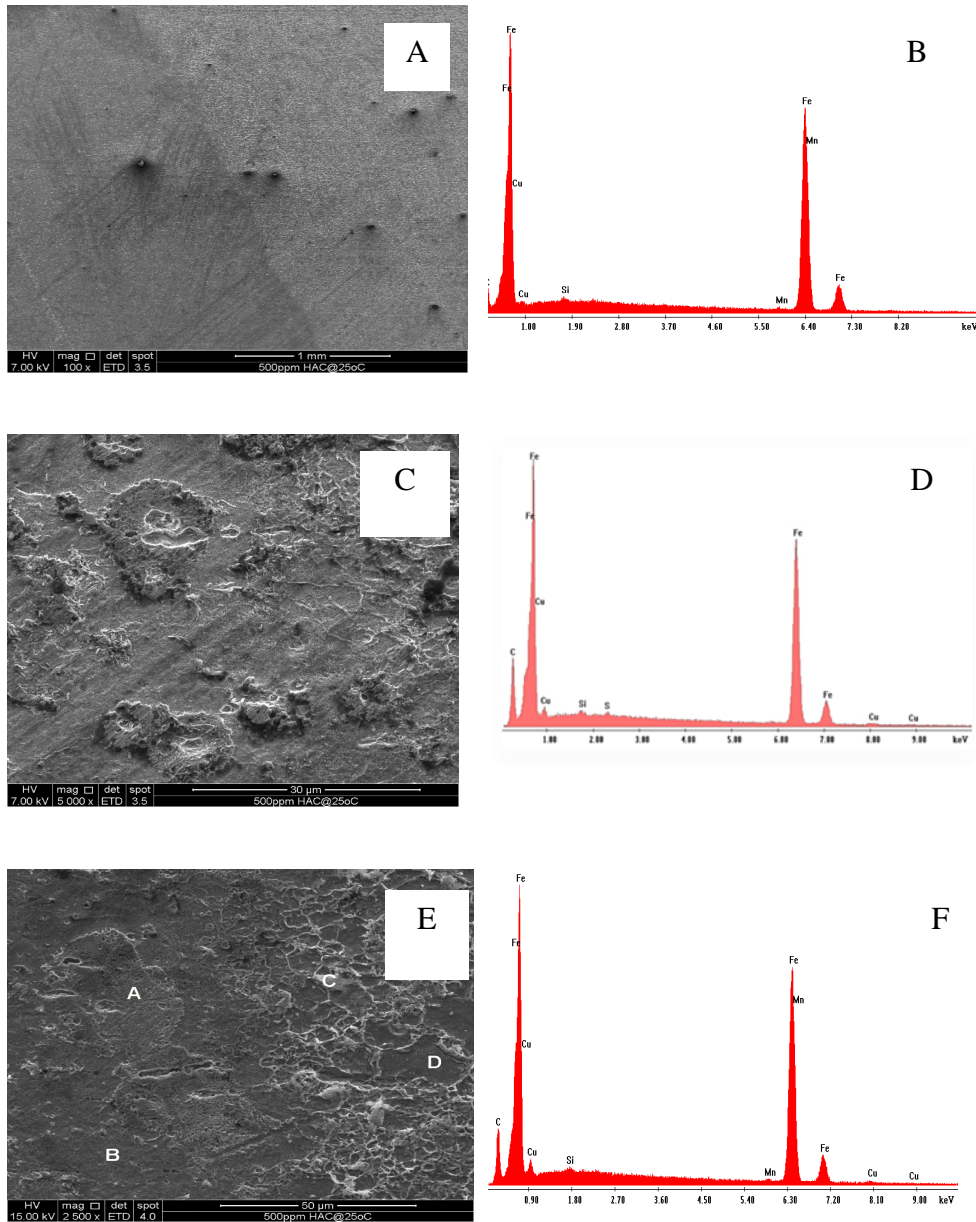


Figure 4-58: SEM images (Left) and EDX spectrum (Right) of carbon steel samples exposed to 3.5% wt. NaCl solution and different concentrations of HAC for 6 hours.[A] 500ppm HAC [B] 1000ppm HAC [C] 2500 ppm HAC.

. This increment is as results of carbon and oxygen atoms of the absorbed MEG on the carbon steel samples. Figure 4-59 (A, D &F) also confirmed that carbonaceous elements containing oxygen and magnesium had covered the surface of the carbon steel samples. The intensity of carbon and oxygen has also increased with increase in concentration of MEG as a results of anions salt been absorbed on the carbon steel. This confirmed with the results obtained by the electrochemical measurement.

4.4.3 SEM observations of samples in solutions with HAc, MEG and corrosion inhibitors

Figure 4-60 presents the SEM results after 6 hours exposure of carbon steel samples in a solutions containing HAc, MEG and inhibitors. Generally, it is confirmed that formation of thin layer is observed as a result of addition of various concentration of inhibitors .The inhibitors are absorbed on the surface of carbon steel resulted in reduction of corrosion rate.

Figure 4-60 (B, D & F) shows EDX spectra obtained for carbon steel samples after 6 hours exposure in 3.5% wt. NaCl solution containing HAc, MEG and inhibitors. In the presence of HAc, the EDX spectra shows some characteristics peaks of the elements contained in the carbon steel samples. Injection of inhibitors to the solutions shows some of the elements greatly increased. This increment is however due to carbon and oxygen atoms of the absorbed MEG and inhibitors on the carbon steel. Figure 4-60 (B, D & F) equally confirmed that a carbonaceous element containing oxygen and magnesium has covered the surface of the carbon steel. The intensity indication of carbon and oxygen also increased with increase in concentration of MEG and inhibitors since more anions and cations salt will be absorbed on the carbon steel. This corresponds with the results obtained by the electrochemical measurements methods.

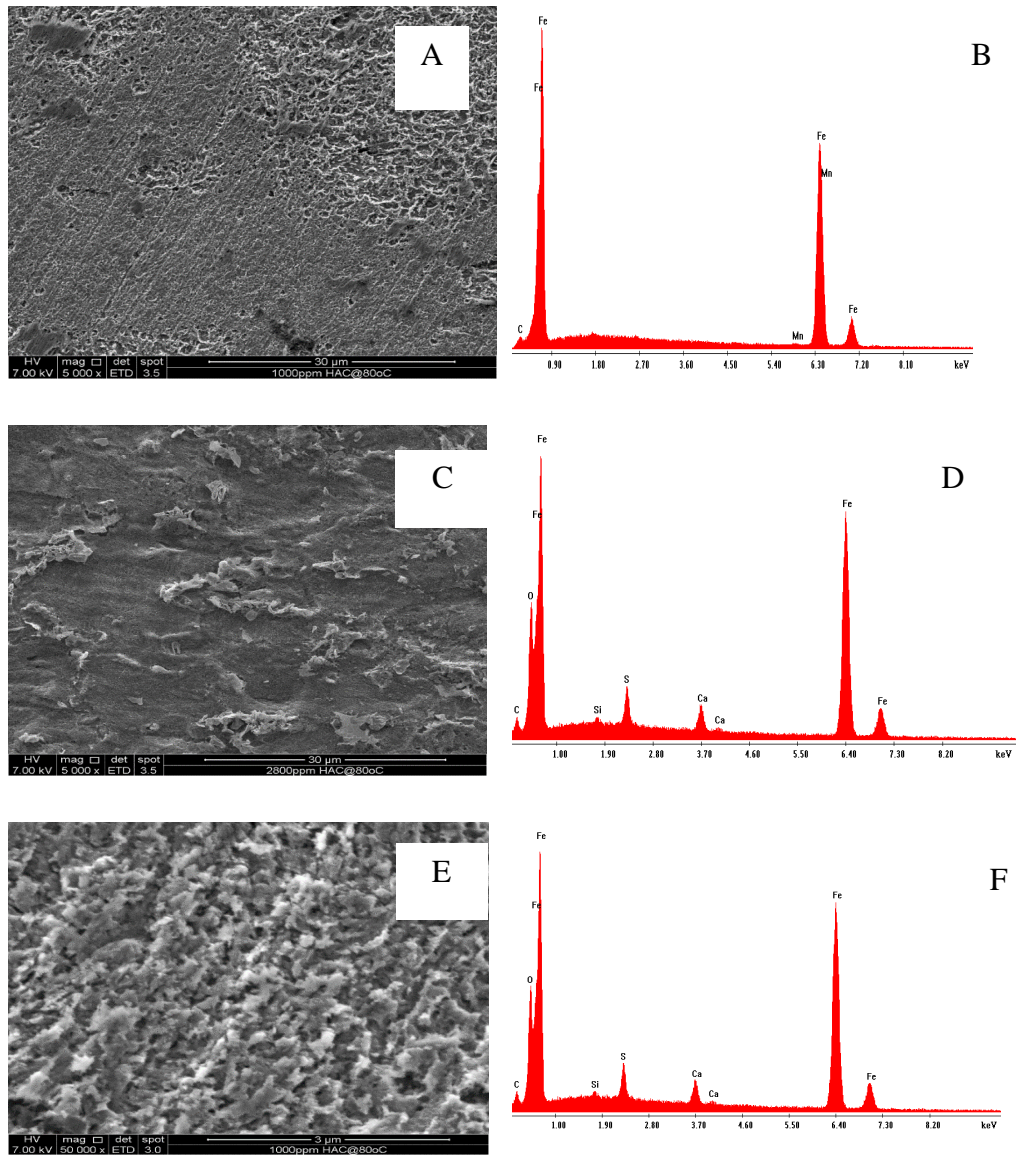


Figure 4-59: SEM images (Left) and EDX spectrum (Right) of carbon steel samples exposed to 3.5% wt. NaCl solution and 1000ppm HAc and different concentrations of MEG for 6 hours. [A] 20% MEG [B] 80% MEG

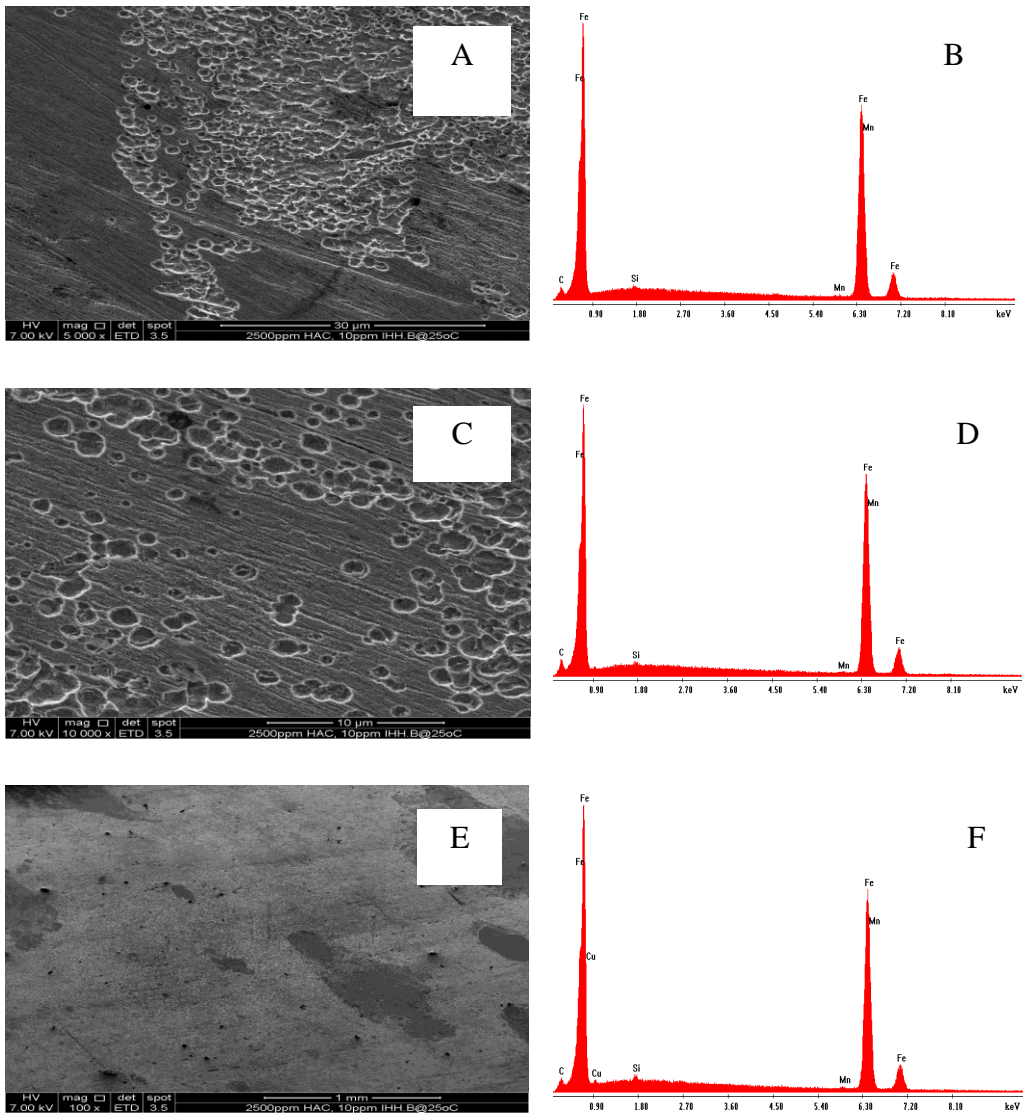


Figure 4-60: SEM images (Left) and EDX spectrum (Right) of carbon steel samples exposed to 3.5% wt. NaCl solution and 1000ppm HAC, 80% MEG and 10ppm of : [A] inhibitor XX [B] inhibitor YY [C] inhibitor ZZ.

4.4.4 XPS spectrum analysis

The XPS measurement technique was employed to analyse the composition of the organic absorbed layer on the surface of the carbon steel sample after exposure to different conditions. As a result, the high resolution peaks for O 1s, C 1s, N 1s, Fe 2p and Cl 2p for carbon steel surface after 6 hours of immersion in 3.5% wt. NaCl solution containing HAc, MEG and inhibitors are shown. All XPS spectra were observed to contained complex forms which were assigned to the corresponding species through a deconvolution fitting procedure using the CasaXPS facility from the University of Manchester apparatus.

i. O 1s spectra

The XPS spectra corresponding to the O 1s region for different test conditions and at different sputtering times are shown in Figure 4-61. In Figure 4-61, it is seen that only one single peak are observed at binding energy of 530 eV. This peak is corresponds to the hydroxyl groupings that results in the chemisorption of water and oxygen. The trend regarding the chemical nature of the species present in the corroded sample layer are the same in all the cases examined Similarly, Figure 4-61 shows that deconvolution of the O 1s spectrum main contributions are from oxygen in the form of oxide and anhydrous ions oxides (O^{2-} and OH^-). These results confirmed that the use of XPS for the identification of different types of oxidized iron species is complex because the core Fe2p region shows a little difference between iron compounds.

ii. C 1s spectra

The XPS high resolution C 1s spectrum obtained on the carbon steel sample immersed in 3.5% wt. NaCl solution are presented in Figure 4-62. The deconvolution of the C 1s and all other spectra was carried out with aid of CasaXPS software from the University of Manchester. In Figure 4-62, it is seen that two peaks, the first peak at 285 eV and the

second peak at 290 eV were identified. The first peak at 285 eV is considered as a result of aromatic or aliphatic carbon atoms together with the carbon atoms of the same type (C-C). The second peak at 290 eV is caused by the carbon atoms linked to oxygen atoms (C-O) or to N atoms (C-N and C+N). The hydrocarbon contribution (C-C/C-H) dominates over the oxidized carbon species. It is observed that when organic molecules are involved on the oxidized iron or carbon electrode surface, the carbon intensity in the XPS measurements are expected to increase compared to that observed in non-treated electrode.

iii. N 1s spectra

The XPS spectrum for N 1s has one single peak at approximately 400 eV as presented in Figure 4-63. This peak is shifted from from 398 eV, the characteristic elemental binding energy of N 1s electron. This change in binding energy may due to the presence of Fe (III) and Zn (II). It is noted that the N 1s peak observed at 399.7 eV could be as a result of presence of (=N-) in the molecule absorbed on the electrode surface. However, the peak at 399.9 eV could be attributed to the neutral imine (-N+) and amine (-N-M) nitrogen atoms.

iv. Fe 2p spectra

The XPS high resolution spectrum for Fe 2p_{3/2} is shown in Figure 4-64. It is noted that deconvolution of the spectrum suggests that two peaks are noticed corresponding to the metallic iron at 710 eV and 730 eV binding energy respectively. The first peak of Fe 2p corresponding to binding energy of 710 eV indicates for the resolution of chemical state of Fe²⁺ in the surface of the electrode materials, while the second peak at 730 eV corresponds to the formation of ferric surface oxidation products of Fe³⁺. The increase of peaks from 710 eV to 730 eV signifies that iron is present in Fe³⁺ state in the electrode surface film. The peak value at 711.0 eV is due to the presence of FeOOH and Fe (OH)₃. This peak corresponds to the mean binding energy of Fe 2p in α -FeOOH as 711.0 \pm 0.2 eV.

The Fe 2p peak values with inhibitors are 711 eV and 725 eV. The peaks value noticed with the presence of inhibitors confirm the presence of Fe₂O₃, Fe₃O₄ and FeOOH and Fe³⁺ on the surface electrode. The film form with the inhibitors is seen as no protective.

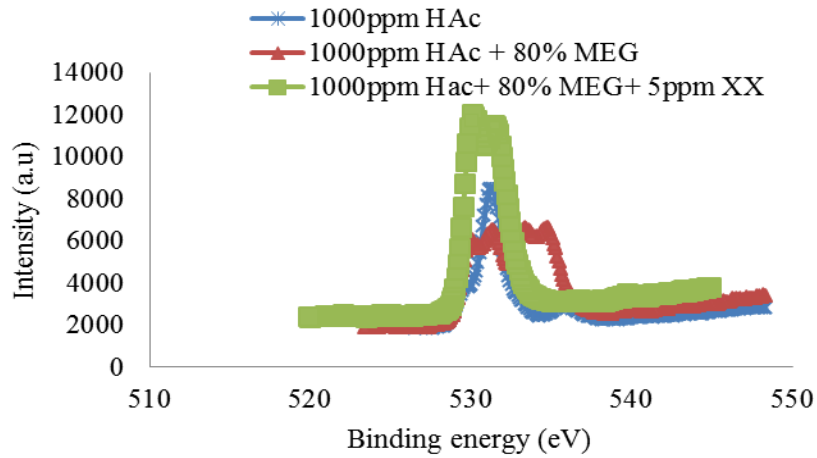


Figure 4-61: The XPS deconvolution profiles for O 1s for carbon steel sample after 6 hours immersion period in 3.5% wt. NaCl solution in the presence of HAc, MEG and inhibitors

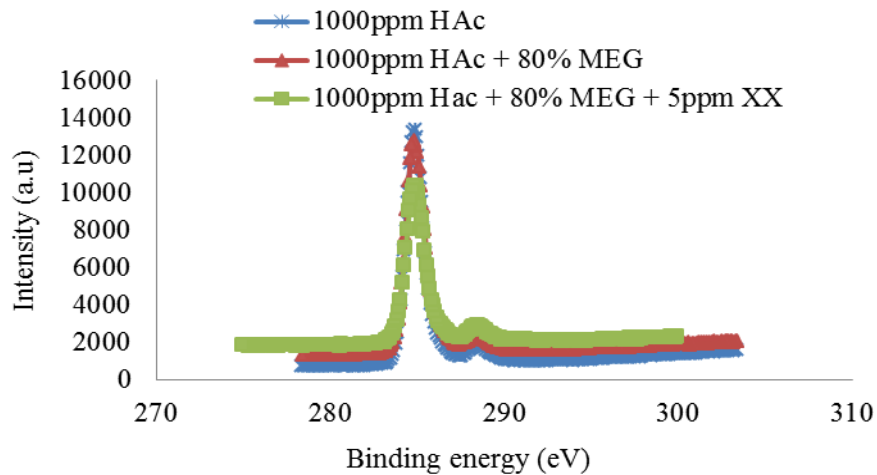


Figure 4-62: The XPS deconvolution profiles for C 1s for carbon steel sample after 6 hours immersion period in 3.5% wt. NaCl solution in the presence of HAc, MEG and inhibitors

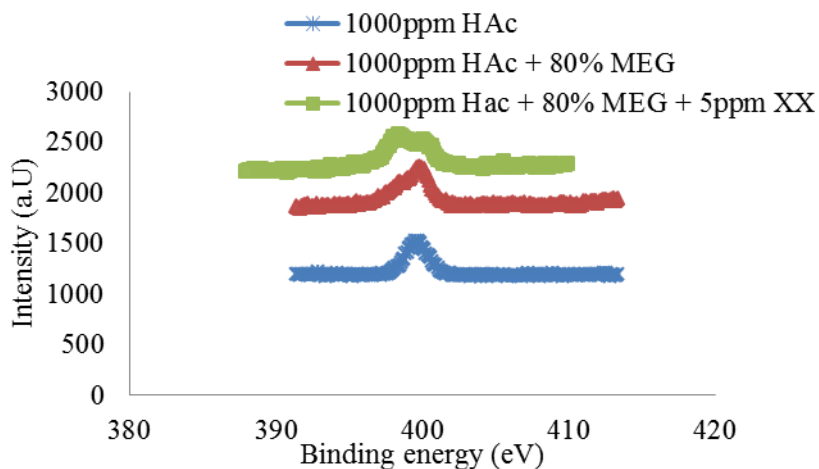


Figure 4-63: The XPS deconvolution profiles for N 1s for carbon steel sample after 6 hours immersion period in 3.5% wt. NaCl solution in the presence of HAc, MEG and inhibitors

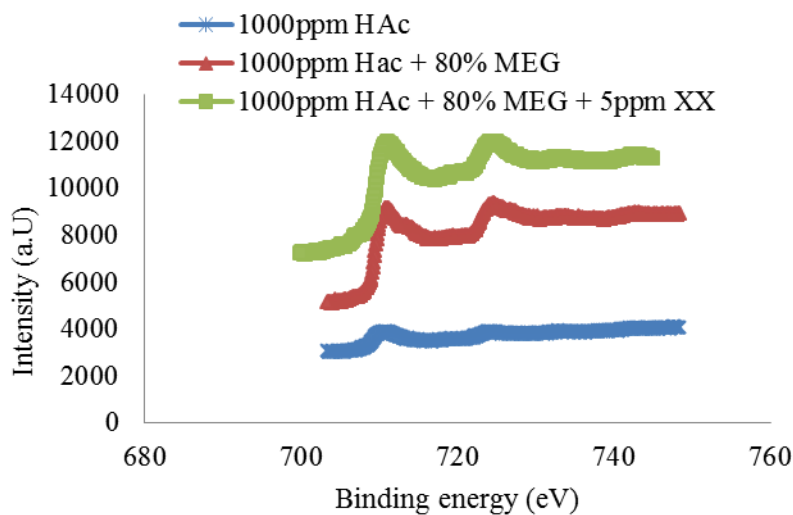


Figure 4-64: The XPS deconvolution profiles for Fe 2p for carbon steel sample after 6 hours immersion period in 3.5% wt. NaCl solution in the presence of HAc, MEG and inhibitors

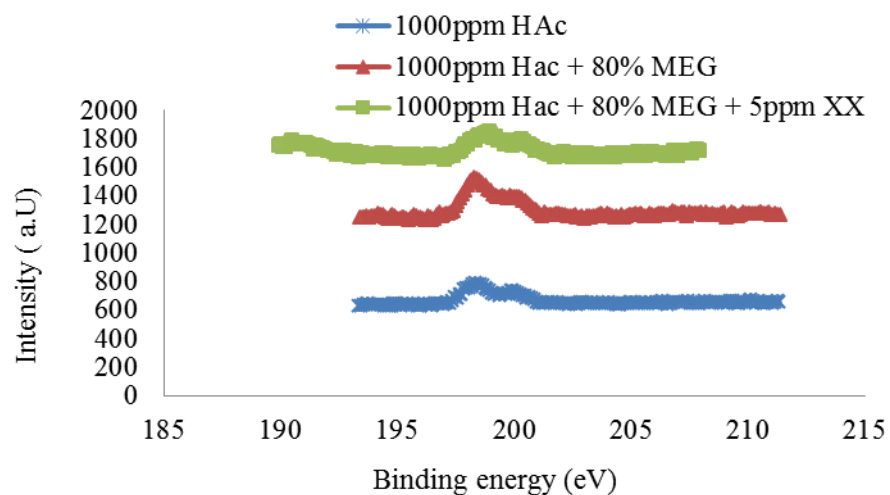


Figure 4-65: The XPS deconvolution profiles for Cl 1s for carbon steel sample after 6 hours immersion period in 3.5% wt. NaCl solution in the presence of HAc, MEG and inhibitors.

Table 4-21: Atomic percentage of XPS deconvolution profiles for carbon steel sample after 6 hours immersion period in 3.5% wt. NaCl solution in the presence of HAc, MEG and inhibitors

Sample	C %	Cl %	Cu %	Fe %	N %	Na %	Ni %	O %	Total
HAc	74.70	0.56	0.28	0.65	1.39	3.58	0.04	18.81	100.00
HAc + MEG	64.25	0.96	1.40	2.94	1.76	0.02	0.66	28.00	100.00
HAc+MEG+Inhibitors	55.40	0.68	2.82	3.51	2.16	0.00	2.36	33.07	100.00

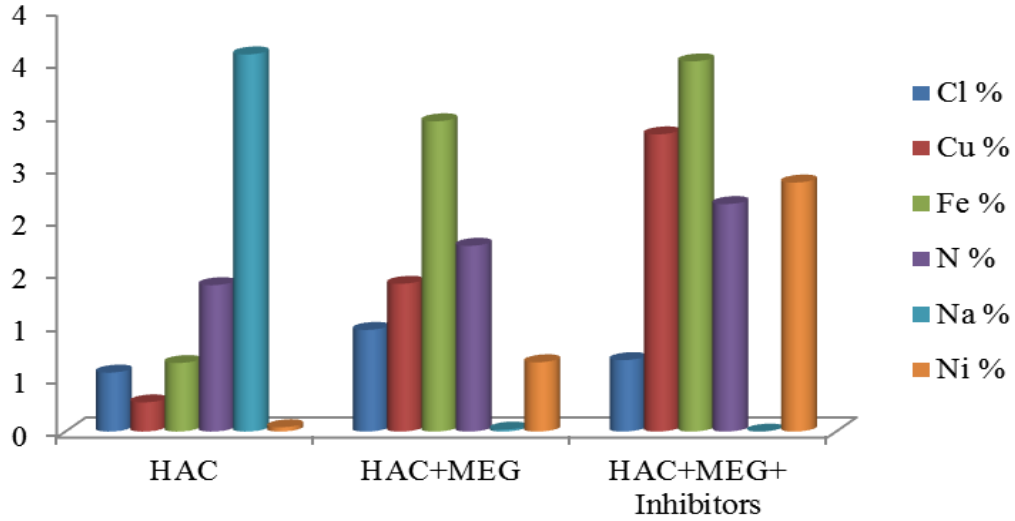


Figure 4-66: Variation of the XPS deconvolution profiles for different samples of carbon steel after 6 hours immersion period in 3.5% wt. NaCl solution in the presence of HAC, MEG and inhibitors

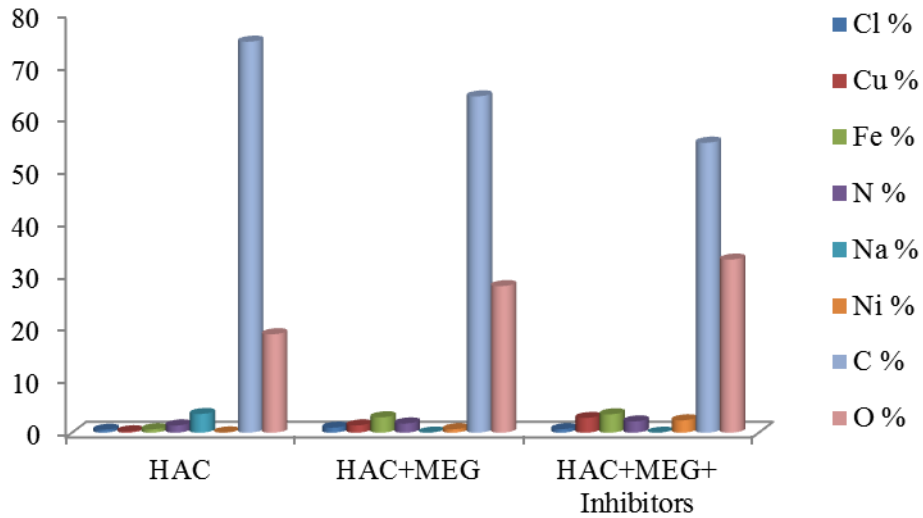


Figure 4-67: Variation of the XPS deconvolution profiles for different samples of carbon steel after 6 hours immersion period in 3.5% wt. NaCl solution in the presence of HAC, MEG and inhibitors including C % and O % respectively.

The next Chapter will give details summaries of this investigations and hence proposed a recommendations for further works to be carried out based on this study.

CHAPTER 5

Conclusions and Further Work

5.1 Conclusions

This Chapter presents summary of conclusions from the experimental investigation of synergistic effects of HAc and MEG on the corrosion of carbon steel in CO₂ saturated environment at three different temperatures of 25°C, 50°C and 80°C, pH of 6.6, 0.54 bar of CO₂ partial pressure, 20% and 80% MEG, different concentrations of HAc and corrosion inhibitors using the weight loss and electrochemical methods. In addition, the inhibitive performance of three organic corrosion inhibitors (namely XX, YY and ZZ) on the CO₂ corrosion of carbon steel in 3.5% wt NaCl solutions containing acetic acid and mono-ethylene glycol were also evaluated. The surface examination of the samples prior to experiment and after exposure at different conditions were also determined to ascertain which elements were present on the electrode surface prior to and after exposure to the solution using the SEM and EDX and XPS. Weight loss and electrochemical measurements using linear polarization resistance LPR, EIS and PDP were employed to establish the relationship between the corrosion rate, corrosion potential and corrosion current density as a function of time. Based on this study and the results, the following conclusions are made:

- The corrosion rate by weight loss (**Phase – I**) per unit area of the carbon steel studied increase steadily as the concentrations of HAc was increased. At 25°C, the

average weight loss on addition of 500ppm HAc was 0.72 mm/yr. Increased in temperature to 80°C leads to the corresponding increase of corrosion rate to approximately 1.05 mm/yr. The results showed a comparable corrosion rate at both temperatures with the addition of different concentrations of HAc.

- It is also show that addition of rich MEG and Lean MEG (20% MEG and 80% MEG) 3.5% wt. NaCl solution reduced the corrosion rate at all temperatures compared the corrosion rate when only HAc are present. The results observed with addition of 20% and 80% MEG demonstrate that there are changes in mechanism of CO₂ corrosion of carbon steel which is as a result of preventing of reactions sites by addition of 20% MEG and thereafter slow down corrosion reaction at high concentration (80%) MEG. Similarly, it is noted and confirmed that addition of 80% MEG (Lean MEG) ensue in a decrease in the corrosion potential, E_{corr} occurred as a result of decrease in corrosion current density as well as corrosion rate.
- The electrochemical (**Phase – II**) measurements have demonstrated that the corrosion rate increases with increase in concentration of HAc, and decreases with the increment of exposition time. This is attributed to the formation of iron carbonate film on the surface of the steel sample.
- The effectiveness of the organic corrosion inhibitor studied in 3.5% wt NaCl solution were confirmed by the polarization and EIS results obtained. However, It was noted that the inhibition efficiency increases as a result of concentrations of the inhibitors. Similarly, the analysis of the equivalent circuit diagram revealed that increase in concentrations of inhibitors from 3 ppm to 10 ppm has decrease the capacitance of the circuit and intensify the polarization resistance of the electrode-electrolyte interface.

- The three corrosion inhibitors studied has showed to inhibit carbon steel corrosion in CO₂ saturated environment. It was noted that the efficiencies of the inhibition increases with the concentrations in the solution and it increased to about 75% when the concentration of the inhibitors were increased to 10ppm.
- The application of corrosion inhibitors for all conditions studied further reduces the corrosion rate to the minimum level. Satisfactory inhibition performance was achieved for all three inhibitors tested with concentrations ranging from 3ppm to 10ppm respectively, compared to the uninhibited samples.
- The Bode and Nyquist plots of the EIS measurement have demonstrated that the diameter of the depressed semicircle decreased as the concentrations of the HAc and MEG increases, and the capacitive semicircle sizes also decreased on addition of 20% and 80% MEG to 3.5% NaCl solutions containing HAc.
- Finally, the SEM (**Phase – III**) analysis shows that a fairly dense layer of iron carbonate was observed in the absence of HAc at 80°C. On addition of HAc, the layers of the film became porous. A high magnification of SEM shows a small pits on the electrode surface submerged in the solution in the presence of HAc and without inhibitors. Also, the EDX spectra for the electrodes shows more lines characteristics for the presence of N, and intensities of C and O are signals are also noticed. Consequently, a charge transfer controlled mechanism was noticed due to the carbonate layer formation irrespective of the concentration of HAc.

5.2 Further work

Using the findings that have been presented in the present investigation for the first time, there are however, work that could be carry out to further study the corrosion of carbon steel in saturated CO₂ environment that can be encountered in the oil and gas industry especially when HAc and MEG are involved. These will assist the corrosion Engineers tackle the problems of internal and localized corrosion in oil and gas industry. The following are recommended as part of future works.

- Experiments should be carry out on the corrosion of carbon steel in the presence of HAc, MEG and inhibitors under flowing conditions using either a flow circulating flow loop, rotating cylinder electrode (RCE) or jet impingement method. This will be done to understand and ascertain the effect of flow velocity and the mechanism occur as a result of high flow rate and compare to the mechanism for no flow conditions.
- Experiments should also be conducted on corrosion of carbon steel in CO₂ environment in the presence of HAc with inhibitors for longer period of time using the electrochemical methods to compare the results with similar results obtained in the field. This will help to understand different corrosion environmental effects.
- The use of surface examination analysis such as XRD, SEM, Interferometry, and FTIR prior to and after each experiment should be applied. In this case, the corrosion product formed on the electrode surface in different conditions will be determined and help to understand different types of corrosion taking place on the examined samples. The exposed carbon steel substrate will need to be further examining at high temperature, long exposure time and at high pressure in CO₂ saturated environment.

- Break down of protective films and localized corrosion is one of the major problems of carbon steel corrosion in CO₂ environment. Further studies should be conducted under scale formation at different conditions to understand the effect on CO₂ corrosion of carbon steel in the presence of HAc and MEG.

REFERENCES

1. Kermani, M.B. and A. Morshed, *Carbon Dioxide Corrosion in Oil and Gas Production—A Compendium*. CORROSION, 2003. 59(8): p. 659-683.
2. G.H.Koch, M.P.H.B., N.G.Thompson, Y.P.Virman, and J.H.Payer, *Corrosion Cost and Prevention Strategies in the United States*. Federal highway administration, U.S. Department of Transportation: McLean VA., 2002.
3. Kermani, M.B. and D. Harrop, *The Impact of Corrosion on Oil and Gas Industry*.
4. Koch, G.H., et al., *Corrosion cost and preventive strategies in the United States*. 2002: Turner-Fairbank Highway Research Center.
5. Schmitt, G. and M. Horstemeier, *Fundamental Aspects of CO₂ Metal Loss Corrosion - Part II: Influence of Different Parameters on CO₂ Corrosion Mechanisms*. 2015, NACE International.
6. Roberge, P.R., *Corrosion basics: An introduction*. 2006, NACE Press Book. p. 56-70.
7. Nešić, S., *Carbon Dioxide Corrosion of Mild Steel*, in *Uhlig's Corrosion Handbook*. 2011, John Wiley & Sons, Inc. p. 229-245.
8. Venkatraman, M.S., et al. *Modeling corrosion of a metal under an aerosol droplet*. in *Materials Science Forum*. 2010. Trans Tech Publications.
9. Gunaltun, Y. and L. Payne, *A New Technique for the Control of Top of the Line Corrosion: TLCC-PIG*. NACE International.
10. Andersen, T.R., et al., *The Influence Of Condensation Rate And Acetic Acid Concentration On Tol-Corrosion In Multiphase Pipelines*. 2007, NACE International.
11. Nafday, O. and S. Nesic, *Iron Carbonate Scale Formation and CO₂ Corrosion in the Presence of Acetic Acid*. NACE International.
12. Abayarathna, D., A. Naraghi, and N. Obeyesekere, *Inhibition of Corrosion of Carbon Steel in the Presence of CO₂, H₂S and S*. NACE International.
13. Gulbrandsen, E., et al., *Effect of Precorrosion on the Performance of Inhibitors for CO₂ Corrosion of Carbon Steel*. NACE International.

14. Pourbaix, M., *Atlas of electrochemical equilibria in aqueous solutions*. 1974: National Association of Corrosion Engineers.
15. Vanloon, G.D., S, *Environmental chemistry - a global perspective*. 2011, Oxford University Press. p. 235-248.
16. Bardal, E., *Corrosion and Protection*. 2004: Springer.
17. Tait, W.S., *An Introduction to electrochemical corrosion testing for practicing engineers and scientists*. 1994, Pair Docs Publications.
18. C.A Barlow, J., *The Electrical Double Layer in physical chemistry: An Advanced Treatise*, in *Electrochemistry*. 1970, Academic press, New York.
19. T.Erdey-Gruz, *Kinetics of Electrode Processes*, in *Wiley Interscience*. 1972, John Wiley & Sons Inc, New York.
20. Sully, J.R.T., D.W, *Electrochemical methods of corrosion testing*. Vol. 13. 1987: Metal Hand book.
21. Burgan, B.A., S.C. Institute, and S.S.A. Centre, *Concise Guide to the Structural Design of Stainless Steel*. 1993: Steel Construction Institute.
22. International, A.S.M., *A.S.M International, Metals Handbook*, . Ninth edition ed. Vol. 13. 1987: Corrosion (ASM Handbook).
23. Schmitt, G. and M. Horstemeier, *Fundamental Aspects of CO₂ Metal Loss Corrosion - Part II: Influence of Different Parameters on CO₂ Corrosion Mechanisms*. 2006, NACE International.
24. Charng, T.L., F., *Review of corrosion causes and corrosion control in a technical facility*. 1982: United States.
25. Dugstad, K.V.a.A., *Film Covered Corrosion, Film Breakdown and Pitting Attack of Carbon Steels in Aqueous CO₂ Environments*. Corrosion Analysis Network, 1988: p. 1 - 18.
26. Bonis, M.R. and J.L. Crolet, *Why So Low Free Acetic Acid Thresholds, in Sweet Corrosion at Low PCO₂?* NACE International.
27. Smart, J., *A review of erosion corrosion in oil and gas production*. J. S. Smart, III. CORROSION 90/10, NACE, Houston, TX. Per Copy\$, 1990.

28. S.Nesic, J.P.a., *Erosion–Corrosion in Single- and Multiphase Flow*. 2011, in Uhlig's Corrosion Handbook: John Wiley & Sons, Inc., Hoboken, NJ, USA. .
29. Venkatesh, E.S., *Erosion Damage in Oil and Gas Wells*. Society of Petroleum Engineers.
30. Schmitt, G.A., et al., *Understanding Localized CO₂ Corrosion of Carbon Steel from Physical Properties of Iron Carbonate Scales*. NACE International.
31. Lillard, R.S., et al., *Using Local Electrochemical Impedance Spectroscopy to Examine Coating Failure*.
32. Oguzie, E.E., et al., *Corrosion and corrosion inhibition characteristics of bulk nanocrystalline ingot iron in sulphuric acid*. Journal of Solid State Electrochemistry, 2008. 12(6): p. 721-728.
33. Videm, K., *"Fundamental Studies aimed at Improving Models for Prediction of CO₂ Corrosion"*, *Progress in the Understanding and Prevention of Corrosion*. Institute of Metals,, London, 1993.
34. Dugstad, A.L., L and Videm, K, *Parametric study of CO₂ corrosion of carbon steel* NACE International, Houston, TX., 1995.
35. Nesic, S., et al., *Mechanistic Modeling for CO₂ Corrosion with Protective Iron Carbonate Films*. NACE International.
36. Sontvedt, E.E.a.T., *Effect of Flow on CO₂ Corrosion Rate in Real and Synthetic Formation Waters*. Corrosion Analysis Network, 1983: p. 1-40.
37. Waard, C.d., U. Lotz, and D.E. Milliams, *Predictive Model for CO₂ Corrosion Engineering in Wet Natural Gas Pipelines*.CORROSION,1991.47(12):p.976-985.
38. WAARD, C.D. and D.E. MILLIAMS, *Carbonic Acid Corrosion of Steel*. CORROSION, 1975. 31(5): p. 177-181.
39. Halvorsen, A.M. and T. Sontvedt, *CO₂ Corrosion Model for Carbon Steel Including Wall Shear Stress Model for Multiphase Flow and Limits for Production Rate to Avoid Mesa Attack*. NACE International.
40. STANDARD, N., *CO₂ corrosion rate calculation model*. 2005.

41. Garsany, Y., D. Pletcher, and B.M. Hedges, *The Role of Acetate in CO₂ Corrosion of Carbon Steel: Has the Chemistry Been Forgotten?* NACE International.
42. Crolet, J.L., N. Thevenot, and A. Dugstad, *Role of Free Acetic Acid on the CO₂ Corrosion of Steels*. NACE International.
43. Nešić, S., *Key issues related to modelling of internal corrosion of oil and gas pipelines—A review*. *Corrosion science*, 2007. 49(12): p. 4308-4338.
44. Perez, T.E., *Corrosion in the Oil and Gas Industry: An Increasing Challenge for Materials*. *JOM*, 2013. 65(8): p. 1033-1042.
45. Gulbrandsen, E., *Acetic Acid And Carbon Dioxide Corrosion Of Carbon Steel Covered With Iron Carbonate*. NACE International.
46. George, K.S. and S. Nešić, *Investigation of Carbon Dioxide Corrosion of Mild Steel in the Presence of Acetic Acid—Part 1: Basic Mechanisms*. *CORROSION*, 2007. 63(2): p. 178-186.
47. Dugstad, A., *Fundamental Aspects of CO₂ Metal Loss Corrosion - Part 1: Mechanism*. NACE International.
48. Pots, B.F.M. and E.L.J.A. Hendriksen, *CO₂ Corrosion Under Scaling Conditions - The Special Case of Top of Line Corrosion in Wet Gas Pipelines*. NACE International.
49. Hedges, B. and L. McVeigh, *The Role of Acetate in CO₂ Corrosion: The Double Whammy*. NACE International.
50. Ueda, M. and H. Takabe, *Effect of Organic Acid on CO₂ Corrosion of Carbon and CR Bearing Steels*. NACE International.
51. Guo, X.P., et al., *Novel quantitative method for evaluation pitting corrosion and pitting corrosion inhibition of carbon steel using electrochemical noise analysis*. *Journal of Materials Science*, 2005. 40(17): p. 4469-4473.
52. Zhang, Q., et al., *Corrosion behavior of Hastelloy C-276 in supercritical water*. *Corrosion Science*, 2009. 51(9): p. 2092-2097.

53. Dugstad, A., M. Seiersten, and R. Nyborg, *Flow Assurance of pH Stabilized Wet Gas Pipelines*. NACE International.
54. Singer, M., et al., *Combined effect of carbon dioxide, hydrogen sulfide, and acetic acid on bottom-of-the-line corrosion*. *Corrosion*, 2011. 67(1).
55. Mendez, C., et al., *On the Mechanism of Corrosion Inhibition by Crude Oils*. NACE International.
56. Oblonsky, L.J., M.P. Ryan, and H.S. Isaacs, *In situ determination of the composition of surface films formed on Fe-Cr alloys*. *JOURNAL OF THE ELECTROCHEMICAL SOCIETY*, 1998. 145: p. 1922-1932.
57. Sun, Y., K. George, and S. Netic, *The Effect of Cl⁻ and Acetic Acid on Localized CO₂ Corrosion in Wet Gas Flow*. NACE International.
58. Okafor, P.C., B. Brown, and S. Netic, *CO₂ corrosion of carbon steel in the presence of acetic acid at higher temperatures*. *Journal of Applied Electrochemistry*, 2009. 39(6): p. 873-877.
59. Zhang, Y., et al., *Modeling steel corrosion under supercritical CO₂ conditions*. *Materials and Corrosion*, 2013. 64(6): p. 478-485.
60. Hurlen, T., et al., *Corrosion and passive behaviour of aluminium in weakly acid solution*. *Electrochimica Acta*, 1984. 29(5): p. 579-585.
61. Guo, S., F. Farelas, and M. Singer, *Effect of Monoethylene Glycol on Sweet Top of the line corrosion*. NACE International.
62. Halvorsen, A.M.K., et al., *The Relationship Between Internal Corrosion Control Method, Scale Control And Meg Handling Of A Multiphase Carbon Steel Pipeline Carrying Wet Gas With CO₂ And Cetic Acid*. NACE International.
63. Pojtanabuntoeng, T., M. Salasi, and R. Gubner, *The Influence of Mono Ethylene Glycol (MEG) on CO₂ Corrosion of Carbon Steel at Elevated Temperatures (80 to 120oc)*. NACE International.
64. Brustad, S., K.P. Løken, and J.G. Waalmann, *Hydrate Prevention using MEG instead of MeOH: Impact of experience from major Norwegian developments on*

- technology selection for injection and recovery of MEG*. Offshore Technology Conference.
65. Lu, H., A.T. Kan, and M.B. Tomson, *Effects of Monoethylene Glycol on Carbonate Equilibrium and Calcite Solubility in Gas/Monoethylene Glycol/Water/Salt Mixed Systems*. Society of Petroleum Engineers.
 66. Svenningsen, G. and R. Nyborg, *Modeling of Top of Line Corrosion with Organic Acid and Glycol*. NACE International.
 67. Wang, C., et al., *Corrosion Study of Carbon Steel in the Presence of Monoethylene Glycol (MEG) and Corrosion Inhibitors in Acid*. NACE International.
 68. Scully, J.R., *The Polarization Resistance Method for Determination of Instantaneous Corrosion Rates: A Review*. NACE International.
 69. Magaña-Zavala, C.R., et al., *Electrochemical impedance spectroscopy (EIS) modelling of different behaviours of Ni and Ni oxide thin films for corrosion prevention in sour media*. *Anti-Corrosion Methods and Materials*, 2010. 57(3): p. 118-125.
 70. Wang, H., et al., *Characterization of Inhibitor and Corrosion Product Film Using Electrochemical Impedance Spectroscopy (EIS)*. NACE International.
 71. Chechirlian, S., et al., *A specific aspect of impedance measurements in low conductivity media. Artefacts and their interpretations*. *Electrochimica Acta*, 1990. 35(7): p. 1125-1131.
 72. Itagaki, M., T. Suzuki, and K. Watanabe, *Anodic dissolution of Fe-Mo in sulfuric acid solution as investigated by electrochemical impedance spectroscopy combined with channel flow double electrode*. *Corrosion Science*, 1998. 40(8): p. 1255-1265.
 73. Pajkossy, T., *Impedance of rough capacitive electrodes*. *Journal of Electroanalytical Chemistry*, 1994. 364(1): p. 111-125.
 74. Mansfeld, F., M. Kendig, and W. Lorenz, *Corrosion inhibition in neutral, aerated media*. *Journal of the Electrochemical Society*, 1985. 132(2): p. 290-296.

75. G1-03, A., *Standard Practice for Preparing, Cleaning, and Evaluating Corrosion Test Specimens*. ASTM International, West Conshohocken, PA, 2011, www.astm.org, 2011.
76. Cottis, R.A., *Lecture notes on Corrosion*. University of Manchester, Corrosion and Protection Center, 2009.
77. Sekine, I., Kawase, T., Kobayashi, M. and Yuasa, M, *The effects of chromium and molybdenum on the corrosion behavior of ferritic stainless steels in boiling acetic acid solutions*. *Corrosion Science*, 1991. 32,: p. pp. 815-825. .
78. Lindsay, R. and S.B. Lyon, *4.25 - Introduction to Control of Corrosion by Environmental Modification*, in *Shreir's Corrosion*. 2010, Elsevier: Oxford. p. 2891-2899.
79. Qiu, J.H. and P.H. Chua, *EIS and XPS study of the corrosion of carbon steel in inhibited natural seawater*. *Surface and Interface Analysis*, 1999. 28(1): p. 119-122.
80. Yong Xiang, M.Y., Yoon-Seok Choi, David Young, Srdjan Nesic, *Time-dependent electrochemical behaviour of carbon steel in MEA*. *International Journal of Greenhouse Gas Control*, 2014. 30: p. 125-132.
81. Galicia, P., N. Batina, and I. González, *The Relationship between the Surface Composition and Electrical Properties of Corrosion Films Formed on Carbon Steel in Alkaline Sour Medium: An XPS and EIS Study*. *The Journal of Physical Chemistry B*, 2006. 110(29): p. 14398-14405.
82. Ochoa, N., et al., *CO 2 corrosion resistance of carbon steel in relation with microstructure changes*. *Materials Chemistry and Physics*, 2015. 156: p. 198-205.
83. Hassan, H.H., E. Abdelghani, and M.A. Amin, *Inhibition of mild steel corrosion in hydrochloric acid solution by triazole derivatives: Part I. Polarization and EIS studies*. *Electrochimica Acta*, 2007. 52(22): p. 6359-6366.
84. Xianghong, L., et al., *Inhibition of the corrosion of cold rolled steel in hydrochloric acid solution by Tween-40*. *Anti-Corrosion Methods and Materials*, 2009. 56(4): p. 232-238.

Appendix A

Electrochemical impedance spectroscopy (EIS) parameters obtained for carbon steel electrodes saturated in 3.5% wt. NaCl solution containing HAc, 20% & 80% MEG, corrosion inhibitors at 25°C, 50°C and 80°C

Appendixes	Title	Page
Appendix – A1	Electrochemical parameters obtained for carbon steel electrode in solutions containing HAc, 20% MEG and inhibitors at 25°C	169
Appendix – A2	Electrochemical parameters obtained for carbon steel electrode in solutions containing HAc, 80% MEG and inhibitors at 25°C.	170
Appendix – A3	Electrochemical parameters obtained for carbon steel electrode in solutions containing HAc, 20% MEG and inhibitors at 50°C	171
Appendix – A4	Electrochemical parameters obtained for carbon steel electrode in 3.5% wt. NaCl solutions containing HAc, 80% MEG and inhibitors at 50°C	172
Appendix – A5	Electrochemical parameters obtained for carbon steel electrode in 3.5% wt. NaCl solutions containing HAc, 20% MEG and inhibitors at 80°C.	173
Appendix – A6	Electrochemical parameters obtained for carbon steel electrode in 3.5% wt. NaCl solutions containing HAc, 80% MEG and inhibitors at 80°C.	174

A-1: Electrochemical parameters obtained for carbon steel electrode in solutions containing HAc, 20% MEG and inhibitors at 25°C

Composition	R_{ct}	R_{sol}	C_{dl}	θ
Uninhibited solution	37	7.1	90	0
Solution + 20% MEG + 500ppm HAc+ 2ppm XX	60	9.80	55	39
Solution + 20% MEG + 500ppm HAc+ 2ppm YY	119	113	49	46
Solution + 20% MEG + 500ppm HAc+ 2ppm ZZ	200	821	44	51
Solution + 20% MEG + 500ppm HAc+ 5ppm XX	42	10.6	32	64
Solution + 20% MEG + 500ppm HAc+ 5ppm YY	55	8.9	54	40
Solution + 20% MEG + 500ppm HAc+ 5ppm ZZ	122	11.3	33	63
Solution + 20% MEG + 500ppm HAc+ 10ppm XX	240	11.8	31	66
Solution + 20% MEG + 500ppm HAc+ 10ppm YY	100	12	39	57
Solution + 20% MEG + 500ppm HAc+ 10ppm ZZ	90	8	28	69
Solution + 20% MEG + 1000ppm HAc+ 2ppm XX	60	6.44	130	31
Solution + 20% MEG + 1000ppm HAc+ 2ppm YY	77	11.0	74	18
Solution + 20% MEG + 1000ppm HAc+ 2ppm ZZ	140	6.5.2	32	64
Solution + 20% MEG + 1000ppm HAc+ 5ppm XX	260	11.8	50	44
Solution + 20% MEG + 1000ppm HAc+ 5ppm YY	69	9.05	45	50
Solution + 20% MEG + 1000ppm HAc+ 5ppm ZZ	78	5.5	33	63
Solution + 20% MEG + 1000ppm HAc+ 10ppm XX	150	10	29	68
Solution + 20% MEG + 1000ppm HAc+ 10ppm YY	238	10.7	46	49
Solution + 20% MEG + 1000ppm HAc+ 10ppm ZZ	240	9.2	22	76
Solution + 20% MEG + 2500ppm HAc+ 2ppm XX	49	9	125	17
Solution + 20% MEG + 2500ppm HAc+ 2ppm YY	78	9.08	35	61
Solution + 20% MEG + 2500ppm HAc+ 2ppm ZZ	305	4.2	41	54
Solution + 20% MEG + 2500ppm HAc+ 5ppm XX	218	10.6	29	68
Solution + 20% MEG + 2500ppm HAc+ 5ppm YY	70	11.5	38	58
Solution + 20% MEG + 2500ppm HAc+ 5ppm ZZ	60	9.8	22	76
Solution + 20% MEG + 2500ppm HAc+ 10ppm XX	114	6.08	52	42
Solution + 20% MEG + 2500ppm HAc+ 10ppm YY	240	10.5	29	68
Solution + 20% MEG + 2500ppm HAc+ 10ppm ZZ	229	8.4	30	67

A-2: Electrochemical parameters obtained for carbon steel electrode in solutions containing HAc, 80% MEG and inhibitors at 25°C.

Composition	R_{ct}	R_{sol}	C_{dl}	,θ
Uninhibited solution	37	8.1	144	0
Solution + 20% MEG + 500ppm HAc+ 2ppm XX	44	5.20	40	72
Solution + 20% MEG + 500ppm HAc+ 2ppm YY	89	9.9	34	76
Solution + 20% MEG + 500ppm HAc+ 2ppm ZZ	190	5.21	49	66
Solution + 20% MEG + 500ppm HAc+ 5ppm XX	43	8.6	22	85
Solution + 20% MEG + 500ppm HAc+ 5ppm YY	64	7.9	56	61
Solution + 20% MEG + 500ppm HAc+ 5ppm ZZ	52	4.15	40	72
Solution + 20% MEG + 500ppm HAc+ 10ppm XX	210	8.8	55	62
Solution + 20% MEG + 500ppm HAc+ 10ppm YY	61	5.7	29	80
Solution + 20% MEG + 500ppm HAc+ 10ppm ZZ	55	6.3	31	78
Solution + 20% MEG + 1000ppm HAc+ 2ppm XX	43	9.1	112	22
Solution + 20% MEG + 1000ppm HAc+ 2ppm YY	66	8.0	30	79
Solution + 20% MEG + 1000ppm HAc+ 2ppm ZZ	125	9.2	34	76
Solution + 20% MEG + 1000ppm HAc+ 5ppm XX	213	6.8	54	63
Solution + 20% MEG + 1000ppm HAc+ 5ppm YY	49	7.05	46	68
Solution + 20% MEG + 1000ppm HAc+ 5ppm ZZ	62	9.2	39	73
Solution + 20% MEG + 1000ppm HAc+ 10ppm XX	90	5.5	51	65
Solution + 20% MEG + 1000ppm HAc+ 10ppm YY	145	6.30	57	60
Solution + 20% MEG + 1000ppm HAc+ 10ppm ZZ	112	11	22	85
Solution + 20% MEG + 2500ppm HAc+ 2ppm XX	33	8.50	109	24
Solution + 20% MEG + 2500ppm HAc+ 2ppm YY	37	10.38	55	62
Solution + 20% MEG + 2500ppm HAc+ 2ppm ZZ	105	10.2	44	69
Solution + 20% MEG + 2500ppm HAc+ 5ppm XX	118	7.65	56	61
Solution + 20% MEG + 2500ppm HAc+ 5ppm YY	60	4.5	64	56
Solution + 20% MEG + 2500ppm HAc+ 5ppm ZZ	54	11	40	72
Solution + 20% MEG + 2500ppm HAc+ 10ppm XX	72	11.07	44	69
Solution + 20% MEG + 2500ppm HAc+ 10ppm YY	111	6.2	34	76
Solution + 20% MEG + 2500ppm HAc+ 10ppm ZZ	132	6.5	28	81

A-3: Electrochemical parameters obtained for carbon steel electrode in solutions containing HAc, 20% MEG and inhibitors at 50°C

Composition	R_{ct}	R_{sol}	C_{dl}	,θ
Uninhibited solution	40	8.1	197	0
Solution + 20% MEG + 500ppm HAc+ 2ppm XX	64	9.20	53	73
Solution + 20% MEG + 500ppm HAc+ 2ppm YY	109	8	70	64
Solution + 20% MEG + 500ppm HAc+ 2ppm ZZ	210	10.21	34	83
Solution + 20% MEG + 500ppm HAc+ 5ppm XX	48	10.6	30	85
Solution + 20% MEG + 500ppm HAc+ 5ppm YY	76	8.9	56	72
Solution + 20% MEG + 500ppm HAc+ 5ppm ZZ	112	10.15	40	80
Solution + 20% MEG + 500ppm HAc+ 10ppm XX	230	11.8	56	72
Solution + 20% MEG + 500ppm HAc+ 10ppm YY	119	8	45	77
Solution + 20% MEG + 500ppm HAc+ 10ppm ZZ	98	7	32	84
Solution + 20% MEG + 1000ppm HAc+ 2ppm XX	57	9.44	50	75
Solution + 20% MEG + 1000ppm HAc+ 2ppm YY	75	7.4.0	69	65
Solution + 20% MEG + 1000ppm HAc+ 2ppm ZZ	130	10.2	34	83
Solution + 20% MEG + 1000ppm HAc+ 5ppm XX	240	8.8	54	73
Solution + 20% MEG + 1000ppm HAc+ 5ppm YY	65	9.05	60	70
Solution + 20% MEG + 1000ppm HAc+ 5ppm ZZ	77	6.95	39	80
Solution + 20% MEG + 1000ppm HAc+ 10ppm XX	120	8.8	50	75
Solution + 20% MEG + 1000ppm HAc+ 10ppm YY	248	10.2	57	71
Solution + 20% MEG + 1000ppm HAc+ 10ppm ZZ	109	7	44	78
Solution + 20% MEG + 2500ppm HAc+ 2ppm XX	45	7.5	104	47
Solution + 20% MEG + 2500ppm HAc+ 2ppm YY	66	9.08	55	72
Solution + 20% MEG + 2500ppm HAc+ 2ppm ZZ	125	5.5	44	78
Solution + 20% MEG + 2500ppm HAc+ 5ppm XX	208	7.65	33	83
Solution + 20% MEG + 2500ppm HAc+ 5ppm YY	58	8.5	64	68
Solution + 20% MEG + 2500ppm HAc+ 5ppm ZZ	65	9.8	40	80
Solution + 20% MEG + 2500ppm HAc+ 10ppm XX	109	7.4	44	78
Solution + 20% MEG + 2500ppm HAc+ 10ppm YY	221	10.5	55	72
Solution + 20% MEG + 2500ppm HAc+ 10ppm ZZ	108	6	33	83

A-4: Electrochemical parameters obtained for carbon steel electrode in 3.5% wt. NaCl solutions containing HAc, 80% MEG and inhibitors at 50°C

Composition	R_{ct}	R_{sol}	C_{dl}	,θ
Uninhibited solution	44	6.9	150	0
Solution + 20% MEG + 500ppm HAc+ 2ppm XX	50	9.20	50	67
Solution + 20% MEG + 500ppm HAc+ 2ppm YY	94	7.5	50	67
Solution + 20% MEG + 500ppm HAc+ 2ppm ZZ	109	10.2	34	77
Solution + 20% MEG + 500ppm HAc+ 5ppm XX	64	10	22	85
Solution + 20% MEG + 500ppm HAc+ 5ppm YY	68	5.7	56	63
Solution + 20% MEG + 500ppm HAc+ 5ppm ZZ	55	8	40	73
Solution + 20% MEG + 500ppm HAc+ 10ppm XX	76	9	61	59
Solution + 20% MEG + 500ppm HAc+ 10ppm YY	44	7	55	63
Solution + 20% MEG + 500ppm HAc+ 10ppm ZZ	38	10	43	71
Solution + 20% MEG + 1000ppm HAc+ 2ppm XX	60	9.44	112	25
Solution + 20% MEG + 1000ppm HAc+ 2ppm YY	44	8.5	56	63
Solution + 20% MEG + 1000ppm HAc+ 2ppm ZZ	38	10.2	44	71
Solution + 20% MEG + 1000ppm HAc+ 5ppm XX	67	11.8	35	77
Solution + 20% MEG + 1000ppm HAc+ 5ppm YY	83	9.05	55	63
Solution + 20% MEG + 1000ppm HAc+ 5ppm ZZ	70	9.95	32	79
Solution + 20% MEG + 1000ppm HAc+ 10ppm XX	113	11	29	81
Solution + 20% MEG + 1000ppm HAc+ 10ppm YY	200	6.5	34	77
Solution + 20% MEG + 1000ppm HAc+ 10ppm ZZ	121	7	38	75
Solution + 20% MEG + 2500ppm HAc+ 2ppm XX	45	7.5	80	47
Solution + 20% MEG + 2500ppm HAc+ 2ppm YY	66	9.08	55	63
Solution + 20% MEG + 2500ppm HAc+ 2ppm ZZ	100	10	44	71
Solution + 20% MEG + 2500ppm HAc+ 5ppm XX	217	6.7	56	63
Solution + 20% MEG + 2500ppm HAc+ 5ppm YY	58	4.6	64	57
Solution + 20% MEG + 2500ppm HAc+ 5ppm ZZ	65	9.8	40	73
Solution + 20% MEG + 2500ppm HAc+ 10ppm XX	96	12	65	57
Solution + 20% MEG + 2500ppm HAc+ 10ppm YY	61	7.2	60	60
Solution + 20% MEG + 2500ppm HAc+ 10ppm ZZ	75	8	55	63

A-5: Electrochemical parameters obtained for carbon steel electrode in 3.5% wt. NaCl solutions containing HAc, 20% MEG and inhibitors at 80°C.

Composition	R_{ct}	R_{sol}	C_{dl}	,θ
Uninhibited solution	44	8.1	70	0
Solution + 20% MEG + 500ppm HAc+ 2ppm XX	46	9.2	44	37
Solution + 20% MEG + 500ppm HAc+ 2ppm YY	167	11	32	54
Solution + 20% MEG + 500ppm HAc+ 2ppm ZZ	65	10.2	28	60
Solution + 20% MEG + 500ppm HAc+ 5ppm XX	80	10.5	22	69
Solution + 20% MEG + 500ppm HAc+ 5ppm YY	50	7.2	33	53
Solution + 20% MEG + 500ppm HAc+ 5ppm ZZ	45	10	40	43
Solution + 20% MEG + 500ppm HAc+ 10ppm XX	68	11	29	59
Solution + 20% MEG + 500ppm HAc+ 10ppm YY	34	6	22	69
Solution + 20% MEG + 500ppm HAc+ 10ppm ZZ	57	9	24	66
Solution + 20% MEG + 1000ppm HAc+ 2ppm XX	50	9.4	33	53
Solution + 20% MEG + 1000ppm HAc+ 2ppm YY	55	9.5	19	73
Solution + 20% MEG + 1000ppm HAc+ 2ppm ZZ	30	10.2	21	70
Solution + 20% MEG + 1000ppm HAc+ 5ppm XX	25	11.8	17.9	74
Solution + 20% MEG + 1000ppm HAc+ 5ppm YY	55	9.05	33	53
Solution + 20% MEG + 1000ppm HAc+ 5ppm ZZ	38	9.95	39	44
Solution + 20% MEG + 1000ppm HAc+ 10ppm XX	40	11	50	29
Solution + 20% MEG + 1000ppm HAc+ 10ppm YY	200	10	57	19
Solution + 20% MEG + 1000ppm HAc+ 10ppm ZZ	34	7	8	89
Solution + 20% MEG + 2500ppm HAc+ 2ppm XX	45	7.5	24	66
Solution + 20% MEG + 2500ppm HAc+ 2ppm YY	66	9.	55	21
Solution + 20% MEG + 2500ppm HAc+ 2ppm ZZ	46	11.2	44	37
Solution + 20% MEG + 2500ppm HAc+ 5ppm XX	61	10.6	56	20
Solution + 20% MEG + 2500ppm HAc+ 5ppm YY	58	11	41	41
Solution + 20% MEG + 2500ppm HAc+ 5ppm ZZ	65	9.8	40	43
Solution + 20% MEG + 2500ppm HAc+ 10ppm XX	39	8	23	67
Solution + 20% MEG + 2500ppm HAc+ 10ppm YY	66	11	22	69
Solution + 20% MEG + 2500ppm HAc+ 10ppm ZZ	57	9	32	54

A-6: Electrochemical parameters obtained for carbon steel electrode in 3.5% wt. NaCl solutions containing HAc, 80% MEG and inhibitors at 80°C.

Composition	R_{ct}	R_{sol}	C_{dl}	,θ
Uninhibited solution	35	7	75	0
Solution + 20% MEG + 500ppm HAc+ 2ppm XX	55	9	45	40
Solution + 20% MEG + 500ppm HAc+ 2ppm YY	41	11	35	53
Solution + 20% MEG + 500ppm HAc+ 2ppm ZZ	48	10	34	55
Solution + 20% MEG + 500ppm HAc+ 5ppm XX	56	11	22	71
Solution + 20% MEG + 500ppm HAc+ 5ppm YY	76	12	56	25
Solution + 20% MEG + 500ppm HAc+ 5ppm ZZ	39	10	40	47
Solution + 20% MEG + 500ppm HAc+ 10ppm XX	31	11	65	13
Solution + 20% MEG + 500ppm HAc+ 10ppm YY	41	8	34	55
Solution + 20% MEG + 500ppm HAc+ 10ppm ZZ	29	4.7	33	56
Solution + 20% MEG + 1000ppm HAc+ 2ppm XX	57	9.4	34	55
Solution + 20% MEG + 1000ppm HAc+ 2ppm YY	35	6.9	41	45
Solution + 20% MEG + 1000ppm HAc+ 2ppm ZZ	40	10.2	34	55
Solution + 20% MEG + 1000ppm HAc+ 5ppm XX	33	11.8	44	41
Solution + 20% MEG + 1000ppm HAc+ 5ppm YY	37	9.05	37	51
Solution + 20% MEG + 1000ppm HAc+ 5ppm ZZ	41	9.95	39	48
Solution + 20% MEG + 1000ppm HAc+ 10ppm XX	39	11	49	35
Solution + 20% MEG + 1000ppm HAc+ 10ppm YY	28	10	57	24
Solution + 20% MEG + 1000ppm HAc+ 10ppm ZZ	22	8	33	56
Solution + 20% MEG + 2500ppm HAc+ 2ppm XX	40	7.5	32	57
Solution + 20% MEG + 2500ppm HAc+ 2ppm YY	28	9.08	55	27
Solution + 20% MEG + 2500ppm HAc+ 2ppm ZZ	33	11.2	44	41
Solution + 20% MEG + 2500ppm HAc+ 5ppm XX	27	10.6	56	25
Solution + 20% MEG + 2500ppm HAc+ 5ppm YY	22	11.5	51	32
Solution + 20% MEG + 2500ppm HAc+ 5ppm ZZ	31	9.8	40	47
Solution + 20% MEG + 2500ppm HAc+ 10ppm XX	11	12	65	13
Solution + 20% MEG + 2500ppm HAc+ 10ppm YY	33	10	39	48
Solution + 20% MEG + 2500ppm HAc+ 10ppm ZZ	40	9	27	64

Appendix B

Potentiodynamic polarization (PDP) parameters obtained for carbon steel electrodes saturated in 3.5% wt. NaCl solution containing HAc, 20% & 80% MEG, corrosion inhibitors at 25°C, 50°C and 80°C

Appendixes	Title	Page
Appendix – B1	Electrochemical parameters for carbon steel samples saturated in 3.5% wt. NaCl solutions containing different concentrations of HAc, inhibitors and 20% MEG at 50°C	176
Appendix – B2	Electrochemical parameters for carbon steel samples saturated in 3.5% wt. NaCl solutions containing different concentrations of HAc, inhibitors and 80% MEG at 25°C	177
Appendix – B3	: Electrochemical parameters for carbon steel samples saturated in 3.5% wt. NaCl solutions containing different concentrations of HAc, inhibitors and 80% MEG at 50°C	178
Appendix – B4	Electrochemical parameters for carbon steel samples saturated in 3.5% wt. NaCl solutions containing different concentrations of HAc, inhibitors and 20% MEG at 80°C	179
Appendix – B5	: Electrochemical parameters for carbon steel samples saturated in 3.5% wt. NaCl solutions containing different concentrations of HAc, inhibitors and 80% MEG at 80°C	180

B-1: Electrochemical parameters for carbon steel samples saturated in 3.5% wt. NaCl solutions containing different concentrations of HAc, inhibitors and 20% MEG at 50°C

Composition	E_{corr}	i_{corr}	CR	η
Uninhibited solution	-740	14	1.03	0
Solution + 20% MEG + 500ppm HAc+ 2ppm XX	-730	9	0.66	35
Solution + 20% MEG + 500ppm HAc+ 2ppm YY	-727	11.2	0.83	20
Solution + 20% MEG + 500ppm HAc+ 2ppm ZZ	-721	9.5	0.70	32
Solution + 20% MEG + 500ppm HAc+ 5ppm XX	-689	11	0.81	21
Solution + 20% MEG + 500ppm HAc+ 5ppm YY	-675	10.2	0.75	27
Solution + 20% MEG + 500ppm HAc+ 5ppm ZZ	-670	6.4	0.47	54
Solution + 20% MEG + 500ppm HAc+ 10ppm XX	-644	7.8	0.58	44
Solution + 20% MEG + 500ppm HAc+ 10ppm YY	-635	3.9	0.29	72
Solution + 20% MEG + 500ppm HAc+ 10ppm ZZ	-610	4.9	0.36	65
Solution + 20% MEG + 1000ppm HAc+ 2ppm XX	-710	8.9	0.66	36
Solution + 20% MEG + 1000ppm HAc+ 2ppm YY	-712	11	0.81	21
Solution + 20% MEG + 1000ppm HAc+ 2ppm ZZ	-715	9.7	0.72	30
Solution + 20% MEG + 1000ppm HAc+ 5ppm XX	-708	10	0.74	28
Solution + 20% MEG + 1000ppm HAc+ 5ppm YY	-699	11	0.81	21
Solution + 20% MEG + 1000ppm HAc+ 5ppm ZZ	-675	7.9	0.58	43
Solution + 20% MEG + 1000ppm HAc+ 10ppm XX	-677	9	0.66	35
Solution + 20% MEG + 1000ppm HAc+ 10ppm YY	-645	7.8	0.58	44
Solution + 20% MEG + 1000ppm HAc+ 10ppm ZZ	-640	11	0.81	21
Solution + 20% MEG + 2500ppm HAc+ 2ppm XX	-645	10	0.74	28
Solution + 20% MEG + 2500ppm HAc+ 2ppm YY	-624	9.8	0.72	30
Solution + 20% MEG + 2500ppm HAc+ 2ppm ZZ	-622	9.4	0.69	32
Solution + 20% MEG + 2500ppm HAc+ 5ppm XX	-618	7.9	0.58	43
Solution + 20% MEG + 2500ppm HAc+ 5ppm YY	-614	10	0.74	28
Solution + 20% MEG + 2500ppm HAc+ 5ppm ZZ	-609	6.9	0.51	50
Solution + 20% MEG + 2500ppm HAc+ 10ppm XX	-627	11	0.81	21
Solution + 20% MEG + 2500ppm HAc+ 10ppm YY	-602	10.4	0.77	25
Solution + 20% MEG + 2500ppm HAc+ 10ppm ZZ	-611	10.5	0.77	25

B-2: Electrochemical parameters for carbon steel samples saturated in 3.5% wt. NaCl solutions containing different concentrations of HAc, inhibitors and 800% MEG at 25°C

Composition	E_{corr}	i_{corr}	CR	η
Uninhibited solution				
Solution + 20% MEG + 500ppm HAc+ 2ppm XX	-638	12	0.88	0
Solution + 20% MEG + 500ppm HAc+ 2ppm YY	-634	9	0.66	25
Solution + 20% MEG + 500ppm HAc+ 2ppm ZZ	-631	8	0.59	33
Solution + 20% MEG + 500ppm HAc+ 5ppm XX	-629	9	0.66	25
Solution + 20% MEG + 500ppm HAc+ 5ppm YY	-625	11	0.81	8
Solution + 20% MEG + 500ppm HAc+ 5ppm ZZ	-623	10	0.74	16
Solution + 20% MEG + 500ppm HAc+ 10ppm XX	-620	8	0.59	33
Solution + 20% MEG + 500ppm HAc+ 10ppm YY	-617	7.7	0.57	35
Solution + 20% MEG + 500ppm HAc+ 10ppm ZZ	-615	11.7	0.86	2
Solution + 20% MEG + 1000ppm HAc+ 2ppm XX	-624	8	0.59	33
Solution + 20% MEG + 1000ppm HAc+ 2ppm YY	-620	9	0.66	25
Solution + 20% MEG + 1000ppm HAc+ 2ppm ZZ	-619	11	0.81	8
Solution + 20% MEG + 1000ppm HAc+ 5ppm XX	-618	11	0.81	8
Solution + 20% MEG + 1000ppm HAc+ 5ppm YY	-608	7.5	0.55	37
Solution + 20% MEG + 1000ppm HAc+ 5ppm ZZ	-604	8.7	0.64	27
Solution + 20% MEG + 1000ppm HAc+ 10ppm XX	-602	10.4	0.77	13
Solution + 20% MEG + 1000ppm HAc+ 10ppm YY	-610	10	0.74	16
Solution + 20% MEG + 1000ppm HAc+ 10ppm ZZ	-609	6.3	0.46	47
Solution + 20% MEG + 2500ppm HAc+ 2ppm XX	-625	6	0.44	50
Solution + 20% MEG + 2500ppm HAc+ 2ppm YY	-622	7.1	0.52	40
Solution + 20% MEG + 2500ppm HAc+ 2ppm ZZ	-621	5	0.37	58
Solution + 20% MEG + 2500ppm HAc+ 5ppm XX	-618	5	0.37	58
Solution + 20% MEG + 2500ppm HAc+ 5ppm YY	-614	10	0.74	16
Solution + 20% MEG + 2500ppm HAc+ 5ppm ZZ	-609	5.5	0.41	54
Solution + 20% MEG + 2500ppm HAc+ 10ppm XX	-606	8.4	0.62	30
Solution + 20% MEG + 2500ppm HAc+ 10ppm YY	-602	10	0.74	16
Solution + 20% MEG + 2500ppm HAc+ 10ppm ZZ	-599	5	0.37	58

B-3: Electrochemical parameters for carbon steel samples saturated in 3.5% wt. NaCl solutions containing different concentrations of HAc, inhibitors and 80% MEG at 50°C

Composition	E_{corr}	i_{corr}	CR	η
Uninhibited solution	--742	13	0.96	0
Solution + 20% MEG + 500ppm HAc+ 2ppm XX	-735	8	0.59	38
Solution + 20% MEG + 500ppm HAc+ 2ppm YY	-731	10	0.74	23
Solution + 20% MEG + 500ppm HAc+ 2ppm ZZ	-720	11	0.81	15
Solution + 20% MEG + 500ppm HAc+ 5ppm XX	-719	8.5	0.63	34
Solution + 20% MEG + 500ppm HAc+ 5ppm YY	-715	6.5	0.48	50
Solution + 20% MEG + 500ppm HAc+ 5ppm ZZ	-716	7	0.52	46
Solution + 20% MEG + 500ppm HAc+ 10ppm XX	-710	11	0.81	15
Solution + 20% MEG + 500ppm HAc+ 10ppm YY	-709	11.5	0.85	11
Solution + 20% MEG + 500ppm HAc+ 10ppm ZZ	-703	12	0.88	7
Solution + 20% MEG + 1000ppm HAc+ 2ppm XX	-699	9.3	0.69	28
Solution + 20% MEG + 1000ppm HAc+ 2ppm YY	-675	11	0.81	15
Solution + 20% MEG + 1000ppm HAc+ 2ppm ZZ	-675	9	0.66	30
Solution + 20% MEG + 1000ppm HAc+ 5ppm XX	-645	5.5	0.41	57
Solution + 20% MEG + 1000ppm HAc+ 5ppm YY	-642	5.9	0.43	54
Solution + 20% MEG + 1000ppm HAc+ 5ppm ZZ	-638	10.6	0.78	18
Solution + 20% MEG + 1000ppm HAc+ 10ppm XX	-633	7	0.52	46
Solution + 20% MEG + 1000ppm HAc+ 10ppm YY	-625	7.5	0.55	42
Solution + 20% MEG + 1000ppm HAc+ 10ppm ZZ	-619	11	0.81	15
Solution + 20% MEG + 2500ppm HAc+ 2ppm XX	-635	6.7	0.49	48
Solution + 20% MEG + 2500ppm HAc+ 2ppm YY	-630	7.8	0.58	40
Solution + 20% MEG + 2500ppm HAc+ 2ppm ZZ	-628	9.5	0.70	26
Solution + 20% MEG + 2500ppm HAc+ 5ppm XX	-626	6.6	0.49	49
Solution + 20% MEG + 2500ppm HAc+ 5ppm YY	-617	9.4	0.69	27
Solution + 20% MEG + 2500ppm HAc+ 5ppm ZZ	-616	11	0.81	15
Solution + 20% MEG + 2500ppm HAc+ 10ppm XX	-614	5.7	0.42	56
Solution + 20% MEG + 2500ppm HAc+ 10ppm YY	-619	4.9	0.36	62
Solution + 20% MEG + 2500ppm HAc+ 10ppm ZZ	-614	7.7	0.57	40

B-4: Electrochemical parameters for carbon steel samples saturated in 3.5% wt. NaCl solutions containing different concentrations of HAc, inhibitors and 20% MEG at 80°C

Composition	E_{corr}	i_{corr}	CR	η
Uninhibited solution	-650	15	1.11	0
Solution + 20% MEG + 500ppm HAc+ 2ppm XX	-642	9	0.66	40
Solution + 20% MEG + 500ppm HAc+ 2ppm YY	-641	7	0.52	53
Solution + 20% MEG + 500ppm HAc+ 2ppm ZZ	-640	11	0.81	26
Solution + 20% MEG + 500ppm HAc+ 5ppm XX	-635	9.4	0.69	37
Solution + 20% MEG + 500ppm HAc+ 5ppm YY	-631	6.7	0.49	55
Solution + 20% MEG + 500ppm HAc+ 5ppm ZZ	-629	10.2	0.75	32
Solution + 20% MEG + 500ppm HAc+ 10ppm XX	-628	6.6	0.49	56
Solution + 20% MEG + 500ppm HAc+ 10ppm YY	-620	6.9	0.51	54
Solution + 20% MEG + 500ppm HAc+ 10ppm ZZ	-619	9.5	0.70	36
Solution + 20% MEG + 1000ppm HAc+ 2ppm XX	-635	7	0.52	53
Solution + 20% MEG + 1000ppm HAc+ 2ppm YY	-633	4.9	0.36	67
Solution + 20% MEG + 1000ppm HAc+ 2ppm ZZ	-630	10.2	0.75	32
Solution + 20% MEG + 1000ppm HAc+ 5ppm XX	-628	8	0.59	46
Solution + 20% MEG + 1000ppm HAc+ 5ppm YY	-626	5.8	0.43	61
Solution + 20% MEG + 1000ppm HAc+ 5ppm ZZ	-615	8.8	0.65	41
Solution + 20% MEG + 1000ppm HAc+ 10ppm XX	-621	10.6	0.78	29
Solution + 20% MEG + 1000ppm HAc+ 10ppm YY	-616	11	0.81	26
Solution + 20% MEG + 1000ppm HAc+ 10ppm ZZ	-625	7.8	0.56	48
Solution + 20% MEG + 2500ppm HAc+ 2ppm XX	-630	11	0.81	26
Solution + 20% MEG + 2500ppm HAc+ 2ppm YY	-625	7.7	0.57	48
Solution + 20% MEG + 2500ppm HAc+ 2ppm ZZ	0623	7.9	0.58	47
Solution + 20% MEG + 2500ppm HAc+ 5ppm XX	-620	10.6	0.78	29
Solution + 20% MEG + 2500ppm HAc+ 5ppm YY	-618	12.4	0.91	17
Solution + 20% MEG + 2500ppm HAc+ 5ppm ZZ	-614	4.9	0.36	67
Solution + 20% MEG + 2500ppm HAc+ 10ppm XX	-616	9.5	0.70	36
Solution + 20% MEG + 2500ppm HAc+ 10ppm YY	-608	8	0.59	46
Solution + 20% MEG + 2500ppm HAc+ 10ppm ZZ	-621	11	0.81	26

B-5: Electrochemical parameters for carbon steel samples saturated in 3.5% wt. NaCl solutions containing different concentrations of HAc, inhibitors and 80% MEG at 80°C

Composition	E_{corr}	i_{corr}	CR	η
Uninhibited solution	-675	13	0.96	0
Solution + 20% MEG + 500ppm HAc+ 2ppm XX	-645	7.9	0.58	39
Solution + 20% MEG + 500ppm HAc+ 2ppm YY	-641	12	0.88	7
Solution + 20% MEG + 500ppm HAc+ 2ppm ZZ	-638	8.5	0.63	34
Solution + 20% MEG + 500ppm HAc+ 5ppm XX	-629	11.6	0.86	10
Solution + 20% MEG + 500ppm HAc+ 5ppm YY	-622	10.9	0.80	16
Solution + 20% MEG + 500ppm HAc+ 5ppm ZZ	-616	5.6	0.41	56
Solution + 20% MEG + 500ppm HAc+ 10ppm XX	-622	8.6	0.63	33
Solution + 20% MEG + 500ppm HAc+ 10ppm YY	-615	11.8	0.87	9
Solution + 20% MEG + 500ppm HAc+ 10ppm ZZ	-610	9.6	0.71	26
Solution + 20% MEG + 1000ppm HAc+ 2ppm XX	-625	10	0.74	23
Solution + 20% MEG + 1000ppm HAc+ 2ppm YY	-624	13.4	0.99	3
Solution + 20% MEG + 1000ppm HAc+ 2ppm ZZ	-619	6.8	0.50	47
Solution + 20% MEG + 1000ppm HAc+ 5ppm XX	-614	7.5	0.55	42
Solution + 20% MEG + 1000ppm HAc+ 5ppm YY	-608	8.8	0.65	32
Solution + 20% MEG + 1000ppm HAc+ 5ppm ZZ	-605	9.5	0.70	26
Solution + 20% MEG + 1000ppm HAc+ 10ppm XX	-602	10.9	0.80	16
Solution + 20% MEG + 1000ppm HAc+ 10ppm YY	-616	5.4	0.40	58
Solution + 20% MEG + 1000ppm HAc+ 10ppm ZZ	-624	8.4	0.62	35
Solution + 20% MEG + 2500ppm HAc+ 2ppm XX	-625	11	0.81	15
Solution + 20% MEG + 2500ppm HAc+ 2ppm YY	-623	7.6	0.56	41
Solution + 20% MEG + 2500ppm HAc+ 2ppm ZZ	-620	10.6	0.78	18
Solution + 20% MEG + 2500ppm HAc+ 5ppm XX	-626	10.2	0.75	21
Solution + 20% MEG + 2500ppm HAc+ 5ppm YY	-618	8.7	0.64	33
Solution + 20% MEG + 2500ppm HAc+ 5ppm ZZ	-619	6.7	0.49	48
Solution + 20% MEG + 2500ppm HAc+ 10ppm XX	-622	10	0.74	23
Solution + 20% MEG + 2500ppm HAc+ 10ppm YY	-613	5.9	0.43	54
Solution + 20% MEG + 2500ppm HAc+ 10ppm ZZ	-611	7.5	0.55	42

Appendix C

List of Publish Papers

Appendix C	Title of paper	Page
C -1	The effect of acetic acid and mono-ethylene glycol on iron carbonate dissolution in de-aerated environment	182-199
C -2	Inhibition performance of mild steel corrosion in the presence of CO ₂ , HAc and MEG	200-216
C -3	Influence of acetic acid and monoethylene glycol on polarization behavior of mild steel corrosion in CO ₂ environment.	217-218

The effects of acetic acid and monoethylene glycol on iron carbonate dissolution in deaerated environment.

L. Ikeh, G.C Enyi and G.G Nasr

Spray Research Group (SRG)

Institute of Material Research (IMR)

School of Computing, Science and Engineering

University of Salford, Manchester

United Kingdom, M5 4WT.

Abstract

Hydrate formation and scale deposition continue to remain a major challenge in oil and gas production and transportation industry. As a result, Monoethylene Glycol (MEG) is introduced into the pipeline as an antifreeze and anticorrosion agent. Recent Investigations have shown that the MEG has to be separated from unwanted substance such as acetic acid (HAc) that are present in the formation water. Internal pipeline corrosion slows and decreases the production of oil and gas when associated with free water and reacts with CO₂ and organic acid by lowering the integrity of the pipe.

In this study, the effect of acetic acid (HAc) and monoethylene Glycol (MEG) on iron carbonate layer corrosion were evaluated at 25°C and 80°C using 3.5% NaCl solution in a semi-circulation flow loop set up. Weight loss and electrochemical measurements using linear polarization resistance (LPR) and electrochemical impedance spectroscopy (EIS) were used in measuring the corrosion rate as a function of HAc and MEG concentrations. Results obtained shows an average corrosion rate increased from 0.5 to 1.8 mm/yr at 25°C, and from 1.2 to 3.5 mm/yr at 80°C in the presence of HAc. However, there are decrease in corrosion rate from 1.8 to 0.95 mm/yr and from 3.5 to 1.6mm/yr respectively

at 25°C and 80°C with the addition of 50% MEG. It is observed that the Fe²⁺ concentration affects the rate of film formation and not the protectiveness. It is also noted that charge transfer control is the main corrosion controlling mechanism under the test conditions. The higher temperature led to faster film dissolution and higher corrosion rate in the presence of HAc. The EIS results indicate that the charge transfer controlled behaviour was as a result of iron carbonate layer accelerated by the addition of MEG concentrations.

Key words: CO₂ corrosion, carbon steel, acetic acid, monoethylene glycol, iron carbonate dissolution

1 Introduction

Natural gas usually contains about 20 to 100lbm of water per MMSCF of gas, depending on the saturated point at the operating conditions. The processing and transportation of this gas in the presence of water was hindered by the formation of corrosion and gas hydrates in pipelines. Corrosion of pipeline will lead to pipeline failure which in turn will reduce gas production/transmission capacity and scale problems [1]

Many studies had been carried out on corrosion of mild steel in CO₂ environment, but none relates to the conditions when acetic acids are present. Gulbrandsen et al [2] reported that MEG altered the anodic half reaction of the corrosion process (dissolution of iron). They related the results to the possible adsorption of MEG on the steel surface. The corrosion rate of steel in the presence of MEG can be lower compared to that without MEG [2, 3]. De Waard and Milliams [3] demonstrated that addition of glycol to wet gas pipeline influenced CO₂ corrosion by lowering the dew point of water and consequently could reduce the severity of Top-of-the-line corrosion. They further reported that the corrosion rate at the bottom of the line decreases when glycol mixes with the water phase

[1-5]. The influence of other parameters such as O₂, H₂S in continuation with MEG had been studied, but the effects of acetic acid are yet to be analysed. [2, 4-6].

The use of pH stabilization in a MEG-containing system has successfully been implemented in the multiphase transportation of natural gas [1, 4, 7]. The pH stabilization often works by reducing the cathodic reaction of the corrosion of steel while encouraging the formation of protective iron carbonate on the surface of the carbon steel pipeline. When formation water is produced from the well, pH stabilization become undesirable method for preventing corrosion as other unwanted scale may form along the pipeline [3, 8].

Similarly, CO₂ corrosion in the presence of acetic acid (HAc) is known as major causes for premature failures in oil and gas pipelines that usually made of carbon steel [9]. Acetic acid (HAc) is often the most abundant volatile organic acids. In oilfield pipelines with low partial pressure of CO₂ (pCO₂), the corrosion issues are easily managed, but when small amounts of acetic acids are present, the corrosivity of the brine can change dramatically [10]. It has been shown that the total quantity of organic acids in produced water in oil and gas system is between 500-3000 ppm of which HAc contributes about 50-90% of organic acids [11]. Similarly, a systematic investigation of field data showed that undissociated HAc concentration higher than 0.1-1 mM was a critical factor for CO₂ corrosion [10]. Garsany et al. [12] proposed that the role of acetic acid is to act as a reactant in the cathodic process which could have a significantly higher rate than the reduction of protons or carbonic acid in oilfield conditions. The three main cathodic reactions involving acetic acid are [12]:



The reaction mechanism and kinetics of the iron dissolution reaction with the overall reaction of equation (3) are affected by acetic acid, CO₂ partial pressure and pH [13]. Dugstad [14] and Gunaltun et al. [15] reported results from field observations and laboratory investigations that the presence of HAc may induce a detrimental effect on the overall corrosion rate and the pitting morphology in sweet systems. Field experienced has also shown that HAc is a key factor in the localized top-of-line corrosion attacks in gas-condensate to pipeline [16]. Moreover, the presence of HAc also tend to solubilize the dissolving iron ions and suppress FeCO₃ or oxide film formation, which can passivate the steel surface [17]. Iron carbonate scale that forms on the carbon steel in CO₂ environments is a frequent concern in the oil and gas production and transportation industry. The iron carbonate film can slow the corrosion process by presenting a diffusion barrier for the species involve and covering up a portion of the steel surface as well as preventing the underlying steel from further dissolution. However, the steel surface corrodes under the film continuously creating a void between the film and the steel surface [18]

There appeared to be many unanswered questions on how MEG affect the CO₂ corrosion mechanism during film formation in the presence of HAc. This paper investigates the corrosion rate of mild steel under the influence of acetic acid and monoethylene glycol during film formation

2 Experimental Procedure

The experiments were performed in a mini circulation flow loop. A peripheral pump circulates the test solution from the reservoir to the test cell. A small diameter pipe maintained a constant liquid volume flow in the cell. The reservoir tank and the test cell were continuously purged with CO₂ to removed oxygen completely from the test solution. Once de-oxygenation has been achieved, the required amount of HAc and MEG were added at the start of every experiment. The temperatures were controlled by means of a heating plate with a temperature sensor in the cell. The pH of the solution was

adjusted to the desired value throughout the experiments by adding sodium bicarbonate (NaHCO_3) or hydrochloric acid (HCl) as needed. Also, the desired concentration of Fe^{2+} was added to the test cell in the form of ferrous chloride ($\text{FeCl}_2 \cdot 4\text{H}_2\text{O}$) crystal pre-dissolved in the deoxygenated water.

2.1 Test set up and procedures

The test specimens used throughout this study are mild steel of having a surface area of 8.11cm^2 and a circular hole toward the top end. A copper wire 0.02 mm diameter was spot welded and used on the test coupon to ensure electrical contact. The test coupons were suspended in the test solution by passing a plastic wire through the coupon and the wire was hung to a plastic rod held in place of the glass cell top holes. Prior to introduction into the test cell, the test coupon were successively ground with 240, 600 and 800 SiC grit paper and polished with 1200 SiC paper. It was then cleaned with acetone, rinsed with distilled water and dried. The general composition of the mild steel samples used is given in Table 1

Table 22: Chemical composition in wt. % of mild steel

Comp.	C	Si	Mn	S	P	Sn	Cr	Ni	Mo	Cu	Al
Val. %	0.08	0.25	1.54	0.01	0.02	0.08	0.04	0.03	0.01	0.12	0.038

Four test solutions were prepared. The first test solution was prepared with 3.5% wt. sodium chloride (NaCl) as the blank solution without HAc and MEG . The second test solution was prepared using 3.5% NaCl solution and HAc concentrations of 1000 ppm and 2000 ppm. The third test solution was prepared using 3.5% NaCl solution, 50% MEG concentration and 1000 ppm of HAc , while the fourth test solution was prepared using 3.5% NaCl , 50% MEG concentrations and 2000 ppm of HAc . Table 2 shows the test matrix for this study.

Table 23: Compositions the test matrix used for the experiments

Parameters	Values
Test solution	3.5% wt. NaCl
Test material	Mild steel
Partial pressure of CO ₂ (bar)	0.54
MEG concentrations	50%
pH	6.6
Temperature (°C)	[25, 80]
C _{Fe2+} (ppm)	250
C _{HAc} (ppm)	[0 -2000]
Surface area (cm ²)	8.11
Test method	[WL, LPR and EIS]

2.1.1 *Measurement Techniques*

Weight loss measurement was performed on mild steel samples in all the test solutions at temperatures of 25°C and 80°C as outlined in ASTM G1. The weight loss is determined and the corrosion rate is calculated using Equation 4:

$$CR = \frac{WL(g)}{\rho \times t \times A} \times K \left(\frac{mm}{yr} \right) \quad (4)$$

Where:

CR = corrosion rate, mm/yr,

ρ = density of the material, 7.86 g/cm³

WL = weight loss, grams,

t = the exposed time, hr

A = the exposed coupon surface area, cm²,

K = conversion factor, 8.76×10⁴

The electrochemical measurements were carried out using a commercial potentiostat. A three-electrode configuration was used in every measurement. The mild steel sample was used as the working electrode, while the Ag/AgCl wire was used as reference electrode. The linear polarization curves were obtained in the potential range of -10 to +10 mV (vs. E_{corr}) with a scan rate of 0.1 mV/s. Electrochemical Impedance measurements were also performed with an excitation of 10mV sinusoidal sign in a frequency range from 10 KHz to 10 mHz and the signal amplitude were fixed at 7 points/decade.

3 Results and Discussion

3.1 *Weight Loss*

The variations of the average weight loss per unit area as a function of time in the presence of HAc are shown below. The weight loss of the first test solution (3.5% wt. NaCl without HAc and MEG) and the second test solution (3.5% NaCl with 1000 ppm and 2000 ppm HAc concentrations and without MEG) were presented in Figures 1A & 1B at temperatures of 25°C and 80°C. The results show an increased in weight loss over time as the concentrations of HAc increases. As can be seen, it is observed that the average weight loss of the mild steel increased at both temperatures, although higher at 80°C than at 25°C. The high weight loss at 80°C is due to the fast reaction rate that occurs at higher temperatures. At 80°C, it is assumed that a protective FeCO_3 corrosion films are formed and remain protective in the presence of HAc provided the super-saturation is high enough. Table 3 presents the summary of the average weight loss per unit area for mild steel used at 25°C and 80°C in the present of acetic acid.

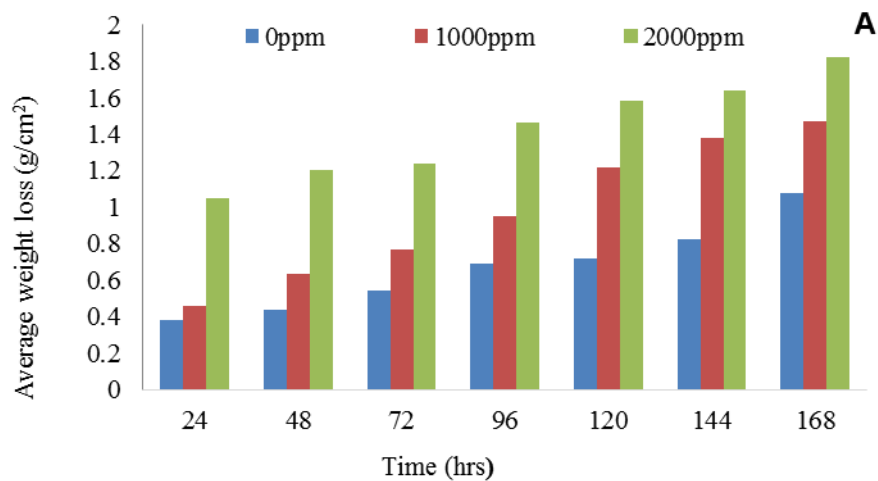


Figure 1A: Average weight loss as a function time for 3.5% wt. solution for pH=6.6, Fe^{2+} =250 ppm and [HAc=0, 1000 2000 ppm at A=25°C.

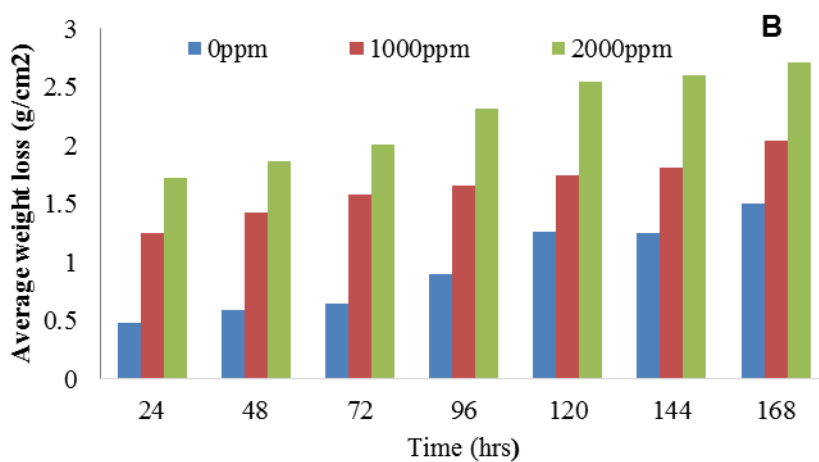


Figure 1B: Average weight loss as a function time for 3.5% wt. solution for pH=6.6, Fe^{2+} =250 ppm and [HAc=0, 1000 2000 ppm at B=80°C

Table 24: Comparison of average weight loss a function of time for mild steel in the presence of HAc at 25°C and 80°C respectively

T(hrs)	Weight loss per unit area (g/cm ²)					
	T=25°C			T=80°C		
	Blank	1000 ppm	3000 ppm	Blank	1000 ppm	3000 ppm
24	0.38	0.46	1.05	0.48	1.25	1.72
48	0.44	0.63	1.2	0.59	1.43	1.86
72	0.54	0.77	1.24	0.65	1.58	2.01
96	0.69	0.95	1.46	0.9	1.66	2.32
120	0.72	1.22	1.58	1.26	1.74	2.55
144	0.82	1.38	1.64	1.25	1.81	2.6
168	1.08	1.47	1.82	1.5	2.04	2.71

Figures 2A & 2B show results of average weight loss as a function of time for mild steel in third test solution (3.5% NaCl, 50% MEG concentration and 1000 ppm of HAc) and fourth test solution(3.5% NaCl, 50% MEG concentration and 2000 ppm of HAc) at 25°C and 80°C. As can be seen, the addition of 50% MEG to the solutions has a significant influence on the weight loss of the materials. From Figure 2A, it is quite obvious that the weight loss reduced drastically from 1.80 g/cm² to 0.77 g/cm² and 1.98 g/cm² to 0.83 g/cm² with addition of 50% MEG to 1000 ppm and 2000 ppm concentrations of HAc at 25°C. Similarly in Figure 2B, the average weight loss over 168 hours reduced approximately from 3.50 g/cm² to 0.81 g/cm², and from 3.58 g/cm² to 0.93 g/cm² on addition of 50% MEG to different concentration of HAc. However, the decrease in weight loss is attributed to the reduction in pH of the solution on addition of the 50% MEG solution. The summary of the average weight loss for the mild steel in the presence of HAc and on addition of 50% MEG concentrations are shown in Table 4.

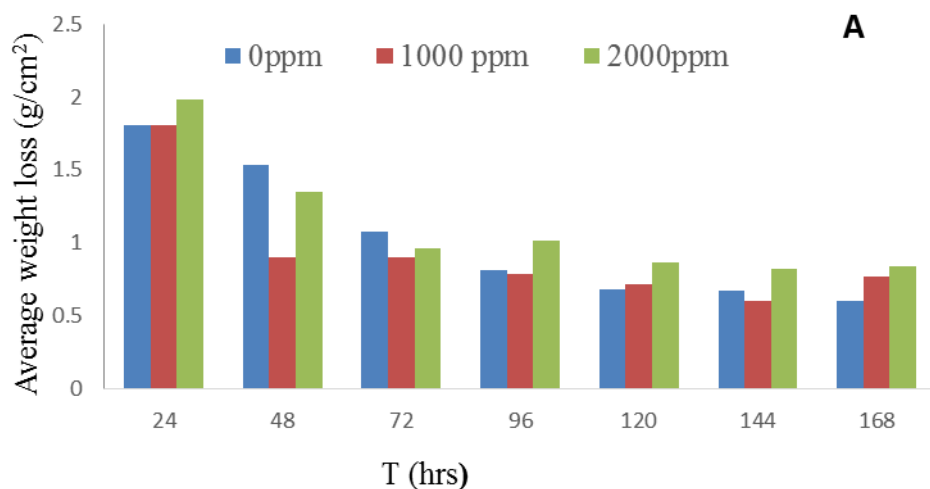


Figure 2: Average weight loss as a function time for 3.5% wt. solution with 50% MEG at pH=6.6, Fe^{2+} =250 ppm and [HAc=0, 1000 2000 ppm]. at T=25°C

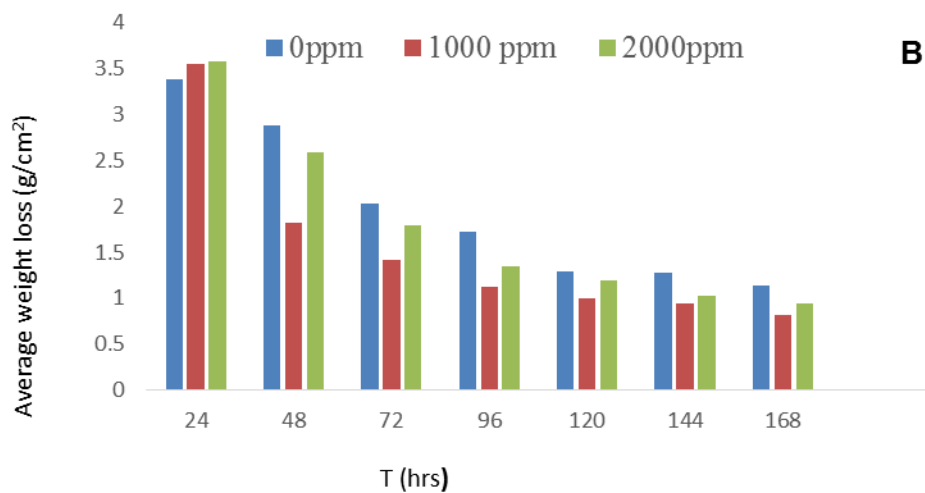


Figure 2: Average weight loss as a function time for 3.5% wt. solution with 50% MEG at pH=6.6, Fe^{2+} =250 ppm and [HAc=0, 1000 2000 ppm] at T=80°C]

Table 25: Average weight loss as a function of time for the mild steel in the presence of HAc at 25°C and 80°C with 50% MEG solution

Time (hrs)	Weight loss per unit area (g/cm ²)					
	T=25°C, 50% MEG			T=80°C, 50% MEG		
	Blank	1000 ppm	2000 ppm	Blank	1000 ppm	2000 ppm
24	1.80	1.80	1.98	3.17	3.55	3.58
48	1.53	0.90	1.35	3.17	1.82	2.58
72	1.08	0.90	0.96	3.17	1.42	1.79
96	0.81	0.78	1.01	2.64	1.12	1.34
120	0.68	0.72	0.86	2.74	0.99	1.19
144	0.67	0.60	0.82	2.50	0.94	1.02
168	0.60	0.77	0.83	2.26	0.81	0.93

3.1.1 Linear Polarization Resistance (LPR)

The effect of HAc and 50% MEG on the corrosion rate of mild steel in CO₂ saturated environment were also evaluated using the LPR measurement technique. Figures 3A and 3B show the variations of measured corrosion rates of steel samples in all the test solutions at 25°C and 80°C

From Figure 3A, the corrosion rate increase steadily as the concentrations of the acetic acid were increased for a while and thereafter remain steady for the remaining period of the experiment. At 80°C (Figure 3B), the corrosion rate increases and thereafter decreases and remain steady throughout the remaining period of the experiment. Though, protective films forms at both temperatures, it is more adherent and protective at 80°C than at 25°C.

It is observed that the Fe^{2+} concentration affects the rate of film formation and not the protectiveness as reported by Nafday et al [19]. It is also noted that charge transfer control is the main corrosion controlling mechanism under the test conditions. The higher temperature led to faster film dissolution and higher corrosion rate in the presence of HAc. The increased corrosion rate is due to the effect of undissociated HAc on the cathodic reactions of the corrosion process. This shows that larger fraction of the FeCO_3 film formed in the corrosion process are lost to the bulk solution.

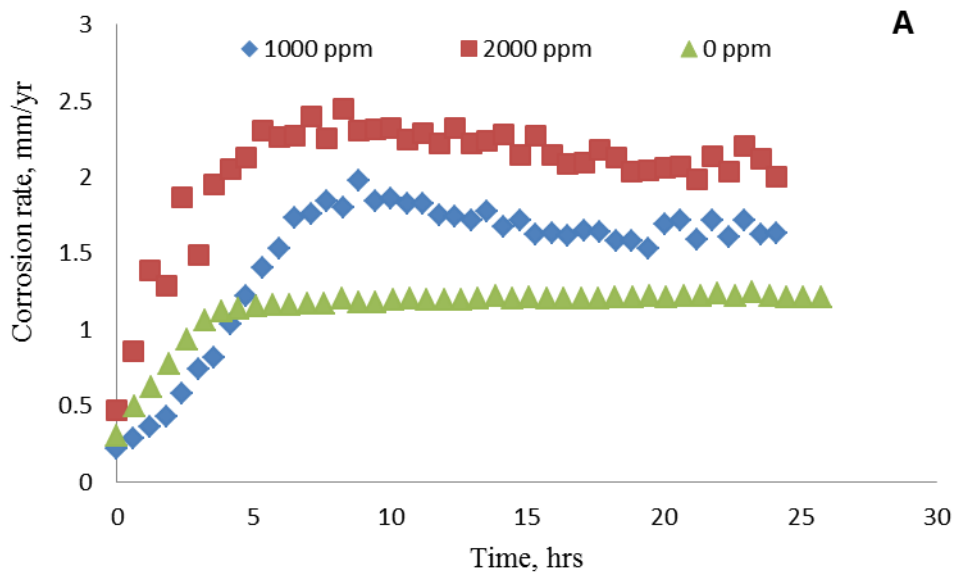


Figure 3: Measured corrosion rate as a function of time for a solution saturated with 0.56 bar of CO_2 , pH=6.6, Fe^{2+} =250 ppm and [HAc=0, 1000 2000 ppm] at A=25°C

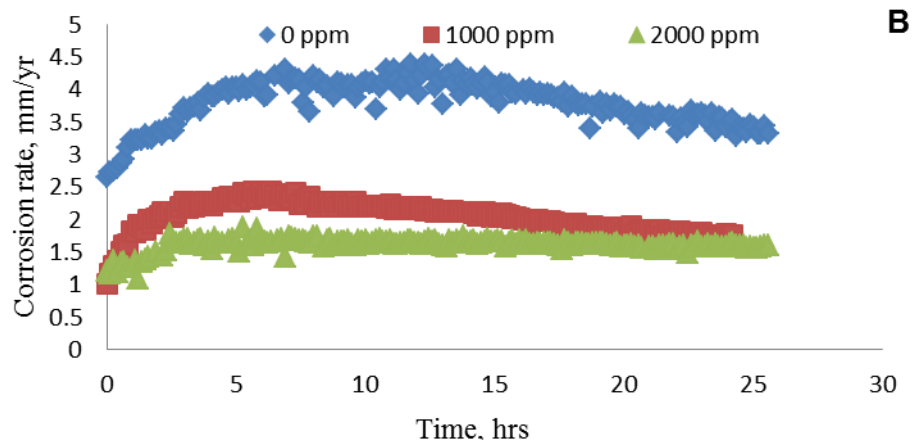


Figure 3: Measured corrosion rate as a function of time for a solution saturated with 0.56 bar of CO_2 , pH=6.6, Fe^{2+} =250 ppm and [HAc=0, 1000 2000 ppm] at B= 80°C

Figure 4 show the variations of measured corrosion rates of steel samples in all the test solutions at 80°C . It is observed that the addition of 50% MEG to the solutions containing HAc reduces the corrosion rates at 80°C . The reduction in corrosion rate is caused by FeCO_3 solubility decreases with MEG, and FeCO_3 super-saturation increase in the presence of MEG.

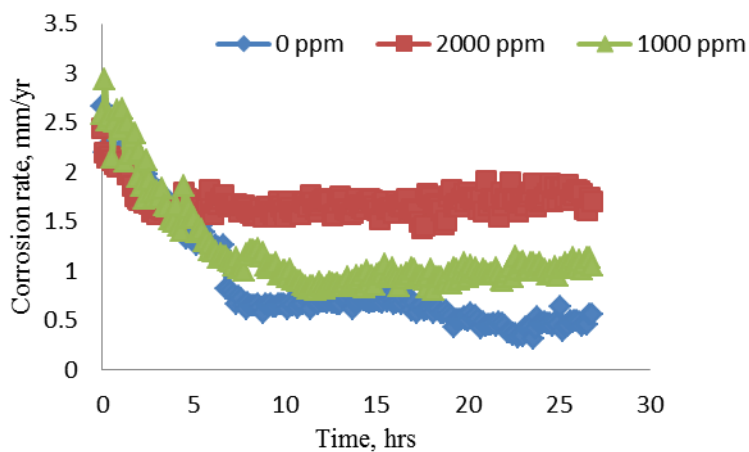


Figure 4: Measured corrosion rate as a function of time for 3.5% NaCl solution saturated with 0.56 bar of CO_2 and 50% MEG, pH=6.6, Fe^{2+} =250 ppm and [HAc=0, 1000 2000 ppm] T= 80°C

3.1.2 Electrochemical Impedance Spectroscopy (EIS)

As the linear polarization resistance (LPR) measurements demonstrates only the change of dissolution of the steel surface under certain conditions, the electrochemical impedance spectroscopy (EIS) was used as an alternative measurement to explain the mechanisms of electrochemical reactions that occur at the metal- electrolyte interface.

Figures 5A & 5B shows the Nyquist plots measured on the mild steel in saturated CO₂ environments at 25°C and 80°C with different concentrations of HAc. The graphs show a large capacitive semicircle at high frequencies which is considered as the capacitance of double electrode layer between the FeCO₃ films and the solutions. With the addition of more concentrations of HAc, the high frequency semicircle decreases in size. The decrease in size shows an increase in corrosion rate as well as decrease in the protectiveness of FeCO₃ layer. However, when the protective layer is completely impact, the corrosion is controlled by a diffusion transfer process, and when there are pores in the protective layers, a charge transfer process at the steel-layer interface occurs.

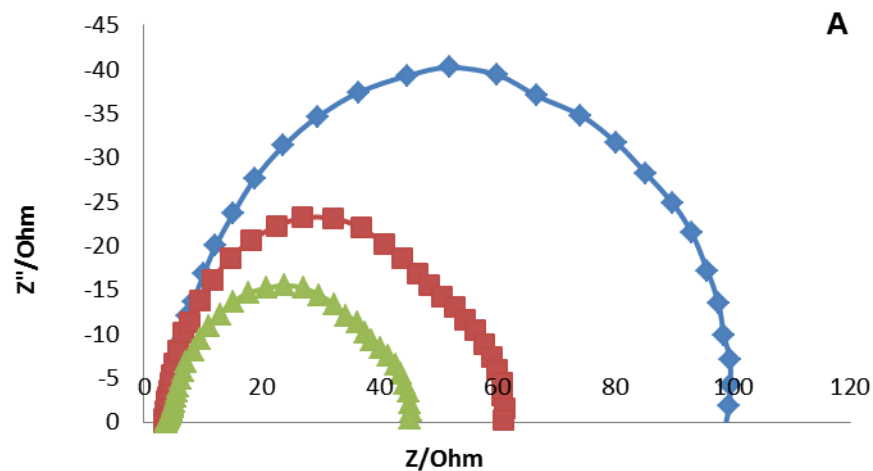


Figure 5: Nyquist plot for mild steel sample in 3.5% wt NaCl solution for 0.54 bar of CO₂ pH=6.6, Fe²⁺=250 ppm and [HAc=0, 1000 2000 ppm] [A = 25°C]

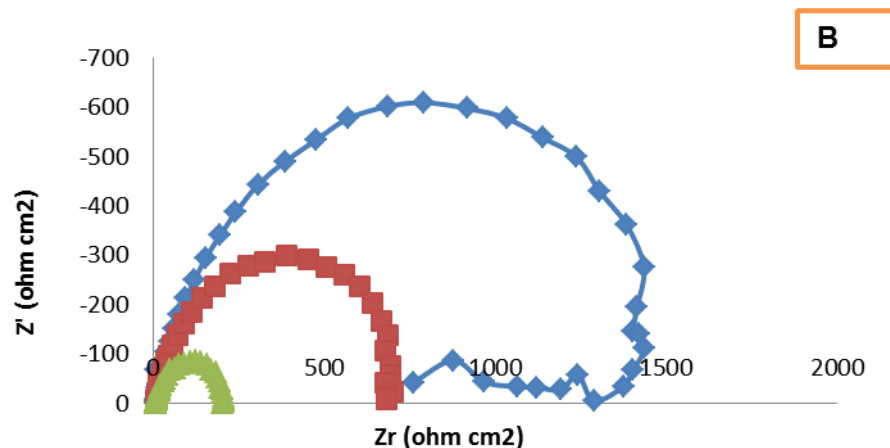


Figure 5: Nyquist plot for mild steel sample in 3.5% wt NaCl solution for 0.54 bar of CO₂ pH=6.6, Fe²⁺=250 ppm and [HAc=0, 1000 2000 ppm] [B=80°C]

Additionally, Figures 6A & 6B shows the EIS results of HAc in the presence of 50% MEG. As can be seen, addition of 50% MEG increases the solution resistance of HAc in solution of 3.5% NaCl. This means that the charge resistance increases with the 50% MEG concentrations. This results is in consistent with the results measured using the linear polarization resistance.

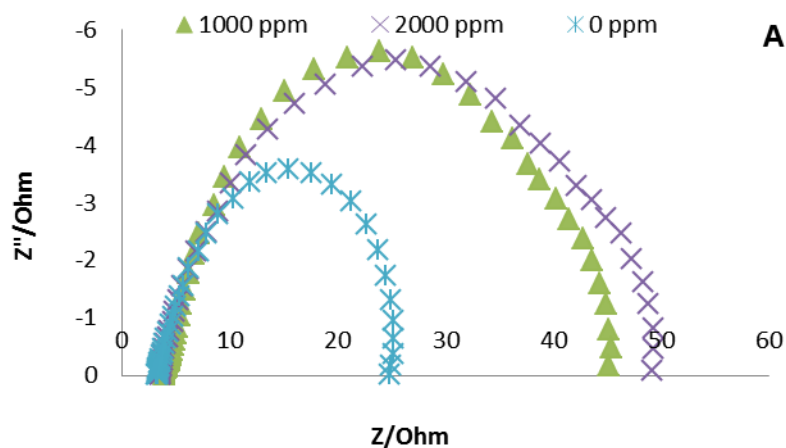


Figure 6: Nyquist plot for mild steel sample in 3.5% wt NaCl solution and 50% MEG for 0.54 bar of CO₂ pH=6.6, Fe²⁺=250 ppm and [HAc=0, 1000 2000 ppm] at A = 25°C

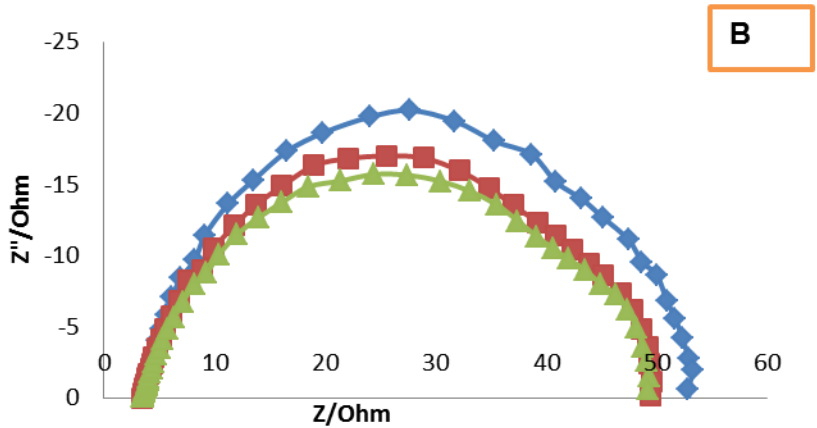


Figure 6: Nyquist plot for mild steel sample in 3.5% wt NaCl solution and 50% MEG for 0.54 bar of CO₂ pH=6.6, Fe²⁺=250 ppm and [HAc=0, 1000 2000 ppm] at B=80°C

4 Conclusions

An experimental study of corrosion of mild steel in CO₂ saturated environment in the presence of HAc and MEG has been carried out. A mini circulation flow loop was used to perform experiments at temperature of 25°C and 80°C, with pH of 6.6, 0.54 bar of CO₂ partial pressure and 50% MEG with different concentrations of HAc. The following observations were deduced:

- The weight loss per unit area of the mild steel increases steadily as the concentrations of HAc were increased. At 80°C, the corrosion rate increased rapidly for some time before decreasing when protective FeCO₃ had formed. The results showed a comparable corrosion rate at both temperatures with the addition of different concentrations of HAc.
- It is also shown that addition of 50% MEG to the solution reduced the corrosion rate at both temperatures compared to the corrosion rate when only HAc were present.

- The electrochemical measurements have shown that the corrosion rate increases with increased in concentration of HAc, and decreases with the increment of exposition time. This however can be attributed to the formation of iron carbonate film on the surface of the steel sample.
- The Nyquist plots of the EIS measurement shows that the diameter of the depressed semicircle decreased as the concentrations of the HAc increases, and the capacitive semicircle sizes also decreased on addition of 50% MEG to the solution.
- Finally, the characterisation and analyses of the corrosion products film formed on the mild steel samples using SEM, XRD and CT scan are on-going. This will be reported in subsequent papers by the authors

5 References

- [1] Gonzalez, J.J., M.E. Alfonso, and G. Pellegrino, *Corrosion of Carbon Steels in Monoethylene Glycol*. NACE International.
- [2] Gulbrandsen, E. and J.H. Morard, *Why Does Glycol Inhibit CO₂ Corrosion?* NACE International.
- [3] de Waard, C., U. Lotz, and D.E. Milliams, *Predictive Model for CO₂ Corrosion Engineering in Wet Natural Gas Pipelines*. Corrosion, 1991. 47(12): p. 976-985.
- [4] Ivonye, I., et al., *Corrosion Study of Carbon Steel in the Presence of Monoethylene Glycol (MEG) and Corrosion Inhibitors in Acid*. NACE International.
- [5] Kvarekval, J., S. Olsen, and S. Skjerve, *The Effect of O₂ on CO₂ Corrosion in pH Stabilized Gas/Condensate Pipelines*. NACE International.
- [6] Kvarekvål, J. and A. Pedersen, *An Electrochemical Study of Corrosion Inhibition of Carbon Steel in Sour Glycol Solutions*. NACE International.
- [7] Elhady, A.A.A., *Operating Experiences of DEG and MEG for Hydrate and Dewpoint Control in Gas Production Offshore Mediterranean*. German National Library of Science and Technology, 2006.

- [8] Dugstad, A., M. Seiersten, and R. Nyborg, *Flow Assurance of pH Stabilized Wet Gas Pipelines*. NACE International.
- [9] George, K. and S. Netic, *Investigation of carbon dioxide corrosion of mild steel in the presence of acetic acid - part 1: Basic mechanisms*. Corrosion Science, 2007(63): p. 178-86.
- [10] Crolet, J.-L. and M.R. Bonis, *Prediction of the Risks Of CO₂ Corrosion in Oil and Gas Wells*. SPE Production Engineering, 1991. 6(4): p. 449-453.
- [11] Gunaltun, Y. and L. Payne, *A New Technique for the Control of Top of the Line Corrosion: TLCC-PIG*. 2003, NACE International.
- [12] Garsany, Y., D. Pletcher, and B. Hedges, *"Speciation and electrochemistry of brines containing acetate ion and carbon dioxide"*. J. Electroanal. Chemistry,, 2002. 538-539: p. 285.
- [13] Crolet, J.L., A. Dugstad, and N. Thevenot, *Role of Free Acetic Acid on the CO₂ Corrosion of Steels*. 1999, NACE International.
- [14] Dugstad, A., *Fundamental Aspects of CO₂ Metal Loss Corrosion - Part 1: Mechanism*. 2006, NACE International.
- [15] Gunaltun, Y.M. and D. Supriyatman, *Top of the Line Corrosion in Multiphase Gas Lines: A Case History*. 1999, NACE International.
- [16] Gunaltun, Y.M. and D. Larrey, *Correlation with calculated water condensation rates*. NACE CORROSION 2000. Paper no. 71.
- [17] Videm, K. and A. Dugstad, *Corrosion of carbon steel in an aqueous carbon dioxide environment, Part 2: Film formation*. Materials Performance, 1989: p. 46-50.
- [18] Sun, W., K. Chokshi, and S. Netic, *Iron Carbonate Scale Growth and the Effect of Inhibition in CO₂ Corrosion of Mild Steel*. NACE International.
- [19] Nafday, O. and S. Netic, *Iron Carbonate Scale Formation and CO₂ Corrosion in the Presence of Acetic Acid*. NACE International.

All final manuscripts will be sent through an XML markup process that will alter the LAYOUT. This will NOT alter the



Society of Petroleum Engineers

SPE-SPE-179942-MS-MS

Inhibition Performance of Mild Steel Corrosion in the Presence of CO_2 , HAc and MEG

Lesor Ikeh, G.C Enyi and G.G Nasr
Petroleum Engineering Research Group (PERG)
School of Computing, Science and Engineering
University of Salford, Manchester
United Kingdom, M5 4WT.

Copyright 2016, Society of Petroleum Engineers

This paper was prepared for presentation at the SPE International Oilfield Corrosion Conference and Exhibition held in Aberdeen, Scotland, UK, 9–10 May 2016.

This paper was selected for presentation by an SPE program committee following review of information contained in an abstract submitted by the author(s). Contents of the paper have not been reviewed by the Society of Petroleum Engineers and are subject to correction by the author(s). The material does not necessarily reflect any position of the Society of Petroleum Engineers, its officers, or members. Electronic reproduction, distribution, or storage of any part of this paper without the written consent of the Society of Petroleum Engineers is prohibited. Permission to reproduce in print is restricted to an abstract of not more than 300 words; illustrations may not be copied. The abstract must contain conspicuous acknowledgment of SPE copyright.

Abstract

The formation of hydrate and scale deposition is a major challenge in the petroleum industry. To avoid corrosion and hydrate formation, monoEthylene glycol (MEG) is been utilized in the pipeline as an antifreeze and anticorrosion agent. It has been observed that the MEG has to be separated from acetic acid (HAc) and acid gases which enhance corrosion of mild steel in the oilfield environments. HAc and MEG also has an

adverse effect of lowering the solubility of mineral salts and causing a higher risk of scale formation.

In this study, the mitigation of corrosion of mild steel in the presence of HAc and MEG in CO₂ saturated environment were investigated at 25°C and 80°C using 3.5% wt. NaCl solution in a semi-circulated loop setup. Weight loss and electrochemical measurements using linear polarization resistance (LPR) were used to evaluate the efficiencies of two corrosion inhibitor based chemicals (the phosphate ester and the Olei imidazoline salt) at different concentrations. Test results obtained show that the corrosion inhibitors are found to be very effective in reducing the corrosion of mild steel in the presence of HAc and MEG at different conditions tested.

Key words: CO₂ corrosion, mild steel, acetic acid, MEG, iron carbonate, inhibitor.

Introduction

Carbon steel pipelines are required to transport oil and gas products from the well, sometimes over long distances. In addition to oil/or gas, It is common that wells produce other products that are likely to cause corrosion, such as water (H₂O), carbon dioxide (CO₂), hydrogen sulphide (H₂S) and acetic acid (CH₃COOH). Pipeline failures due to corrosion could be very costly in terms of safety, cost or environmental damage [1]

The processing and transportation of this gas is hindered by corrosion due to water content and formation of gas hydrates in pipelines. Water can condense along the pipeline due to temperature gradients between the source and process plant, and this can lead to more corrosion and gas hydrate formation [2]. MonoEthylene glycol is usually injected into the pipeline as an antifreeze and anticorrosion agent. In most gas production system, thermodynamic hydrate inhibitors are applied to prevent the formation of

hydrates that can block the pipelines. More importantly, MEG is used in inhibitor prevention because it is less toxic than methanol and has low density [3-6]. Also, MEG has corrosion inhibition properties, but the corrosion inhibition of MEG is normally inadequate to protect the carbon steel used in the construction of oil and gas pipeline [5].

Several mitigation measures have been developed to reduce the corrosion rate in such pipelines to acceptable limits, which includes Injection of corrosion inhibitors or stimulating the growth of protective corrosion film [7, 8]. Wong and Park [9] explored the interactions of iron carbonate with three corrosion inhibitor generic actives (quaternary amine monomer, imidazoline, and phosphate ester. They noticed that the presence of quaternized amine monomer increases the precipitation rate of iron carbonate scale. They also reported that the presence of phosphate ester and imidazoline at concentrations above 25ppm prevents the growth of iron carbonate scale. Evidence suggests that iron and phosphate ester interact to form a more protective film on the surface [9]. Bilkova and Gulbrandsen in their studies established that the CO₂ corrosion inhibition was composed of two processes, a rapid process connected to hydrophobically driven adsorption of the inhibitor leading to inhibition of the anodic part reaction, and a slower process leading to a reduction in the corrosion rate through inhibition of the cathodic part reactions. They clearly stated that the performance of CO₂ corrosion inhibitors in many cases was hindered when the steel corroded before inhibition. However, the corrosion deposit may reduce access of the inhibitor to the steel surface and inhibitor performance might differ significantly from what is seen on bare carbon steel surfaces [10]. McMahon [18] noted that corrosion inhibitor performance is being affected by the use of hydrate inhibitors.

Kowata and Takahashi [11] devoted some work to corrosion inhibition at steel surfaces covered with corrosion product layers. They reviewed the work done on rusted surfaces, and showed that some inhibitors are able to penetrate deep into the rust layer. Hausler [12] in his research considered inhibition of CO₂ corrosion under conditions where

FeCO₃ films predominated. The concept of interphase inhibition has also been developed to describe inhibition in porous corrosion product layers as opposed to interface inhibition at bare surfaces [13]. Al-Maslamani et al [14] conducted a test on how well corrosion inhibitors perform under high velocity flows or flows containing solid particles. They noted that in some cases, inhibitors may be stripped from the surface they are supposed to protect by hydrodynamic forces or by the impingement of solid particles. For inhibitor that depends on the formation of a corrosion product for maximum efficiency, it may be the scale that is destroyed by erosive forces. Jasinski [15] found that commercial filming amine corrosion inhibitors transformed the morphology of the corrosion product scale that forms in CO₂ saturated systems into a more compact form. Based on his findings, corrosion rate was found to be related to the morphology of the scale with the denser scales corresponding to the lower corrosion rates. It was speculated that the denser corrosion scales formed when an inhibitor is present are more erosion resistant than scales formed without benefit of inhibitor. This means that using an inhibitor may also offer a means of controlling erosion-corrosion. Hence, it would be beneficial using corrosion inhibitors to reduce the corrosion rate of steel in CO₂ environment, but so far none published work on the inhibiting performance of mild steel corrosion in CO₂ saturated environment especially when both MEG and acetic acid are present.

In this study, two CO₂ corrosion inhibitors (phosphate ester and an oleic imidazoline salt) would be used to study the interaction of MEG and HAc on mild steel in CO₂ environment.

The oleic imidazoline salt (OI) contains an imidazoline group and a C₁₇ hydrocarbon chain with a double bond, and it is a reaction product of diethylenetriamine and a fatty acid [16]. Oleic imidazoline salt has been reported to partition preferentially to water. The adsorption of oleic imidazoline salt onto iron surface was found to be a fast process. Recent studies of oleic imidazoline by atomistic simulation methods suggest that a self-assembled monolayer forms [17]. Also, Moon et al found that the maximum of the inhibition efficiency was reached at about the same concentration as the minimum of the oil-water interface tension was reached

Several studies have been carried out on the corrosion inhibiting properties of phosphate esters [18] but not with MEG and or HAc in CO₂ saturated conditions. The general structure of the corrosion inhibitors considered are shown in Table 1.


Description and Application of Equipment and Processes.

The experiments were performed in a mini circulation flow loop. A peripheral pump circulates the test solution from the reservoir to the test cell. A small diameter pipe maintained a constant liquid volume flow in the cell. The reservoir tank and the test cell were continuously purged with CO₂ to removed oxygen completely from the test solution. Once de-oxygenation has been achieved, the required amount of HAc, MEG and inhibitors were added at the start of every experiment. The temperatures were controlled by means of a heating plate with a temperature sensor in the cell. The pH of the solution was adjusted to the desired value throughout the experiments by adding sodium bicarbonate (NaHCO₃) or hydrochloric acid (HCl) as needed.

Corrosion Inhibitors

The corrosion inhibitors that were tested in this study includes the phosphate ester and the oleic imidazoline salt, with their molecular formula and chemical structure showed in Table 1 below.

Table 1: Structures of corrosion inhibitors tested in the experiment

Inhibitor	Active component	Chemical formula	Molecular structure
A	The phosphate ester	H_3PO_4	$\begin{array}{c} O \\ \\ HO-P-OCH_3 \\ \\ OH \end{array}$
B	The Oleic imidazoline salt(OI)	$C_{18}H_{33}NaO_2$	

Test set up and procedures

The test specimens used throughout this study are mild steel having a surface area of 8.11cm^2 and a circular hole toward the top end. A copper wire of 0.02 mm diameter was spot welded and used on the test coupons to ensure electrical contact. The test coupons were suspended in the test solution by passing a plastic wire through the coupon and the wire was hung to a plastic rod held in place of the glass cell top holes. Prior to introduction into the test cell, the test coupon were successively ground with 240, 600 and 800 SiC grit paper and polished with 1200 SiC paper. It was then cleaned with acetone, rinsed with distilled water and dried. The general composition of the mild steel samples used is given in Table 2.

Four test solutions were prepared. The first test solution was prepared with 3.5% wt. sodium chloride (NaCl) as the blank solution without HAc, MEG and inhibitors. The

second test solution was prepared using 3.5% NaCl solution and 1000ppm HAc. The third test solution was prepared using 3.5% NaCl solution, 1000ppm HAc and 50% MEG, while the fourth and fifth test solution was prepared using 3.5% NaCl, 1000ppm HAc, 50% MEG, 10ppm and 50ppm of inhibitors A and B respectively. Table 3 summarizes the composition of test matrix used for this study.

Table 2: Chemical composition of mild steel (wt. %).

Comp.	C	Si	Mn	S	P	Sn	Cr	Ni	Mo	Cu	Al
Val. %	0.08	0.25	1.54	0.001	0.019	0.008	0.04	0.03	0.01	0.12	0.038

Table 3: Compositions of the test matrix used for the experiments

Parameters	Values
Test solution	3.5% wt. NaCl
Test material	Mild steel
Partial pressure of CO ₂ (bar)	0.54
MEG concentrations	50%
Inhibitor A(ppm)	[10, 50]
Inhibitor B(ppm)	[10, 50]
pH	6.6
Temperature (°C)	[25, 80]
C _{HAc} (ppm)	[0 -2000]
Surface area (cm ²)	8.11
Test method	[WL, and LPR]

Measurement Techniques

Weight loss measurement was performed on mild steel samples in all the test solutions at temperatures of 25°C and 80°C. The weight loss is measured and determined and the corrosion rate calculated using Equation 1:

$$= \frac{WL(g)}{\rho \times t \times A} \times K \left(\frac{mm}{yr} \right) \quad (1)$$

Where:

CR = corrosion rate, mm/yr,

ρ = density of the material, 7.86 g/cm³

WL = weight loss, grams,

t = the exposed time, hr

A = the exposed coupon surface area, cm²,

K = conversion factor, 8.76×10⁴

Also, the electrochemical measurements were carried out using a commercial potentiostat. A three-electrode configuration was used in every measurement. The mild steel sample was used as the working electrode, while the Ag/AgCl wire was used as reference electrode. The linear polarization curves were obtained in the potential range of -10 to +10 mV (vs. E_{corr}) with a scan rate of 0.1 mV/s.

Results and Discussion

Weight loss test

The results from the weight loss tests for the performance of two corrosion inhibitors evaluated at 25°C and 80°C are given in Figures 1-4 and are summarised in Table 4 and 5. In the first set of experiments, the weight loss of the first test solution (3.5% wt. NaCl without HAc, MEG and inhibitors), the second test solution (3.5% wt. NaCl with 1000ppm HAc), the third test solution (3.5% wt. NaCl with 1000 ppm HAc and 50% MEG), the fourth test solution (3.5% wt. NaCl with 1000ppm HAc and 50% MEG and inhibitor A) and the fifth test solution (3.5% wt. NaCl and 1000ppm HAc and 50% MEG and inhibitor B) evaluated at 25°C are presented in Figures 1 and 2 and Table Table 4, while the results of the second set of experiments, the weight loss of the first test

solution(3.5% wt. NaCl without HAc, MEG and inhibitors), the second test solution(3.5% wt. NaCl with 1000ppm HAc), the third test solution(3.5% wt. NaCl with 1000 ppm HAc and 50% MEG), the fourth test solution(3.5% wt. NaCl with 1000ppm HAc and 50% MEG and inhibitor A) and the fifth test solution(3.5% wt. NaCl and 1000ppm HAc and 50% MEG and inhibitor B) evaluated at 80°C are presented in Figures 3 and 4 and Table 5 respectively.

As can be seen from Figures 1 and 2 at 25°C, the two inhibitors tested performed better as expected. Both inhibitors show higher efficiencies by reducing the corrosion rate for the duration of the test, compared to the corrosion rate when HAc and MEG were tested alone. In Figure 1 with inhibitor A, the average corrosion rate reduced from 0.95 mm/yr to 0.35 mm/yr with 10ppm of inhibitor A, and from 0.98 mm/yr to 0.15 with 50 ppm of inhibitor A. Figure 2 (with inhibitor B) also show that the corrosion rate decreases from 0.88 mm/yr to 0.43 mm/yr with 10 ppm of inhibitor B and from 0.90 to 0.18 mm/yr on when applying 50ppm of inhibitor B. Table 4 summarizes the results of the average corrosion rate of the uninhibited and inhibited mild steel tested at 25°C

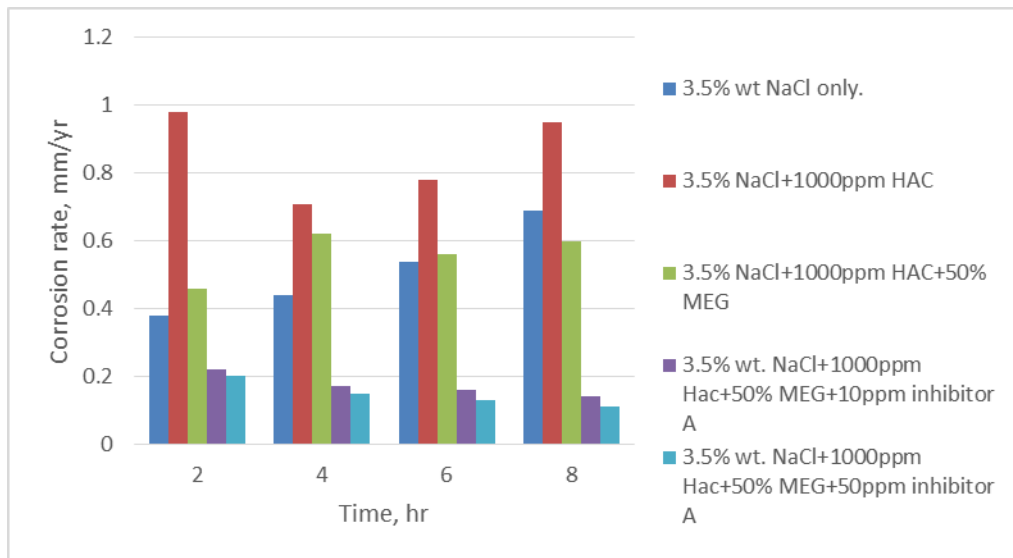


Figure 1: Effect of corrosion inhibitors on mild steel in 3.5% wt. NaCl solution at 25°C (3.5% wt. NaCl+1000ppm HAc+50% MEG+ inhibitor A)

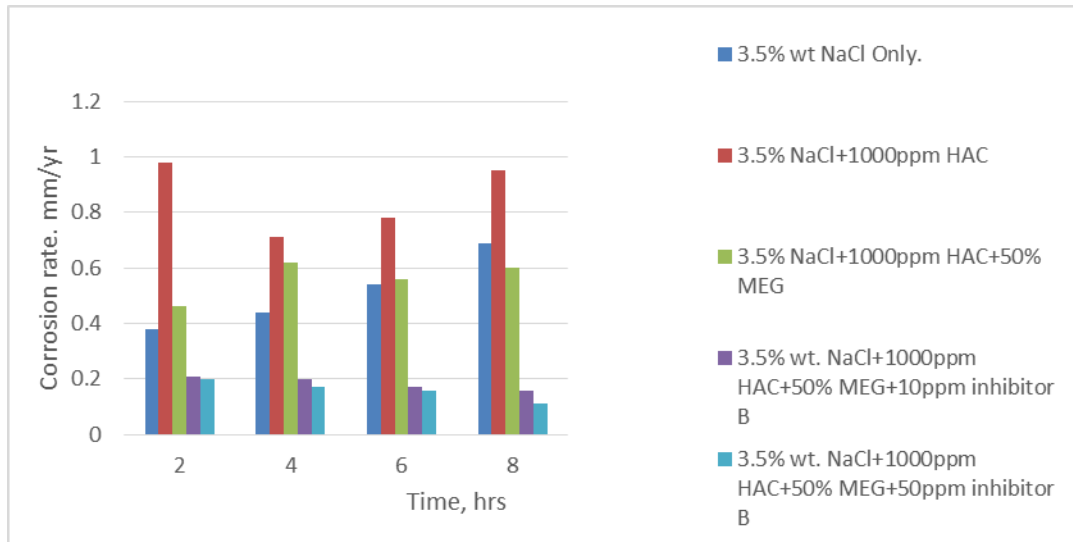


Figure 2: Effect of corrosion inhibitors on mild steel in 3.5% wt. NaCl solution at 25°C(3.5% wt. NaCl+1000ppm HAC+50% MEG+ inhibitor B)

Table 4: Summary results for corrosion inhibition performance for mild steel in 3.5% wt. NaCl solution saturated with CO₂ for inhibitors A and B at 25°C

T(hrs)	Blank	1000 ppm	1000 ppm	10 ppm	50 ppm	10 ppm	50 ppm
T(hrs)	0ppm	Hac only	50% MEG	Inb. A	Inb. A	Inb. B	Inb. B
2	0.38	0.98	0.46	0.22	0.2	0.21	0.22
4	0.44	0.71	0.62	0.17	0.15	0.18	0.16
6	0.54	0.78	0.56	0.16	0.13	0.14	0.09
8	0.69	0.95	0.6	0.14	0.11	0.9	0.05

Similarly, Figures 3 and 4 shows the average corrosion rate for both inhibitors tested at 80°C. As noticed, it is worthwhile to know that effective inhibitions were achieved with the inhibitors concentrations of 10ppm and 50ppm on the samples tested. The average corrosion rate obtained on the inhibited steel decreases from 0.35 mm/yr to 0.20 mm/yr with 10ppm of inhibitor B and from 0.18 mm/yr to 0.09 mm/yr with 50ppm of inhibitor B compared to non-inhibited steel. Table 5 summarizes the results of the inhibited and the un-inhibited steel tested at 80°C.

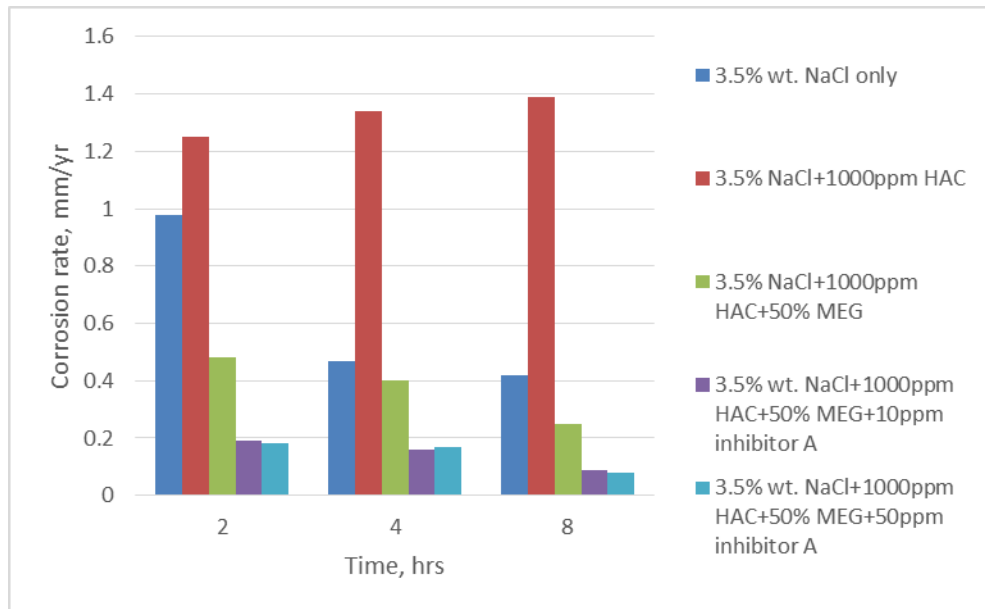


Figure 3: Effect of corrosion inhibitors on mild steel in 3.5% wt. NaCl solution at 80°C (3.5% wt. NaCl+1000ppm HAC+50% MEG+ inhibitor A)

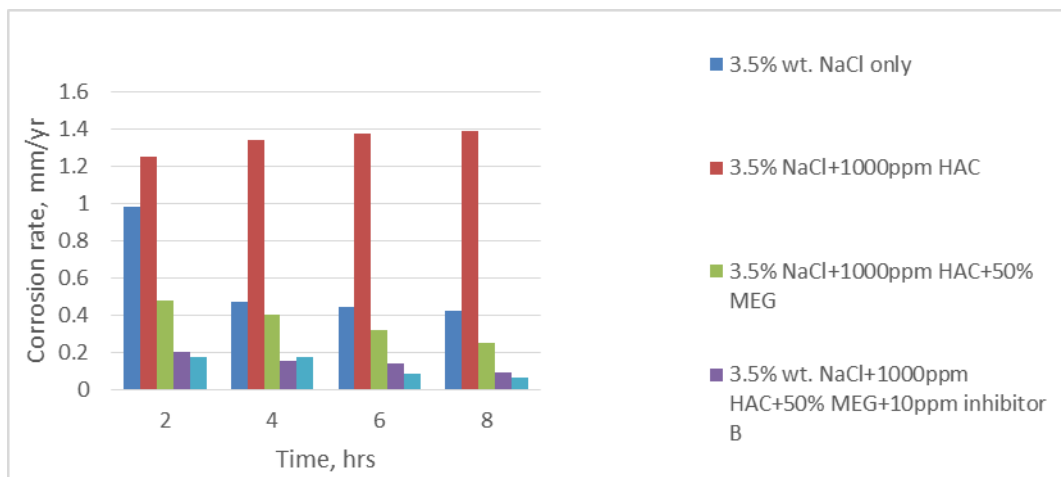


Figure 4: Effect of corrosion inhibitors on mild steel in 3.5% wt. NaCl solution at 80°C (3.5% wt. NaCl+1000ppm HAC+50% MEG+ inhibitor B)

Table 5: Summary results for corrosion inhibition performance for mild steel in 3.5% wt. NaCl solution saturated with CO₂ for inhibitors A and B at 80°C

	Blank	1000 ppm	1000 ppm	10 ppm	50 ppm	10 ppm	50 ppm
T(hrs)	0ppm	Hac only	50% MEG	Inb. A	Inb. A	Inb. B	Inb. B
2	0.98	1.25	0.48	0.2	0.19	0.17	0.19
4	0.47	1.34	0.4	0.16	0.16	0.14	0.16
6	0.44	1.38	0.32	0.15	0.15	0.08	0.08
8	0.42	1.39	0.25	0.09	0.07	0.04	0.03

Linear Polarization Resistance (LPR) Measurements

The performance of two corrosion inhibitors on the corrosion rate of mild steel in CO₂ saturated environment were also evaluated using the electrochemical measurement technique.

Linear polarization resistance curves of mild steel in different inhibitors concentrations in 3.5% wt. NaCl solution saturated in CO₂ at 25°C and 80°C are shown in Figures 5 and 6. The results indicates that corrosion reaction is inhibited by addition of the two inhibitors to the solutions. As can be seen, it is obvious that the corrosion rate for the inhibited samples reduces drastically to less than 0.1 mm/yr compared to the uninhibited samples with HAc and MEG alone.

At 25°C (Figure 5),

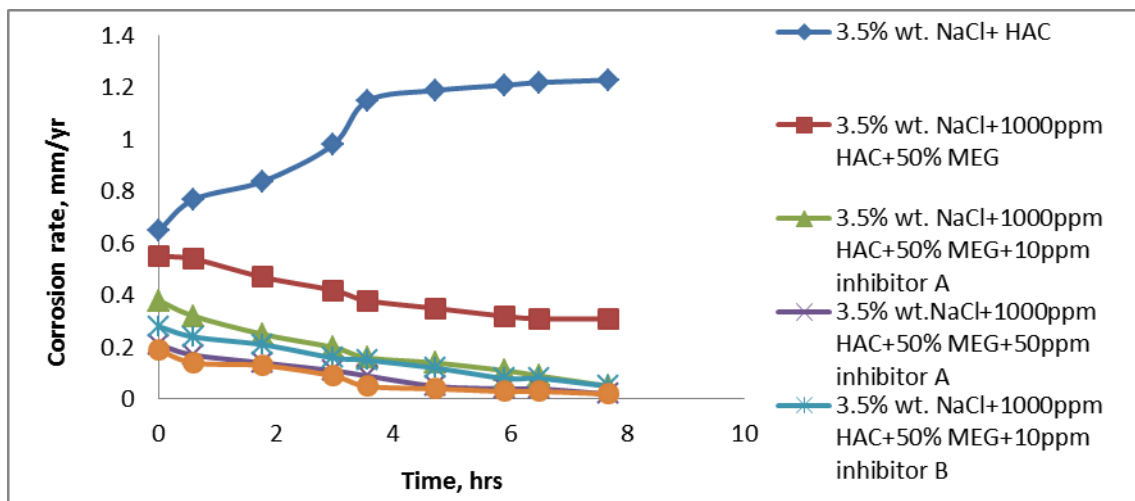


Figure 5: Performance of corrosion inhibition as a function of time for inhibitors A and B in 3.5% wt. NaCl solution at 25°C (3.5% wt. NaCl+1000ppm HAC+50% MEG+ inhibitors A and B).

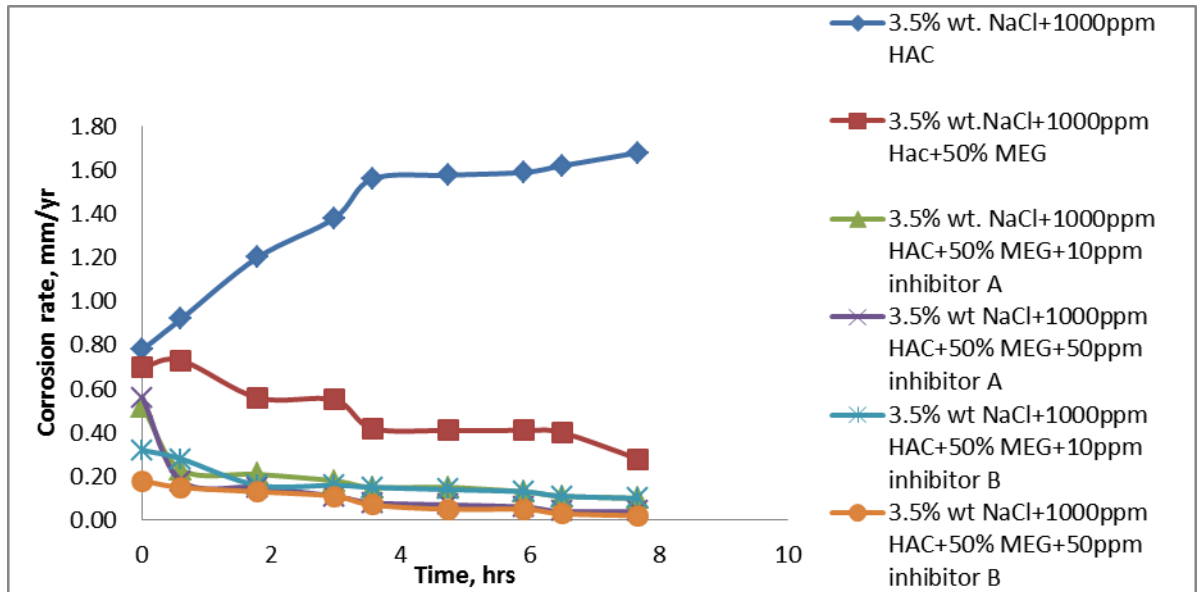


Figure 6: Performance of corrosion inhibition as a function of time for inhibitors A and B in 3.5% wt. NaCl solution at 80°C (3.5% wt. NaCl+1000ppm HAC+50% MEG+ inhibitors A and B).

Conclusions

In this study, the corrosion inhibition performance of mild steel in CO₂ saturated environment were carried out in the presence of HAc, MEG and two different types of corrosion inhibitors at 25°C and 80°C, pH of 6.6, CO₂ partial pressure of 0.54 bar and 50% MEG. Test results obtained show changes in mechanism of corrosion rate with time at different concentrations of the inhibitors.

The weight loss method gives a more reliable results of the inhibition performance of the mild steel samples tested. It is observed that the presence of HAc with the 3.5% wt. NaCl solution increases the corrosion rate of mild steel at both temperatures for the entire duration of the test

but, addition of 50% MEG to the test solution decreases the corrosion rate rapidly compared to the corrosion rate with 1000ppm concentrations of HAc.

The application of corrosion inhibitors for all the conditions tested further reduces the corrosion rate to the minimum. However, satisfactory performance was achieved for the

two inhibitors tested with concentrations ranging from 10ppm to 50ppm compared to the uninhibited steel. However, Inhibitor A (the phosphate ester) exhibited the highest inhibitor efficiency both at 10ppm and 50ppm and reduced the corrosion rate below 0.02 mm/yr than Inhibitor B.

Acknowledgments

The authors will like to thank the Petroleum Engineering Research Group and the Spray Research Group of the University of Salford for their support.

Nomenclature

HAc	=Acetic acid
MEG	=Monoethylene glycol
Ppm	=Parts per million (mg/Kg)
CI	= Corrosion Inhibitor
Mm/yr	= Millimetres per year

References

1. Executive, H.a.S.L.f.t.H.a.S., *Reliable corrosion inhibition in the oil and gas industry*. HSE, 2014.
2. Gonzalez, J.J., M.E. Alfonso, and G. Pellegrino, *Corrosion of Carbon Steels in Monoethylene Glycol*. NACE International.
3. Elhady, A.A.A., *Operating Experiences of DEG and MEG for Hydrate and Dewpoint Control in Gas Production Offshore Mediterranean*. German National Library of Science and Technology, 2006.
4. Brustad, S., K.P. Løken, and J.G. Waalmann, *Hydrate Prevention using MEG instead of MeOH: Impact of experience from major Norwegian developments on technology selection for injection and recovery of MEG*. Offshore Technology Conference.
5. Gulbrandsen, E. and J.H. Morard, *Why Does Glycol Inhibit CO2 Corrosion?* NACE International.

6. Wang, C., et al., *Corrosion Study of Carbon Steel in the Presence of Monoethylene Glycol (MEG) and Corrosion Inhibitors in Acid*. NACE International.
7. Dugstad, A., *Mechanism of Protective Film Formation During CO₂ Corrosion of Carbon Steel*. NACE International.
8. Jovancicevic, V., S. Ramachandran, and P. Prince, *Inhibition of CO₂ Corrosion of Mild Steel by Imidazolines and Their Precursors*. NACE International.
9. Wong, J.E. and N. Park, *Further Investigation On The Effect Of Corrosion Inhibitor Actives On The Formation Of Iron Carbonate On Carbon Steel*. NACE International.
10. Rozenfeld, I.L., *Corrosion inhibitors*. 1981: New York : McGraw-Hill, .
11. Kowata, K. and K. Takahashi, *Interaction of Corrosion Inhibitors With Corroded Steel Surface*. NACE International.
12. Hausler, R. *Corrosion Inhibition in the Presence of Corrosion Product Layers*. in R. H. Hausler, *Petrolite Corp., St. Louis, MO, Proceedings of the 6 th European Symposium on Corrosion Inhibitors(6 SEIC) Ann. Univ. Ferrara, N. S., Sez. V, Suppl.* 1985.
13. Lorenz, W.J. and F. Mansfeld, *Interface and interphase corrosion inhibition*. *Electrochimica Acta*, 1986. **31**(4): p. 467-476.
14. Al-Maslamani, M. and apos, *Performance Of (UNS 8028) Production Tubing Material In Sour Service Environment Of Khuff Gas Formation*. Society of Petroleum Engineers.
15. Jasinski, R.J., *Corrosion of Low-Alloy Steel in Crude oil /Brine/CO₂ Mixtures*. *Proc.Electrochemical Society* 1986. V. 86-7: p. pp. 139-48.
16. McMahan, A.J., *The mechanism of action of an oleic imidazoline based corrosion inhibitor for oilfield use*. *Colloids and Surfaces*, 1991. 59: p. 187-208.
17. Sunder Ramachandran , B.-L.T., Mario Blanco , Huey Chen , Yongchun Tang , and William A. Goddard *Self-Assembled Monolayer Mechanism for Corrosion Inhibition of Iron by Imidazolines*. *Langmuir*, 1996. 12 (26), pp 6419–6428.
18. Alink, B.A., et al., *Mechanism of CO₂ Corrosion Inhibition by Phosphate Esters*. NACE International.

Influence of Acetic Acid and MonoEthylene Glycol on Polarization behaviour of Mild Steel Corrosion in CO₂ Environment

Lesor Ikeh, G.C Enyi and G.G Nasr

Petroleum Engineering Research Group (PERG)

School of Computing, Science and Engineering

University of Salford, Manchester

United Kingdom, M5 4WT

Abstract

Mild steel pipelines are required to transport oil and gas products from the well, sometimes over long distances. In addition to oil/or gas, It is common that wells produce other products that are likely to cause hydrate and corrosion, such as water (H₂O), carbon dioxide (CO₂), hydrogen sulphide (H₂S) and acetic acid (CH₃COOH).

MonoEthylene glycol (MEG) is usually injected into the pipeline as an antifreeze and anticorrosion agent, but it has been observed that the MEG need to be separated from organic acids and acid gases which enhance corrosion of mild steel in the oilfield environments. In addition, MEG also has an adverse effect of lowering the solubility of mineral salts and causing a higher risk of scale formation.

In this study, the effect of acetic acid and monoEthylene glycol on cathodic and anodic polarization resistance of mild steel corrosion in CO₂ environment were evaluated at 25°C and 80°C using 3.5% wt. NaCl solution in a semi-circulation flow loop set up. Electrochemical measurements such as Potentiodynamic sweeps were employed in measuring the variations of Fe²⁺ dissolution and mitigation as a function of time on the mild steel coupons.

Preliminary results shows that the concentrations of HAc and MEG used both affect the metal dissolution as well as the cathodic polarization and not the anodic reaction. In addition, X-ray diffraction (XRD), scanning electron microscopy (SEM) and energy dispersive spectrum (EDS) techniques would be employing to analyse both the inhibited and uninhibited surfaces.

Key words: Acetic acid, MonoEthylene glycol, internal corrosion, mild steel, Potentiodynamic.